UNIVERSITÀ DEGLI STUDI DI MILANO

DIPARTIMENTO DI CHIMICA

PhD COURSE IN CHEMISTRY, XXX CYCLE

Synthesis of RGD Peptidomimetic-Drug Conjugates for the Tumor-Targeted Delivery of Cytotoxic Agents

CHIM/06 Organic Chemistry

André Filipe RAPOSO MOREIRA DIAS

R11167

Tutor: Prof. Dr. Cesare GENNARI (University of Milan)

Co-Tutor UNIMI: Dr. Luca PIGNATARO (University of Milan)

Co-Tutor MAGICBULLET: Prof. Dr. Norbert SEWALD (University of Bielefeld)

PhD Course Co-ordinator: Prof. Dr. Emanuela LICANDRO

A.Y. 2017/2018

To my parents and brother

ACKNOWLEDGMENTS

The work herein described was mainly performed at the University of Milan at the Department of Chemistry, in collaboration with Nerviano Medical Sciences (Milan, Italy), National Institute of Oncology (Budapest, Hungary) and Italfarmaco (Milan, Italy), in the period from June 2015 to May 2018 under the supervision of Prof. Cesare Gennari.
During these three years I also completed two secondment periods abroad: 1) University of Bielefeld (Bielefeld, Germany), from October 2016 to March 2017 under the supervision of Prof. Norbert Sewald and 2) Italfarmaco S.p.A. (Milan, Italy) from January 2018 to March 2018 under the supervision of Dr. Christian Steinkühler.

Firstly, I would like to thank my PhD supervisors: Prof. Cesare Gennari, Dr. Luca Pignataro and Prof. Norbert Sewald for giving me the opportunity to participate in this research project. I am extremely thankful for their continuing support, availability, leadership, and critical spirit during these three years of thesis, that helped me to grow as a person and chemist.

In terms of collaborations, I would like to thank:

- Prof. Norbert Sewald, Dr. Marcel Frese and all the OCIII group (University of Bielefeld, Germany) for all your kindness, guidance, scientific spirit and receiving me from October 2016 to March 2017.
- Dr. Michele Caruso and Dr. Fabio Gasparri (Nerviano Medical Sciences) for their availability to test our compounds (biological assays), advices and criticism;
- Prof. József Tóvári and Msc. Ivan Randelovic (National Institute of Oncology, Budapest) for their biological assays;
- Dr. Christian Steinkühler, Msc. Ana Martins and all Italfarmaco team for the collaboration from January 2018 to March 2018;
- Dr. Daniela Arosio for the support and the binding affinity assays during these years;
- Prof. Laura Belvisi for all the precious advices and collaboration during these three years;
- Dr. Hans-Georg Lerchen and Beatrix Stelte-Ludwig (Bayer AG, Germany) for their precious advices on the elastase topic.

For the financial support, I am grateful to the European Union's Horizon 2020 research and innovation programme that financed this project (ETN MAGICBULLET project, Marie Skłodowska-Curie grant agreement No 642004), granting me a "Marie Curie Fellowship".

A particular mention is dedicated to a friend and colleague Dr. Alberto Dal Corso that during these three years helped, gave support and taught me most part of the things on this topic.

I would like to thank all my group (a special word for Dr. Simone Zanella, Arianna Pina and Paula Rivas) and people from our corridor (Prof. Bernardi's group) with whom I shared my life in the laboratory. Without you would not be possible to complete these three years. Thank you!

I am eternally grateful to all my friends in Portugal and here in Milan, that helped and gave me support here and at distance.

My parents and brother receive my greatest wholeheartedly gratitude for their constant support, understanding, helpfulness, inspiration and encouragement they gave me all my life and through this unforgettable experience!

Grazie mille a tutti!

Table of Contents

Abbreviations

Aba	Azabicycloalkane
Ac	Acetyl
ADC	Antibody-drug conjugate
Ampro	4-Aminoproline
aq.	Aqueous solution
APT	Attached proton test
Asc	Ascorbate
Bn	Benzyl
Boc	*tert*-Butyloxycarbonyl
Bu	Butyl
Bz	Benzoyl
CA	Carbonic anhydrase
Cy5	Cyanine5
CPT	Camptothecin
CuAAC	Copper-Catalyzed Azide-Alkyne Cycloaddition
DAVB	Desacetyl vinblastine
DEPT	Distortionless Enhancement by Polarization Transfer
DHFR	Dihydrofolate reductase
DKP	Diketopiperazine
DMAP	4-Dimethylaminopyridine
DMF	*N*,*N*-Dimethylformamide
DMSO	Dimethyl sulfoxide
DNA	Deoxyribonucleic acid
DOX	Doxorubicin
ECM	Extracellular Matrix
EDC	1-Ethyl-3-(3-dimethylaminopropyl)carbodiimide
EEDQ	*N*-Ethoxycarbonyl-2-ethoxy-1,2-dihydroquinoline
EPR	Enhanced permeability and retention
equiv.	Equivalents
ESI	Electrospray ionisation
Et	Ethyl
FAK	Focal adhesion kinase
FACS	Fluorescence Assisted Cell Sorting
FH_4	Tetrahydrofolic acid
Fmoc	9-Fluorenylmethoxycarbonyl
GSH	Glutathione
FR	Folate Receptor
HATU	O-(7-azabenzotriazol-1-yl)-tetramethyl-uronium hexafluorophosphate
Her/neu	Receptor tyrosine-protein kinase erbB-2
HOAt	1-Hydroxy-7-azabenzotriazole
HPLC	High performance liquid chromatography
HRMS	High resolution mass spectrometry
Igs	Immunoglobulins
iPr$_2$NEt	N,*N*-Diisopropylethylamine (DIPEA)
J	Scalar coupling constants
K_d	Dissociation Constant
MTT	3-(4,5-dimethylthiazol-2-yl)-2,5-diphenyltetrazolium bromide
mAb	Monoclonal antibody
MALDI	Matrix-assisted laser desorption ionization
MC/SD	Monte Carlo/Stochastic Dynamics
Me	Methyl
MED	Minimum Effective Dose
MMAE	Monomethyl auristatin E
MMAF	Monomethyl auristatin F
MMP	Matrix metalloproteinase
MS	Mass spectroscopy
MTD	Maximum tolerated dose
MW	Molecular weight
NMR	Nuclear Magnetic Resonance
NHS	*N*-Hydroxysuccinimide
PABC	*para*-amino benzyl carbamate
PBS	Phosphate-buffered saline
PCa	Prostate cancer
PEG	Polyethylene glycol
ppm	Part per million

PSMA	Prostate specific membrane antigen	RAFT	Regioselectively Addressable Functionalized Templates
PTX	Paclitaxel		
quant.	Quantitative	RP	Relative Potency
R_f	Retention factor	TFA	Trifluoroacetic acid
SAR	Structure–activity relationship	THF	Tetrahydrofuran
RT	Room temperature	TI	Targeting Index
SIP	Small Immune Proteins	TMS	Tetramethylsilane
SMAC	Second mitochondrial activator of caspases	t_R	Retention time
		$t_{1/2}$	Half-life time
SMDC	Small molecue-drug conjugate	unc	Uncleavable
SPECT	Single-photon emission computed tomography	VEGFR	Vascular Endothelial Growth Factor Receptor
SSTR	Somatostatin receptor	WHO	World Health Organization
S	Selectivity	δ	Chemical shift
RNA	Ribonucleic acid		

Amino acid*	**One-letter code**	**Three-letter code**
Alanine	A	Ala
Arginine	R	Arg
Asparagine	N	Asn
Aspartic	D	Asp
Cysteine	C	Cys
Glutamine	Q	Gln
Glutamic acid	E	Glu
Glycine	G	Gly
Histidine	H	His
Isoleucine	I	Ile
Leucine	L	Leu
Lysine	K	Lys
Methionine	M	Met
Phenylalanine	F	Phe
Proline	P	Pro
Serine	S	Ser
Threonine	T	Thr
Tryptophan	W	Trp
Tyrosine	Y	Tyr
Valine	V	Val

* D-amino acids are described by D-Xaa in the three-letter code and with the small letter in the one-letter code.

General Introduction

The use of cytotoxic agents (i.e. chemical compounds capable of killing cells) is a core component of pharmacological approaches for the therapy of cancer. Ideally, cytotoxic agents should preferentially kill tumor cells while sparing healthy tissue. In practice, the scenario is much more complex: many anticancer drugs inhibit cells in rapid proliferation and thus act against healthy tissues, in which they accumulate. This drawback typically results in severe side-effects, limiting therapeutic benefits.

Different approaches to overcome the drawbacks of traditional chemotherapy have been investigated so far, pointing at the selective delivery of cytotoxic agents to cancer cells. This goal has been pursued by improving the tumor accumulation of anticancer drugs through their covalent conjugation to specific ligands (antibodies or 'small molecules') of tumor-associated receptors. While Antibody-Drug Conjugates (ADCs) represent a mature technology, which has already reached the market, increasing research efforts have been recently put into Small Molecule-Drug Conjugates (SMDCs), which have the potential advantage of better pharmacokinetic properties and more sustainable preparation.

One of the tumor receptors that has been studied as target for SMDCs is integrin $\alpha_V\beta_3$ (a heterodimeric transmembrane glycoprotein), owing to its high expression in the tumor neovasculature as well as on the surface of several tumor cells. Thus, in this PhD thesis, the synthesis of new SMDCs targeting $\alpha_v\beta_3$ integrin is described. The structure of such SMDCs consists in the connection of three core components: i) LIGAND - the *cyclo*[DKP-RGD] peptidomimetic, developed by the Gennari and Piarulli group, has been used as integrin-targeting moiety in all the new constructs; ii) CYTOTOXIC PAYLOAD - three different cytotoxic agents (i.e. paclitaxel, monomethyl auristatin E and monomethyl auristatin F) have been included as anticancer drugs; iii) LINKER - specific functional groups (i.e. peptides) have been used to connect the drug and ligand, aiming at the selective drug release in the intra or extracellular tumor environment.

These new SMDCs have been subjected to a panel of biochemical and biological assays, for the assessment of both their structural features (e.g. stability, cleavage experiments of the

linkers, kinetics of drug release, etc.) and biological activity (e.g. affinity for the purified integrin $\alpha_V\beta_3$ receptor, selective cytotoxicity against $\alpha_v\beta_3$-expressing or non-expressing cells, etc.).
Thus, the main structure of the present PhD thesis is reported here:

- Chapter I provides a general overview of the tumor-targeting research area through an in-depth survey of the most relevant and recent literature in the field. The contribution of our group in the field is also reported here.
- Chapter II describes the development of a new library of multimeric *cyclo*[DKP-RGD]-PTX conjugates (monomeric, dimeric, trimeric and tetrameric conjugates) bearing lysosomally-cleavable linkers and their full biological *in vitro* evaluation. The results achieved with these first compounds prompted the design of next-generation *cyclo*[DKP-RGD]-PTX conjugates, reported in the following chapters.
- Chapter III describes the synthesis and *in vitro* evaluation of *cyclo*[DKP-RGD]-PTX conjugates bearing extracellularly-cleavable peptide linkers, capable of releasing the payload in the tumor microenvironment, rather than inside cancer cells: this mechanism can be promoted by tumor-associated enzymes present in the tumor stroma (e.g. elastase), which can efficiently cleave the linker and set the drug free to diffuse within the tumor mass.
- Chapter IV consists in the development of a small library of conjugates containing the *cyclo*[DKP-RGD] ligand, a lysosomally-cleavable peptide linker and the highly potent toxins monomethyl auristatin E or F (MMAE and MMAF) as the cytotoxic payloads, which are state-of-the-art tools for targeted anticancer therapy.
- Finally, all the experimental details of synthetic and biological procedures are included in Experimental Section, together with spectroscopic data and HPLC profiles of the newly synthesized compounds.

Chapter I

Drug Targeting to Cancer

DRUG TARGETING TO CANCER

1.1 General Introduction

Cancer is one of the main causes of human mortality and morbidity in both developed and developing countries.[1] As stated by the World Health Organization (WHO), approximately 14 million new incidences and 8.2 million cancer-related deaths were reported in 2014, affecting populations in all continents (Figure 1). The number of incidences is expected to increase to 22 million within the next two decades. Among the world population, the most common identified cancer types were lung, breast, colon/rectum, liver, prostate and stomach (Figure 1).[2] Cancer is triggered by complex processes, which are directly connected to the alteration of a fundamental process of life, *i.e.* cell division (mitosis). Cancer might be induced by down and/or upregulation of endogenous molecules, being characterized by uncontrolled cell growth and fast proliferation properties leading to tumor formation.

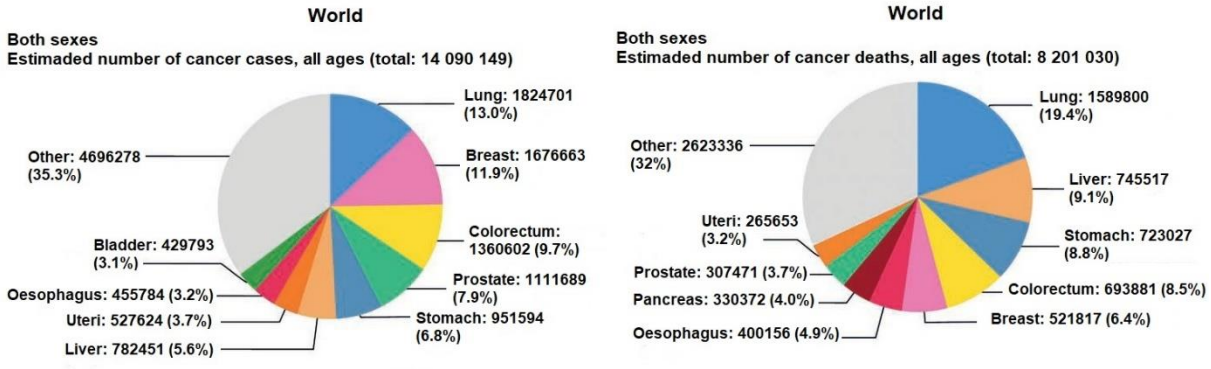

Figure 1. Estimated world cancer incidences and mortality proportions by WHO, in both genders, 2014.[1]

Treatment of cancer has been one of the key goals of medicine and medicinal chemistry research. Combinations of surgery, radiotherapy and chemotherapy interventions remain the backbone of cancer treatment. The traditional pharmaceutical approaches consist on the administration of small cytotoxic molecules aimed at stopping the rapid cell proliferation and inducing apoptosis by interfering with fundamental cellular functions (e.g. DNA replication, cell division).[3]

Cytotoxic agents are commonly classified on the basis of their biological targets:[4,5]

- **DNA-targeting groups**:[6] these class of compounds are divided into DNA-alkylating agents (e.g. mechlorethamine, chlorambucil, Figure 2) and DNA metalating agents (e.g. cisplatin, oxaliplatin, picoplatin, Figure 2). DNA-alkylating agents are known as a class of compounds that directly modify DNA bases, forming crosslinks in DNA or intercalating between bases. Developed as a derivative of nitrogen mustard gas, Mechlorethamine (**1**, Figure 2) can be considered the first compound of such class to be evaluated as anticancer agent: it is a bifunctional alkylating agent, containing electrophilic residues, which react with guanine bases on the DNA sequence.

  On the other hand, DNA-metalating agents are described as a panel of molecules containing Pt(II)-complexes, capable of irreversibly crosslink DNA strands, upon reaction with N^7-position of guanine bases.
- **Antimetabolites and Nucleoside analogs**: this group of anticancer drugs consists on synthetic variants of endogenous fundamental building blocks, which interfere with the elongation of DNA strands (e.g. thioguanine, 5-fluoruracil, gemcitabine, Figure 2).
- **Anti-folates**:[6,7] This class consists of inhibitors of crucial enzymes involved in the synthesis of DNA and its precursors. Methotrexate and pemetrexed (see Figure 2) are the most representative examples of this class. Their mechanism of action involves the inhibition of DHFR (dihydrofolate reductase) preventing the formation of tetrahydrofolate, an essential intermediate of purine and pyrimidine biosynthesis. Particularly, interferences with FH4 (tetrahydrofolate cofactors - series of the reduced form of folate) metabolism hamper important biochemical processes, such as methylation reactions, that essential for the biosynthesis of purine ribonucleotides and thymidine monophosphate (TMP).
- **Topoisomerase Inhibitors**:[6] this class of anticancer drugs interferes with DNA synthesis by inhibiting topoisomerase I and II. These enzymes are involved in crucial steps of the DNA structure organization. Topoisomerase I permits the passage of single DNA strands through a temporary single-strand break, originated in the complementary strand of the double helix. Topoisomerase II cleaves both double helix strands to allow the passage of a complete helix to the supercoiled DNA (unwind form). For example, camptothecin (**11**, Figure 2) and its analogs stabilize the DNA-topoisomerase I cleavable complex, thus inhibiting the rejoin step of DNA. On the other hand, topoisomerase II is one of the targets of Anthracyclines antibiotics (e.g. doxorubicin, daunorubicin, epirubicin and idarubicin, Figure 2), which are known to intercalate DNA leading to cell death.[8]
- **Antimitotic drugs**:[9] this class of cytotoxic agents interfere with microtubule dynamics, which are crucial in the mitosis process. Microtubule destabilizing agents, such as Vinca Alkaloids (e.g. Vinblastine and Vincristine, Figure 2), inhibit tubulin polymerization, thus blocking the formation of microtubules. By contrast, Taxanes (e.g. Paclitaxel and Docetaxel,

Figure 2) are the most known microtubule-stabilizing agents, which also trigger apoptosis in highly-proliferating cells. These drugs, inhibit tubulin depolymerization, thus blocking the formation of free tubulin.

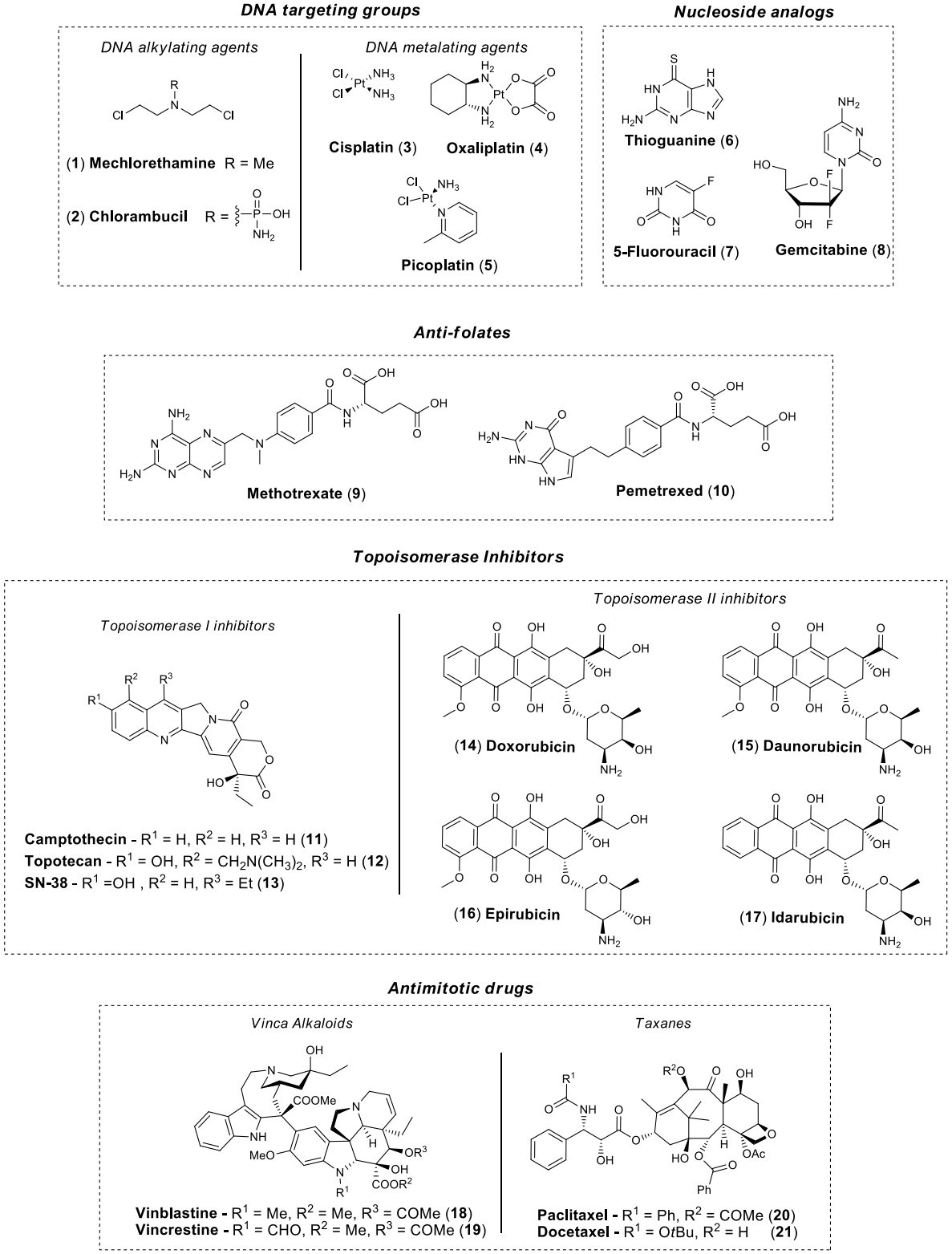

Figure 2. Molecular structures of selected conventional chemotherapeutics divided by different groups.

In general, the systemic administration of traditional anticancer agents does not result in the selective drug accumulation to the diseased tissue. In fact, these compounds can interact with healthy cells, leading to considerable side effects (low molecular-weight cytotoxic drugs do not preferentially accumulate in solid tumors)[10] and preventing the administration of anticancer drugs to doses that are high enough to be effective.[11] This low accumulation of chemotherapeutics at the tumor site can be ascribed to different factors, such as the increased interstitial pressure in several solid tumors and the rapid elimination from systemic circulation of small molecule drugs, which eventually accumulate in excreting organs (e.g. liver and kidney).[12]

Studies in mice have shown that injection of paclitaxel (PTX),[13] or doxorubicin (DOX)[14] led to poor tumor accumulation compared to the amount of injected drug detected in healthy organs such as liver and lung (1:10 – 1:20, after organ weight normalization). The same trend has been observed in human patients treated with a bolus injection of ^{11}C-docetaxel: the product did not show any significant accumulation in the hepatic tumor.[15]

Another drawback is the so-called drug resistance, which heavily affects the chemotherapy efficacy. In particular, due to their high heterogenicity and mutation rates, tumor cells can be considered as rapidly changing targets. A certain population of cancer cells may be less affected by the treatment and it can then overgrow, leading to a drug-resistant tumor mass.[16]

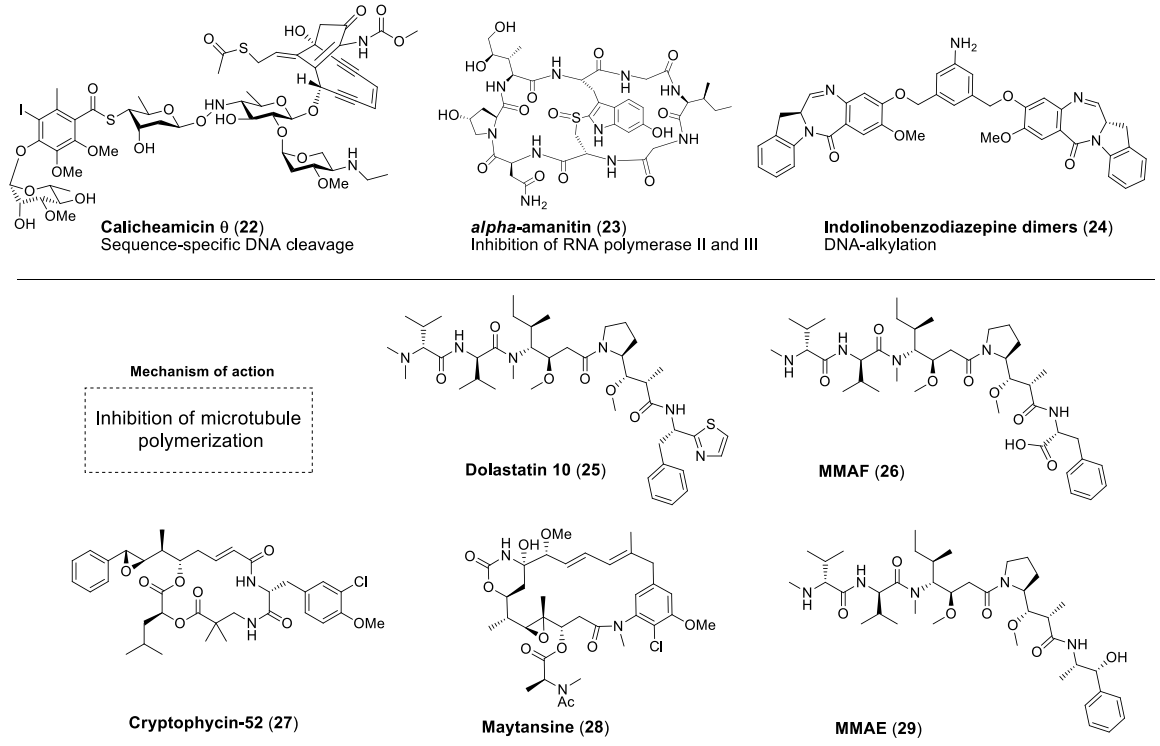

Figure 3. Molecular structures and mechanism of action of some potent cytotoxic agents used in chemotherapy.

As consequence of all these facts, traditional anticancer agents are characterized by a small "therapeutic window", which is commonly described as the difference between the lowest

administered dose resulting to clinical benefits (minimum effective dose, MED) and the highest dose found to be free of undesired toxicities (maximum tolerated dose, MTD). To overcome the drawbacks mentioned above, multidrug therapy was one of the first approaches tried by the clinic.[12] Unlikely, severe side-effects were observed in patients. During the past three decades, efforts have been done to discover new more potent small anticancer agents with improved anticancer efficacy. A wide range of new anticancer drugs have been discovered from natural sources and developed as anticancer agents (Figure 3). New DNA- and RNA-targeting agents (e.g. derivatives of calicheamicin, indolinobenzodiazepines and α-amanitin) and tubulin-targeting molecules (e.g. cryptophycins, maytansinoids, dolastatins) were found to inhibit cell proliferation at the picomolar and subnanomolar range.[17,18,19,20,21,22] However, most of these new cytotoxic molecules showed harsh side effects at low administration doses, indicating that the increased potency does not extend the therapeutic window of systemic cytotoxics. As a result, these ultrapotent cytotoxic agents were discontinued from the clinic at early stages, unveiling the need for new pharmacologic approaches.

1.2. Targeted Therapies for Cancer

The selective delivery of cytotoxic agents at the tumor site is still a major concern to improve current chemotherapy outcome. Regarding this issue, targeted delivery approaches rely on the ability of specific molecular constructs to selectively accumulate at the diseased site, improving the therapeutic window of cytotoxic agents. A particular group of such molecules (e.g. micelles, liposomes, polymers, nanoparticles and macromolecules) can have tumor-topic activity (i.e. the ability to **passively** accumulate into solid tumors).[12] The so-called EPR (Enhanced Permeability and Retention) effect has been described as the main mechanism of action of these large molecules , which take advantage of the absence of lymphatic drainage and the leakage of tumor vasculature.[23] For example, different types of nanoparticles have been used to encapsulate cytotoxic agents, with the aim to force drug accumulation within the tumor vasculature, following different mechanisms of action.[24] However, clinical success of nanomedicine has been limited so far to pegylated (Doxil™) and non-pegylated (Myocet™) liposomal forms of doxorubicin for the treatment of metastatic ovarian cancer, liposome-encapsulated daunorubicin (DaunoXome™) for the treatment of leukemia, and albumin-based paclitaxel (Abraxane™) for the treatments of breast cancer.[25]

On the contrary, **active** drug targeting systems use ligands (e.g. monoclonal antibodies, small molecule ligands such as vitamins, peptides or peptidomimetics) directed against specific tumor antigens (i.e. particular proteins showing predominant expression in tumors, located either on the surface of cancer cells, or in the tumor stroma or vasculature, see Fig. 4).[26]

Typically, one or more cytotoxic drugs are covalently attached to the targeting ligand through a specific linkers. Such systems will be hereafter referred to as ligand-drug conjugates. These conjugates are generally administered systemically to patients and the efficient extravasation (i.e. the migration from the circulation to the tissues) is fundamental for the conjugate to reach and bind the tumor antigen. Ideally, the binding leads to the selective conjugate accumulation in the diseased tissue expressing the target antigen, (Fig. 4), whereas in healthy tissues, binding does not occur and the conjugate is cleared quickly. Upon ligand binding, it has previously been described that target antigen-conjugate complexes must internalize into the diseased cells (i.e. internalization of the conjugate through receptor-mediated endocytosis).[20,27] The modified intracellular environment (e.g. lysosomal proteases, endosomal reducing agents, lowered pH) would then trigger the linker cleavage and the release of the cytotoxic cargo.[28] By contrast, other approaches have been investigated, where the drug release takes place in the extracellular space (i.e. *"non-internalizing"* tumor targeting). In this strategy, the drug can later act against tumor cells and other cellular targets (e.g. tumor endothelial cells or tumor cells with low antigen expression) by passive diffusion.[29]

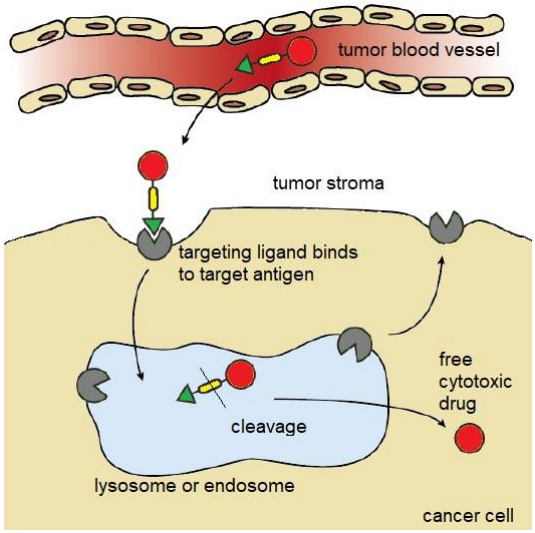

Figure 4. Active drug targeting approach. A ligand-drug conjugate (green-yellow-red) diffuses to the tumor stroma and interacts with its tumor-associated antigen. After internalization, the smart linker (yellow) between the ligand (green) and drug (red) is intracellularly cleaved, releasing its cytotoxic drug. Adapted from[20]

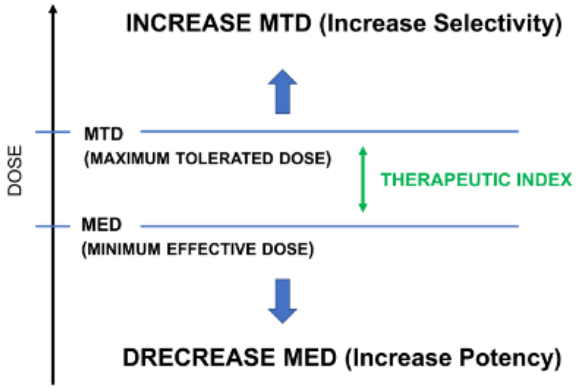

Figure 5. Strategy for the optimization of the therapeutic index of anticancer ligand-drug constructs.[30]

A variety of ligand-drug conjugates have been successfully developed to treat cancer according to these strategies. Generally, by combining a homing device (e.g. antibodies or small molecule ligands) with an active drug, it is possible to locally increase the concentration of the anticancer drug, thus decreasing the dose-limiting toxicities and improving the overall

therapeutic index of the drug (Figure 5).[30] As a result, while some of these constructs have already reached the market, others can be considered as promising technologies for future oncology.

1.3 Antibody-Drug Conjugates (ADCs)

1.3.1. Antibodies – an overview

Antibodies, also known as immunoglobulins (Igs), are endogenous-occurring proteins biosynthesized by plasma cells and B-lymphocytes in mammals.[31] Antibodies can bind with high affinity and selectivity to virtually any kind of antigen, expressed in viruses, bacteria, cancer cells or other disease-causing organisms. In the context of immune response, antibodies play two main functions: 1) recognition (i.e. specific binding and blockade of pathogen molecules), and 2) recruitment of humoral immune components (e.g. complement proteins) and cellular immune components (e.g. cytotoxic T-lymphocytes or phagocytes activation for the release of cytokines and interaction with the antigen of interest) with the goal of destroying the pathogen.[31]

1.3.2. From Discovery to Development

In 1890, Emil von Behring and Kitasato Shibasaburo described a “molecule” that could neutralize diphtheria infection in the blood stream. Hence, rats, rabbits and pigs were immunized with attenuated forms of the infectious molecules causing diphtheria. Then, the serum produced by these animals was later injected in non-immunized animals that had previously been infected with diphtheria bacterium: all animals recovered from the infection.[32] Some years after, in 1987, Paul Ehrlich developed the concept of “magic bullets” (i.e. antibodies), being secreted on the cell membrane surface of immune system in response to “strange” antigens.[33] Such “magic bullets” would only attack specific pathogens (e.g. viruses, bacteria). During the decade of 1940, Linus Pauling proved that the theory of Paul Ehrlich was correct, fully describing the way of interaction between an antibody and the recognized antigen (i.e. lock-and-key theory). In 1976, Susumu Tonegawa showed the first rearrangement of Ig genes, being the key role for the development of sequence diversity in antibodies.[34] In 1975, Georges Köhler and César Milstein developed the hybridoma technology,[35] which allowed the synthesis of large amounts of a single-purified monoclonal antibody (mAb). The hybridoma technology made possible the specific targeting of a single epitope of the antigen of interest, which was then a springboard to the clinical use of mAbs as therapeutic agents for cancer and other indications. Therefore, antibody-based constructs are one of the largest and fastest

growing family of drugs, putting pressure on the development of new targeted anticancer molecules.

1.3.3. Antibody Engineering and Structure

A typical mAb molecule features a Y-shaped structure, which carries two similar peptidic heavy (H) and light (L) chains (Figure 6A). Both heavy (~50 kDa) and light (~25 kDa) chains are connected by an intramolecular disulfide bond and heterodimerized by non-covalent interactions. Two copies of heterodimers are covalently linked at the level of the heavy chains by two extra disulfide bonds at the hinge region, leading to a full antibody structure of ~150 kDa. Each chain is known to be composed by a variable domain at its N-terminus (V_L and V_H for the light and heavy chain, respectively), which is responsible for antigen biding, and one or more C-terminus constant domains (C_L and C_H for the light and heavy chain, respectively). Finally, the general Y-shape of mAbs is divided into Fab (antigen recognition) and Fc (effector) domains. The latter is glycosylated at a conserved Asn 297 amino acid residue.[26]

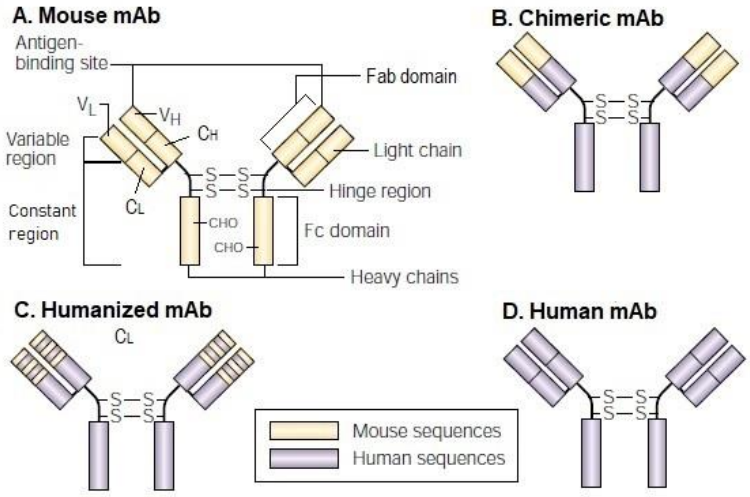

Figure 6. Antibody general structure and evolution of antibody engineering. A. Mouse antibody; B. Chimeric antibody; C. Humanized antibody; D. Human antibody. The mAb subdomains are reported. Fab: Fragment antigen-binding; Fc: fragment crystallizable domain; V_H: heavy-chain variable; V_L: light-chain variable; C_H: heavy-chain constant; C_L: light-chain constant.[26]

While the enormous therapeutic potential of mAbs became evident since the early discovery, a considerable limitation was identified when murine antibodies showed severe immunogenicity in humans. Moreover, murine mAbs show low binding to human Fc receptors (i.e. receptor found on the cell surface of, for example, B-lymphocytes and macrophages), resulting in inefficient effector functions and leading to fast clearance (Figure 6A). To overcome these limitations, advances in recombinant DNA techniques made possible the modification of the mAb structure, allowing the generation of engineered mAbs containing human sequences. In other words, the variable domains of a murine mAb are installed onto the constant domains

of a human mAb, forming the “chimeric antibodies” (Figure 6B). Thus, immunogenic response is reduced and stronger binding affinity is allowed for its target antigen (e.g. Fc receptors). Later on, “humanized antibodies” were developed, where only the murine complementary determining regions (CDRs) are grafted on human antibodies (Figure 6C). The origin of fully human antibodies (Figure 6D) was achieved in the 1990s after the development of phage display techniques by George P. Smith and the revolutionary work of Sir Gregory Winter on mAbs field. Other techniques including the use of transgenic mice (bearing the immunized gene loci of human mAb with the antigen of interest) or ribosome and yeast display, have also been developed as valuable tools to produces fully human antibodies.[30]

1.3.4. mAbs as Carriers for the Tumor Targeted Delivery of Anticancer Agents

Due to the success achieved by the development of “chimeric”, “humanized” and “fully human” mAbs (i.e. the half-life of 21 days in humans[36] and 6-8 days in mice[37] is way longer than the half-life of murine mAbs), pharmaceutical industry have been using such macromolecules as single agents, for cancer treatment. The first mAb to receive marketing authorization for cancer treatment was the chimeric mAb Rituxan™ (rituximab, Biogen-Idec in 1997): approved for treatment of patients with non-Hodgkin’s lymphoma, it became rapidly a blockbuster.[30] On the contrary, the development of antibodies for the treatment of solid tumors is generally more cumbersome.[38] Accordingly, mAbs are usually given in combination with traditional anticancer drugs or other mAbs. For instance, Roche/Genentech’s Herceptin™ (trastuzumab) was approved for the treatment of Her/neu positive metastatic breast cancer in combination with doxorubicin or paclitaxel.[30] Moreover, the use of mAbs to stimulate the immune system to attack cancer cells should be mentioned here: the success of the so-called checkpoint inhibitors (e.g. Nivolumab and Ipilimumab) is now established and the products are receiving marketing authorization for an increasing number of indications.[39]

Over the past two decades, antibodies have been studied as interesting tools to carry several cytotoxic agents at the tumor site.[20,30] Since traditional cytotoxic drugs exhibit their action inside the cell, the observation that specific antibodies can enter cells upon binding to a transmembrane antigen (i.e. receptor-mediated endocytosis) stimulated the mAb functionalization with cytotoxic drugs through specific linkers, giving rise to the so-called antibody-drug conjugates (ADCs).[20,40] The release of the payload inside the targeted cancer cell would increase the selectivity and therapeutic efficacy of these constructs and it is made possible either by the linker cleavage or after intracellular degradation of the antibody structure – Figure 7A.[20,40]

By contrast, it has been recently understood that mAb internalization may not be essential for selective drug release (e.g. ADCs specific to extracellular matrix proteins have been showing strong anti-tumor activity) if equipped with extracellularly cleavable linkers – Figure 7B.[27,29,41] Considering the mechanism of action of ADCs, it is conceivable that the linker plays a key role: ideally, this moiety should be stable in circulation for days and be efficiently cleaved during the receptor-mediated endocytosis (Fig. 7A) or in the tumor microenvironment (Fig. 7B). In fact, premature release of the drug in the blood circulation would lead to systemic toxicity and a lower therapeutic index.[29,30]

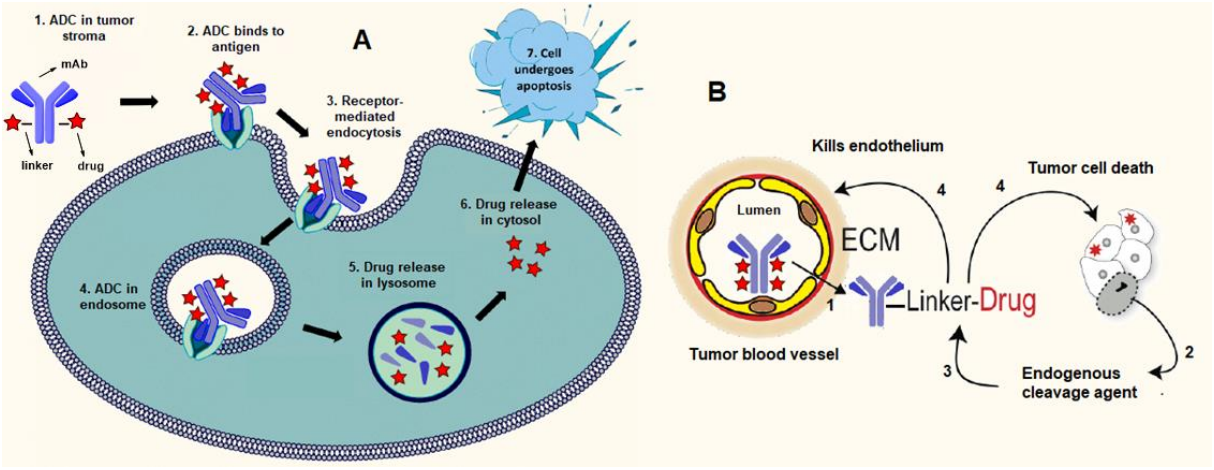

Figure 7. Structure and different drug delivery mechanisms of ADCs. **A)** Upon binding to tumor cell surface antigens, the ADC-receptor complex is internalized into the cell. This receptor-mediated endocytosis leads to drug release in intracellular compartments (e.g. endosomes and lysosomes). **B)** In case of non-internalizing antigens, the ADC remains bound to the receptor on the cell surface. Here, depending on the linker, the cytotoxic drug may be released in the extracellular environment and enter the cell by passive diffusion.[29,30]

In the development of 1st-generation ADCs, the chimeric mAb (BR96), targeting the LewisY tetrasaccharide (LeY) tumor antigen, was linked to eight unities of doxorubicin (**14**, Fig. 2) through an acid-labile hydrazone linker.[42] Low anti-tumor activity and undesired cytotoxicity were observed. Whereas the non-human form of the mAb structure was associated to significant immunogenicity, the occurrence of severe toxicity was probably due to the short half-life of the hydrazone linker ($t_{1/2}$ = 43 h), which was not compatible with the long circulation time of the BR96 mAb ($t_{1/2}$ = 12 days).[43] Another 1st-generation ADC was the K1S/4 mAb, which was connected to desacetylvinblastine (a vinca alkaloid), through an esterase-labile hemisuccinate or an acid-labile hydrazone linkers. Also in these two cases, no considerable anti-tumor activity emerged from clinical trials.[44]

Following these clinical failures, it was proved that a rational linker development would play an essential role in the evolution of the next generations of ADCs, as well as the use of more potent cytotoxic drugs. Moreover, “humanized” and “fully human” antibodies were used to reduce immunogenicity and the rapid clearance of the ADCs from circulation.

New generations of ADCs were developed accordingly and, so far, four ADCs have been approved by the FDA for cancer therapy: the CD30-targeting brentuximab vedotin (Adcetris™ from Seattle Genetics, compound **30** – Figure 8) is used for the treatment of Hodgkin lymphoma and anaplastic large cell lymphoma, and HER2-targeting ado-trastuzumab emtansine (Kadcyla™ from Roche, compound **31** – Figure 8) for the treatment of metastatic breast cancer. More recently, the CD33-targeting gemtuzumab ozogamicin (Mylotarg™ from Pfizer, compound **32** – Figure 8) was approved for treatment of acute myeloid leukemia. This ADC had been withdrawn in 2010, due to an inadequate efficacy/side effect relationship, but a dose-treatment revision led to the re-approval of the biotherapeutic (FDA news release, 2017). [45] Lastly, the newly CD22-targeting inotuzumab ozogamicin (Besponsa™ from Pfizer, compound **33** – Figure 8) was approved during the previous year for treatment of acute lymphoblastic leukemia.[45] Moreover, around 60 ADCs are now running the clinical trials, while many drug candidates are being investigated at preclinical level.[46]

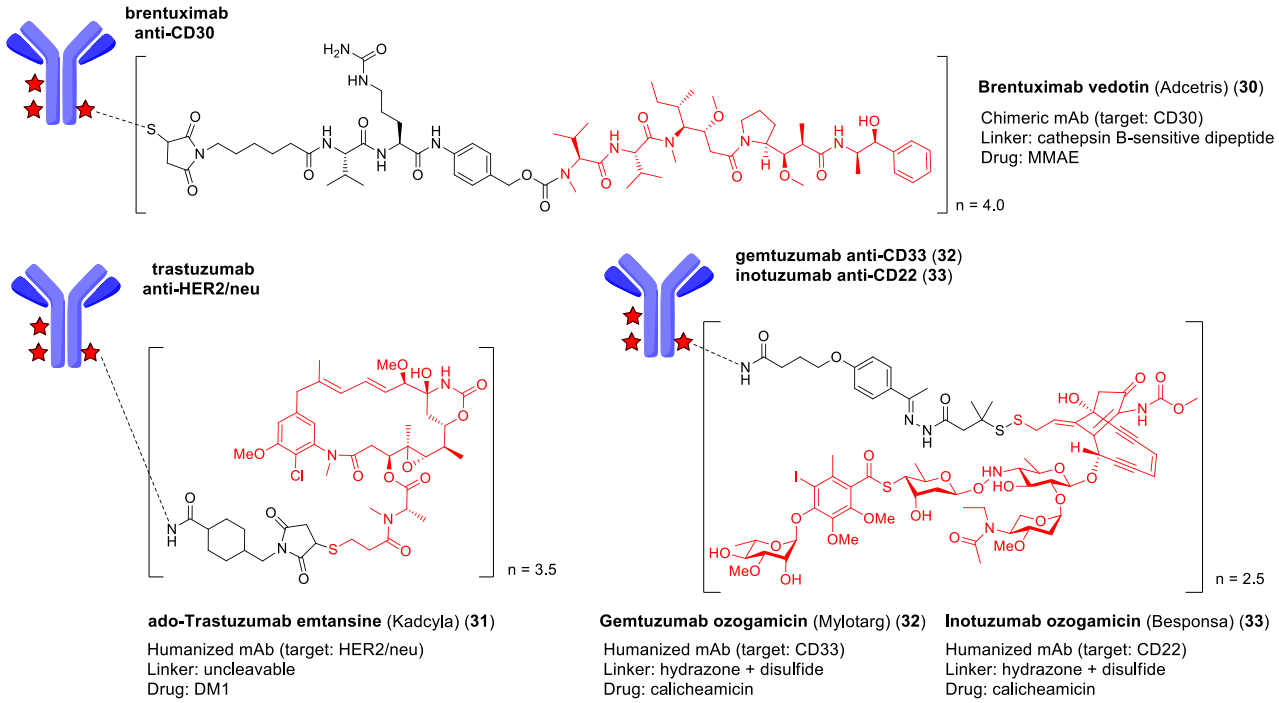

Figure 8. Molecular structures and mAb/linker/drug system of ADCs that were, so far, approved for cancer therapy. DM1: mertansine (i.e. a thiol-bearing maytansinoid); MMAE: monomethyl auristatin E.[45]

1.3.5. Drawbacks of Antibodies

As already mentioned, mAbs have been chosen as selective targeted delivery vehicles of cytotoxic agents, due to their strong binding affinity properties and accumulation at the tumor site in patients. Although ADCs show a variety of benefits over traditional anticancer

approaches, the *in vivo* pharmacodelivery of the cytotoxic agent by an antibody is limited by a number of factors:[47]

- the large size of antibodies delays the ADC extravasation and the diffusion into the tissues. Moreover, only a little fraction of the conjugates penetrates into the tumor mass, being immediately trapped by antigens located on perivascular tumor cells (i.e. the so-called antigen barrier effect). This particular feature may prevent the drug to reach all cells in the tumor mass; to circumvent this limitation, smaller formats of ADCs (SIP, diabody etc.) have been proposed, but this approach is currently being investigated only at the preclinical level.
- As mentioned above, the ADC efficacy can be substantially affected by the occurrence of anti-mAb immune response, not only depending on the type (i.e. chimeric, humanized or fully humanized) but also on the format (i.e. diabody, miniantibody or small immune proteins) of the mAb structure.
- From the manufactory point of view, the large-scale assembly of ADCs is an expensive process, requiring providers to simultaneously handle biologic materials in sterile conditions and manipulate highly potent cytotoxic compounds. As a result, the high manufacturing costs limit the clinical evaluation of new ADCs and, importantly, they impact dramatically on the final costs of the treatment.

  Considering these drawbacks of the ADC technology, the development of other active targeting devices, is now gaining high interest among the pharmaceutical industry.

1.4. Small Molecule-Drug Conjugates (SMDCs)

1.4.1. Why SMDCs? – an overview

The development of low-molecular-weight compounds (i.e. small organic ligands) may represent an alternative to antibodies for pharmacodelivery applications.[47] However, while it is now possible to develop antibodies against virtually any protein antigen, the development of potent small molecular binders is not a general process and so far only few ligands have been investigated for drug delivery purposes.[48] Small molecule-drug conjugates (SMDCs) that bind with high affinity to tumor-overexpressed receptors are now designed to rapidly extravasate, accumulate in the tumor mass homogeneously, without being immunogenic.[48] Moreover, in case of absence of good binding (e.g. recognition of extracellular matrix proteins or membrane antigens) lower molecular weight compounds quickly diffuse back to blood stream for excretion.[48] Furthermore, due to their synthetic accessibility, the large-scale production of SMDCs is more sustainable at the industrial level.[48]

Similarly to ADCs, the mechanism of drug release for SMDCs depends on the targeted receptor (Figure 9).[17] Usually, most of the SMDCs are internalized into the cell through receptor-mediated endocytosis. The drug is then released upon linker cleavage by specific mechanisms in intracellular compartments. By contrast, in the case of SMDCs bearing a linker which can be cleaved in the extracellular milieu, the cytotoxic drug can be released in the tumor microenvironment and it can then penetrate the cancer cell by passive diffusion.[49,50]

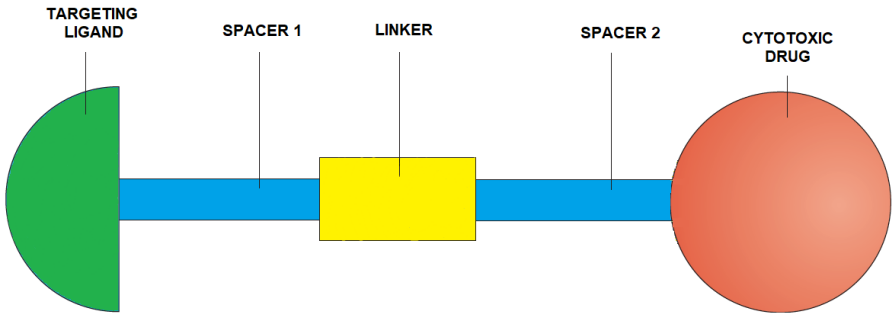

Figure 9. General structure of small molecule-drug conjugates (SMDCs). Ligand (green) for targeting, Spacer 1 and Spacer 2 (blue), to modify the conjugate's physicochemical properties (e.g. solubility) or to improve the kinetic of drug release, linker (yellow) to achieve intra or extracellular cytotoxic drug release, and drug (red) to get therapeutic effect after release. Adapted from [49]

Ideally, the cytotoxic payload should be stably connected to the targeting moiety while the SMDC is in circulation. On the contrary, the drug should be efficiently released at the tumor site in its unmodified form.

1.4.2. Linkers and Spacers

The nature of the linker shows direct impact on the efficacy and stability of the SMDC construct. Several parameters, such as type of connection bond on the targeting ligand (e.g. ester, carbonate, carbamate, oxime), polarity, hydrophobicity and drug release mechanisms, may contribute to the SMDC performance.[17,51] Depending on the chemical bonds lability on the linker structure, linkers can be divided into two categories: cleavable and uncleavable. The latter rely on the complete stability of the whole conjugate, being usually exploited for diagnosis purposes (i.e. connection of fluorophores to the targeting ligand). On the other hand, environmental factors such as the acidic or reductive conditions of cytoplasm and extracellular matrix or the presence of specific enzymes in lysosomes are some of the exploited intra- and extracellular promoters of drug release from cleavable linkers.[50,52]

Regarding that, a variety of chemical structures have been used as linkers to release the drug under different conditions at the tumor site:

- **Reductively cleavable linkers**: the high intracellular concentration of reduced glutathione (~2-10 mM) and other reductants (e.g. cysteine, thioredoxin, peroxiredoxins, and nicotinamide adenine dinucleotides) in cancer cells inspired the development of delivery systems containing reducible moieties, such as disulfide linkers. The drug release from disulfide bonds mainly occurs in the cytoplasm upon endocytosis, through disulfide exchange reactions with glutathione and other cysteine-containing proteins. However, it has been claimed that the high reducible environment at the tumor stroma can cleave the disulfide bond extracellularly and the drug can be taken up, passively, by the cancer cell. Upon S-S bond cleavage, the resulting reduced thiol group triggers the drug release through a cyclization onto electrophilic functional groups (e.g. carbonates and carbamates, Scheme 1).[17,52]

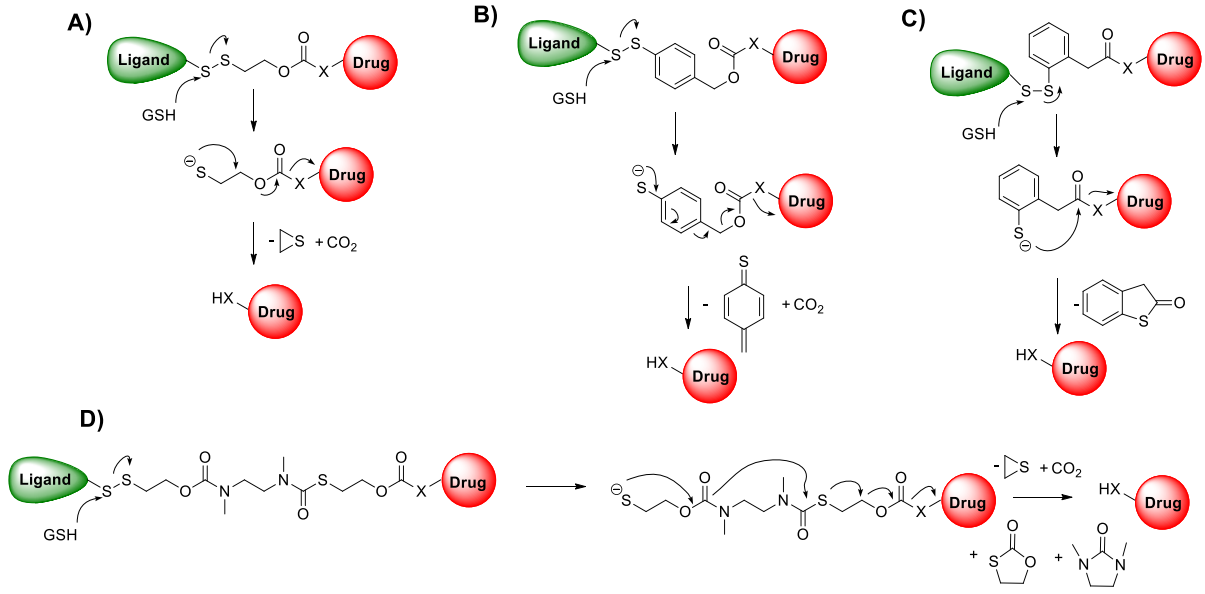

Scheme 1. Drug release mechanism of SMDCs bearing reductively cleavable linkers. After cleavage by glutathione, the free drug is released leading to the formation of different byproducts: A) thiirane; B) thioquinone methide; C) thiolactone; D) thiirane, 1,3-oxathiolan-2-one, and 1,3-dimethyl-2-imidazolidinone. GSH = glutathione; X=NH or O.[52]

- **Acid-labile linkers**: the receptor-mediated endocytic process is known to proceed through a progressive acidification of the intracellular compartments (i.e. pH 4.5-5.0 in lysosomes and 5.0-6.5 in endosomes). Moreover, tumors are often characterized by a remarkable acidity of their extracellular milieu, as a result of the high metabolic rates of aggressive tumors. Therefore, linkers that are rapidly hydrolyzed under acidic conditions can be exploited for delivery of anticancer drugs. An example, in addition to esters, is the acidic hydrolysis of the *para*-alkoxybenzylidene methoxy (Scheme 2A), where the electron-donating effect of the *para*-alkoxy functional group in the aromatic ring gives increasing stability to a *para*-alkoxybenzylonium cation, facilitating the cleavage and consecutive drug release. Hydrazones are also acid-labile linkers, especially when connected by direct

coupling of a carbonyl-containing drug to hydrazide linker. This approach relies on the linker hydrolysis within the endosomes (Scheme 2B), but the poor stability of such linker avoids significant drug accumulation at the tumor site and negligible release of the payload into the blood stream.[17,52]

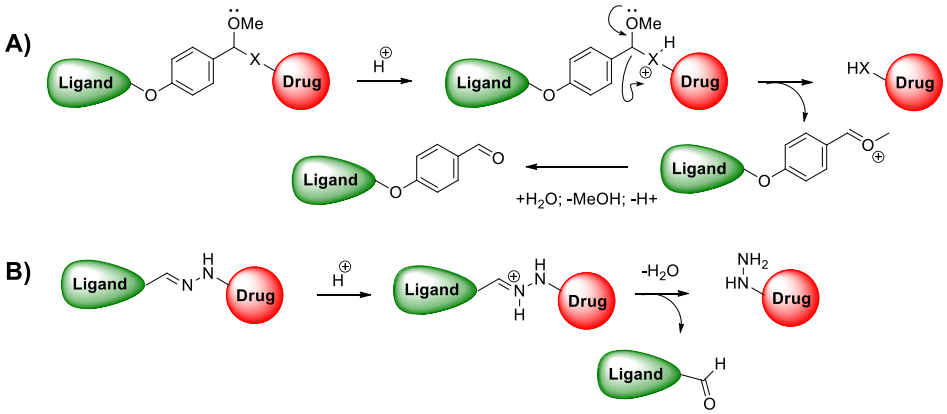

Scheme 2. Examples of drug release mechanism, upon hydrolysis, of SMDCs bearing acid-labile linkers. A) *para*-alkoxybenzylidene acetal; B) hydrazones; X=NH or O.[52]

- **Enzyme-cleavable linkers**: the abundance of hydrolytic enzymes inside cancer cells and within the tumor stroma differs from their presence in the blood stream. As a consequence, linkers composed by specific peptide sequences or sugar moieties can be selectively recognized and cleaved by a variety of enzymes (i.e. proteases or glycosidases). Depending on the location of these effectors, the linker cleavage can take place at different sites of the cancer cell (e.g. tumor stroma, cell membrane, lysosomes and endosomes). Being composed by peptide bonds, enzymatically labile linkers show high stability under different pH conditions. In these drug-delivery systems, a self-immolative spacer is often present to decrease the steric hindrance around the peptide sequence, thus allowing a more efficient enzymatic action. The proteolytic cleavage generates a nucleophilic functional groups (e.g. hydroxy, amino, or thiol groups) which reacts intramolecularly through different mechanisms (mainly cyclization and electronic cascade over conjugated double bonds), releasing the free drug (see Scheme 3).[52]
- **Uncleavable linkers:** unlike uncleavable linkers in ADCs (where the mAb structure is proteolytically degraded inside the cell, eventually releasing the cytotoxic agent), uncleavable linkers in SMDCs are generally stable both in circulation and inside the cell (i.e. blood stream and tumor site). The typical functional groups used for these linkers are triazoles, carbamates, and amides. Due to this high stability, these bonds are typically not indicated for drug delivery purpose, whereas they can be used for diagnosis, conjugating a fluorophore to the targeting ligand (i.e. SMDCs for cancer diagnosis).[52]

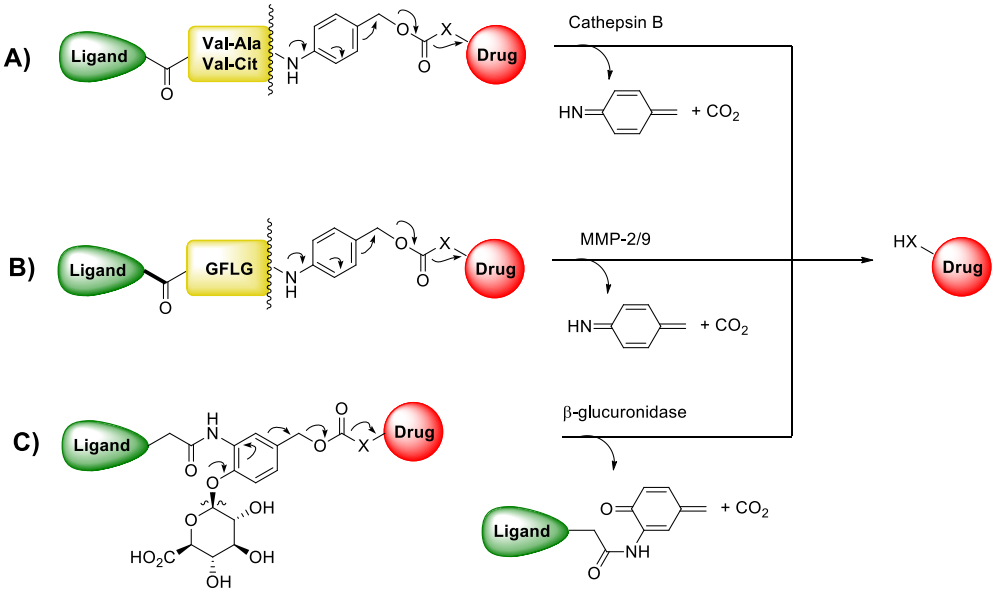

Scheme 3. Examples of enzyme-cleavable linkers bearing a self-immolative spacer. The cleavage by different located enzymes (intracellular for cathepsin B, extracellular for MMP-2/9 and intra/extracellular for β-glucuronidase) gives rise to liberation of the free drug after 1,6-elimination of the *p*-amino or *p*-hydroxy benzoxycarbonyl spacers. X= O or NH.[17]

The choice of the linker is normally dependent on the target protein and its biological features (e.g. location in the tumor mass, internalization pathway etc.), as intra- or extracellular processes contribute to the fully active drug release.[50,52]

From the structural point of view, the linker moiety is often functionalized at both sides with different kinds of spacers (see Figure 9). As mentioned above, self-immolative spacers between linker and payload (spacer 2, Figure 9) are important to release the drug in the active form upon linker cleavage (e.g. most common in literature is the 1,6-elimination of the *para*-amino benzoxycarbonyl spacers, Scheme 3). Many other self-immolative spacers are reported in literature, considering different connection bonds (e.g. 1,8-elimination concerning chromanone rings and 1,4-elimination concerning phenyl rings). Moreover, additional chemical structures between linker and ligand are often included for different reasons.

For instance, as linkers and cytotoxic agents are usually highly lipophilic, the spacer between the cleavable linker and targeting ligand is often included to improve the solubility in aqueous media of the entire SMDC (e.g. through the use of PEG chains or short peptide sequences bearing hydrophilic residues - spacer 1, Figure 9).[52] In some cases, the spacer minimizes possible steric hindrance from the cytotoxic drug that can interfere with the ligand affinity for its receptor. Moreover, modifications of the spacer structure have been used to modulate the pharmacokinetic properties of the SMDC, as well as to allow multipresentation of ligands and drug moieties.[53]

It is now established that cancer cells express specific receptors on their surface which are present in a higher number of copies compared to healthy cells. In the case of SMDCs, a

variety of antigens have been investigated as targeted receptors: among all, some of the most studied targeted receptors will be described in the following sections [e.g. folate receptor (FR), prostate-specific membrane antigen (PSMA), somatostatin receptor (SSTR), carbonic anhydrase IX and integrin receptor]. Moreover, other receptors have been also described [e.g. cholecystokin receptor (CCKR), sigma-2 receptor, tropomyosin receptor kinase (Trk), hormones receptors (androgen, estrogen and progesterone), biotin receptor, CD13 receptor] but they will not be debated here in detail.[56]

1.4.3. SMDCs Targeting Folate Receptors (FRs)

Among all vitamin receptors, FRs are the most studied as cancer biomarkers. Vitamins are required for the survival of all living cells, and especially tumor cells require them in large quantities to sustain fast growth.[54] Folic acid is a crucial dietary factor that is converted by enzymatic reduction to a series of tetrahydrofolate (FH_4) cofactors, providing methyl groups for the synthesis of DNA precursors (e.g. thymines and purines) and RNA (e.g. purines). Due to the importance of folic acid for fast-growing cells, FR is overexpressed on the surface of different cancer cells.[55] For this reason, folic acid (folate, Figure 10 in green) is considered the first small molecule to be used as ligand in SMDCs and the research activity done on folate-drug conjugates represents a milestone in the development of tumor-targeting cytotoxic agents. Impressive work by Philip Low and co-workers at Endocyte, has been done in the applications of folate conjugates for tumor targeting.[56] The most studied SMDCs from Endocyte are EC145 (vintafolide, Vynfinit™ compound **34**, Figure 10) and the analog, peptidoglycan-based, EC0489 (compound **35**, Figure 10). Both compounds are known to enter the cell by FR-mediated endocytosis and, during this internalization pathway, the compounds are carried to the endosome.[52] From the structural point of view, both compounds are folate-desacetylvinblastine hydrazide (DAVBH) conjugates, bearing a disulfide linker and hydrophilic spacers. EC145 showed considerable efficacy in preclinical mouse models and it is now being evaluated in Phase II clinical trials for solid tumors (i.e. ovarian, neck and colorectal). However, the clinical reports of EC145 highlighted side effects such as fatigue and constipation ascribable to the hepatic clearance and metabolism of the conjugate, which leads to the release of free drug (i.e. vinca alkaloid) to gastrointestinal organs. Subsequently, EC0489 (**35**), containing a peptidoglycan-based spacer was developed to reduce hepatic clearance and metabolism. Here, the hydrophilic spacer that connects the drug to the folate (Figure 10) was found to allow better affinity for the receptor (i.e. without any further data, authors stated that a rigid hydrophilic spacer might avoid the decrease of affinity) which prevents unspecific uptake by healthy cells. This conjugate is now undergoing Phase I clinical trials.[52] Other drugs have been conjugated to folate ligand by Endocyte, as cryptophycin, through a carbonate bond.

Compound **36** (Figure 10) displayed cell cytotoxicity *in vitro* at low nanomolar concentrations, while data of *in vivo* antitumor activity are currently not available.[57]

Besides FRs, other vitamin-targeted receptors have been explored.[54] For example, the conjugation of potent drugs to biotin has been investigated, due to the overexpression of biotin receptors (BR) in tumor cells.[58]

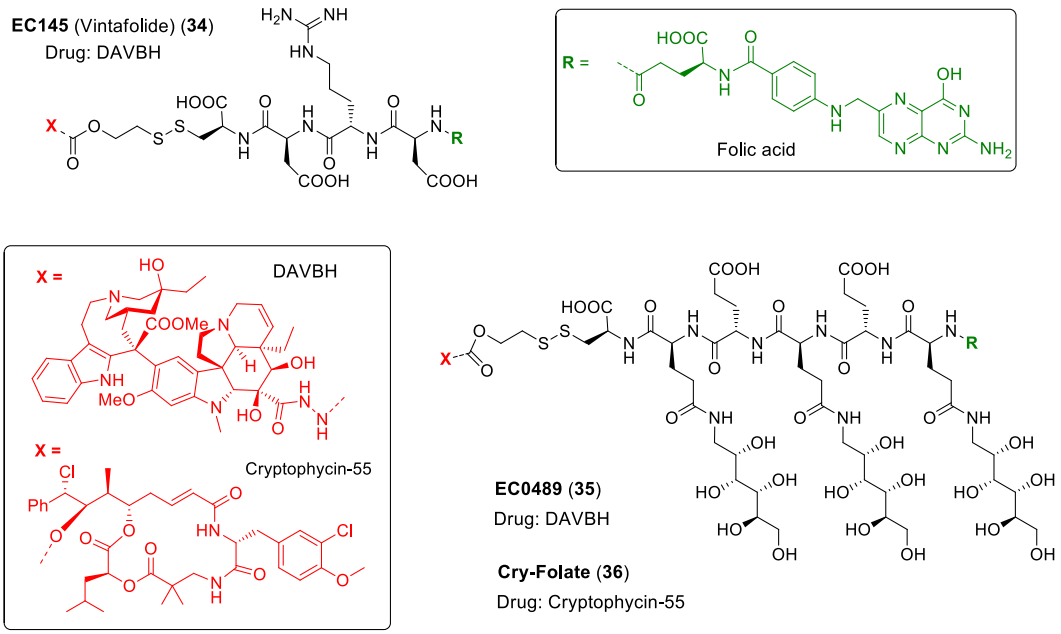

Figure 10. Molecular structures of three examples of FR-targeted SMDCs.

1.4.4. SMDCs Targeting Prostate-Specific Membrane Antigen (PSMA)

PSMA (also known as folate hydrolase I or glutamate carboxypeptidase II) is a plasma membrane protein, and it is the second most upregulated protein in prostate cancer (PCa).[59] This antigen represents an ideal cell surface protein for tumor-specific targeting. In addition to its expression on both prostate cancer cells and on the neovascular tissue of other solid tumors, PSMA is present at low concentrations in healthy tissues. Physiologically, this transmembrane glycoprotein cleaves glutamate residues from biological substrates (e.g. *N*-acetylaspartyl glutamate) and, upon ligand binding, this cell-surface receptor undergoes endocytosis through clathrin-coated pits, recycling then to the cell surface.[60]

Also in this case, Endocyte has been doing considerable efforts in PSMA-targeting SMDCs field. A variety of analogs of *N*-acetylaspartyl glutamate have been prepared and linked to cytotoxic agents or radioisotopes. For example, in EC0652 (compound **37**, Figure 11) the ligand 2-[3-(1,3-dicarboxypropyl)ureido]pentanedioic acid (DUPA, Fig. 11) was conjugated to the radioisotope technetium Tc-99m (^{99m}Tc), that can potentially be used as a radio-imaging agent for PSMA-overexpressing tumor cells. After cell uptake and SPECT (i.e. single-photon emission computed tomography) imaging, PSMA-positive tumor cells can be observed and identified. Furthermore, PSMA-overexpression has been correlated to the targeting skills and

the efficacy of certain PSMA-targeting cytotoxic agents. Compound **37** showed remarkable tumor accumulation in seven patients without reported toxicities, being now in phase I/II trials with a larger number of patients.[56] Another example of successful radioligand is ^{177}Lu-PSMA-617 (compound **38**, Figure 11) developed by Endocyte and now in Phase III clinical trials.[61] The DUPA ligand in ^{177}Lu-PSMA-617, is chemically attached to a therapeutic radioactive isotope called Lutetium-177 (^{177}Lu), which releases an energetically active β- particle as a cytotoxic radiation at the site of disease (i.e. PSMA-positive cells). DUPA ligand was also conjugated to a potent antimitotic agent tubulysin hydrazide through a disulfide linker (EC1169, compound **39**). Treatment of compound **39** in a *in vivo* model (i.e. nude mice bearing subcutaneous LNCaP tumor) showed regression in all treated animals, with 2/7 achieving complete tumor eradication (i.e. no tumor regrowth until 90 days), with no apparent toxicities. Compound **39** is now being evaluated in phase I clinical trials.[56]

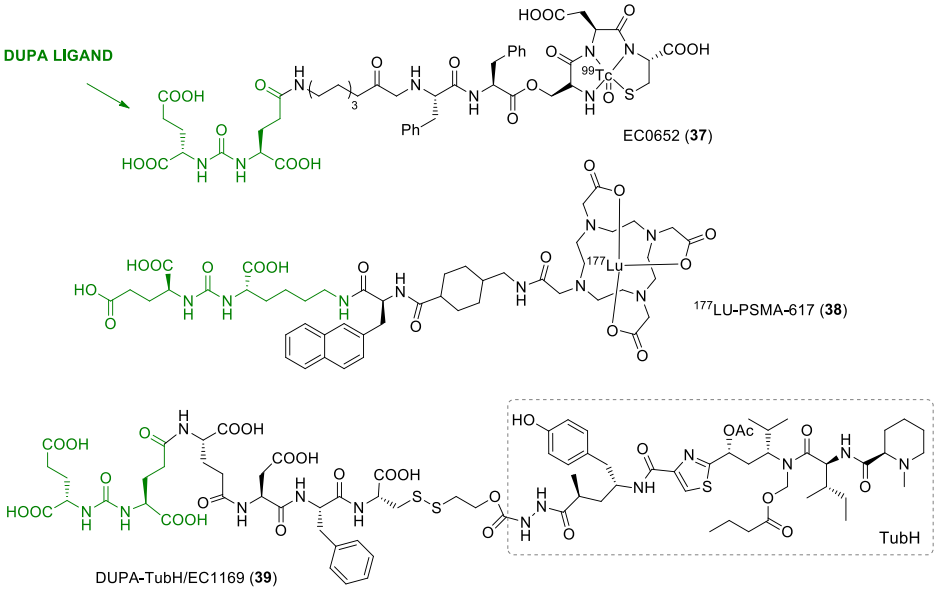

Figure 11. Molecular structures of three examples of PSMA-targeted SMDCs. DUPA ligand is represented in green.

1.4.5. SMDCs Targeting Somatostatin Receptors (SSTRs)

Specific hormone receptors are considered suitable targets for anticancer therapy, due to their high expression in different cancer cells. Among different hormone receptors (e.g. gonadotropin-releasing hormone or GnRH, steroid hormones, etc.), hormone somatostatin receptors (SSTRs, in particular subtypes 2, 3 and 5) are widely expressed in cancer cells, in particular in neuroendocrine tumors.[62] The most studied subtypes are SSTR2 and SSTR5. In particular, synthetic cyclic peptides such as octreotide and seglitide have been developed as somatostatin analogs. These compounds are particularly selective for SSTR2, rather than SSTR5 (14-fold and 130-fold higher affinity for SSTR2 isolated receptor, respectively).[63] Interestingly, a correlation was observed between somatostatin and its analogs to bind to the

SSTR2 subtype and its capability to constrain angiogenesis (i.e. the growth of new ramified blood vessels, which is significantly faster in aggressive and metastatic tumors).[63] For instance, somatostatin analog octreotide has been coupled through a labile ester bond at the 2'-O position of paclitaxel (PTX, **20**, Fig. 2), showing considerable antitumor efficacy in mouse models, with potent inhibition of tumor growth and lower systemic toxicity compared to PTX alone.[64,65,66]

Moreover, ligands consisting of octreotide analogs have been also used to improve the anticancer efficacy of octreotide-DM1 SMDC, through a disulfide cleavable linker, against SSTR2-expressing tumor model (Fig. 12). A recent work from Tarveda Therapeutics showed the significant *in vivo* antitumor efficacy of compound **40** (Figure 12) in several SSTR2-positive lung xenograft models with. Antitumor activity was superior to that observed with standard of cytotoxic agents, cisplatin/etoposide. Remarkably, compound **40** showed no antitumor effect in a SSTR2-negative xenograft model.[67]

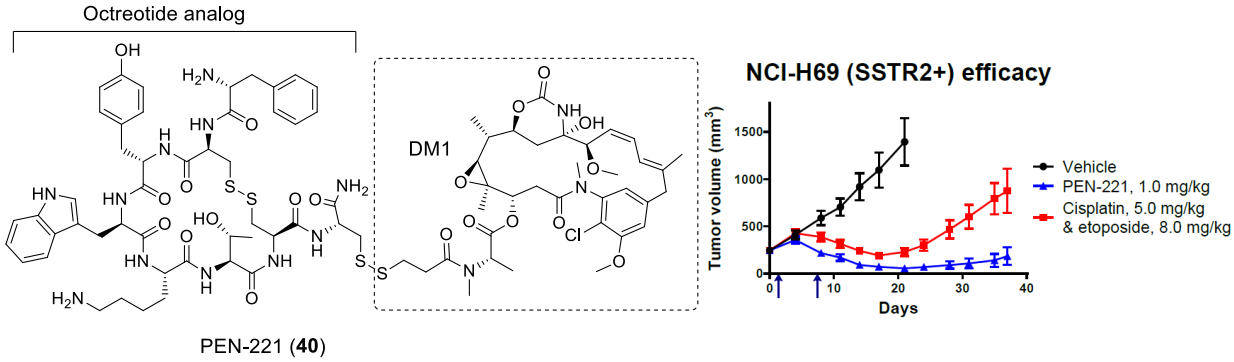

Figure 12. Molecular structure of PEN-221 conjugate (**40**) developed by Tarveda Therapeutics and effect on the growth of small cell lung cancer NCI-H69 xenograft model in comparison with standard cytotoxic agents.[67]

1.4.6. SMDCs Targeting Carbonic Anhydrases (CA)

Carbonic anhydrase is described as a zinc metalloprotein located in cervical cancer cells. This metalloenzyme catalyzes the reversible hydration of carbon dioxide to hydrogen carbonate and H^+ ($CO_2 + H_2O \leftrightarrow H^+ + HCO_3^-$), being responsible by physiological pH homeostasis. In humans, this enzyme is expressed in 16 known isoforms varying their catalytic activities, cellular localizations, and vulnerability to different inhibitors. Among these isoforms, carbonic anhydrase IX (CAIX) is considered an excellent tumor antigen, being overexpressed in different cancer types (e.g. glioblastoma, colorectal and breast cancer) as a marker of hypoxia.[68]

Due to its high and localized expression, a group of highly specific SMDCs based on CAIX ligands has been developed. Although it is now clear that CAIX-targeting ligands do not enter the cell through receptor-mediated endocytosis, different CAIX-targeted SMDCs have been developed, and their antitumor properties were evaluated *in vivo*.[69] Over the past decade,

Neri and co-workers, have synthesized several SMDCs bearing a CAIX inhibitor acetalozamide (AAZ, Figure 13 in green). A first fluorescent conjugate carrying the AAZ CAIX-targeting ligand, allowed the confirmation of the high affinity of AAZ ligand, which showed nanomolar K_d values (K_d = 12.6 nM) for the receptor, while exhibiting good tumor accumulation *in vivo*, 1 hour post-administration (the tumor accumulation was 22-fold higher than the negative control ligand confirming the selectivity of the ligand).[69] The development of SMDC compounds based on AAZ ligand showed that the combination of a disulfide linker and duocarmycin drug led to modest tumor volume inhibition. On the contrary, the use of a maytansinoid payload (in compound **41**, Fig. 13) resulted in a potent antitumor effect.[69]

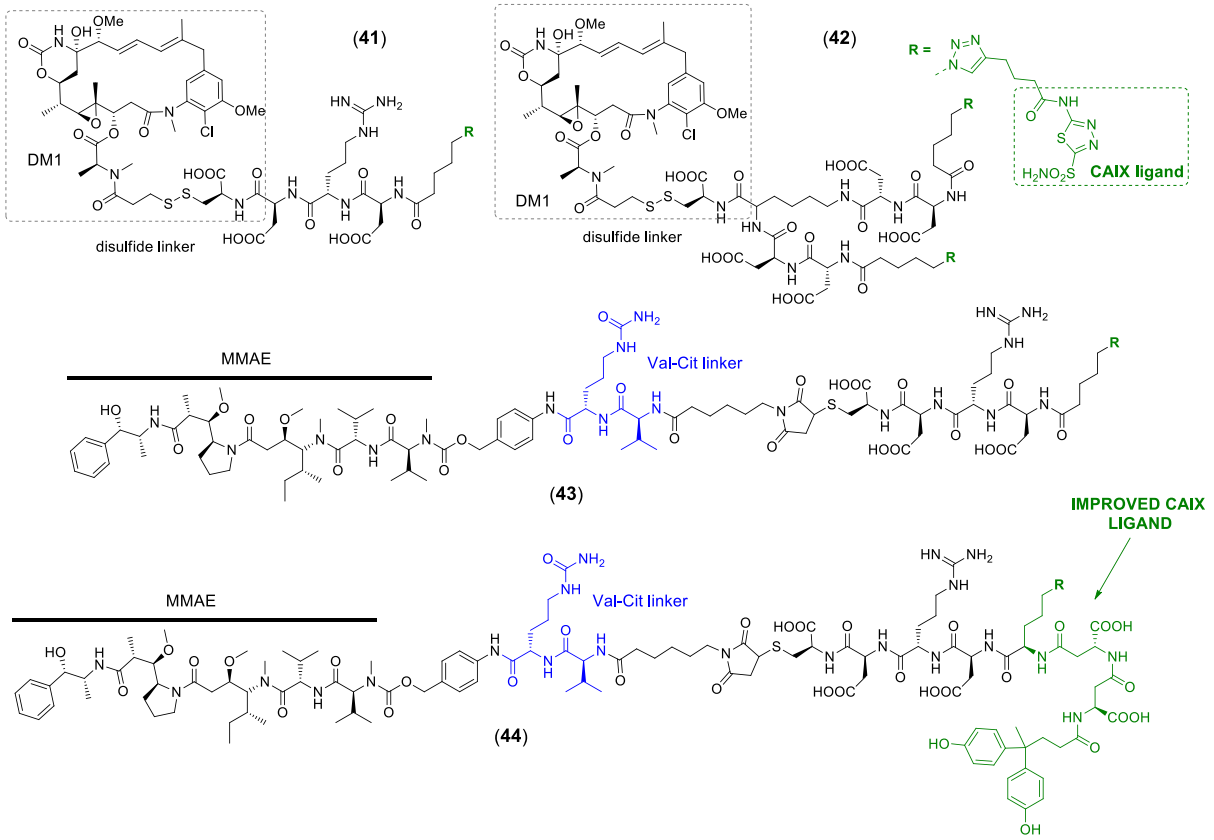

Figure 13. Molecular structures of SMDCs bearing CAIX as targeting ligand (**41**-**44**), developed by Neri and co-workers. CAIX ligands are represented in green. Compounds **41**-**42** have DM1 as payload, while compounds **43**-**44** show MMAE (**29**) as payload. Disulfide linkers are represented in compounds **41**-**42** and lysosomally-cleavable linkers for **43**-**44**.

In the same frame, a bivalent AAZ-(DM-1) SMDC **42** (Fig. 13) illustrated how the increased ligand avidity can lead to substantial modification of the SMDC performances [displayed better results when compared with SMDC **41**]: In particular, the dimeric ligand showed 1) high affinity with no apparent dissociation from CAIX coated surface (binding affinity measured with Surface Plasmon Resonance – SPR); 2) approximately 3-fold higher tumor accumulation than SMDC **41**; and 3) longer tumor residence (24 hours after administration, bivalent **42** showed 40% total fluorescence signal when compared with 14% of monovalent **41**). Moreover, SMDC **42** showed better antitumor activity *in vivo* than monomeric **41**, which is the result of the

improved and extended tumor accumulation.[70] More recently, the same group, showed that variations of the linker moiety (i.e. introduction of cathepsin-B cleavable linker Valine-Citruline compound **43**, Fig. 13) and of the cytotoxic agents (i.e. MMAE and PNU-159682) can improve the antitumor activity, leading in some situations to complete cancer eradication in the case of conjugate bearing MMAE as payload.[71] Remarkably, with the use of a non-internalizing ligand and intracellularly cleavable linker, the authors observed *in vivo* therapeutic efficacy.[71] Neri and co-workers claim that cathepsin B, which is originally an intracellular enzyme, might be secreted to the extracellular environment by dying cells but also by tumor cells, initiating extracellularly proteolytic cascades to help tumor growth.[71,72] Against the widely-accepted assumption that internalization is a strict requirement for the conjugate efficiency, these data indicate that the delivery of cytotoxic agents to the tumor extracellular environment is also a promising strategy to achieve anticancer efficacy.[71] The ligand fragment of these compounds has been recently improved through an innovative affinity-maturation experiment, performed through development and screening of DNA-encoded chemical library technologies (DNA-ECL).[73,74] A new CAIX ligand was achieved from DNA-ECL allowing the development of a new SMDC **44**, displaying a K_d = 10 nM by SPR.[75] In terms of therapeutic efficacy, SMDC **44** showed no substantial improvement of the anticancer activity exhibited by compound **43**, with the authors claiming that the release of the drug might be too slow (i.e. a more labile linker could rise the rate of tumor cell killing to show more therapeutic efficacy).[75]

1.5. Integrin $\alpha_v\beta_3$ as Tumor Target Receptor

Another group of receptors that have been largely studied in cancer therapy are integrins. These proteins are a family of heterodimeric membrane glycoproteins formed by non-covalently associated α- and β- subunits (Fig. 14).[76] This large group is composed by 18 α and 10 β subunits that can assemble leading to 24 identified heterodimers (Fig. 14), giving the possibility to act in crucial biochemical processes of the cell biology (i.e. cell replication, survival, migration, and intracellular signal transduction).[76,77] For example, it has been described that immunoglobulins and cytokines interact with integrin receptors and trigger signaling pathways by activating receptor tyrosine kinases (i.e. well-known receptor overexpressed in different types of cancer).[78] Particularly, each subunit is featured by: 1) an

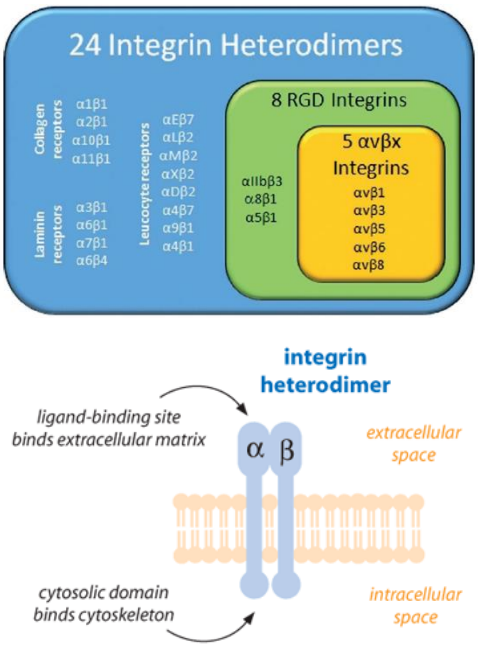

Figure 14. up) The integrin family; down) Schematic representation of the two integrin subunits. Adapted from[76]

extracellular domain; 2) a single transmembrane domain; and 3) a cytoplasmic region (Figure 14).[77] As main function, integrins mediate cell-cell and cell-extracellular matrix (ECM) adhesion, playing key roles in the cytoskeleton organization during cell adhesion and migration.[79] Indeed, the name “integrin” was given to designate the role of such protein as an integral membrane complex involved in the transmembrane association between the extracellular matrix and the inner part of the cell.[79] This kind of proteins are also responsible for the regulation of many biochemical processes at the cellular level which happen during the formation and in the progression of several diseases (e.g. prostate carcinoma, breast cancer, pancreatic tumor and glioblastoma).[78] It has been reported that tumor cells enhance the expression of specific integrins, stimulating their proliferation, invasion and survival.[78]

Among these integrins, $\alpha_v\beta_3$ is strongly involved in the regulation of angiogenesis. Particularly, the quantity of integrin $\alpha_v\beta_3$ in tumor neovasculature is often higher with respect to healthy tissues, resulting in a continuous stimulation of angiogenesis.[80] The role of integrin $\alpha_v\beta_3$ is not only important in natural biochemical processes (e.g. wound healing, tissues remodeling, embryogenesis, and female reproductive cycle), but also for growth and survival of tumors. As a matter of fact, $\alpha_v\beta_3$ integrin is not only overexpressed in angiogenic endothelial cells, but it is also upregulated in several tumors (e.g. glioblastoma, pancreatic, breast, prostate and cervical carcinoma, and melanoma).[80] Besides, $\alpha_v\beta_3$ is involved in ECM remodeling and degradation, which are crucial processes for tumor invasion and metastasis. For example, $\alpha_v\beta_3$ integrin is able to recruit and activate specific extracellular proteases [i.e. metalloproteinase-2 (MMP-2) and plasmin] which degrade different components of the extracellular and interstitial matrixes (i.e. angiogenesis event arises from interaction between $\alpha_v\beta_3$ and MMP-2, which destroys the collagen matrix) thus promoting the migration of cancer cells.[80]

1.5.1 RGD Integrin Ligands

Endogenous proteins (e.g. fibrinogen, vitronectin, plasminogen) presenting the tripeptide sequence arginine-glycine-aspartic acid (Arg-Gly-Asp, or RGD) can interact with different integrin receptors (e.g. $\alpha_v\beta_3$, $\alpha_v\beta_5$, $\alpha_5\beta_1$), which have been associated to cancer development, metastasis and tumor angiogenesis.[81] For instance, Rouslahti and co-workers described that the cell-adhesion ability of fibronectin is mediated by the RGD peptide sequence (Fig. 15), included in one of the protein domains.[82,83]

For this reason, different research groups designed and synthesized a variety of peptides and peptidomimetics displaying the RGD recognition motif (see Figure 15) to target and bind these specific integrins and, among all, some were found to bind integrin $\alpha_v\beta_3$ with high affinity.[81]

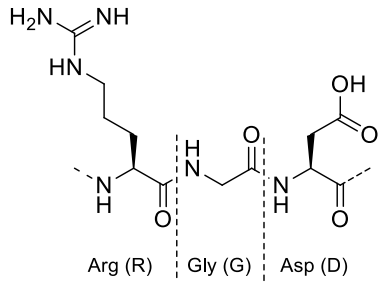

Figure 15. The RGD recognition motif.

So far, several strategies were implemented to exhibit the RGD recognition motif in a stable conformation. Indeed, it was reported that the constrain of the RGD sequence in small cyclic structures leads to high-affinity ligands, showing low conformational flexibility (i.e. flexibility of flanking residues is limited).[84] Numerous RGD-based binders are described in literature. Among them, Kessler's research group was pioneer in developing the potent integrin ligand Cilengitide (**45**, Fig. 16).[85,86] The structural rationale for the observed high ligand-receptor affinity was provided by Xiong and co-workers, which reported X-ray analysis of the structure of integrin $\alpha_v\beta_3$ co-crystalized with Cilengitide.[87] The latter study was able to describe an extended conformation of the RGD sequence in the binding pocket, characterized by a crucial 9-Å distance between C-β atoms of the Arg and Asp residues: this essential interaction relies on the establishment of two bridge salts, where the first is located between the arginine side chain and negatively charged residues in the α subunit, and the other involving the β-carboxylate moiety of aspartic and the Mn^{2+} divalent metal cation of the metal ion-dependent adhesion site (MIDAS) region in the β subunit (Figure 16).[88]

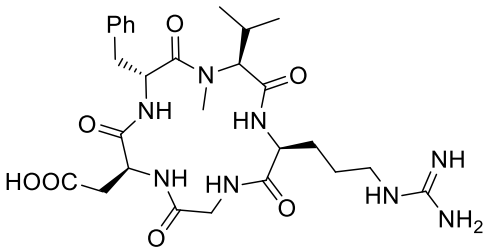

Cilengitide (**45**)
Kessler and co-workers
IC_{50} $\alpha_v\beta_3$ = 0.61 nM
IC_{50} $\alpha_v\beta_5$ = 8.4 nM

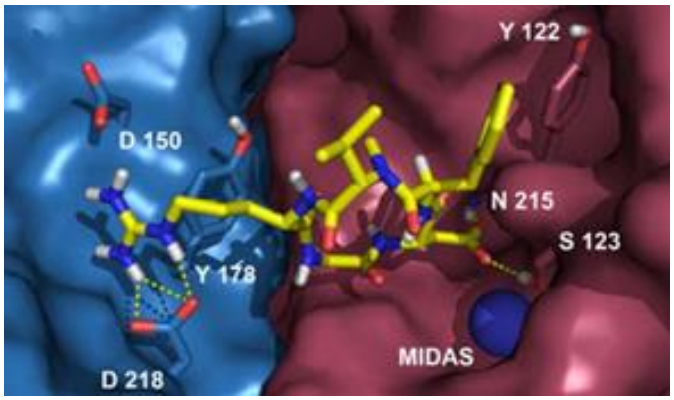

Figure 16. The potent integrin ligand Cilengitide showing selectivity for $\alpha_v\beta_3$ over $\alpha_v\beta_5$ integrin receptors and Cilengitide bound to $\alpha_v\beta_3$. IC_{50} values from[89] and figure adapted from[88]

Due to its high binding affinity to $\alpha_v\beta_3$ integrin receptor, Cilengitide was first developed as antiangiogenic molecule, thus being directly used as anticancer drug. Cilengitide reached clinical trials and, although it was found to be well tolerated in patients, its anti-angiogenic activity has been debated. By contrast, after the initially reported results, in specific

experimental conditions, Cilengitide was shown to act as an angiogenesis agonist, which caused the interruption of the clinical evaluation.[76,81,88]

However, the significant work on the structural information and interaction between Cilengitide and $\alpha_v\beta_3$ integrin led to the development of cyclic RGD peptidomimetic and semi-peptidic ligands towards $\alpha_v\beta_3$ integrin. Some examples are shown in Figure 17, where the common feature of ligands **46**-**51** is the presence of the RGD tripeptide sequence within a cyclic structure, to limit the flexibility of the structure backbone.

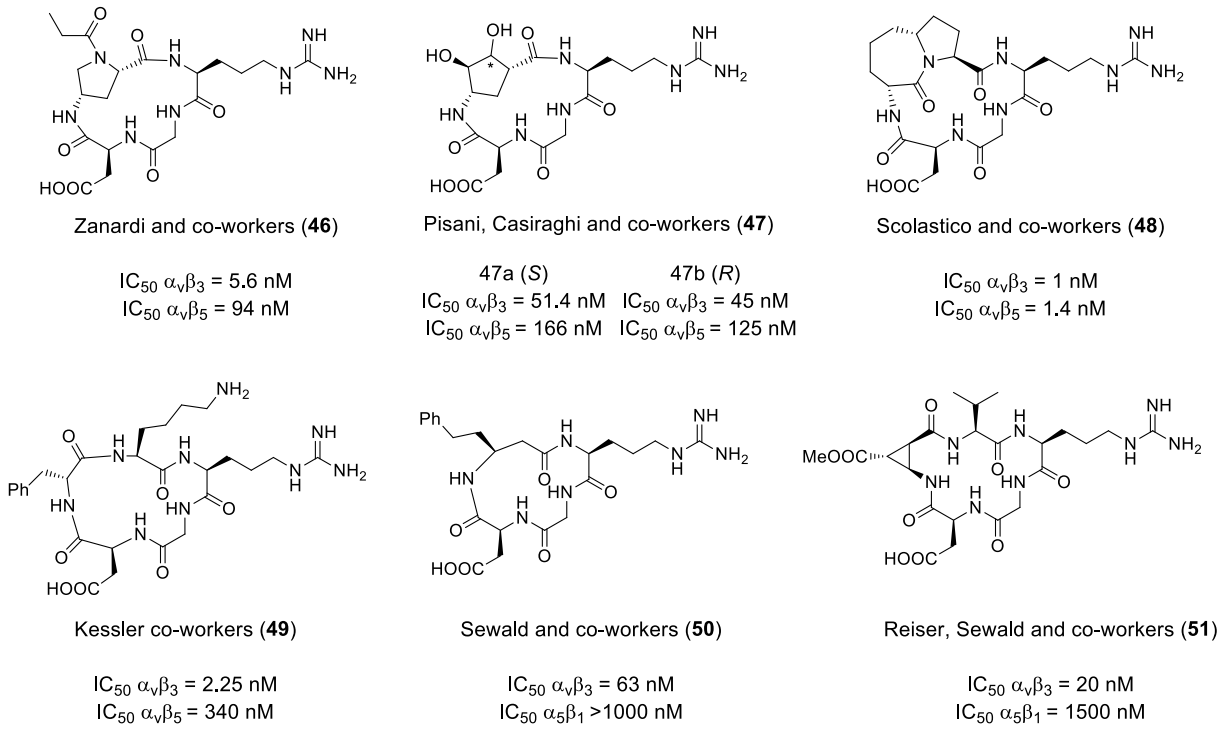

Figure 17. Selected examples of integrin ligands (**46**-**51**) and relative integrin affinity, expressed as IC_{50} value. The IC_{50} values were taken from literature: for compound **46**,[90] **47**,[91] **48**,[92] **49**,[89] **50**,[81] and **51**[81].

Even after the clinical failure of Cilengitide, several $\alpha_v\beta_3$- and $\alpha_v\beta_5$-targeting ligands were able to enter clinical trials as well, due to their potent activity against tumor angiogenesis (i.e. this approach in cancer therapy was not successful).[93] Besides the use of $\alpha_v\beta_3$ integrin ligands as anti-angiogenic agents a different strategy arose, consisting in their use as tumor targeting agents. Due to the ability of these compounds to recognize overexpressed $\alpha_v\beta_3$ integrins on the membrane of tumor cells, different RGD-based small molecules have been used as carriers to deliver selectively: nanoparticles,[94] liposomes,[95] imaging agents,[96,97,98] and chemotherapeutics.[50,56,99,100]

1.5.2. RGD Integrin Ligands for the Delivery of Cytotoxic Drugs in Tumor Therapy

Many different radiolabeled constructs containing RGD-based ligands were developed and validated in cancer imaging at the clinical level.[97,101,102] Alternatively, RGD-containing SMDCs are still under investigation and far from clinic. As previously mentioned, the overexpression of integrin $\alpha_v\beta_3$ by cancer cells can be exploited for the selective delivery of cytotoxic drugs by RGD-based SMDCs. Different dynamics of internalization-recycling of integrin receptors have been described. Upon interaction with their ligands, these processes are mediated by specific proteins (i.e. caveolin and clathrin), capable of activating the receptor insertion into characteristic vesicles that are delivered to endosomes.[103] In the case of integrin $\alpha_v\beta_3$, two pathways are available: 1) protein degradation by specific enzymes in endosomes or lysosomes and, 2) restoration to the cell membrane (i.e. recycling). Consequences of these processes involve cell migration and activation of other receptor families by cross-talk mechanisms (e.g. VEGFR-2, involved in angiogenesis).[104]

Among the cytotoxic drugs used in traditional chemotherapy, doxorubicin (**14**, Fig. 2) was the first chemotherapeutic coupled to an RGD-bearing peptide (RGD4C, Fig. 18) in order to target integrin $\alpha_v\beta_3$. The RGD4C-doxorubicin SMDC developed by Ruoslahti and co-workers, triggered tumor growth inhibition of human breast cancer xenografts (i.e. MDA-MB-435 breast cancer cell line which features a high level of expression of α_v integrins) in nude mice compared to the free cytotoxic drug. Furthermore, the RGD4C-doxorubicin SMDC showed decreased cardio- and hepatotoxicity than free cytotoxic drug as revealed by histopathological studies.[105] By contrast, the presence of stable amide linker showed some unspecific cleavage. For this reason, enzymatically cleavable linkers have been investigated to avoid non-specific cleavage. In 2002, De Groot and co-workers connected the bicyclic RGD4C ligand (Fig. 18) to doxorubicin, through a peptide substrate of protease plasmin (i.e. a tumor-associated enzyme, and involved in tumor invasion and metastasis) as cleavable linker, the D-Ala-Phe-Lys tripeptide sequence (**52**, Figure 18).[106] SMDC **52** showed inhibition of vitronectin binding to HUVEC (human umbilical vein endothelial cells) cells at nanomolar concentration and the efficient linker cleavage by plasmin protease was confirmed.[107] However, only 30% of SMDC **52** was found to be converted into free doxorubicin. In the presence of protease, SMDC **52** was nearly as potent as the free drug against HT1080 and HUVEC cell lines (IC_{50} = 0.28 μM and IC_{50} = 0.75 μM).[106] Later on, Ryppa and co-workers developed two dimeric integrin-targeted doxorubicin SMDCs conjugated through an amide bond (**53**, Fig 18) and a peptide linker (**54**, Fig. 18).[108] The conjugates were designed to improve the affinity towards the target receptor by exploiting the multi-presentation of the recognition sequence. Such constructs were obtained after reaction of the thiolated divalent E-[c(RGDfK)$_2$] linker with: 1) a maleimido functionalized doxorubicin, or 2) doxorubicin functionalized with a MMP2/9 cleavable octapeptide (**53**-**54**, Fig. 18). The MMP2/9 cleavable conjugate was efficiently cleaved in OVCAR-

3 cancer cells (i.e. human ovarian carcinoma), releasing the free doxorubicin. On the other hand, the release of free doxorubicin from the amide-bearing conjugate was not observed, showing the specificity of the MMP cleavable octapeptide. Unfortunately both SMDCs did not display considerable effect in mice xenograft model bearing the OVCAR-3 cancer cell line.[108]

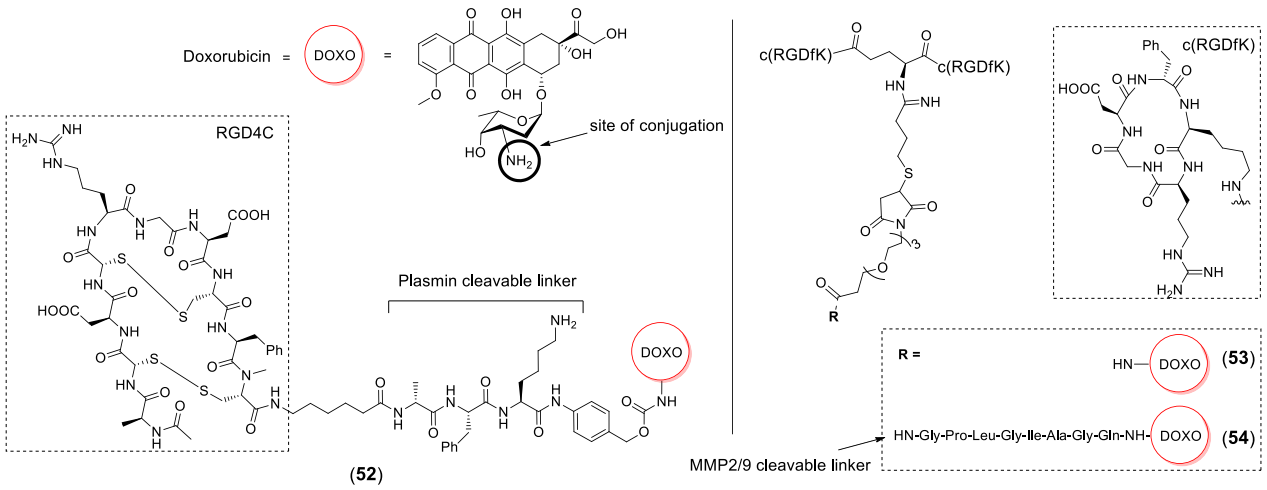

Figure 18. Integrin-targeted DOXO SMDCs. Molecular structures of SMDCs bearing RGD-based integrin-targeting ligand and DOXO through enzymatically cleavable linkers **52** and **54** and amide bond **53**.

Camptothecin (CPT **11**, Fig. 2) and hydrophilic derivatives such as Topetocan (**12**) and SN38 (**13**) are another group of cytotoxic drug used for the development of SMDCs targeting integrin $\alpha_v\beta_3$.[107] Dal Pozzo and co-workers reported in 2010 the synthesis and biological evaluation of integrin-targeted SMDCs (compounds **55**-**56**, Figure 19), in which a CPT analog was conjugated to an RGD cyclopentapeptide through a hydrazone linker. The SMDCs showed good binding affinity to $\alpha_v\beta_3$ ($\alpha_v\beta_3$ IC_{50} = 6-11 nM) and the cytotoxic activity of **55**-**56** was measured against PC3, A498 and A2780 cancer cell lines: despite the high cytotoxicity of this compound, the linker was reported to be poorly stable *in vitro*, resulting in a premature hydrazone cleavage and an non-specific drug release *in vivo*.[109]

SMDC analogs of Cilengitide, conveniently modified with specific groups for conjugation, as well as derivatives of CPT at position 7, were described in a patent by Sigma-Tau.[110,111,112] The RGD targeting ligand was conjugated to CPT through stable linkers at physiological conditions, but promptly cleaved when the conjugate is internalized. Such conjugates present an enzymatically peptide cleavable linker, and short PEG spacer to increase the solubility, without affecting the RGD ligand binding affinity towards $\alpha_v\beta_3$/$\alpha_v\beta_5$ integrins.[107] Indeed, the binding affinity to $\alpha_v\beta_3$/$\alpha_v\beta_5$ isolated receptors ($\alpha_v\beta_3$ IC_{50} = 30-40 nM) and cytotoxicity against ovarian and prostate carcinoma cancer, were remarkable for all the SMDCs.[107] Interestingly, *in vivo* ability of SMDC **57** (Fig. 19) showed good antitumor efficacy with full tumor regression being observed at 25 mg/kg dose (i.e. in a mouse xenograft model of A2780 ovarian cancer cells). Good tolerability and effect persistence were observed after the treatment.[107, 111,112]

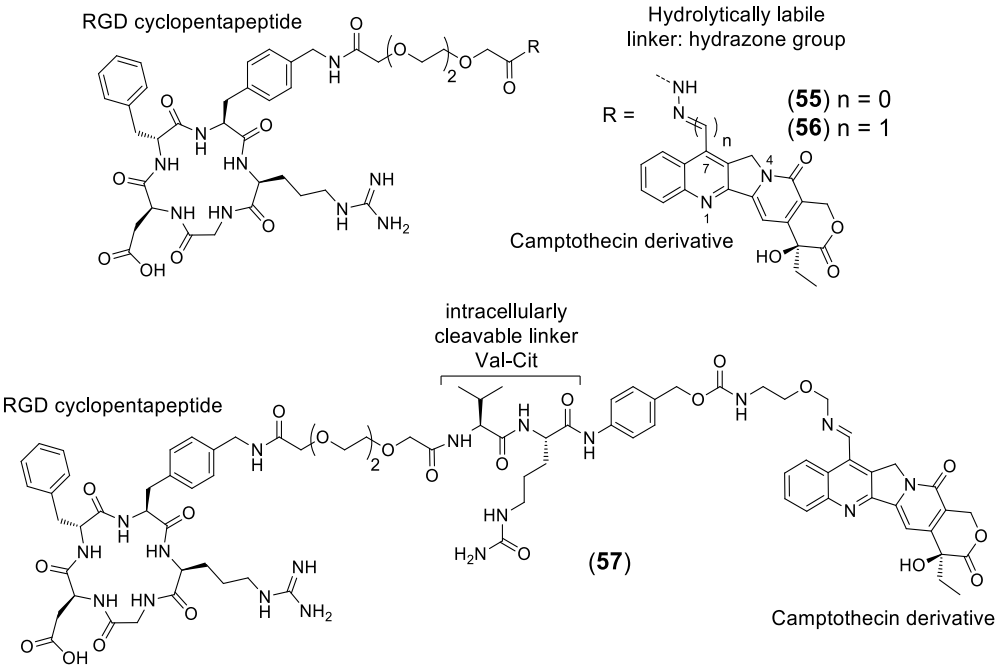

Figure 19. Integrin-targeted CPT SMDCs. Molecular structures of SMDCs bearing RGD-based integrin-targeting ligand and CPT through hydrolytically labile linker **55**-**56** and enzymatically cleavable linker **57**.

Another class of cytotoxic drugs that has been investigated as payloads in RGD-based SMDCs is Crytophycin-52 (**27**, Cry-52, Fig. 3). The latter was the first derivative of this drug family to reach clinical trials (developed by Eli Lilly).[113,114] While the use of free Cryptophycin resulted to severe neurotoxicity in patients,[18,115] the synthesis of targeted cryptophycin derivatives, aimed at improving the drug's safety profile, has been an attractive research area, particularly pursued by the group of Prof. Sewald. Several cryptophycin derivatives were developed, as well as an RGD-(Cry-52) SMDC (**58**, Fig. 20A), bearing a triazole linkage.[116] Cell viability assays were performed in human cervix cancer cell lines KB-V1 and KB-3-1, through cell-based resazurin assay. SMDC **58** displayed low cytotoxicity when compared with free drug **27** (**58** IC_{50} = 55.8 nM in KB-3-1 cells and **58** IC_{50} = 1.8 nM in KB-V1 cells vs. free drug IC_{50} = 15.5 pM in KB-3-1 cells and free drug IC_{50} = 0.26 nM in KB-V1), probably due to the stable triazole connection. The RGD-(Cry-52) compound was derivatized with fluorescein, leading to a *c*RGDfK-fluorescein-(Cry-52) conjugate (**59**), which was used for imaging studies in terms of internalization and cell localization. It was proved that in 15 min, **59** was internalized through integrin-mediated endocytosis and it was localized in the lysosomes of WM-115 tumor cells (see Figure 20A).[116]

Besides the contribution of Sewald and coworkers, the development of "theranostic" devices is now facilitating the overall understanding of the mechanism of $\alpha_v\beta_3$-targeted drug delivery. MMAE (**29**, Fig. 3) has also been conjugated to RGD peptides for theranostic applications (e.g. RGD-PLGC(Me)AG-MMAE-ACPP) by Tsien and co-workers).[117] The RGD ligand was conjugated to MMAE via a PEG spacer, an activable cell penetrating peptide (ACPP), a far-red fluorophore (Cy5), and an intracellularly cleavable linker Val-Cit (SMDC **60**, Fig. 20B).

ACPPs can help the cell uptake and they are generally structured with a polyanion, a polycationic peptide, and a metalloproteinase (MMP2/9) extracellularly cleavable linker (PLGC(Me)AG) - Fig. 20B. SMDC **60** displayed increased cellular uptake in U87MG glioblastoma cancer cells when compared with the RAD-bearing negative control (i.e. RAD-ACPP-PLGC(Me)AG-MMAE), proving the targeting ability of RGD sequence. As for the *in vivo* studies, SMDC **60** displayed better tumor volume regression in MDA-MB-231 breast cancer when compared with cyclic-RAD-PEG-6-MMAE and MMAE negative controls (i.e. MMAE therapeutic dose of 0.2 mg/kg).[117]

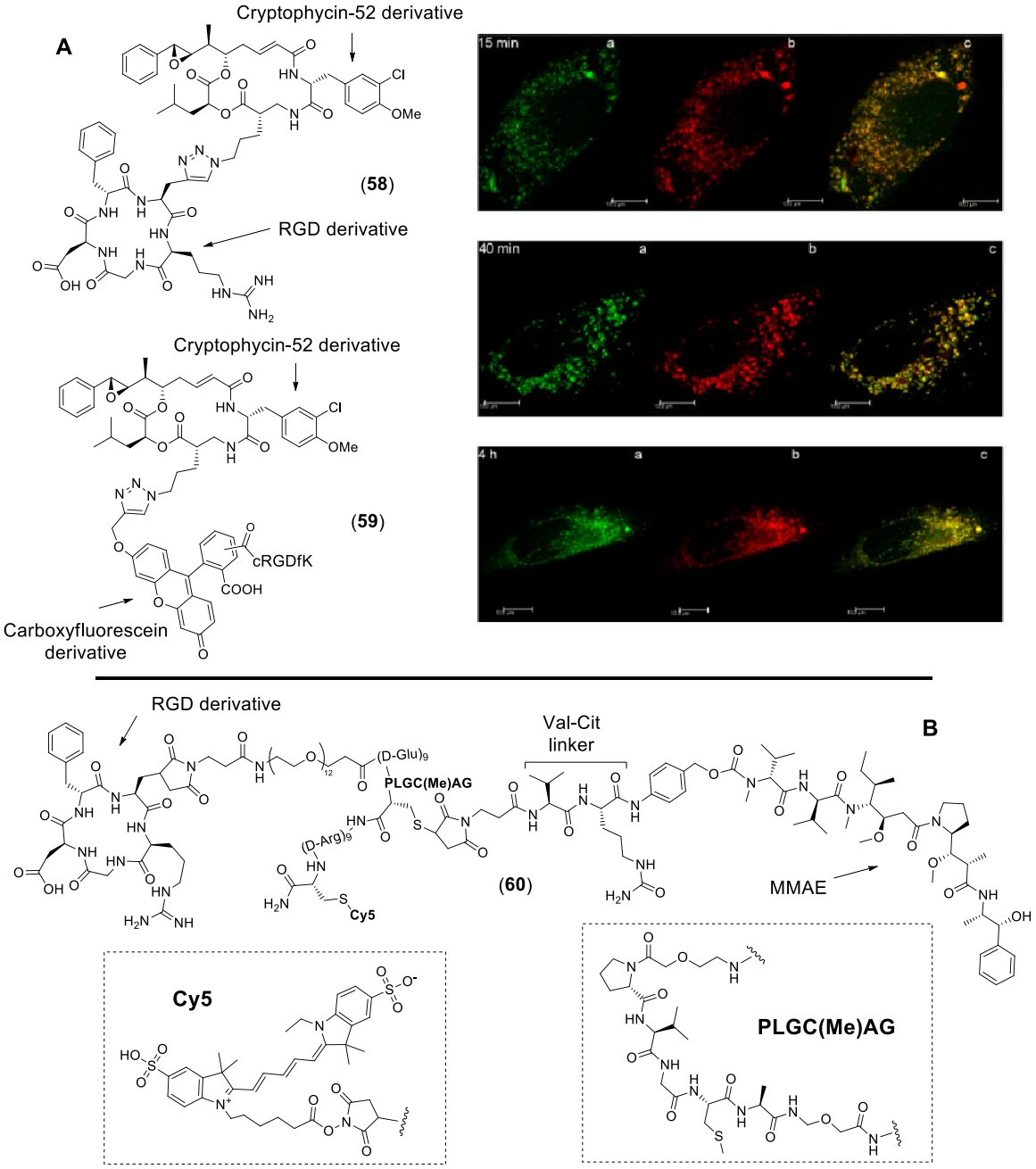

Figure 20. A) Integrin-targeted Cry-52 SMDCs **58**-**59**. On the right: Confocal microscopy. Incubation of WM-115 melanoma cells with conjugate **59** for (I) 15 min, (II) 40 min, (III) 4 h. (Green) The fluorescent conjugate **59** (λ_{ex} = 458 nm) is localized intracellularly. (Red) Lysosomes are stained with LysoTrackerRed (λ_{ex} = 561 nm). (Yellow) The overlay clearly proves colocalization.[116] B) Molecular structure of the "theranostic" (*c*RGD)-ACPP-PLGC(Me)AG-MMAE SMDC **60**.

As already mentioned, an important feature to increase the therapeutic efficacy is the affinity and selectivity of the conjugate. This can be achieved by the concept of multivalency (i.e. multivalent conjugates can carry two or more targeting units). The development of RAFT (i.e. regioselectively-addressable functionalized template) cyclodecapeptide scaffold by Boturyn and co-workers helped the synthesis of multi-presented constructs.[118] Moreover, reducible Pt(IV) complexes have been proved to be particularly useful as linkers in tumor-targeting. After internalization into $\alpha_v\beta_3$/$\alpha_v\beta_5$-expressing cells, the Pt(IV) reduction triggers the release of the Pt(II) complex (i.e. picoplatin active form). For example, Marchán and co-workers developed a mono (**62**, Fig. 21) and a tetrameric (**63**, Fig. 21) RGD-containing SMDCs by conjugation of the picoplatin Pt(IV) prodrug **61** bearing a succinic axial group.[119] Cytotoxicity assays were performed in $\alpha_v\beta_3$/$\alpha_v\beta_5$ integrin expressing SK-MEL-28 melanoma cancer cells, and in 1BR3G and CAPAN-1 cell lines (both showing low integrin expression). The tetrameric SMDC **63** was tested in all three cell lines and IC_{50} values were compared with IC_{50} values of monomeric conjugate and free drug. Tetrameric conjugate displayed 20-fold and 2.6-fold higher cytotoxicity in SK-MEL-28 integrin-expressing cell line when compared to free drug **5** and monomeric **62**, respectively. No antiproliferative activity was shown in $\alpha_v\beta_3$-negative cells (1BR3G and CAPAN-1). ICP-MS technique was used to measure intracellular accumulation of platinum, proving that the increase of cytotoxicity is associated to the level of integrin expression of the cell line and, consequently to the number of targeting units of the SMDC.[119]

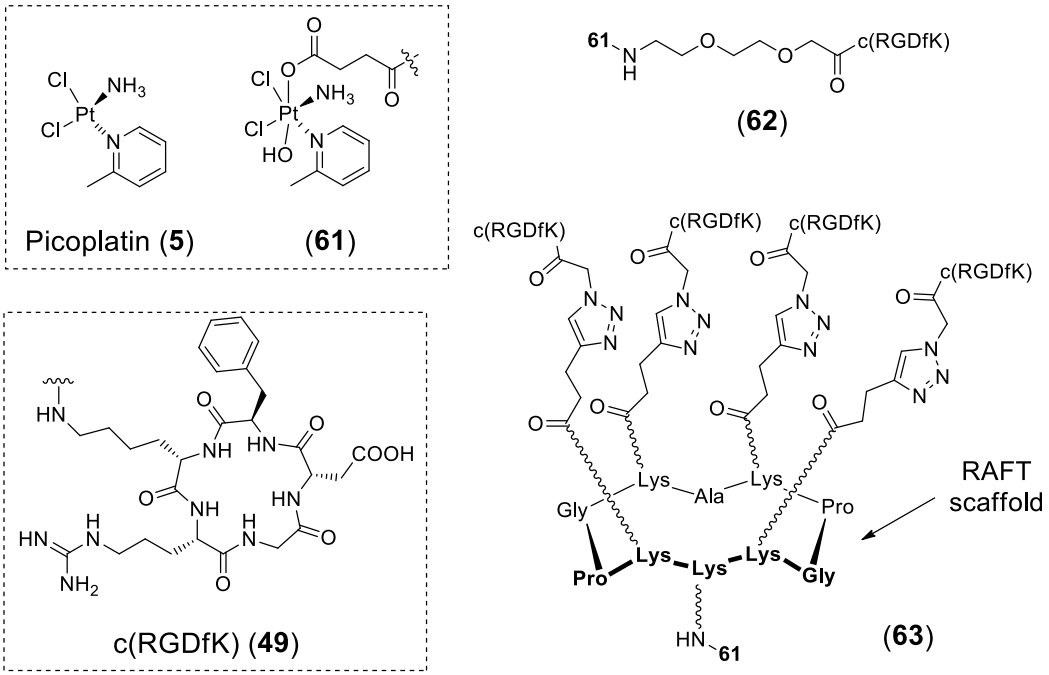

Figure 21. Molecular structures of integrin-targeted platinum SMDCs **62** (monomeric) and **63** (tetrameric) bearing Pt(IV) complexes.

Finally, paclitaxel (PTX, **20**, Fig. 2) is one of the most widely employed in the construction of RGD-containing SMDCs. PTX is usually derivatized at the 2'-OH functional group, which is

crucial for the biological activity of the drug. This position has been often functionalized with targeting agents through ester linkers: this strategy increased the selectivity of paclitaxel in *in vivo* tests.[120] However, such PTX esters showed poor stability even in aqueous buffers and the premature release of the drug was observed, limiting the overall applicability of this kind of SMDCs. As a representative example of such PTX SMDCs, in 2009 Ryppa and co-workers synthesized conjugate **64** (Fig. 22), a divalent RGD compound designed to improve the affinity towards the target receptor, and its anti-proliferative activity was studied on HUVEC cell line. The short half-life of **64** (*ca.* 2 hours in phosphate buffer solution at 37 °C) compromised the targeting ability of the integrin binding portions.[121]

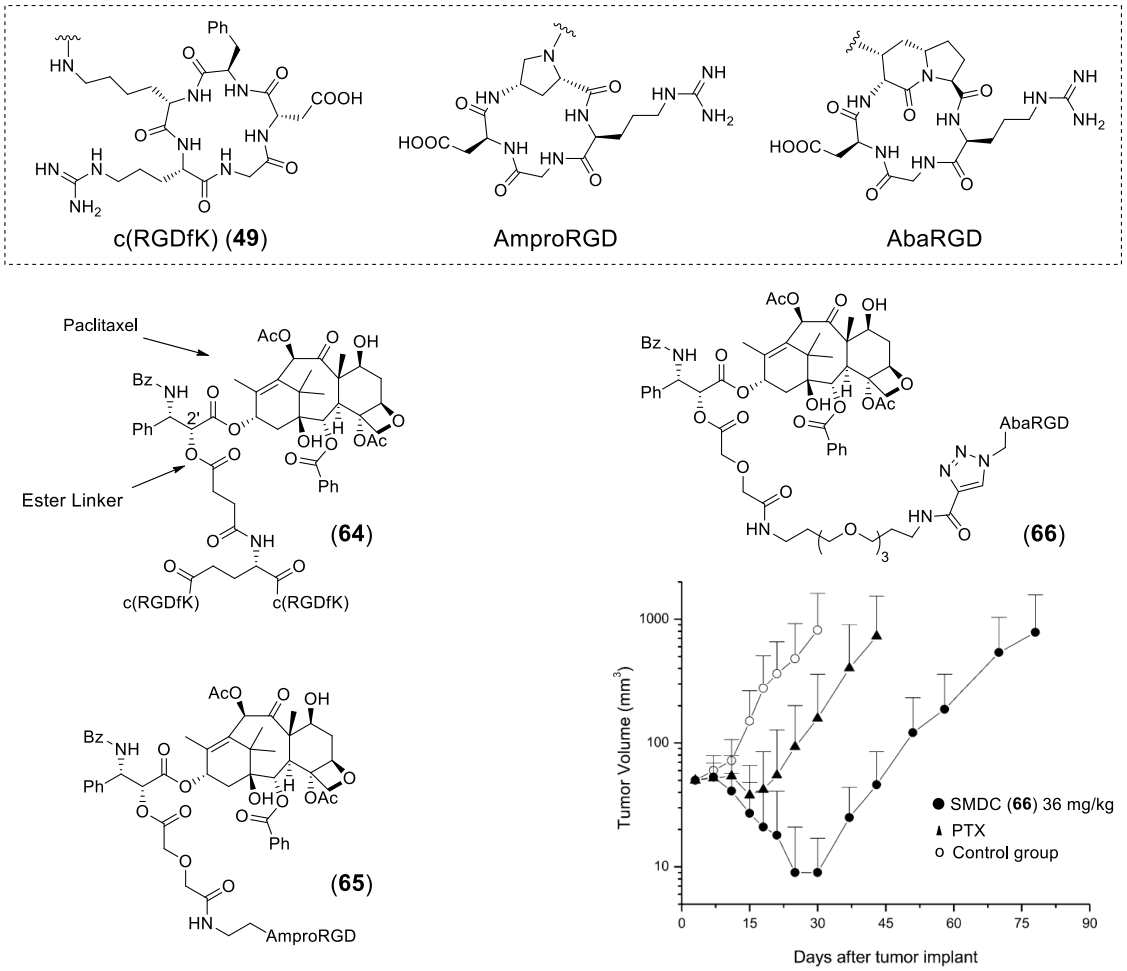

Figure 22. Molecular structures of integrin-targeted PTX SMDCs **64**-**66** bearing an RGD-based structure as targeting ligand and PTX as cytotoxic drug. The graphic corresponds to the *in vivo* effect of **66** on ovarian carcinoma IGROV-1/Pt1. SMDC **66** was administered every fourth day four times.[122]

In 2012, Zanardi, Manzoni and co-workers used cyclic RGD ligands based on modified aminoproline (Ampro) and azabicycloalkanes (Aba) moieties (Fig. 22).[122] These AmproRGD and AbaRGD ligands (i.e. displaying $\alpha_v\beta_3$ affinity) were used to the targeted delivery of PTX (**65**-**66**, Fig. 22). The SMDCs were obtained connecting the 2'-O position of PTX with AmproRGD and AbaRGD via succinic or diglycolic esters and different spacers (i.e. varying the hydrophilicity and length of the spacer). All synthesized conjugates showed good binding

affinity to $\alpha_v\beta_3$ integrin isolated receptor. At the same time, *in vitro* cytotoxicity assays on a panel of $\alpha_v\beta_3/\alpha_v\beta_5$-expressing cancer cell lines was evaluated. Also in this case, all conjugates displayed remarkable cytotoxic activity. Furthermore, *in vivo* efficacy was evaluated for one of the SMDCs (**66**), in a Pt-resistant (IGROV-1/Pt1) ovarian cancer xenograft model (Fig. 22). SMDC **66** displayed improved activity at a molar dose 50% lower than the one of free PTX.[122] In an additional study, the same group exploited the potential of multivalency, with the goal of increase binding affinity of the SMDCs to $\alpha_v\beta_3/\alpha_v\beta_5$ integrins. This work will be described in Chapter II.

Other examples of $\alpha_v\beta_3$-targeted SMDCs are described in literature.[50,56,107,110] In conclusion, despite the notable efforts made in this research field, such type of SMDCs are still far from being evaluated in the clinic. Preclinical data supporting the potential of this pharmacologic approach are still missing and optimizations of each single fragments of integrin-targeted SMDCs may lead to deeper understanding of this drug delivery constructs.

1.6. Work of Our Research Group in the Field – State of the Art

Between 2009 and 2012, our research group developed a new library of cyclic integrin ligands where the 2,5-diketopiperazine (DK1-DK8, Fig. 23A) scaffold had the function of constrain the RGD tripeptide sequence. In addition to the decrease of flexibility of the peptide backbone, the cyclic peptidomimetic structure prevents metabolic cleavage of amide bonds in α-amino peptides. Furthermore, the DKP ring itself is able to participate to ligand-receptor interactions, owing to the presence of hydrogen bond donors and acceptors, such as amide protons and carbonyl groups, respectively. Thus, a better interaction with the biological target can be achieved by introducing diversity in the DKP ring at four positions. In this frame, our research group synthesized a small library of DKP scaffolds, varying the configuration at C3 and C6 and the substitution at N1 and N4 (DKP1-DKP8, Fig. 23A). Later on, with these DKPs in hands, a group *cyclo*[DKP-RGD] peptidomimetics bearing the RGD recognition motif was prepared (**67**-**74**, Fig. 23B).[123,124]

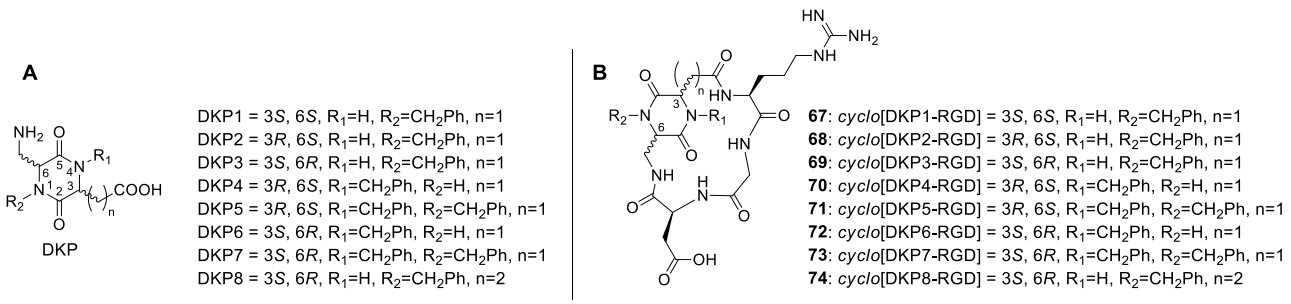

Figure 23. A) DKP1-DKP8 scaffold library and the B) corresponding *cyclo*[DKP-RGD] peptidomimetics (**67**-**74**).[124]

In vitro binding assays on the isolated $\alpha_v\beta_3$ and $\alpha_v\beta_5$ integrin receptors (i.e. ability to compete with the endogenous ligand fibronectin for binding to integrins) qualified the previously

prepared ligands **67**-**74** as low nanomolar binders for $\alpha_v\beta_3$ and demonstrated that the DKP ring strongly influences the ligand affinity for the receptor.[124] In contrast to reference compound Cilengitide (**45**, Fig. 16), these peptidomimetics displayed a higher $\alpha_v\beta_3/\alpha_v\beta_5$ selectivity ration for $\alpha_v\beta_3$ integrin receptor.[124] Compounds **67**-**74** were studied by NMR technique and MC/SD simulations, to elucidate their conformational preferences: the highest affinity for the $\alpha_v\beta_3$ receptor was associated to a defined and extended arrangement of the RGD tripeptide, due to the presence of intramolecular hydrogen bond patterns locking the backbone flexibility. Due to its low-nanomolar affinity for the $\alpha_v\beta_3$ receptor and to its relatively easy synthetic preparation, supplementary *in vitro* biological studies were performed on *cyclo*[DKP3-RGD] (**69**): the tested compound efficiently inhibited angiogenesis in HUVECs.[125] Additionally, ligand **69** has been recently classified as a $\alpha_v\beta_3$ antagonist, due to its inhibitory effect on integrin-mediated FAK/Akt transduction pathways and cell infiltration processes. For this reason, it is important to highlight the difference between *cyclo*[DKP-RGD] ligand ($\alpha_v\beta_3$ antagonist) and the well-known Cilengitide (**45**, $\alpha_v\beta_3$ agonist). Besides, ligand **69** did not affect other cellular aspects (e.g. cell viability and proliferation).[126]

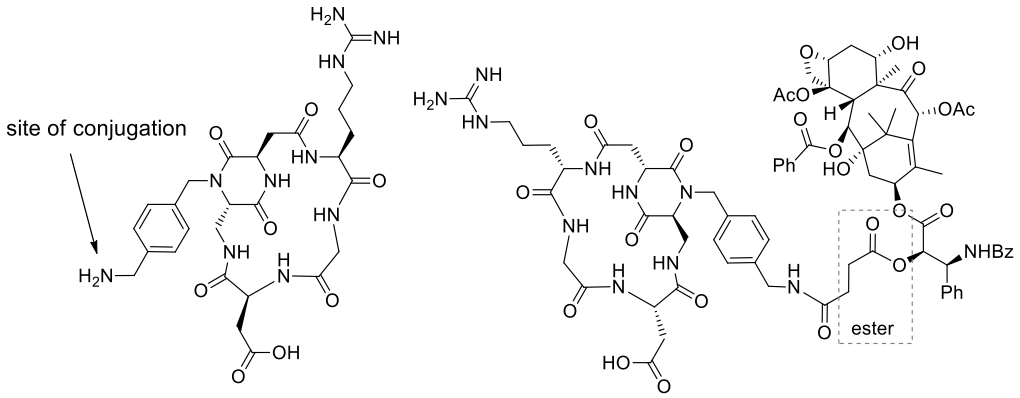

cyclo[DKP-RGD] (**75**) *cyclo*[DKP-RGD]-PTX (**76**)

Figure 24. Molecular structures of *cyclo*[DKP-RGD] (**75**) integrin ligand and of *cyclo*[DKP-RGD]-PTX conjugate (**76**).[127]

As the *cyclo*[DKP3-RGD] (**69**) was selected as hit compound, our research group functionalized the DKP scaffold of peptidomimetic **69** with a benzylamino moiety. This nucleophilic group on the new *cyclo*[DKP-RGD] ligand (compound **75**, Fig. 24)[127] has been used as attaching point for the conjugation of different compounds, such as PTX,[127] a pro-apoptotic SMAC mimetic compound[128] and an anti-angiogenic peptide.[129] Particularly, PTX was connected to the *cyclo*[DKP-RGD] targeting ligand (*cyclo*[DKP-RGD]-PTX **76**, Fig. 24) through a succinate moiety and, despite the increased steric hindrance on the *cyclo*[DKP-RGD] part, conjugate **76** retained a low nanomolar affinity and a high selectivity towards $\alpha_v\beta_3$ integrin [IC_{50} ($\alpha_v\beta_3$) = (5.2 ± 2.3) nM and IC_{50} ($\alpha_v\beta_5$) = (219 ± 124) nM]. Antitumor assays of conjugate **76** in nude mice xenografted with IGROV-1/Pt1 cancer cells (i.e. an $\alpha_v\beta_3$-overexpressing cell line) showed a better efficacy of the conjugate with respect to the free PTX.

Indeed, due to the active integrin targeting, the antitumor activity of **76** was superior than the free drug despite the lower molar dose administered to the animal (Fig. 25C), thus revealing that the conjugation with the *cyclo*[DKP-RGD] ligand improves the antitumor effect of PTX. However, while conjugate **76** showed stability for at least 7 days in physiological solution (Fig. 25A), the ester linker proved to be less stable in plasma, and the release of free PTX occurred with half-lives of 143 min and 165 min in human and murine plasma respectively (Fig. 25B).[127]

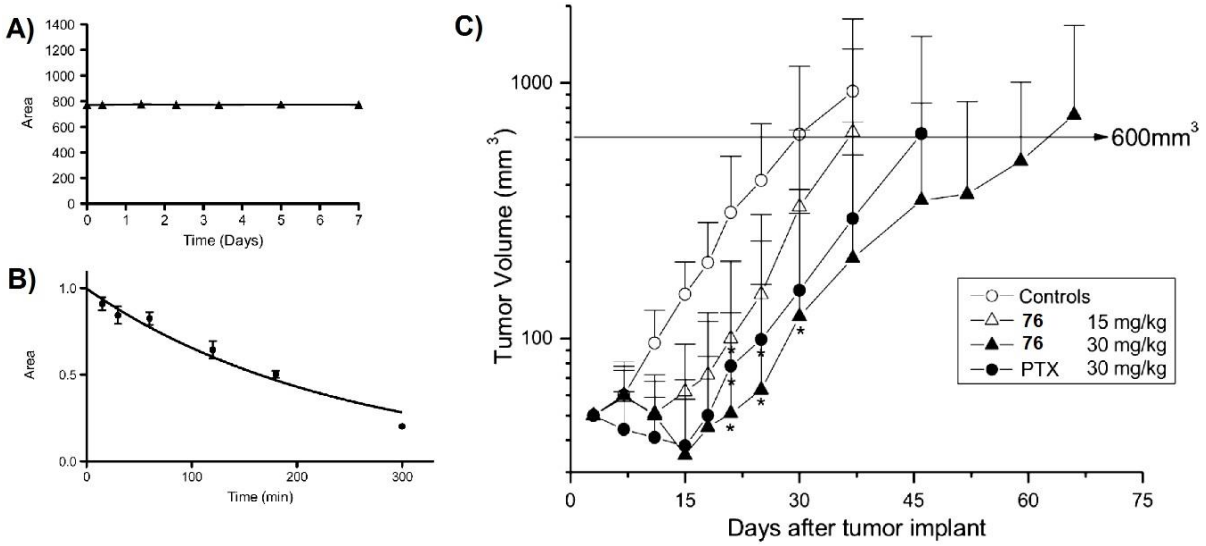

Figure 25. A) Stability of conjugate **76** (1.28 mM) in physiological solution; B) Stability of **76** in murine plasma; C) biological evaluation of **76** *in vivo* compared to paclitaxel (PTX) on IGROV-1/Pt1 ovarian carcinoma. Adapted from.[127]

Such *in vivo* studies with conjugate **76** pointed out the advantage of using *cyclo*[DKP-RGD] integrin ligands as targeting compound for the selective tumor-targeted delivery of cytotoxic agents. At the same time, the plasma stability of this ester linker showed to be too low to exclude a premature drug release in circulation, confirming that the linker system is a critical point for the efficacy of the conjugate and its essential role in the selective release of the cytotoxic drug within the tumor site. These findings prompted the development of different systems to link the portions of the conjugate.

In 2015, our research group synthesized the conjugate *cyclo*[DKP-RGD]-Val-Ala-PTX (**77**, Fig. 26).[130] Conjugate **77** was composed by the integrin ligand *cyclo*[DKP-RGD], the cytotoxic agent (PTX), the dipeptide linker (valine-alanine, Val-Ala) and two different spacers (i.e. the spacer between the dipeptide linker and PTX allowed the conjugation through a carbamate bond, which is known to be more stable in plasma than esters or carbonates). The mechanism of drug release of this construct is similar to the one described for enzyme-cleavable linkers (Paragraph 1.4.2., Scheme 3A). Conjugate **77**, showed a high affinity to the purified $\alpha_v\beta_3$ receptor [IC_{50} ($\alpha_v\beta_3$) = (13.3 ± 3.6) nM and IC_{50} ($\alpha_v\beta_5$) = (924 ± 290) nM]. At the same time, noticeable selectivity was displayed for the integrin over-expressing cell line CCRF-CEM $\alpha_v\beta_3$ with respect to the isogenic cell line CCRF-CEM devoid of the target receptor [i.e. the ratio

between the cytotoxicity in $\alpha_v\beta_3$(-) and $\alpha_v\beta_3$(+) cell lines (i.e. IC_{50} values) highlighted the selectivity (*S*) of such conjugate (*S* = 66.9)].[130]

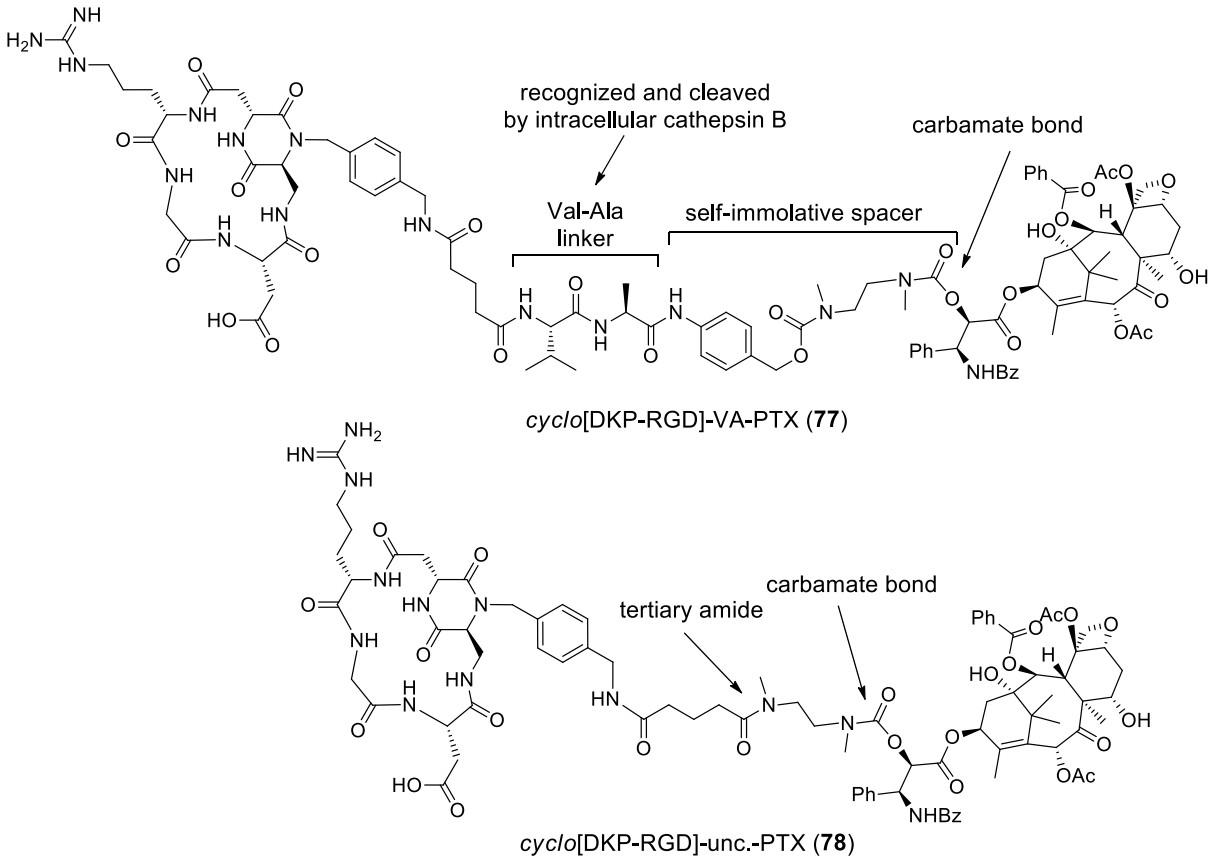

Figure 26. Molecular structures of the conjugates *cyclo*[DKP-RGD]-Val-Ala-PTX (**77**) and *cyclo*[DKP-RGD]-uncleavable-PTX (**78**).

The analog conjugate *cyclo*[DKP-RGD]-uncleavable-PTX **78** was designed to be unable to release of PTX, and thus used as negative control in anti-proliferative assays: the conjugate showed no cytotoxic activity against the tumor cell lines. Curiously, free PTX itself showed a marked selectivity against CCRF-CEM $\alpha_v\beta_3$(+) cells (*S* = 7.4), allowing the correction of the selectivity value of conjugate **77,** by taking into account the different biological activity of PTX in the two cell lines (Targeting Index, TI). TI was calculated as follows:

$$\mathrm{T.I.} = \frac{Selectivity_{\mathrm{SMDC\ 77}}}{Selectivity_{\mathrm{Free\ Drug}}}$$

Interestingly, conjugate **77** displayed a TI = 9.0, showing a remarkable value for the direct evaluation of the tumor-targeting ability of **77** *in vitro*.[130] Moreover, conjugate **77** has been evaluated *in vitro* with different cellular models.[131]

Additionally, our research group has also been developing different SMDCs targeting $\alpha_v\beta_3$ integrin receptor. In particular, the use of reductively cleavable disulfide linkers was explored with the synthesis of a *cyclo*[DKP-RGD]-SS-CPT conjugate. The compound showed TI = 0

due to the low stability of the α,α-unsubstituted disulfide bond in the cell medium.[132] Moreover, new payloads were employed, such as the natural product α-amanitin. Conjugates *cyclo*[DKP-RGD]-Val-Ala-α-amanitin from our group displayed reduced potency in $\alpha_v\beta_3$(+) and $\alpha_v\beta_3$(-) cell lines when compared with free drug (i.e. α-amanitin). Moreover, no targeting was observed against $\alpha_v\beta_3$(+) cell line.[133]

In order to improve the TI value of our conjugates, an intense analysis on the increase of the conjugates valency (i.e. exploitation of multivalency concept), the exploration of different linker structures and the implementation of more potent cytotoxic payloads have been proposed as strategies to achieve and develop more efficient integrin-targeted prodrugs. The mentioned topics will be discussed in the following Chapters.

Chapter II

Multimeric cyclo[DKP-RGD]-PTX Conjugates

Multimeric *cyclo*[DKP-RGD]-PTX Conjugates

Part of the work described in this Chapter was published in the following articles:

- A. Raposo Moreira Dias, A. Pina, A. Dal Corso, D. Arosio, L. Belvisi, L. Pignataro, M. Caruso, C. Gennari, *Chem. Eur. J.* **2017**, *23*, 14410-14415.
- P. L. Rivas, I. Ranđelović, A. Raposo Moreira Dias, A. Pina, D. Arosio, J. Tóvári, G. Mező, A Dal Corso, L. Pignataro, C. Gennari, *Eur. J. Org. Chem.* **2018**, 2902-2909.

2.1 Introduction

The choice of the linker is fundamental for the SMDC efficacy, being the key of the correct equilibrium between the linker stability in circulation and its fast cleavage at the tumor site. Besides, previous data reported by our research group (Chapter I, Paragraph 1.6) established that precise modifications of the linker structure are crucial for the achievement of good selectivity. It is important to note that most of the publications in the field of $\alpha_v\beta_3$-targeted chemotherapeutics do not report the required data for the calculation of the Targeting Index (TI), such as the *in vitro* cell antiproliferative activity of conjugate and free drug against two cancer cell lines, with different $\alpha_v\beta_3$ integrin expression. Considering all available literature reporting sufficient data for the calculation of this parameter, the TI of 9.0 achieved by *cyclo*[DKP-RGD]-Val-Ala-PTX **77** is still the highest ever reported.[50] Moreover, the TI of 9.0 demonstrates that the use of the Val-Ala linker may be a promising starting point for the development of new-generation SMDCs, based on RGD ligands and the Paclitaxel payload. On the other hand, this TI value is still far from the data relative to a large number of ADC products. For instance, TI values in the order of 1000-2000 have been frequently reported for some ADCs, which indicates these biotherapeutics as the best-in-class in the active drug delivery field (Table 1).[50] However, some remarkable TI values can be calculated with literature data available for some SMDC products, specific to non-integrin targets. Nevertheless, TI values reported for SMDC constructs are often one order of magnitude lower than for ADCs. Generally, small molecules as tumor-homing devices are frequently described as weaker binders than mAbs. This is due to the different structural basis of antigen recognition: while most of small ligands bind to a small and specific binding pocket (e.g. the active site of an enzyme), high-affinity antibodies normally interact with a larger antigen surface (epitope), whose shape is complementary to the mAb's variable region. As a result, it is

conceivable to correlate such lower binding affinity to the *in vitro* and *in vivo* selectivity displayed by the corresponding SMDCs, and consequently, the TI values.

As an example, for ADCs, Table 1A and Fig. 27 demonstrate the highly selective antiproliferative activity of the PSMA-targeted ADC **79** against the PSMA expressing cancer cell line MDA PCa2b, achieving a TI of 1716.[134]

Table 1. Antiproliferative activity of the PSMA-targeted ADC **79** (A)[134], Her2-targeted ADC **80** (B)[135], folate receptor-targeted SMDC **81** (C)[21], and SMDC **77** from our group (D)[130] against cancer cell lines with different expressions of PSMA, Her2, FR and $\alpha_v\beta_3$, respectively. [a] Selectivity (*S*): IC_{50}(receptor −)/IC_{50}(receptor +); [b] Targeting index (TI): selectivity/selectivity observed with free drug.

Structure	IC_{50} (nM)		*S*[a]	T.I.[b]
	Negative Antigen	Positive Antigen		
A	**PC3 (PSMA −)**	**MDA PCa2b (PSMA +)**		
Monomethyl auristatin E (MMAE, **29**)	0.970	0.363	2.7	1
mAb(PSMA)-Val-Cit-MMAE (**79**)	83.4	0.018	4633.3	**1716**
B	**MDA-MB-231 (Her2 −)**	**SK-BR-3 (Her2 +)**		
Monomethyl auristatin E (MMAE, **29**)	0.038	0.004	9.5	1
mAb(Her2)-Gal-MMAE (**80**)	No cytotoxicity	0.009	>1000	**>1000**
C	**A549 (FR −)**	**KB (FR +)**		
Monomethyl auristatin E (MMAE, **29**)	0.872	0.240	3.6	1
Folate-MMAE (**81**)	195.2	0.240	813.5	**226**
D	**CCRF-CEM ($\alpha_v\beta_3$ −)**	**CCRF-CEM ($\alpha_v\beta_3$ +)**		
Paclitaxel (PTX, **20**)	155	21	7.4	1
cyclo[DKP-RGD]-VA-PTX (**77**)	5153	77	66.9	**9.0**

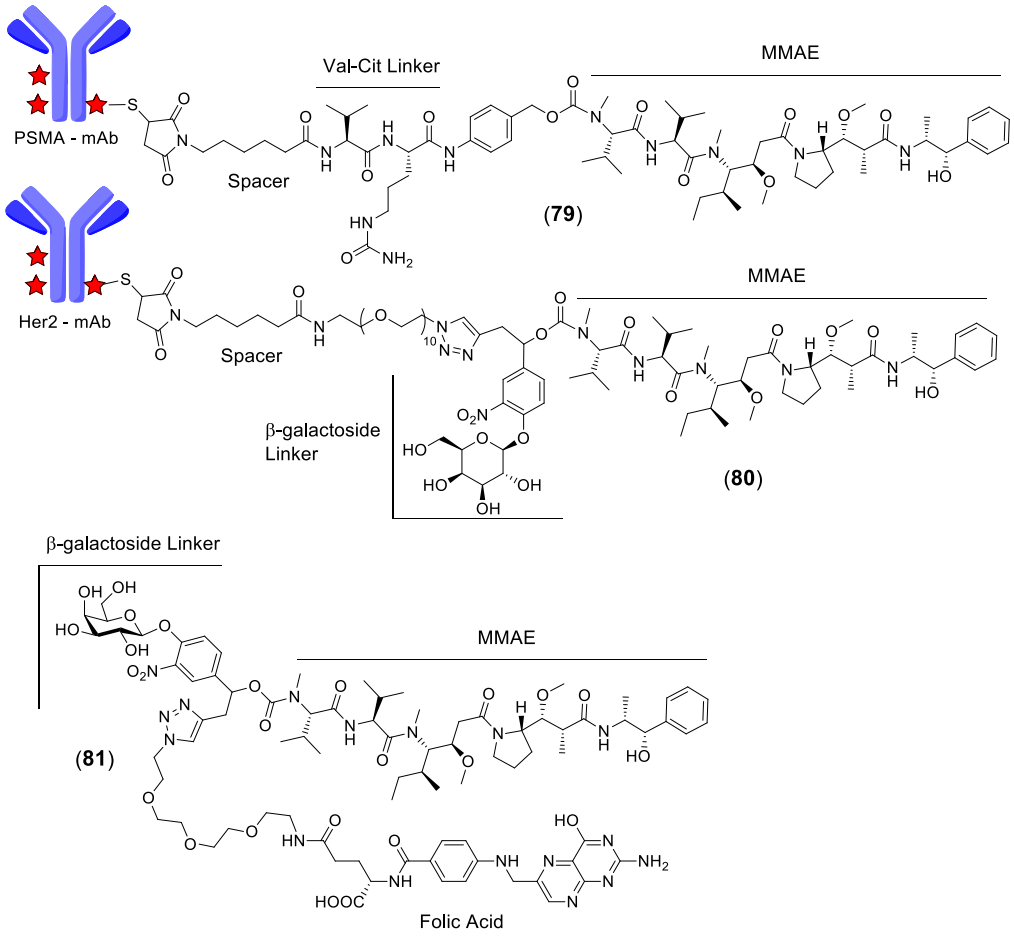

Figure 27. Molecular structures of the examples described in Table 1.

Another successful example of selective ADC development is the recent effort of Papot and co-workers (Table 1B), where a highly selective ADC construct was designed for the treatment of breast cancer.[135] Indeed, this construct displayed better therapeutic efficacy than commercial trastuzumab emtansine (Kadcyla **31**, Fig. 8). Table 1B shows the noticeable antiproliferative activity of the Her2-targeted ADC **80** against the Her2-expressing cancer cell line SK-Br-3 (values obtained were in the picomolar range).[135] By contrast, ADC **80** did not show activity against Her2-non-expressing MDA-MB-231 cancer cells, leading to a remarkable TI. Regarding literature data about SMDCs, the TI value of one of the best conjugates targeting folate (compound **81**, Fig. 27) was around 226 (Table 1C), indicating that it is actually possible to calculate TI values higher than 9.0 using SMDC products.[21]

A well-known strategy to increase the binding affinity and selectivity of a SMDC towards the cells overexpressing integrin $\alpha_V\beta_3$ is the formation of multivalent interactions between the ligand and the target antigen. This strategy is the most common approach to increase this binding strength, according to a biomolecular principle often referred to as “avidity”.[136]

Accordingly, this Chapter aimed at synthesizing new multimeric $\alpha_v\beta_3$-targeted SMDCs, in order to increase their binding avidity, potentially resulting in higher T.I. values.

2.1.1. Multivalency

Multivalent interactions are used by nature to generate stronger binding between two units (e.g. ligand/receptor). For instance, viruses, antibodies, protein complexes are multivalent entities possessing a high number of recognition units or binding moieties (e.g. targeting ligands) able to interact with another multivalent entity (Fig. 28).[137] Essentially, the interesting feature of multivalent interactions is the ability of enhancing the avidity of multivalent species, resulting in an apparent enhancement of the binding affinity of each individual binding unit.[138,139,140] Indeed, the increased ligand binding strength in multivalent constructs can derive from several different mechanisms: 1) receptor/protein aggregation or clustering, 2) chelation, and 3) statistical rebinding (Fig. 28).[141]

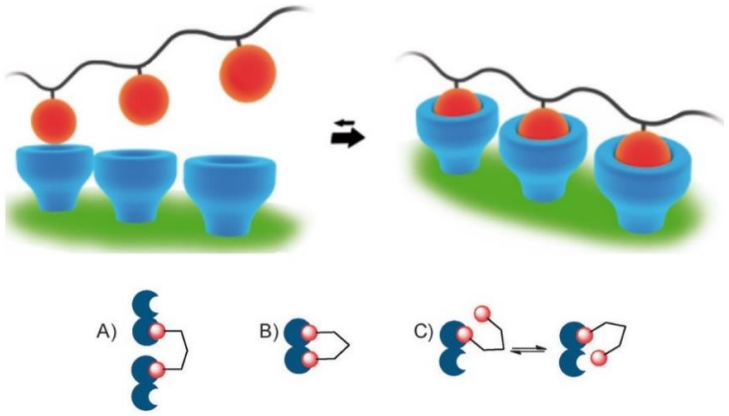

Figure 28. Up) Example of multivalent interactions between two entities to increase the binding strength.[136] Down) A) binding to a cluster of receptors; B) chelation to a divalent protein; C) statistical rebinding with the increase of ligand concentration, enhancing the rebinding rate and, consequently, the binding strength.[141]

Translating this for tumor-targeted therapy or diagnosis, a variety of radiotracers for tumor imaging have been conjugated to multimeric RGD peptides, showing increased tumor uptake and reduced site accumulation to other organs.[142,143,144,145] Besides the applications for tumor imaging *in vivo*, which have reached the clinic, the advantages of using multimeric ligands have been also studied *in vitro*.[102,120,146,147] In particular, a large contribution in this field has been given by Boturyn and co-workers,[148] who developed a RAFT scaffold for the use of multipresentation in RGD constructs, as previously mentioned in Paragraph 1.5.2.[149,150,151] Notably, it was demonstrated that a tetrameric probe **82** (RAFT-c[RGDfK]$_4$-Cy5) displayed higher binding affinity for the isolated integrin $\alpha_v\beta_3$ receptor when compared to monomeric analog (K_d = 3.87 nM for tetrameric construct vs K_d = 41.70 nM for the monomeric analog). Interestingly, when the RGD ligand was replaced by a non-targeting RAD ligand (RAFT-c[RADfK]$_4$-Cy5), the construct lost the affinity for the receptor (K_d > 10000 nM). Later on, the same research group proved that the tetrameric construct **82** increased the endocytosis of a fluorescent probe in HEK293 cells (i.e. β_3-transfected human kidney cell line) by 12%, compared to the monomeric analog, after incubation for 10 minutes.[152]

This study proved that multimeric $\alpha_v\beta_3$-targeting systems can exhibit higher binding affinity to the receptor when compared to monomeric analogs, which reflects in a higher cell adhesion and in a more efficient receptor-mediated endocytosis.[153,154]

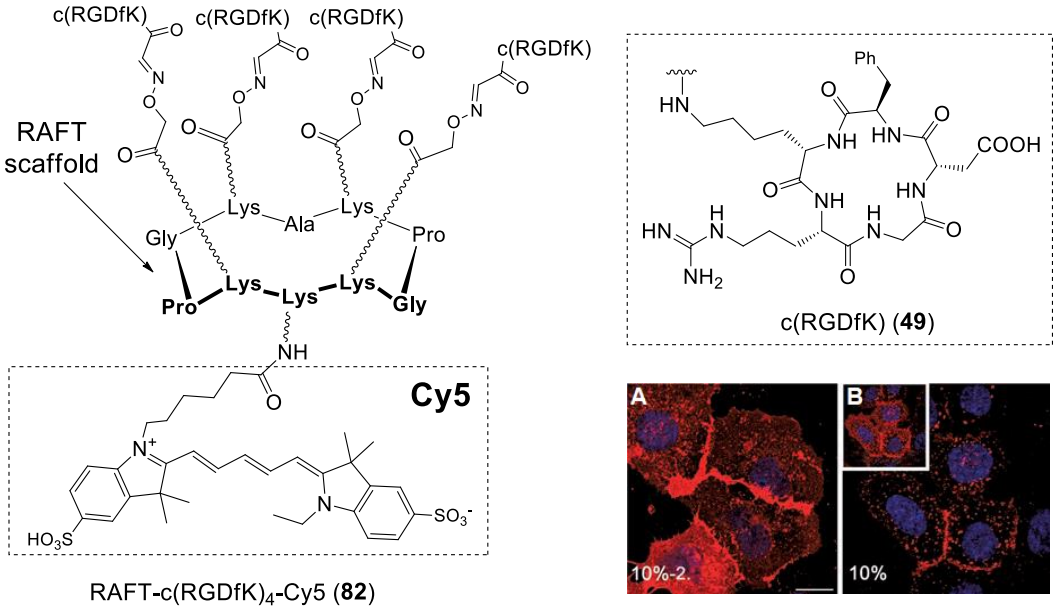

Figure 29. Molecular structure of RAFT-c(RGDfK)$_4$-Cy5 (**82**) and confocal analysis on HEK293(β_3) cells (A – incubation with 1 μM of tetrameric **82** and B - 1 μM of monomeric c(RGDfK)-Cy5 compound) after 10 minutes. Cells were analyzed at 633 nm.[152]

The use of multimeric $\alpha_v\beta_3$-targeted compounds for delivery of cytotoxic payloads has been investigated by Zanardi,[122] Manzoni and co-workers.[155] In 2012, a monomeric and dimeric conjugates [i.e. [AmproRGD]-PTX (**65**) and [AmproRGD]$_2$-PTX (**83**)] carrying AmproRGD as targeting ligand (Fig. 30) were developed. Later on, the same group evaluated the use of

AbaRGD (Fig. 30) as targeting ligand, preparing monomeric (**66**), dimeric (**84**) and tetrameric (**85**) $[AbaRGD]_n$-PTX SMDCs (n = 1, 2 or 4).

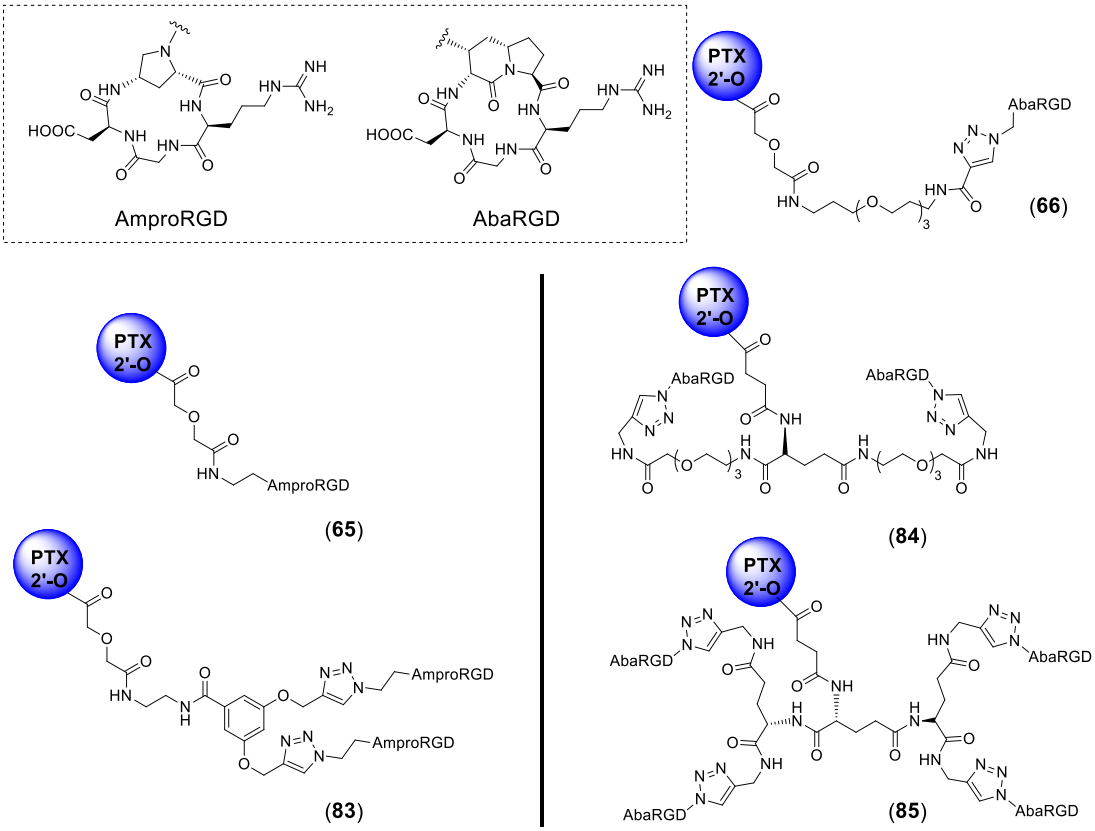

Figure 30. Molecular structures of mono and multimeric conjugates synthesized bearing AmproRGD and AbaRGD as targeting ligands. Molecular structures of **65** and **83** taken from ref.[122] and **66**, **84** and **85** from ref.[155]

Table 2. Cytotoxicity assays of conjugates bearing AmproRGD and AbaRGD as targeting ligands and free PTX in IGROV-1 and IGROV-1/Pt1 cell lines. Table adapted from[122,155].

Cpd	Structure	IC_{50} (nM)	
		IGROV-1 ($\alpha_v\beta_3$ −)	**IGROV-1/Pt1 ($\alpha_v\beta_3$ +)**
65	[AmproRGD]-PTX	43.1 ± 6.8	3.4 ± 2.4
83	$[AmproRGD]_2$-PTX	28.0 ± 2.2	1.6 ± 0.5
20	PTX	23.4 ± 8.2	2.2 ± 0.8
		IGROV1 ($\alpha_v\beta_3$ −)	**IGROV-1/Pt1 ($\alpha_v\beta_3$ +)**
66	[AbaRGD]-PTX	1.6 ± 0.9	1.6 ± 1.1
84	$[AbaRGD]_2$-PTX	32.67 ± 7.5	6.65 ± 3.76
85	$[AbaRGD]_4$-PTX	12.18 ± 1.00	8.81 ± 2.14
20	PTX	58.55 ± 11.71	4.3 ± 1.17

These works represented the proof of concept that the apparent integrin affinity can be increased by multipresentation of RGD units.[122,155] However, the increased avidity was not found to correlate with the selective anticancer activity of the conjugates for $\alpha_v\beta_3$-expressing cells. In fact, cell antiproliferative tests were run against two cell lines expressing different

integrin levels: in particular, the IC_{50} values reported for all tested conjugates highlighted a remarkable potency of the SMDCs against the $\alpha_v\beta_3$ integrin-expressing cell line. However, such intrinsic selectivity is also displayed by the free PTX. This lack of selectivity is probably due to the fast hydrolysis of the ester linker, as already reported in the literature.[127]

Inspired by these literature data, we set to design new multimeric (*cyclo*[DKP-RGD]-PEG-4)$_n$-VA-PTX conjugates (n = 1-4) for tumor targeting (Fig. 31), aiming at improving the binding affinity and TI towards $\alpha_v\beta_3$-expressing cells shown by the monomeric *cyclo*[DKP-RGD]-VA-PTX (**77**).

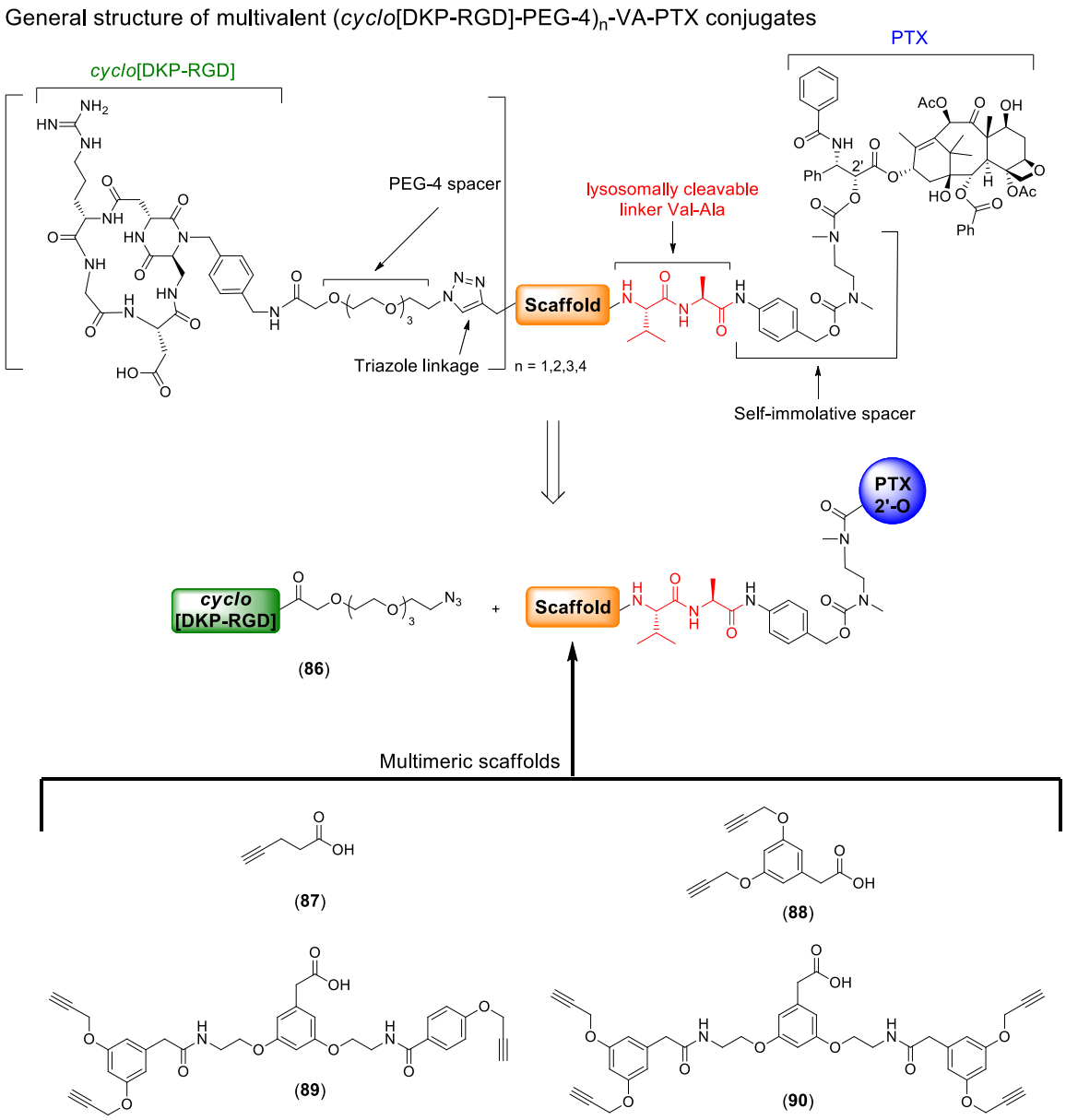

Figure 31. General structure of multimeric (*cyclo*[DKP-RGD]-PEG-4)$_n$-VA-PTX conjugates (n = 1-4) and retrosynthetic analysis of multimeric conjugates (disconnection into azide **86** and different alkyne intermediates bearing multimeric scaffolds **87**-**90**).

In order to allow an easy and general synthetic preparation, a mono- (**86**) and polyalkyne scaffolds (**87**-**90**) were connected to the N-terminus of the Val-Ala linker. The monomeric scaffold (commercial 4-pentynoic acid **87**) was included for the synthesis of a monomeric conjugate, to be used as control for the biological evaluations of the multimeric analogs. The scaffolds were chosen taking into account the central connection of such molecules, which need to be balanced in terms of rigidity and flexibility, so that the loss of conformational entropy can be minimized.[156] Therefore, the terminal alkyne moieties of the paclitaxel prodrug (Fig. 31) were used as anchoring point for the installation of one, two, three or four *cyclo*[DKP-RGD] integrin ligands, through Cu-catalyzed azide-alkyne cycloaddition (CuAAC).[157] A derivative of the RGD peptidomimetic bearing an azido-tetraethylene glycol spacer (compound **86**) was designed and synthesized to be coupled to the alkyne moieties, in the final conjugation reaction. This particular molecular structure was chosen as it is known that polyethylene glycol (PEG) spacers are ”inert” to nonspecific adsorption to proteins, promoting the specific binding of each individual unit to the receptor.[158] Moreover, this flexible layout could help the SMDC to adapt to the target $\alpha_v\beta_3$ integrin.[141] Finally, besides improving the SMDC solubility in aqueous media, short PEG spacers are known to minimize the generation of bulky loops, that can limit the ligand avidity to the antigen.[111]

2.2. Synthesis and Biological Evaluation of a New Monomeric cyclo[DKP-RGD]-PEG-4-VA-PTX Conjugate

2.2.1. Synthesis of a New Monomeric *cyclo*[DKP-RGD]-PEG-4-VA-PTX Conjugate

Following the retrosynthetic scheme represented in Figure 31, the synthesis of fragments **86** and paclitaxel derivative containing commercial alkyne **87** converged to the final isolation of the new PEG-containing monomeric *cyclo*[DKP-RGD]-PEG-4-VA-PTX conjugate.

As for the synthesis of the functionalized integrin ligand with the azido-tetraethylene glycol spacer **86** is shown in Scheme 4.

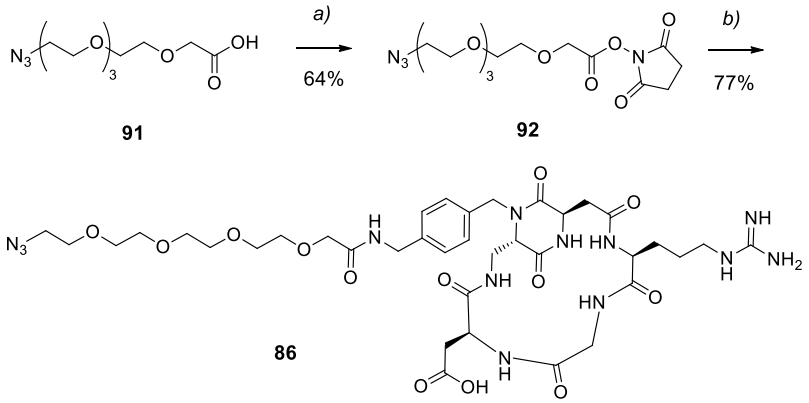

Scheme 4. Synthesis of *cyclo*[DKP-RGD]-PEG-4-Azide (**86**). Reagents and conditions: a) EDC·HCl, N-Hydroxysuccinimide, CH_2Cl_2, overnight; b) *cyclo*[DKP-RGD] (**75**), MeCN/PBS pH 7.5 (1:1), overnight.

Azido-acid **91** was synthesized according to a previously reported methodology, starting from commercially available tetraethylene glycol.[159] Azido-acid **91** was transformed into the corresponding *N*-hydroxysuccinimidyl ester, which was purified by flash chromatography, affording the activated ester **92** with 64% yield. The purified electrophile **92** was then reacted with the *cyclo*[DKP-RGD] ligand (**75**),[127] affording the final azide **86** in 77% yield, after purification by semi-preparative HPLC and freeze-drying. As a well-established procedure from our group, this conjugation step was run at controlled pH, since at pH < 7.0 the reaction does not proceed, whereas at pH > 7.6 the hydrolysis of the NHS ester competes significantly with the desired coupling. The pH was maintained in the 7.3-7.6 range by adding aliquots of 0.2 M aq. NaOH to the reaction mixture.[130]

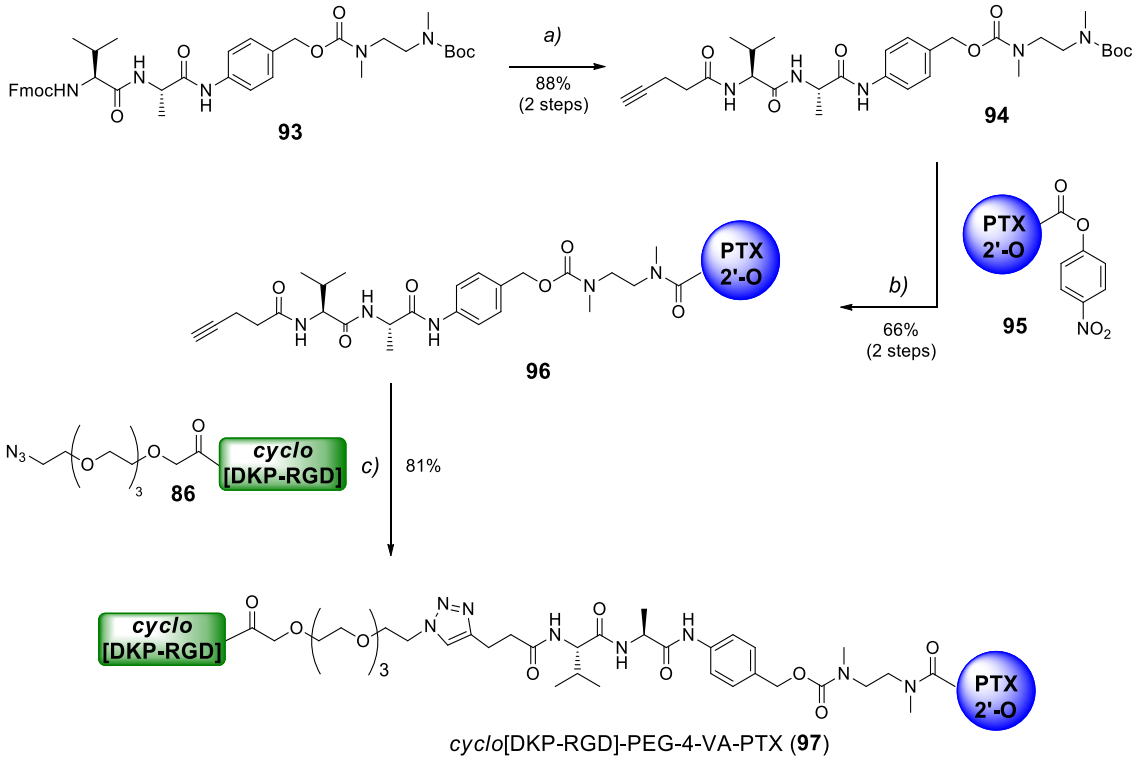

Scheme 5. Synthesis of monomeric *cyclo*[DKP-RGD]-PEG-4-VA-PTX conjugate **97**. Reagents and conditions: a) 1) piperidine, DMF, r.t., 2 h; 2) 4-pentynoic acid **87**, HATU, HOAt, *i*Pr$_2$NEt, DMF, r.t., overnight; b) 1) 1:2 TFA/CH_2Cl_2, 45 min; 2) **95**, *i*Pr$_2$NEt, DMF, r.t., overnight; c) **86**, $CuSO_4 \cdot 5H_2O$, NaAsc, 1:1 DMF/H_2O, 35 ºC, overnight.

After the synthesis of the necessary azide fragment **86** for the construction of the final conjugate, the monomeric *cyclo*[DKP-RGD]-PEG-4-VA-PTX, featuring the alkyl scaffold (**97**), was synthesized by coupling of the free alkyne present in Val-Ala-PTX (**96**, Scheme 5) moiety with the azide **86** – Scheme 5. The alkyne derivative of PTX (**96**) was synthesized starting from the protected Val-Ala linker **93** (previously synthesized and described by our laboratory)[130] that was treated with piperidine for the Fmoc removal and then coupled with commercial 4-pentynoic acid to give the alkyne **94** (88% yield). Later on, the Boc group in amide **94** was removed and the corresponding free amine was reacted with 2'-(4-nitrophenoxycarbonyl)paclitaxel (**95**, previously synthesized and described by our

laboratory)[130] affording carbamate **96** with 66 % yield over two steps. A Cu-Catalyzed Azide-Alkyne Cycloaddition (CuAAC)[160] was performed between alkyne **96** and azide **86**, affording the monomeric conjugate *cyclo*[DKP-RGD]-PEG-4-VA-PTX (**97**) in 81% yield after HPLC purification and freeze-drying.

2.2.2. Cell Proliferation Analysis

In order to first assess the ability of the synthesized monomeric conjugate (**97**) to selectively target $\alpha_v\beta_3$ integrin in human cancer cells, the antiproliferative activity of *cyclo*[DKP-RGD]-PEG-4-VA-PTX (**97**) was tested in parallel with other monomeric RGD-PTX conjugates developed by our research group (Figure 32).[161] In particular, the tested compounds differed from the targeting ligand (RGDfK or *cyclo*[DKP-RGD]), the spacer between the linker and the homing-device (glutarate or PEG spacer) and the lysosomally-cleavable peptide linker (Gly-Phe-Leu-Gly or Val-Ala) (**77**, **98**-**101**, Fig. 32).

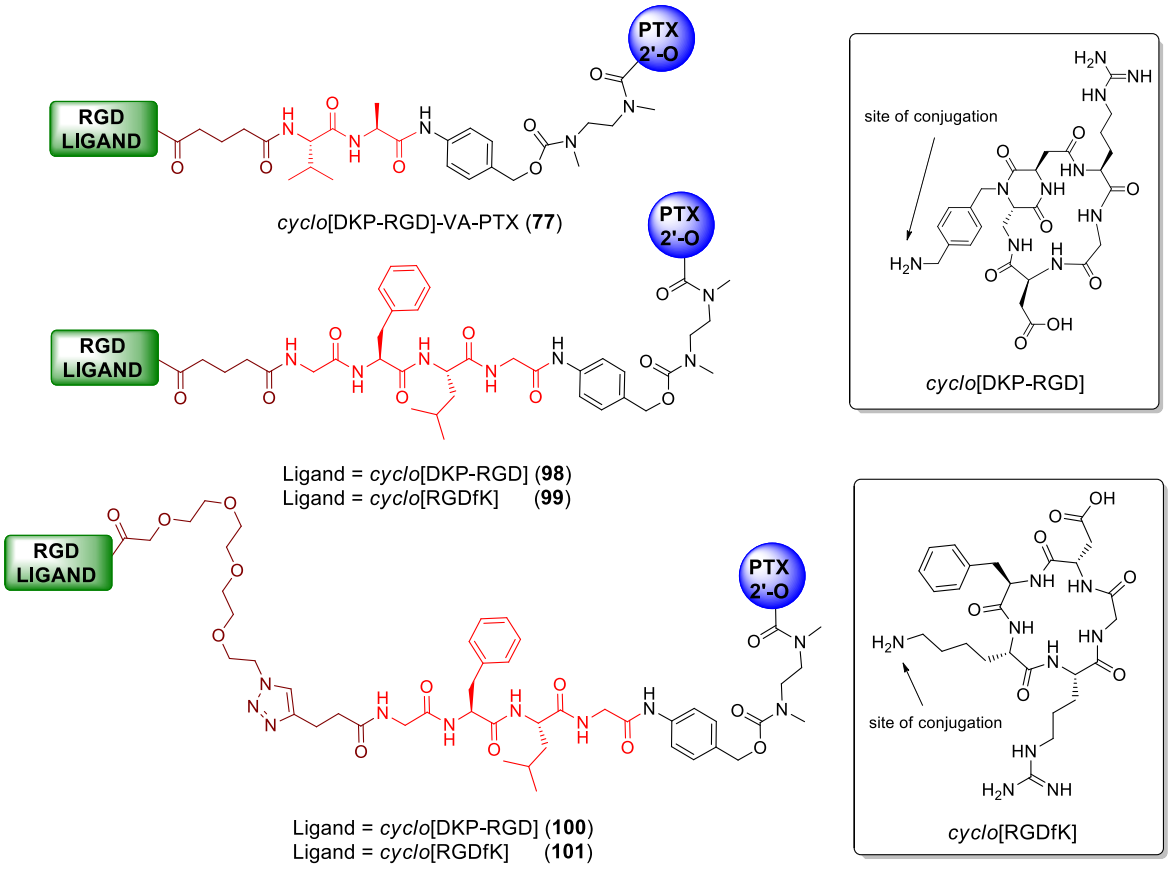

Figure 32. Molecular structures of *cyclo*[DKP-RGD]-VA-PTX (**77**), *cyclo*[DKP-RGD]-GFLG-PTX (**98**), *cyclo*[RGDfK]-GFLG-PTX (**99**), *cyclo*[DKP-RGD]-PEG-4-GFLG-PTX (**100**) and *cyclo*[RGDfK]-PEG-4-GFLG-PTX (**101**).

In collaboration with the National Institute of Oncology in Budapest, Hungary (Prof. József Tóvári) all six compounds (**77** and **97**-**101**) were tested in two different cell lines expressing the integrin receptor at different levels: 1) the human colorectal adenocarcinoma cell line HT29

($\alpha_v\beta_3$ −) and, 2) the human glioblastoma cell line U87 ($\alpha_v\beta_3$ +). The different $\alpha_v\beta_3$ expression on the cell membrane of the two cell lines was confirmed by treatment the cells with a fluorescein-labeled $\alpha_v\beta_3$-selective mAb, followed by cell immunofluorescence analysis and flow cytometry (Fluorescence Activated Cell Sorter - FACS). The graphics of $\alpha_v\beta_3$ expressions for each cell line are shown in the Experimental Section (Figures 45-46).

The two cell lines were incubated with increasing doses of free PTX and conjugates (**77** and **97**-**101**). After 96 hours, the cell viability was analyzed by MTT assay (3-(4,5-dimethylthiazol-2-yl)-2,5-diphenyl-tetrazolium bromide).

The measured IC_{50} values are shown in Table 3.

Table 3. Cytotoxicity assays of conjugates **77** and **97**-**101** and free PTX in U87 and HT29 cell lines.

Cpd	Structure	IC_{50} (nM)[a]		RP_{U87}[b]	RP_{HT29}[c]	TI[d]
		U87 ($\alpha_v\beta_3$ +)	HT29 ($\alpha_v\beta_3$ −)			
20	PTX	1.8 ± 1.9	32.7 ± 21.8	1	1	1
77	*cyclo*[DKP-RGD]-VA-PTX	2686 ± 589	6452 ± 1723	0.01216	0.0002821	43
97	*cyclo*[DKP-RGD]-PEG-4-VA-PTX	432.6 ± 129.3	12840 ± 2730	0.07550	0.0001417	533
98	*cyclo*[DKP-RGD]-GFLG-PTX	2031 ± 454	3413 ± 983	0.01608	0.00053	30
99	*cyclo*[RGDfK]-GFLG-PTX	1250 ± 293.6	2692 ± 676	0.02613	0.000692	38
100	*cyclo*[DKP-RGD]-PEG-4-GFLG-PTX	854.7 ± 165.1	1979 ± 252	0.03821	0.0009196	42
101	*cyclo*[RGDfK]-PEG-4-GFLG-PTX	506.20 ± 113.60	1272 ± 156	0.06452	0.001431	45

[a] IC_{50} values were calculated as the concentration of compound required for 50% inhibition of cell viability. Both cell lines were treated with different concentrations of PTX and compounds **77**, **97-101** for 96 hours. The samples were measured in triplicate; [b] Relative Potency in U87 cell line (RP_{U87}): IC_{50} PTX in U87/ IC_{50} Conjugate in U87; [c] Relative Potency in HT29 cell line (RP_{HT29}): IC_{50} PTX in HT29/ IC_{50} Conjugate in HT29; [d] Targeting Index (TI): RP_{U87}/RP_{HT29}.

From the *in vitro* assays emerged that all conjugates displayed a significant loss of potency (higher IC_{50} values) when compared to the free drug PTX **20** (i.e. for U87 and HT29 cell lines). In general, all conjugates featuring a PEG spacer (**97** and **100**-**101**) proved 2.4-6.2 times more potent (compared to the analogs having a glutarate spacer – **77** and **98**-**99**) against the $\alpha_v\beta_3$-expressing cell line (U87). This is in line with the benefits of PEG spacers in terms of hydrophilicity and flexibility, possibly facilitating the binding to the antigen.[141] Moreover, the replacement of the *cyclo*[DKP-RGD] ligand moiety with the well-known *cyclo*[RGDfK] did not influence significantly the targeting properties. Relative Potencies (RP) were calculated (i.e. RP = IC_{50}PTX / IC_{50}SMDC) for the conjugates in both cell lines. This parameter was introduced as a normalization of conjugates' potency considering the sensitivity of each cell line for free PTX. Accordingly, it can be observed that for all conjugates, the RP in HT29 cell line ($\alpha_v\beta_3$-) was 1-2 orders of magnitude lower than in $\alpha_v\beta_3$-expressing cell line (U87). This suggests that the loss of potency of the conjugates with respect to PTX is more evident when $\alpha_v\beta_3$ receptor is not presented on the surface of tumor cells. Moreover, good TI's were detected for all conjugates (Table 3), with values between 30-45. To our delight, the new monomeric conjugate

cyclo[DKP-RGD]-PEG-4-VA-PTX (**97**) displayed a TI = 533, becoming the best throughout the series. Additionally, competition experiments demonstrated that the potency of **97** against $\alpha_V\beta_3$-positive cells (U87) was decreased by the presence of a large excess of free ligand *cyclo*[DKP-RGD] in the cell medium, in keeping of the hypothesis of conjugate internalization by $\alpha_V\beta_3$-mediated endocytosis.[161]

Finally, conjugate *cyclo*[DKP-RGD]-PEG-4-VA-PTX (**97**) led to the best targeting performances, which prompted its use as starting point for the development of the multimeric library (Figure 31) previously mentioned.

2.3. Synthesis and Biological Evaluation of Multimeric (cyclo[DKP-RGD]-PEG-4)$_n$-VA-PTX Conjugates (n = 1-4)

2.3.1. Synthesis of Multimeric (*cyclo*[DKP-RGD]-PEG-4)$_n$-VA-PTX (n = 1-4) Conjugates

Following the retrosynthetic analysis shown in Figure 31, four different (*cyclo*[DKP-RGD]-PEG-4)$_n$-VA-PTX (n = 1-4) conjugates have been synthesized, and their molecular structures are reported in Fig. 33. In addition to the three multimeric (*cyclo*[DKP-RGD]-PEG-4)$_n$-VA-PTX (n = 2-4) conjugates (**103**-**105**), a new monomeric construct (**102**) was prepared, in which the aliphatic scaffold of monomeric conjugate **97** is replaced by an aromatic scaffold. This derivative was designed to investigate the biological contribution of the aromatic scaffolds present in the multimeric conjugates (**103**-**105**).

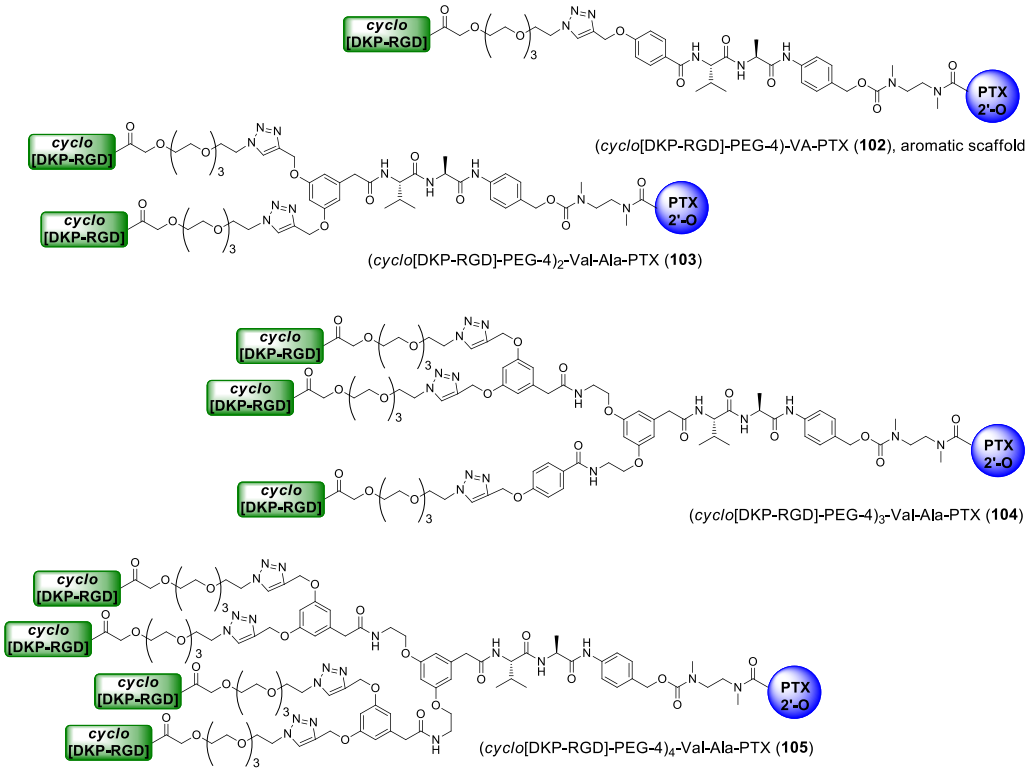

Figure 33. Molecular structures of monomeric (**102**) and multimeric (**103**-**105**) (*cyclo*[DKP-RGD]-PEG-4)$_n$-VA-PTX (n = 1-4).

As a further step, the mono-alkyne (**109**, Scheme 6) and polyalkyne scaffolds **87**-**90** (Schemes 7-9) were synthesized to be connected to the Val-Ala-PTX module, at the N-terminus of the peptide linker. (Fig. 31). The mono-alkyne scaffold **109** was synthesized starting from 4-hydroxybenzoic acid **106**, which was firstly converted in the corresponding ester **107**. Compound **107** was mixed with propargyl bromide affording **108** and then saponified giving **109** with high overall yield – Scheme 6.

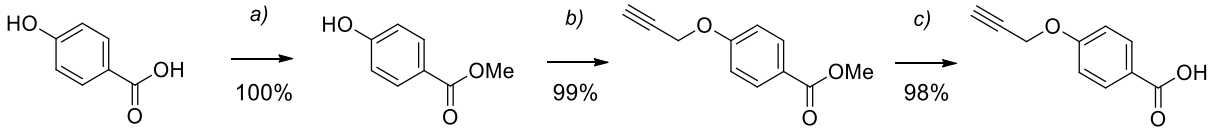

106 **107** **108** **109**

Scheme 6. Synthesis of monomeric aromatic scaffold (**109**). Reagents and conditions: a) H_2SO_4, MeOH, reflux, 4 h; b) propargyl bromide, K_2CO_3, acetone, r.t., 24 h; c) NaOH, MeOH/H_2O (3:1), r.t., 5 h.

The dimeric scaffold was synthesized starting from commercially available methyl 3,5-dihydroxyphenyl acetate (**110**), which was reacted with propargyl bromide allowing the isolation of **111** and then saponified, affording carboxylic acid **88**, with quantitative yields – Scheme 7.

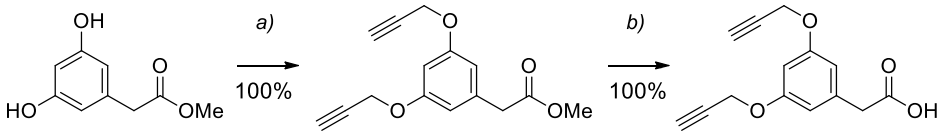

110 **111** **88**

Scheme 7. Synthesis of dimeric scaffold (**88**). Reagents and conditions: a) propargyl bromide, K_2CO_3, acetone, r.t., 24 h; b) LiOH·H_2O, THF/H_2O (2:1), 0 °C, 1.5 h.

As for the trimeric scaffold **89** (Scheme 8), the commercially available methyl 3,5-dihydroxyphenylacetate **110** was firstly refluxed in acetone in presence of commercially available 2-(Boc-amino)ethyl bromide and base, affording the fully protected diamine **112** in 87% yield. Later on, two reactions were carried out in parallel: 1) first, the Boc protecting groups were removed by reaction with TFA, yielding the salt **113**, and 2) dimeric scaffold **88** was activated in presence of thionyl chloride for one hour in CH_2Cl_2 affording the acyl chloride **114**. The coupling between **113** and **114** was then performed in a 5:1 molar ratio, respectively, at 0 ºC, leading to the mono amine **115**. The latter, without being isolated, was coupled to monomeric scaffold **109**, affording the trimeric alkyne ester **116** in 30% yield after three steps (Scheme 8). Finally, trimeric scaffold **89** was obtained after saponification reaction of **116** in presence of LiOH and flash chromatography purification (99% yield).

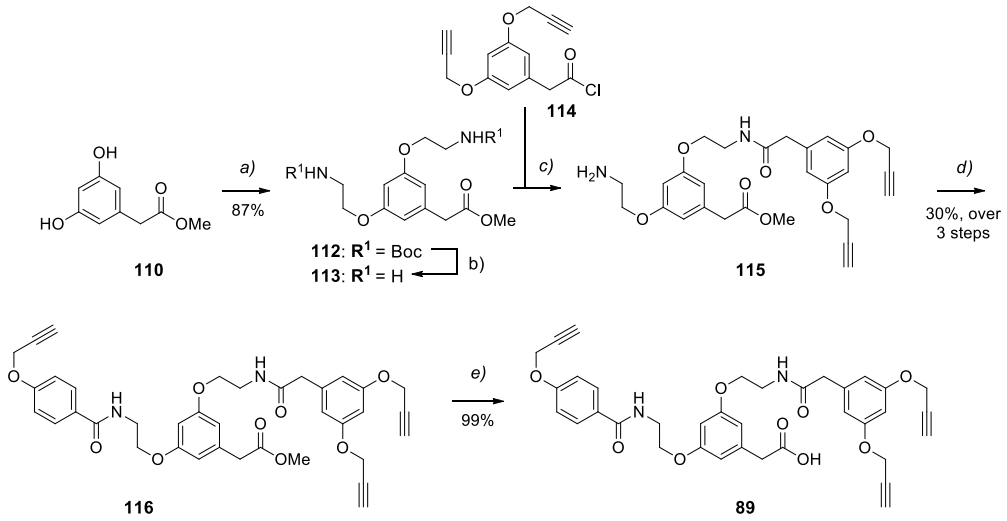

Scheme 8. Synthesis of trimeric scaffold (**89**). Reagents and conditions: a) 2-(Boc-amino)ethyl bromide, K_2CO_3, acetone, reflux, overnight; b) TFA/CH_2Cl_2 (1:2), r.t., 45min; c) **114**, Et_3N, DMF, r.t., overnight; d) **109**, HATU, HOAt, *i*Pr_2NEt, DMF, overnight; e) LiOH·H_2O, THF/H_2O (2:1), 0 °C, 1.5 h.

In the synthesis of the tetrameric aromatic scaffold **90**, the commercially available methyl 3,5-dihydroxyphenylacetate **110** was again refluxed in acetone in the presence of commercially available 2-(Boc-amino)ethyl bromide and potassium carbonate, affording the fully protected diamine **112** in 87% yield. The Boc protecting groups were removed in the presence of TFA, and the resulting diamine-TFA salt **113** was coupled with bis-alkyne **85**, which in turn had been prepared from methyl 3,5-dihydroxyphenylacetate **110** (by treatment with propargyl bromide and ester hydrolysis) – Scheme 7. The coupling of **113** with **88** was carried out in the presence of HATU, HOAt and base in DMF, affording amide **117** in 77% yield. The latter compound **117** was deprotected, affording the desired tetrameric aromatic scaffold **90** in 85% yield (Scheme 9).

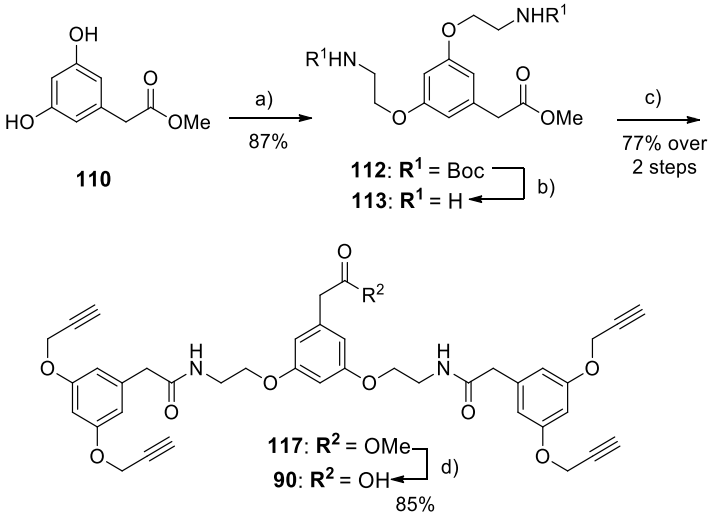

Scheme 9. Synthesis of tetrameric scaffold (**90**). Reagents and conditions: a) 2-(Boc-amino)ethyl bromide, K_2CO_3, acetone, reflux, overnight; b) TFA/CH_2Cl_2 (1:2), r.t., 45 min; c) **88**, HATU, HOAt, *i*Pr_2NEt, DMF, overnight; d) LiOH·H_2O, THF/H_2O (2:1), 0 °C, 1.5 h.

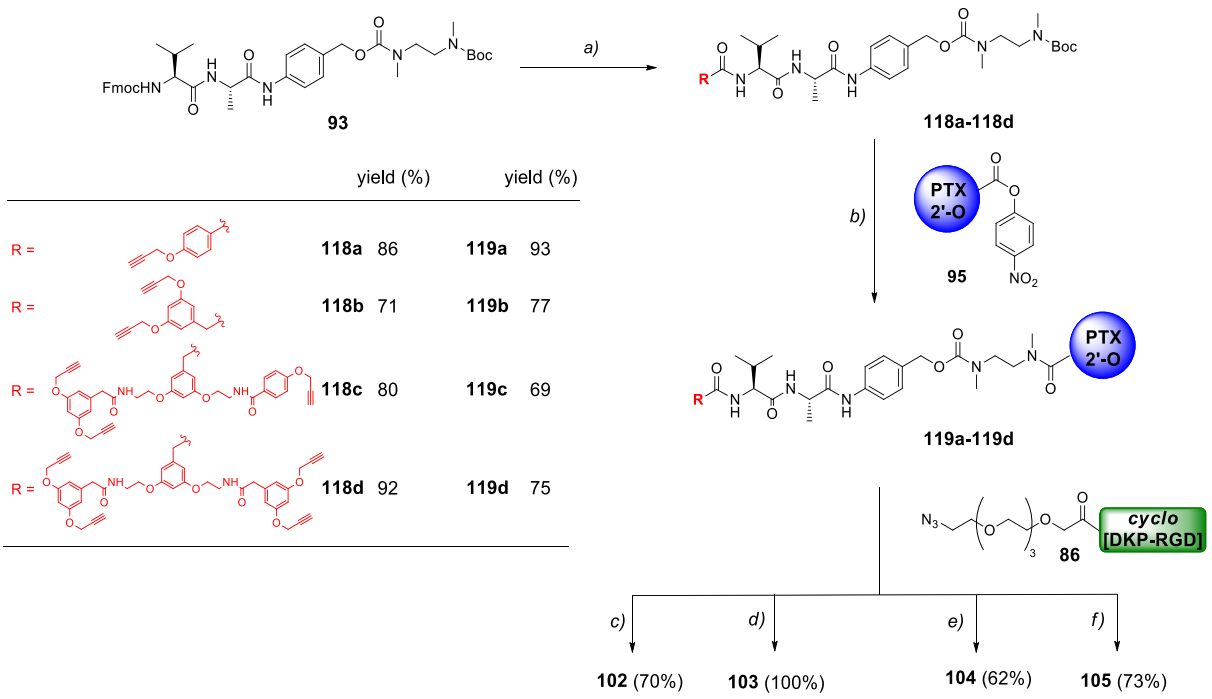

Scheme 10. Synthesis of (*cyclo*[DKP-RGD]-PEG-4)$_n$-VA-PTX (n = 1-4) conjugates **102**-**105**. Reagents and conditions: a) 1) piperidine, DMF, r.t., 2 h; 2) acids **109**, **88**-**90**, HATU, HOAt, *i*Pr$_2$NEt, DMF, r.t., overnight (**118a**-**118d**); b) 1) 1:2 TFA/CH_2Cl_2, 45 min; 2) **95**, *i*Pr$_2$NEt, DMF, r.t., overnight; c) **86**, **119a** (1.5 equiv), $CuSO_4 \cdot 5H_2O$, NaAsc, 1:1 DMF/H_2O, 35 ºC, overnight; d) **119b** (1 equiv), **86** (3 equiv) $CuSO_4 \cdot 5H_2O$, NaAsc, 1:1 DMF/H_2O, 35 ºC, overnight; e) **119c** (1 equiv), **86** (3.6 equiv), $CuSO_4 \cdot 5H_2O$, NaAsc, 1:1 DMF/H_2O, 35 ºC, overnight; f) **119d** (1 equiv), **86** (4.8 equiv) $CuSO_4 \cdot 5H_2O$, NaAsc, 1:1 DMF/H_2O, 35 ºC, overnight.

The monomeric *cyclo*[DKP-RGD]-PEG-4-VA-PTX, featuring an aromatic scaffold (**102**, Figure 33), was synthesized using the same synthetic strategy described above for the monomeric conjugate bearing an alkyl scaffold (**97**, Scheme 5). Thus, conjugate **102** (Figure 33) was prepared through the convergent synthesis shown in Scheme 10. Also in this case, the Boc group of amide **118a** was removed, and the corresponding free amine was reacted with 2'-(4-nitrophenoxycarbonyl)paclitaxel (**95**), leading to carbamate **119a** in 93% yield. The final CuAAC was performed using alkyne **119a** and azide **86**, affording the *cyclo*[DKP-RGD]-PEG-4-VA-PTX (**102**, Fig. 33) possessing an aromatic scaffold, in 70% yield (after HPLC purification and freeze-drying).

Later on, with the dimeric (**88**), trimeric (**89**), and tetrameric (**90**) scaffolds in hands, the synthesis of the multimeric (*cyclo*[DKP-RGD]-PEG-4)$_n$-VA-PTX (n = 2-4) conjugates (**103**-**105**, Fig. 33) was performed following the same synthetic pathway (Scheme 10). Protected Val-Ala fragment **93** was treated with piperidine for Fmoc removal, and subsequent coupling with the acids **88**-**90** led to compounds **118b**-**118d** with good yields (71-92%, Scheme 10). The Boc group of amides **118b**-**118d** was then removed, and the corresponding free amines were reacted with 2'-(4-nitrophenoxycarbonyl)paclitaxel (**95**) to afford carbamates **119b**-**119d** with moderately good yields (69-75%, Scheme 10).

Copper(I)-catalyzed azide-alkyne cycloadditions were performed by varying the relative stoichiometric amounts of azide **86** (Scheme 10): while alkyne derivatives of PTX (**119b**-**119d**)

were used as limiting agent, the amount of azide **86** varied considering the valency of the conjugate. As for the dimeric conjugate (**103**), the excess of azide was 1.5 equivalents for each alkyne, affording (*cyclo*[DKP-RGD]-PEG-4)$_2$-VA-PTX **103** (Fig. 33) in quantitative yield after HPLC purification and freeze-drying – Scheme 10. The final "click" reaction for trimeric and tetrameric conjugates (**104**-**105**, Fig. 33) was performed with a 20% excess of azide **86**, with respect to the alkyne (3.6 and 4.8 equivalents, respectively). The final (*cyclo*[DKP-RGD]-PEG-4)$_3$-VA-PTX **104** and (*cyclo*[DKP-RGD]-PEG-4)$_4$-VA-PTX conjugates **105** were isolated with good yields (62 and 73%, respectively) after HPLC purification and freeze-drying.

2.3.2. Integrin Receptor Competitive Binding Assays

As reported for previous conjugates developed in our research group (e.g. **76**-**77**), the newly synthesized monomeric *cyclo*[DKP-RGD]-PEG-4-VA-PTX (**97** and **102**) and multimeric (*cyclo*[DKP-RGD]-PEG-4)$_n$-VA-PTX (n = 2-4) **103**-**105** conjugates were evaluated *in vitro* for their ability to compete with vitronectin for the binding to the purified $\alpha_v\beta_3$ integrin. Screening assays were carried out through incubation of the immobilized integrin receptors with serial dilutions of the tested compounds (concentration values in the 10^{-12}-10^{-5} M range) in the presence of a constant concentration of biotinylated vitronectin (1 μg/mL), and measuring the concentration of bound upon equilibration. The IC_{50} values obtained are listed in Table 4.

Table 4. Inhibition of biotinylated vitronectin binding to purified integrin $\alpha_v\beta_3$.

Cpd	Structure	$\alpha_v\beta_3$ IC_{50} [nM][a]
97	*cyclo*[DKP-RGD]-PEG-4-VA-PTX (aliphatic scaffold)	14.8 ± 3.9
102	*cyclo*[DKP-RGD]-PEG-4-VA-PTX (aromatic scaffold)	27.3 ± 9.8
103	(*cyclo*[DKP-RGD]-PEG-4)$_2$-VA-PTX	4.0 ± 0.1
104	(*cyclo*[DKP-RGD]-PEG-4)$_3$-VA-PTX	1.2 ± 0.5
105	(*cyclo*[DKP-RGD]-PEG-4)$_4$-VA-PTX	1.3 ± 0.3
69	*cyclo*[DKP3-RGD]	4.5 ± 0.1

[a] IC_{50} values were calculated as the concentration of compound required for 50% inhibition of biotinylated vitronectin binding as estimated by GraphPad Prism software. All values are the arithmetic mean ± the standard deviation (SD) of triplicate determinations.

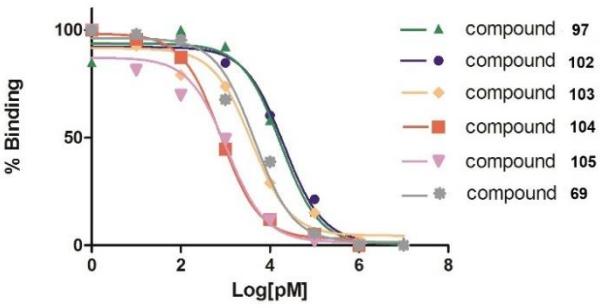

Figure 34. Inhibition of biotinylated vitronectin binding to purified integrin $\alpha_v\beta_3$. X-axis shows the [tested compounds] in log scale; Y-axis shows the % of inhibition of the binding of biotinylated vitronectin in the presence of conjugates.

As expected, all conjugates displayed binding affinity in the nanomolar range. As highlighted in Table 4, the two monomeric conjugates (**97** and **102**), bearing a single *cyclo*[DKP-RGD] targeting ligand moiety, showed little reduction of binding avidity when compared to the free ligand *cyclo*[DKP3-RGD] (**69**). In particular, while the free ligand showed a IC_{50} value of 4.5 nM, conjugate **97** (aliphatic scaffold) and conjugate **102** (aromatic scaffold) showed IC_{50} values of 14.8 and 27.3 nM, respectively. As expected, when the number of targeting moieties in the

constructs raised from one to three (**102**-**104**), a clear tendency of binding affinity increments as well as the decrease of IC_{50} values was detected (IC_{50} conjugate **97** and **102** > **103** > **104**), reaching lower IC_{50} values than the one of free *cyclo*[DKP3-RGD] ligand (**69**) – Table 4.[162]
In particular, a plateau is reached with the trimeric conjugate **104** (IC_{50} = 1.2 ± 0.5 nM), evidencing no further improvement with the tetrameric conjugate **105** (Fig. 34). Although the increment of steric bulk seems to affect the binding affinity (plateau reached with **104**), the binding potency of the trimeric conjugate was slightly higher than the one of free *cyclo*[DKP3-RGD] ligand (i.e. 1.2 and 4.5 nM, respectively).

2.3.3. Cell Proliferation Analysis

Multimeric conjugates were tested for their ability to selectively target $\alpha_v\beta_3$ integrin in human cancer cells, in comparison with previously tested monomeric conjugate **97**. Among the synthesized two monomeric conjugates, the latter was included in this test as a consequence of its higher binding affinity, compared to conjugate **102**, endowed with the aromatic scaffold. Following the same approach of previous *in vitro* assays, (Paragraph 2.2.2.), two different cell lines were chosen expressing the integrin receptor at different levels: 1) the human colorectal adenocarcinoma cell line HT29 ($\alpha_v\beta_3$ −) and, 2) the human glioblastoma cell line U87 ($\alpha_v\beta_3$ +). The two cell lines were incubated with increasing doses of free PTX and conjugates **97** and **103-105**. After 96 hours, the cell viability was analyzed by MTT assay.
The calculated IC_{50} values are shown in Table 5.

Table 5. Cytotoxicity assays of conjugates **97**, **103**-**105** and free PTX in U87 and HT29 cell lines.

Cpd	Structure	IC_{50} (nM)[a]		RP_{U87}[b]	RP_{HT29}[c]	TI[d]
		U87 ($\alpha_v\beta_3$ +)	HT29 ($\alpha_v\beta_3$ −)			
20	PTX	24.1 ± 13.3	2.5 ± 1.2	1	1	1
97	*cyclo*[DKP-RGD]-PEG-4-VA-PTX (aliphatic scaffold)	682.6 ± 169.6	6591 ± 1236	0.035335	0.000375	94.3
103	(*cyclo*[DKP-RGD]-PEG-4)$_2$-VA-PTX	2360 ± 955	7349 ± 1192	0.01022	0.000336	30.4
104	(*cyclo*[DKP-RGD]-PEG-4)$_3$-VA-PTX	13580 ± 8297	12910 ± 1700	0.001776	0.000191	9.3
105	(*cyclo*[DKP-RGD]-PEG-4)$_4$-VA-PTX	11140 ± 5908	9006 ± 1669	0.002165	0.000274	7.9

[a] IC_{50} values were calculated as the concentration of compound required for 50% inhibition of cell viability. Both cell lines were treated with different concentrations of PTX and compounds **97**, **103**-**105** for 96 hours. The samples were measured in triplicate; [b] Relative Potency in U87 cell line (RP_{U87}): IC_{50} PTX in U87/ IC_{50} Conjugate in U87; [c] Relative Potency in HT29 cell line (RP_{HT29}): IC_{50} PTX in HT29/ IC_{50} Conjugate in HT29; [d] Targeting Index (TI): RP_{U87}/RP_{HT29}.

As reported for similar compounds investigated previously, all conjugates showed reduced potency (IC_{50} values) when compared to PTX (i.e. for U87 and HT29 cell lines). Importantly, our data showed that the valency increase in the multimeric conjugates was associated to a decrease of cytotoxic activity against both cell lines. These data seemed to discredit the hypothesis that the increased binding affinity could promote the ligand internalization and the

resulting SMDC efficiency, even though this concept has been extensively supported by literature data.[148,152,163] Although a loss of potency can be noticed, all conjugates resulted substantially more potent in U87 cells ($\alpha_v\beta_3$+) in comparison with HT29 cells ($\alpha_v\beta_3$−). The added value of these data is the 10-fold enhanced selectivity of PTX for the $\alpha_v\beta_3$-negative cells. The observation that the PTX conjugation resulted in the alteration (or in the inversion, in mono and dimeric conjugates) of the intrinsic selectivity of the payload, it can be ascribed to an $\alpha_v\beta_3$-targeting effect.

Considering RP values, TI's were calculated (TI = RP$\alpha_v\beta_3$+ / RP$\alpha_v\beta_3$−) and the best targeting performances was shown by the monomeric conjugate **94** (TI = 94.3).

2.4. Results and Discussion

Overall, the reported experiments indicate that multipresentation of RGD ligands can efficiently lead to enhanced functional affinity for $\alpha_v\beta_3$ integrin receptor through different structural design. In our constructs, ligands were connected to easily accessible multimeric scaffolds through short PEG spacers, with final conjugation with efficient and chemoselective synthesis. On the other hand, complex biological mechanisms requiring more than a simple receptor binding (e.g. internalization and linker cleavage), may be highly dependent on the different design of the construct. In particular, our multimeric conjugates (**103**-**105**) showed relatively low RP and TI values, even though these compounds proved more selective than other multimeric RGD-PTX devices developed in the past (see Table 2 in this Chapter). The observed loss of selectivity could be explained by the increased steric bulk around the peptide linker, which is likely to affect significantly the intracellular proteolytic action, thus affecting progressively the drug release. Cleavage experiments on multimeric conjugates in the presence of lysosomal extract are currently in progress, with the aim to provide a rationale for the *in vitro* assays. Moreover, it is important to note that monomeric conjugate **97** has been tested twice under the same experimental conditions: the observed TI values were found to be 533 (Table 3) and 94 (Table 5). These data reflect the limit of the TI value measurement, which takes into account the IC_{50} values relative to four different experiments (i.e. cell antiproliferative activity of both free PTX and SMDC against two different cell lines) and it is therefore subjected to high variability. On the other hand, both TI values indicate the high targeting potency of conjugate **97**, which can be considered as a new hit compound in the field of $\alpha_v\beta_3$-integrin-targeting SMDCs.

While showing remarkable selectivity, the best-performing conjugate **97** was found to be much less potent than the free toxin, even against the $\alpha_v\beta_3$-positive cells. In general, this observation is common for most therapeutic prodrugs reported in the literature, consisting in a stable, chemical functionalization of the parent drug. However, our data may indicate that the

conjugate is poorly internalized by the targeted cell. A different approach can be also used in presence of different type of “smart linkers” (e.g. extracellularly-cleavable linkers) or more effective drugs (e.g. auristatins), improving the potency of such anticancer prodrugs for therapeutic use.

Chapter III

cyclo[DKP-RGD]-PTX Conjugates bearing an Extracellularly-Cleavable Linker

cyclo[DKP-RGD]-PTX Conjugates bearing an Extracellularly-Cleavable Linker

3.1 Introduction

As discussed in Paragraph 2.4, a quantification of the targeting ability of RGD-containing conjugates to $\alpha_v\beta_3$-expressing cells has been rarely described in the literature. Despite the remarkable selectivity displayed by the monomeric and multimeric conjugates (described in the previous Chapter), the drop of potency displayed by such constructs, as compared to the activity of the free PTX payload, limits their *in vivo* application.

An alternative strategy is here reported, aimed at improving the drug delivery efficacy and to achieve a more potent therapeutic activity. This approach consists in the development of conjugates that can be cleaved in the vicinity, rather than inside, of targeted cancer cells. Generally, it is assumed that ADCs and SMDCs should be internalized through the tumor-associated antigens and activated by intracellular agents, to exhibit their therapeutic effect and to avoid undesired cytotoxic activity against healthy tissues. However, this assumption has been recently challenged, as non-internalizing ADC and SMDC products have shown excellent therapeutic profiles *in vivo*.[45] This approach relies on the synthesis of nontoxic SMDCs that can recognize non- or poorly internalizing tumor antigens (either specific ECM proteins or transmembrane receptors, Fig. 35, step 1): this selective binding is required to improve the accumulation of the cytotoxic agent at the site of disease. Later on, the linker cleavage is triggered in the extracellular environment, by a tumor-associated enzyme (Fig. 35, step 2). While this approach focused originally on proteases expressed in the tumor stroma (e.g. Carboxylesterase 1C,[164] Matrix Metalloproteinases -2 and -9,[165]

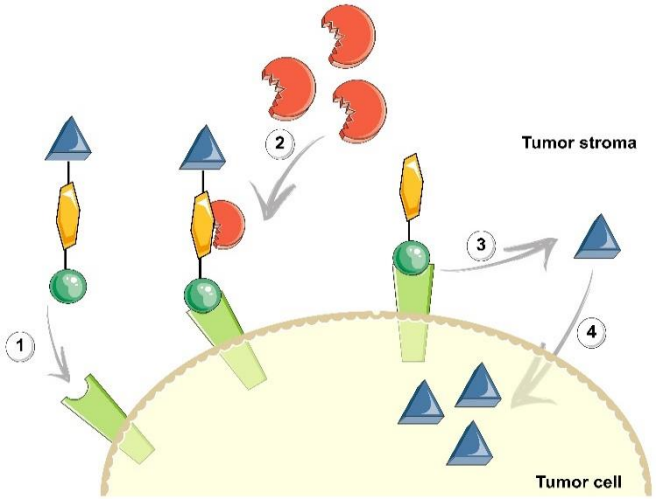

Figure 35. The principle of tumor targeting in presence of tumor-associated enzymes and extracellularly-cleavable conjugates. Targeting ligand (green ball), extracellularly-cleavable linker (yellow), cytotoxic drug (blue) and enzyme (red).

Elastase[166]), it has been demonstrated that other types of proteases that are originally located in the intracellular compartments, can be released externally, for instance by dead cells in necrotic tumors (e.g. Cathepsin B).[71,167] In this context, the active anticancer drug can be released extracellularly within the tumor microenvironment (Fig. 35, step 3), and diffuse in the tumor tissue (Fig. 35, step 4).[45] Here, the cytotoxic agent would be free to kill a large variety of cells (e.g. endothelial cells, cancer cells devoid of the target antigen, etc.) and the resulting localized damage may have therapeutic benefits against certain indications.

In this Chapter, we focused on an extracellularly-cleavable linker by elastase as tumor-associated enzyme. Elastase is a serine protease secreted from activated neutrophils upon inflammation and, for this reason, it is known to be involved in the progress of certain inflammatory diseases (e.g. cystic fibrosis and arthritis) and of certain solid tumors (e.g. breast, lung and skin cancers).[168] The pro-inflammatory nature of these tumors is characterized by a high number of tumor-invading leucocytes, such as neutrophils, resulting in a high expression of elastase in the tumor stroma.[169] Therefore, elastase can be used as extracellular trigger for $\alpha_v\beta_3$ integrin-targeted SMDC products, aimed at releasing the free drug in the vicinity of tumor cells, rather than in intracellular compartments.

Among the few elastase tetrapeptide cleavable linkers that have been used to conjugate anticancer drugs (e.g. Ala-Ala-Pro-X, X = Val, Nal or Nva),[170] we focused on the Asn-Pro-Val (NPV) tripeptide sequence described by Lerchen and co-workers for the synthesis of $\alpha_v\beta_3$ integrin ligands-CPT conjugates (**120**, Fig. 36).[171] This tripeptide linker is selectively cleaved by elastase at the Valine C-terminus.[171] The authors proved the efficiency of this approach by evaluating the stability of **120** in cellular medium supplemented with elastase, which resulted in the full release of the CPT payload within 24 hours.[171]

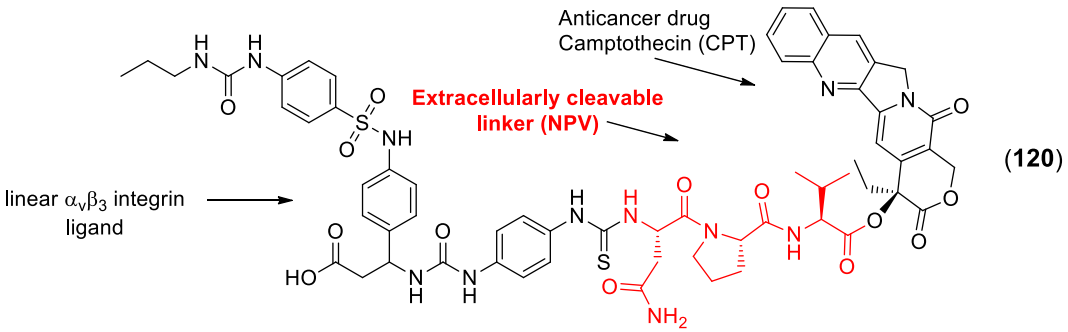

Figure 36. Molecular structure of a conjugate **120** bearing extracellularly-cleavable linker NPV designed by Lerchen and co-workers[171]

Thus, we designed an extracellularly-cleavable SMDC (**121**, Fig. 37) in which the $\alpha_v\beta_3$ integrin ligand *cyclo*[DKP-RGD] (**75**) is connected to PTX via a self-immolative spacer, an elastase-cleavable tripeptide linker (Asn-Pro-Val), a triazole linkage and a PEG-4 spacer. In order to allow an easy and general synthetic preparation, an alkyne-bearing alkyl scaffold was

connected to the N-terminus of the Asn-Pro-Val linker. Similarly to the preparation of the monomeric conjugate **97** (described in Chapter II), the single terminal alkyne moiety of the PTX prodrug (compound **122**, Fig. 37) was used as anchoring point for the connection of the *cyclo*[DKP-RGD] integrin ligand **86**, through CuAAC "click" reaction. Moreover, the PEG-4 spacer emerged from the screening of previous RGD-PTX conjugates (see Chapter II) was maintained in this structure.[161]

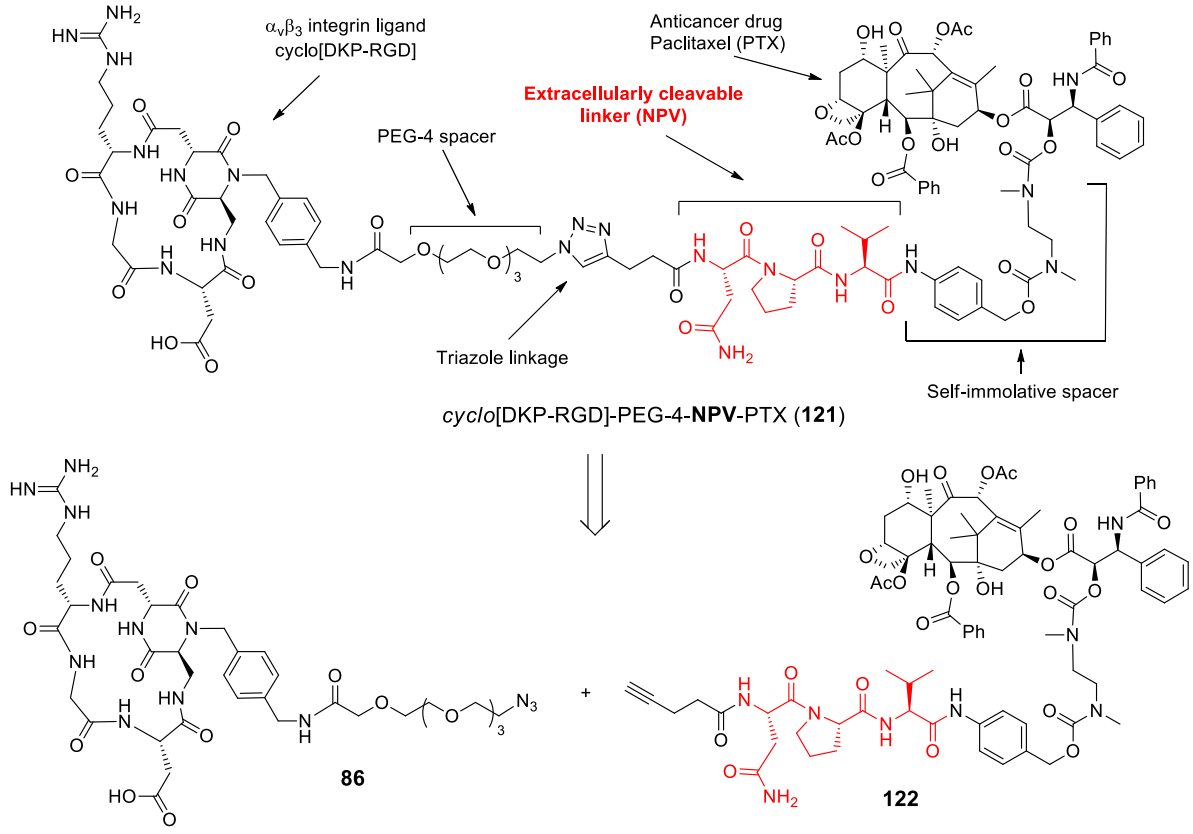

Figure 37. Molecular structure of the conjugate **121** bearing extracellularly-cleavable linker designed by our group and described in this chapter. Retrosynthetic analysis of **121** is also present: disconnection into alkyne **122** and azide **86**.

3.2. Synthesis of cyclo[DKP-RGD]-PEG-4-NPV-PTX conjugate bearing an Extracellularly-Cleavable Linker

Three different *cyclo*[DKP-RGD]-PTX conjugates have been synthesized, and their molecular structures are reported in Fig. 38.

In addition to the peptide linker-bearing conjugate *cyclo*[DKP-RGD]-PEG-4-NPV-PTX (**121**), another *cyclo*[DKP-RGD]-PEG-4-NP-[D]-V-PTX conjugate (**123**), featuring the non-natural amino acid [D]-Valine, was also prepared as negative control for cleavage experiments in the presence of elastase. Furthermore, a third conjugate (compound **124**) was prepared, in which

the tripeptide moiety is replaced by a tertiary amide bond. This proteolytically-stable or "uncleavable" linker was designed as negative control for the evaluation of the biological performances of conjugate **121**.

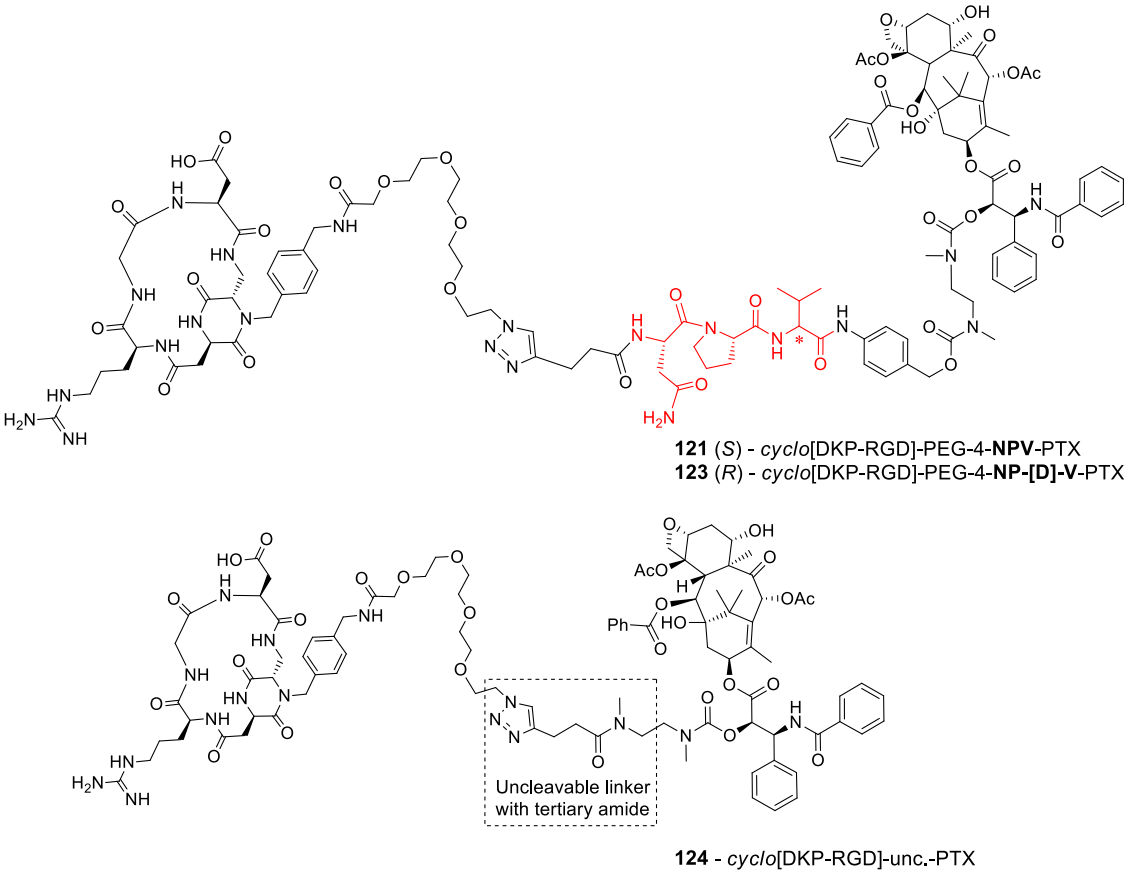

Figure 38. Molecular structures of the SMDCs synthesized in this: *cyclo*[DKP-RGD]-PEG-4-NPV-PTX **121**, *cyclo*[DKP-RGD]-PEG-4-NP-[D]-V-PTX **123**, and *cyclo*[DKP-RGD]-uncleavable-PTX **124**.

Similarly to the preparation of *cyclo*[DKP-RGD]-PEG-4-VA-PTX **97**, the new conjugate *cyclo*[DKP-RGD]-PEG-4-NPV-PTX **121** was synthesized as described in Scheme 11, starting with the preparation of the new tripeptide linker. In particular, Fmoc-Asn(Trt)-OH **125** was activated with *N*-(3-Dimethylaminopropyl)-*N'*-ethylcarbodiimide (EDC) and *N*-hydroxysuccinimide (NHS) in CH_2Cl_2, affording the corresponding activated ester. The latter was reacted with L-proline in the presence of sodium hydrogen carbonate as base in a THF/H_2O mixture, affording dipeptide **126** in moderate yield (52%). The same procedure was used to obtain the tripeptide **127,** featuring L-valine. The next coupling was carried out with a pre-activation of the carboxylic acid **127** with 2-ethoxy-1-ethoxycarbonyl-1,2-dihydroquinoline (EEDQ) in CH_2Cl_2/MeOH: the activated ester formed *in situ* was directly reacted with 4-aminobenzyl alcohol affording the resulting benzyl alcohol, which was directly activated as 4-nitrophenyl carbonate **128** with moderated yield (54% over two steps). The latter, was reacted with mono-Boc protected *N,N'*-dimethylethylenediamine (synthesized according to previously reported procedures),[130] affording carbamate **129** with 80% yield. The Fmoc protecting group

was efficiently removed in the presence of piperidine and the resulting free amine was treated with 4-pentynoic acid, which led to amide **130** in high yield (90% over two steps). Treatment of **130** with trifluoroacetic acid (TFA) for the removal of Trityl and Boc protecting groups afforded the corresponding primary amide and secondary amine, respectively. The latter was reacted with 2'-(4-nitrophenoxycarbonyl)paclitaxel **95**[130] affording carbamate **122** in good yield (71%, over two steps). Finally, alkyne **122** was linked to *cyclo*[DKP-RGD]-PEG-4-N_3 (**86**), through a CuAAC reaction, as previously reported in Chapter II, affording SMDC **121** in high yield (94%).

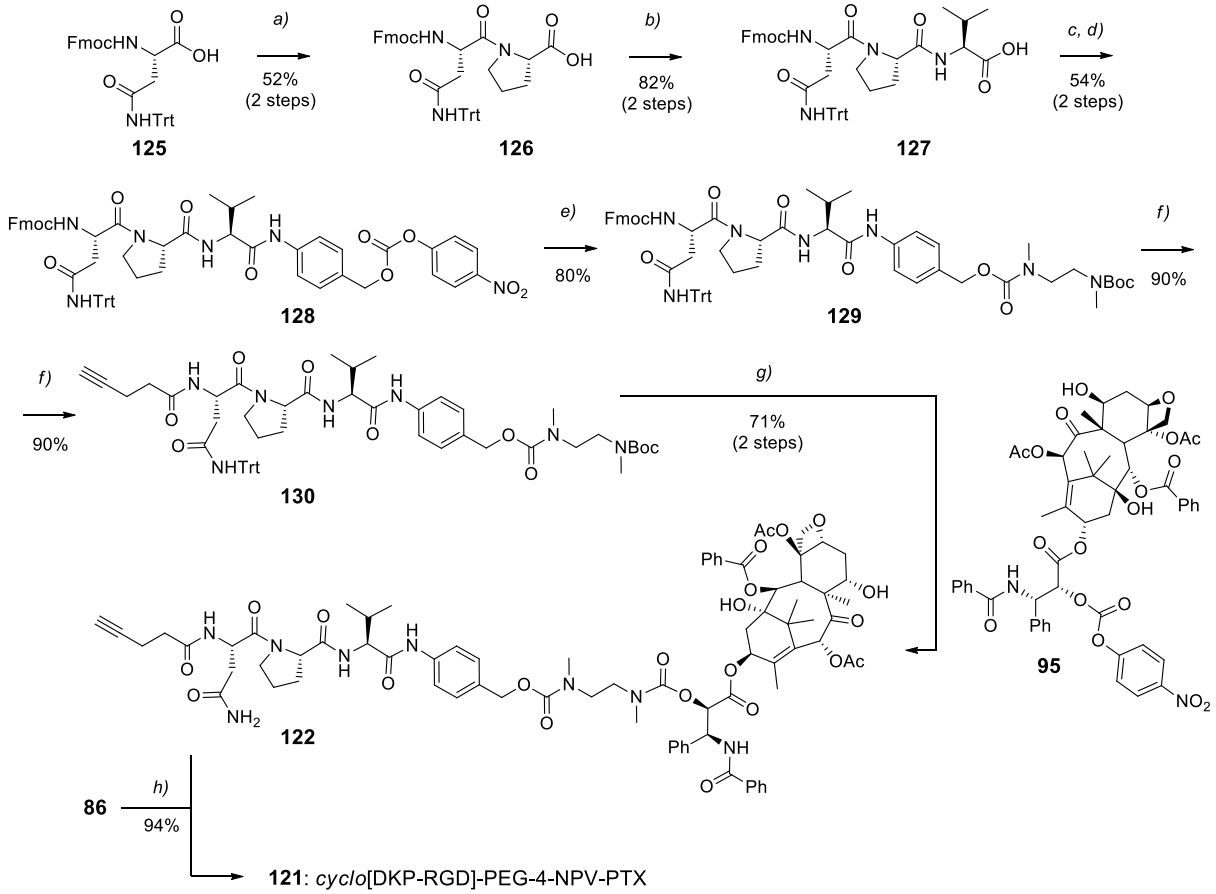

Scheme 11. Synthesis of *cyclo*[DKP-RGD]-PEG-4-NPV-PTX conjugate (**121**). Reagents and conditions: a) 1) NHS, EDC·HCl, CH_2Cl_2, r.t., overnight; 2) L-Proline, $NaHCO_3$, THF/H_2O (1:1), r.t., overnight; b) NHS, EDC·HCl, CH_2Cl_2, r.t, overnight; 2) L-Valine, $NaHCO_3$, THF/H_2O (1:1), r.t., overnight; c) 4-aminobenzyl alcohol, EEDQ, CH_2Cl_2/MeOH (2:1), r.t., overnight; d) 4-nitrophenyl chloroformate, pyridine, r.t., THF, 2 h; e) *N*-(Boc)-*N,N'*-dimethylethylenediamine, *i*Pr_2NEt, r.t., THF, overnight: f) 1) piperidine, DMF, r.t., 2 h; 2) 4-pentynoic acid, HATU, HOAt, *i*Pr_2NEt, DMF, r.t., overnight; g) 1) TFA/CH_2Cl_2 (1:2), 15 min; 2) **95**, *i*Pr_2NEt, DMF, r.t., overnight; h) *cyclo*[DKP-RGD]-PEG-4-N_3 **86**, $CuSO_4 \cdot 5H_2O$, NaAsc, DMF/H_2O (1:1), 30 ºC, overnight.

The synthesis of *cyclo*[DKP-RGD]-PEG-4-NP-[D]-V-PTX conjugate **123** is reported in Scheme 12. In this case, the tripeptide sequence Asn-Pro-[D]-Val was produced starting from the C-terminus (D-Valine) due to epimerization problems. As a matter of fact, it was observed that the coupling of the Asn-Pro-OH fragment with [D]-Val-NH_2 resulted in a mixture of epimers, even at lower temperatures (0-5 ºC). Hence, Fmoc-[D]-Val-OH **131** was activated with EEDQ *in situ*, and then reacted with 4-aminobenzyl alcohol affording compound **132** in 84% yield (Scheme 12). The conversion of **132** into the corresponding amine after treatment with

piperidine was followed by the coupling with Fmoc-L-proline through traditional peptide coupling protocols (i.e. pre-activation of the acid with HATU, HOAt, DIPEA in DMF, followed by addition of the amine). The formation of **133** was observed but the large amount of DIPEA and complications during the work-up (i.e. presence of a free benzylic alcohol significantly enhances the partition easily allows the partition of the product into the aqueous layer) did not allow the isolation of **133**. The same happened during the coupling with Fmoc-[L]-Asn(Trt) **134**, but upon activation of the benzyl alcohol by conversion into the corresponding 4-nitrophenyl carbonate, the purification was possible to afford the intermediate **135**, in 47% yield over five steps (Scheme 12, **132**-**135**).

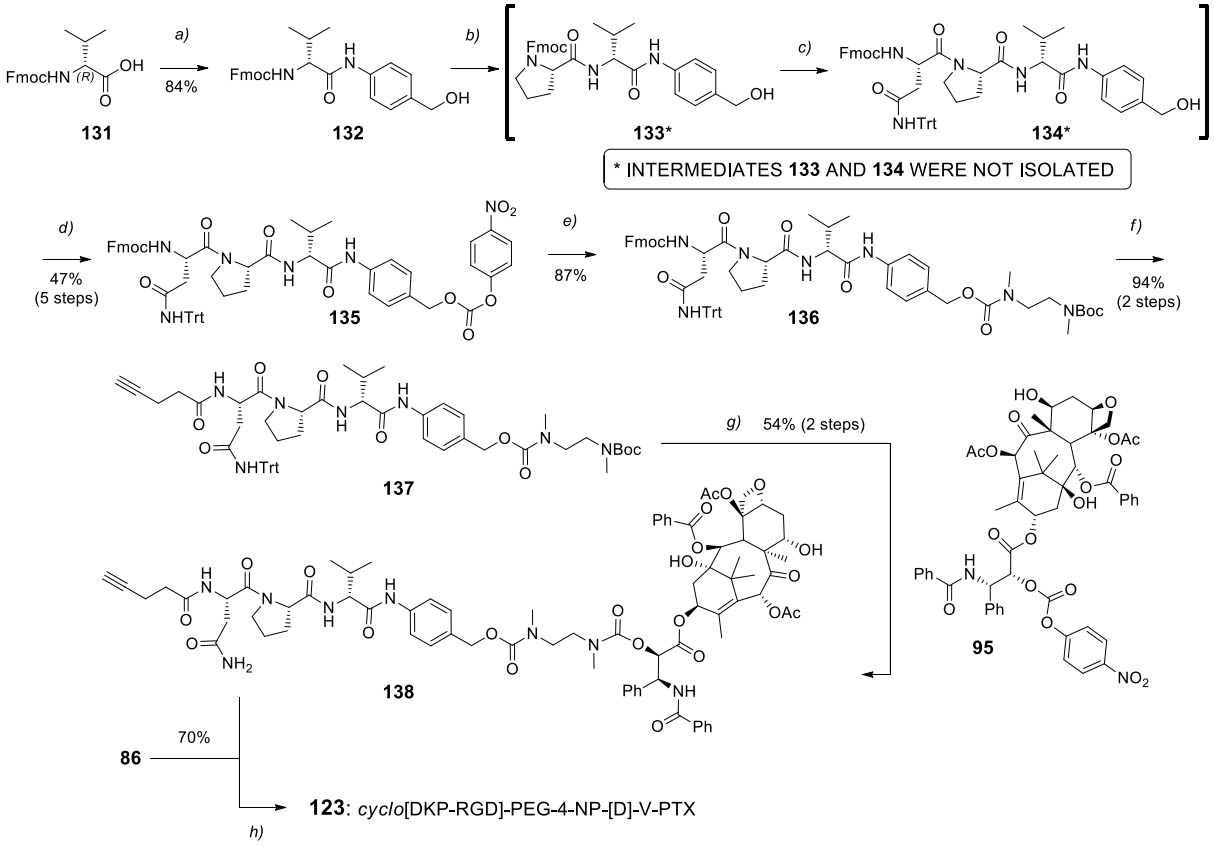

Scheme 12. Synthesis of *cyclo*[DKP-RGD]-PEG-4-NP-[D]-V-PTX conjugate (**123**). Reagents and conditions: a) 4-aminobenzyl alcohol, EEDQ, CH_2Cl_2/MeOH (2:1), r.t., overnight; b) 1) piperidine, DMF, r.t., 2 h; Fmoc-L-Proline, HATU, HOAt, *i*Pr_2NEt, DMF, r.t., overnight; c) 1) piperidine, DMF, r.t., 2 h; 2) Fmoc-L-Asn(Trt), HATU, HOAt, *i*Pr_2NEt, DMF, r.t., overnight; d) 4-nitrophenyl chloroformate, pyridine, r.t., THF, 2 h; e) *N*-(Boc)-*N*,*N'*-dimethylethylenediamine, *i*Pr_2NEt, r.t., THF, overnight; f) 1) piperidine, DMF, r.t., 2 h; 2) 4-pentynoic acid, HATU, HOAt, *i*Pr_2NEt, DMF, r.t., overnight; g) 1) TFA/CH_2Cl_2 (1:2), 15 min; 2) **95**, *i*Pr_2NEt, DMF, r.t., overnight; h) *cyclo*[DKP-RGD]-PEG-4-N_3 **86**, $CuSO_4 \cdot 5H_2O$, NaAsc, DMF/H_2O (1:1), 30 ºC, overnight.

From this step, the final compound was assembled analogously to conjugate **121**. The reaction of **135** with *N*-(Boc)-*N*,*N'*-dimethylethylenediamine led to carbamate **136** in high yields (87%) and a fast deprotection of the N-terminus of the asparagine residue followed by coupling with 4-pentynoic acid afforded the terminal alkyne-functionalized compound **137**. The deprotection of Boc and Trityl groups and the amine conjugation with the carbonate-derivative of PTX **95** led to the carbamate **138** in moderate yield (54% over two steps). Finally, from the click

reaction between alkyne **138** and azide **86**, the final *cyclo*[DKP-RGD]-PEG-4-NP-[D]-V-PTX conjugate **123** was formed.

The synthesis of the RGD-paclitaxel conjugate featuring the “uncleavable” linker (**124**) is reported in Scheme 13. Here, 4-pentynoic acid was reacted with the mono-protected diamine **139** affording tertiary amide **140**. The Boc group was removed at this stage, and the resulting secondary amine was reacted with paclitaxel derivative **95** to yield compound **141**. Again, as described for previous conjugates, a final click reaction afforded *cyclo*[DKP-RGD]-uncleavable-PTX (**124**) in quantitative yield.

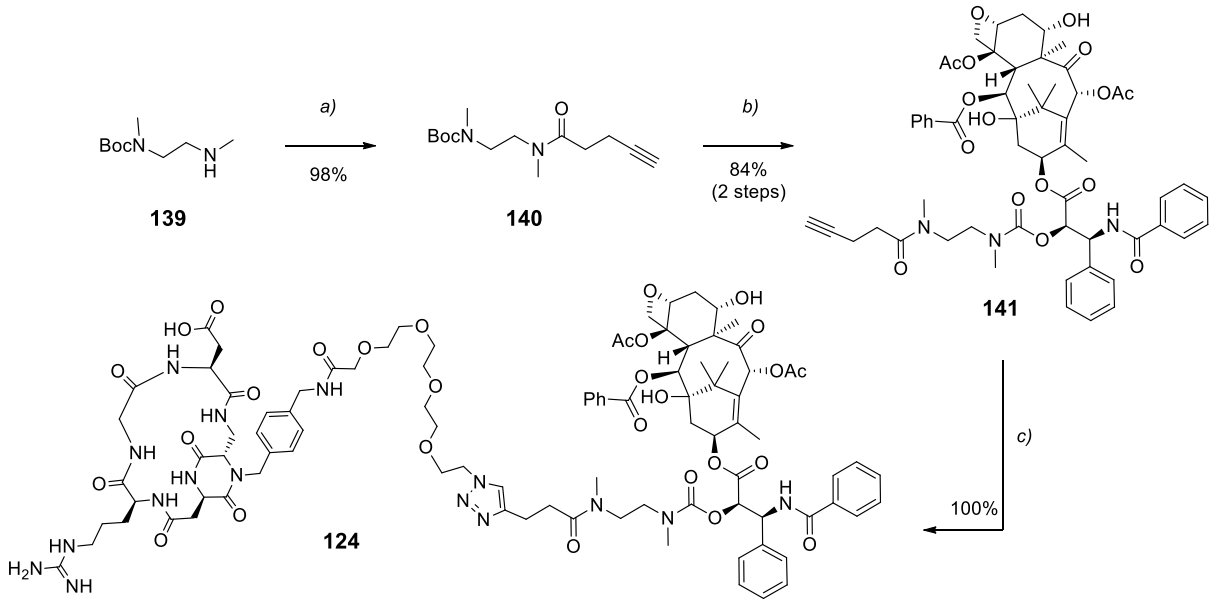

Scheme 13. Synthesis of *cyclo*[DKP-RGD]-uncleavable-PTX conjugate (**124**). Reagents and conditions: a) 4-pentynoic acid, HATU, HOAt, *i*Pr$_2$NEt, DMF, r.t., overnight; b) 1) TFA/CH$_2$Cl$_2$ (1:2), 45 min; 2) **95**, *i*Pr$_2$NEt, DMF, r.t., overnight; c) *cyclo*[DKP-RGD]-PEG-4-N$_3$ **86**, CuSO$_4$·5H$_2$O, NaAsc, DMF/H2O (1:1), 30 ºC, overnight.

The final compounds **121**, **123**-**124** were all purified by semi-preparative HPLC and freeze-dried before being subjected to biological assays.

3.3. In vitro Biological Evaluation

3.3.1. Integrin Receptor Competitive Binding Assays

Analogously to all the SMDCs described so far, the newly synthesized *cyclo*[DKP-RGD]-PTX **121**, **123**-**124** conjugates were evaluated in competitive assays for the binding to the purified $\alpha_v\beta_3$ integrin, in the presence of biotinylated vitronectin. The IC_{50} values obtained are shown in Table 6.

Table 6. Inhibition of biotinylated vitronectin binding to isolated $\alpha_v\beta_3$ receptor.

Cpd	Structure	$\alpha_v\beta_3$ IC_{50} [nM][a]
121	*cyclo*[DKP-RGD]-PEG-4-NPV-PTX	12.9 ± 1.4
123	*cyclo*[DKP-RGD]-PEG-4-NP-[D]-V-PTX	24.9 ± 2.1
124	*cyclo* [DKP-RGD]-uncleavable-PTX	5.8 ± 1.2
69	*cyclo*[DKP3-RGD]	4.5 ± 0.1

Also in this case, the results showed that despite their remarkable steric bulk, the conjugates' affinity for the purified $\alpha_v\beta_3$ receptor is comparable to that of the free ligand **69**. Remarkably, the high affinity observed towards the $\alpha_v\beta_3$ receptor (IC_{50} = 5.8-24.9 nM), demonstrates that the use of a new tripeptide sequence as cleavable linker in the presence of this type of constructs does not impair the binding to the integrin receptor.

3.3.2 Cleavage Experiments in Presence of Elastase and Stability Assays

To evaluate the effective cleavage of the tripeptide linker and the subsequent paclitaxel release in the presence elastase, conjugate **121** was treated with human elastase, and metabolites were detected by HPLC-MS analysis (in collaboration with Nerviano Medical Sciences, Milan). The enzymatic cleavage of the tripeptide linker in compound **121** was observed over a 2 h period, at 37 ºC. First of all, elastase was inactivated in presence of trifluoroacetic acid (TFA), and the intact conjugate **121** was detected as major metabolite, indicating its stability under such conditions (Fig. 39A). In a second experiment, conjugate **121** was subjected to the same conditions, in the presence of activated elastase. In particular, the metabolite analysis of this compound revealed the presence of *N*,*N'*-dimethylethylenediamine spacer-bearing paclitaxel (i.e. compound **142**, "Pro-PTX", Fig 39B) as the main product. Moreover, this result confirms the cleavage of conjugate **121** at valine C-terminus and the release of the drug through the mechanism described in Paragraph 1.4.2 (Scheme 3).

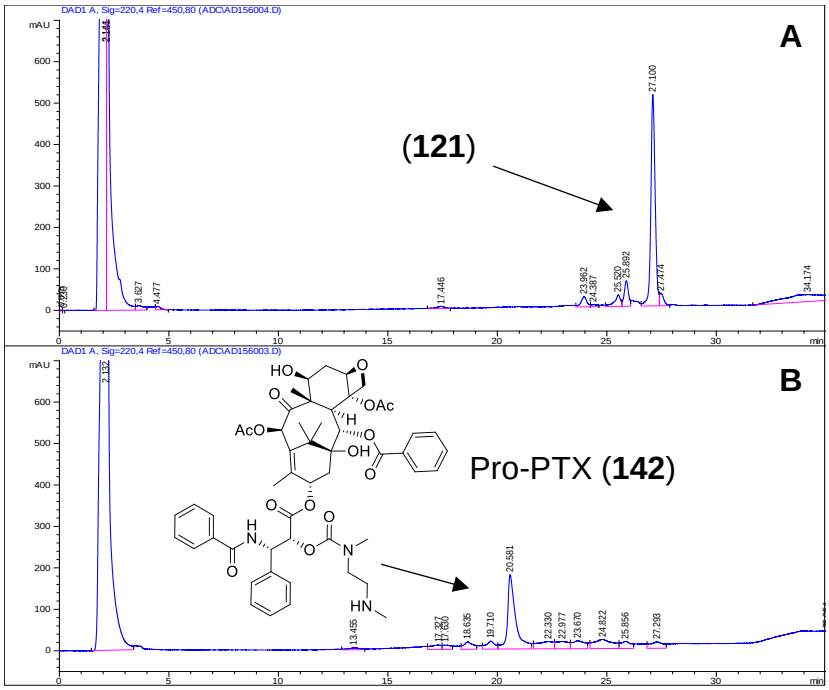

Figure 39. HPLC-MS chromatograms from cleavage experiments of conjugate **121**. A) Analysis of conjugate **121** in presence of inactivated elastase; B) Analysis of conjugate **121** in presence of activated elastase. Signal detected for m/z 968.4 was attributed to compound **142**.

The detection of metabolite **142** is consistent with the drug release mechanism described by Scheeren and co-workers for prodrugs featuring both the dimethylethylenediamino chain and the *p*-aminobenzylcarbamate (PABC) structures: among the two mechanism of self-elimination, the cyclization of the diamine spacer was claimed as the rate-limiting step of the drug release.[172,173]

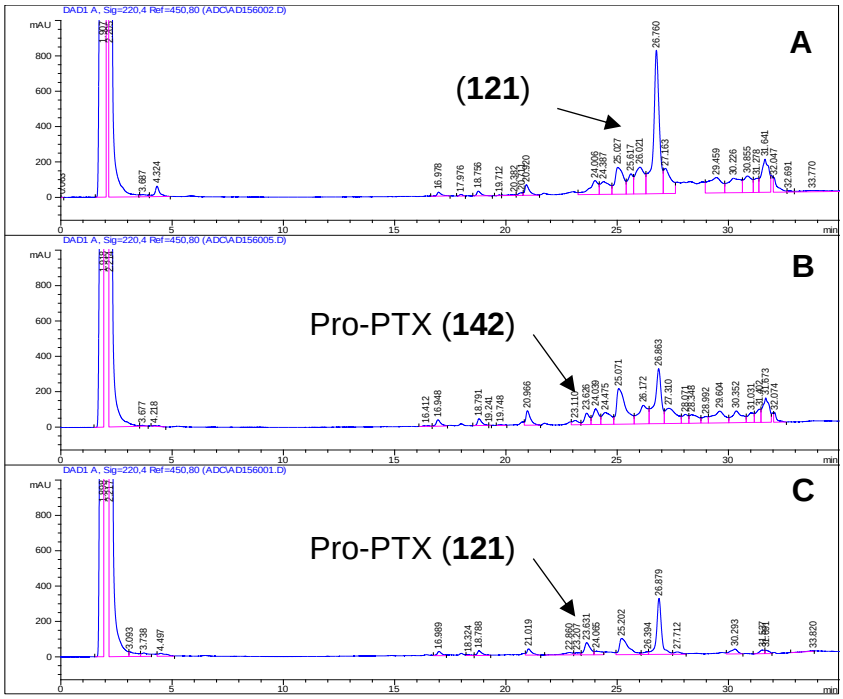

Figure 40. HPLC-MS chromatograms from cleavage experiments of conjugate **121**. A) Analysis of conjugate **121** in presence of inactivated lysosomal extract; B) Lysosomal extract digestion in the presence of cysteine proteases inhibitor (E-64) and; C) Lysosomal extract digestion.

In order to analyze more in detail the selectivity of the linker cleavage, SMDC **121** was treated with lysosomal extract and the cysteine proteases inhibitor E-64 was also included to gain insights into the effector enzymes involved in the cleavage. The effect of protease inhibition, evaluated by HPLC-MS, is shown in Fig. 40. Firstly, lysosomal enzymes were inactivated in presence of TFA (Fig. 40A). Noticeably, SMDC **121** was digested only partially by the lysosomal extract upon 2 hours (Fig. 40C), with conjugate **121** detected as the main species present. 'Pro-PTX' **142** was slightly detectable, which may indicate the presence of lysosomal elastase in the extract.[174] This hypothesis was supported by the observation of metabolite **142** also in the presence of the E-64 inhibitor, (Fig. 40B) indicating that cysteine proteases are not responsible for the cleavage of this linker.

To our delight, these results showed that the tripeptide Asn-Pro-[L]-Val linker is mainly cleaved by elastase and partially digested by other components of the lysosomal extract (e.g. lysosomal elastase or other lysosomal proteases). Conjugates **97** and **123** (i.e. Val-Ala linker and NP-[D]-V at the cleavage site as negative control, respectively) are now being subjected to the same cleavage tests in order to confirm the substrate selectivity of this NP-[L]-V tripeptide.

While these stability tests confirmed the efficacy of the linker system, from these assays it was not possible to gain information on the actual release of the free PTX, as the Pro-PTX **142** was always detected as main metabolite. According to literature data, while in 2015, our research group reported the release of Pro-PTX after enzymatic cleavage,[130] Scheeren and co-workers described the release of free PTX from a similar construct within 47 minutes after proteolysis.[173] To clarify this issue, we set up a model to investigate the kinetic of free PTX release, after cyclization of *N*,*N'*-dimethylethylenediamine spacer and formation of the cyclic urea imidazolidinone.

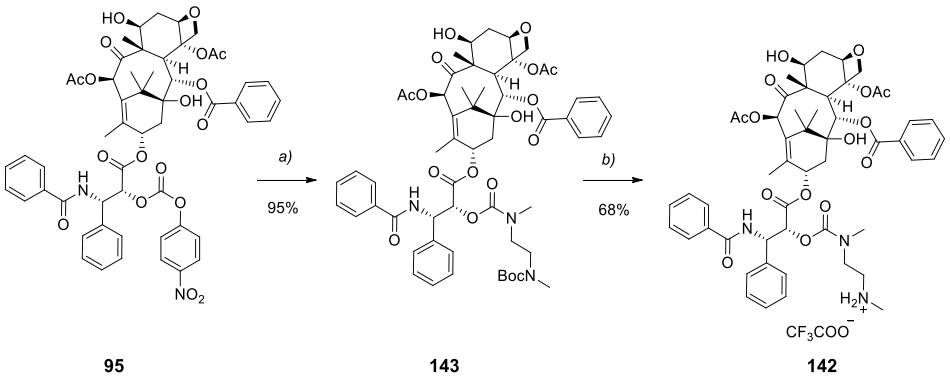

Scheme 14. Synthesis of "Pro-PTX" intermediate (**142**). Reagents and conditions: a) *N*-(Boc)-*N*,*N'*-dimethylethylenediamine, *i*Pr$_2$NEt, DMF (2:1), r.t., overnight; b) TFA/CH_2Cl_2 (1:2), 20 min, 0 ºC.

The synthesis of Pro-PTX **142** is shown in Scheme 14. As mentioned, PTX derivative **95** was synthesized according to previously described protocol by our group.[130] Later on, the

secondary amine of *N*-(Boc)-*N*,*N'*-dimethylethylenediamine **139** was reacted with **95** to yield compound **143** (95% yield). The latter was treated with TFA leading to the TFA salt of **142** in 68% yield, after purification by semi-preparative HPLC and lyophilization.

In order to evaluate the half-life ($t_{1/2}$) of Pro-PTX (**142**), we followed a similar stability assay described by Scheeren and co-workers.[173] In particular, the cyclization of the amine spacer at 37 ºC was measured in a 250 μM DMSO:PBS (1:1) solution at pH 7.5. Aliquots were taken at different time points and analyzed by HPLC, revealing 50% of free PTX release after approximately 8 hours ($t_{1/2(\text{Pro-PTX})}$ ~ 8 h, Fig. 41) - all chromatograms are shown in the Experimental Section.

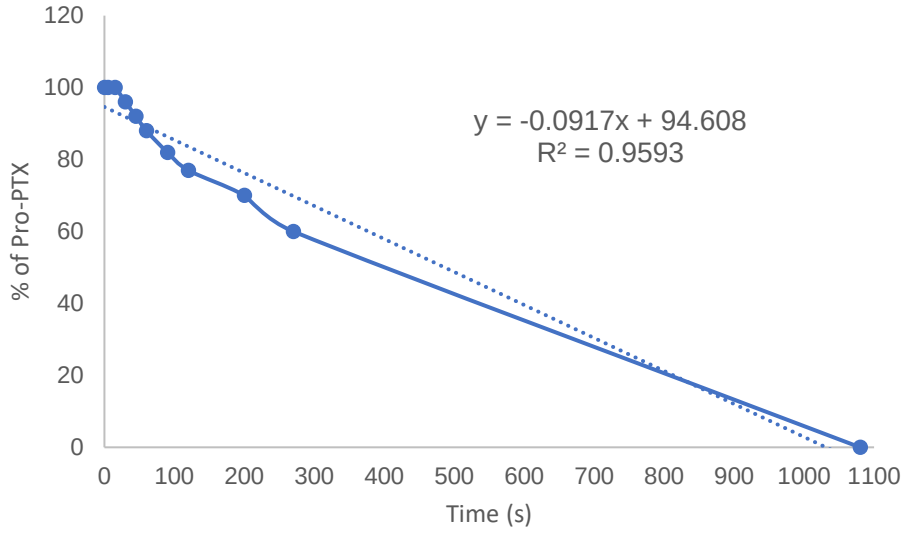

Figure 41. Graphic concerning the linear regression between cyclization of Pro-PTX **142** (Y-axis) over the time (X-axis). The linear equation (y=-0.0917x+94.608) was used to calculate the $t_{1/2}$ when 50% of Pro-PTX is already cyclized.

This result proved that free PTX is released slowly, which may be the cause of the observed loss of cytotoxicity displayed by our RGD-PTX conjugates, as compared to the free drug. However, this analysis contrasts the data shown by Scheeren and co-workers, who observed the release of free PTX after 47 minutes. This discrepancy may be explained by the different concentration of starting Pro-PTX **142** in the experimental conditions, or by the differences in the buffer used to monitor the cyclization reaction.[173]

Additionally, SMDC **121** was tested in 5 μM blank mouse plasma for 24 hours at 37 ºC. Notably, conjugate **121** showed a $t_{1/2}$ in mouse plasma of 35.3 hours (for more details, see Experimental Section). This result indicates that, in case of good *in vitro* antiproliferative assays, SMDC **121** is a promising candidate for *in vivo* studies. As for the chemical stability under different chemical conditions, our group reported that conjugate **77** (i.e. *cyclo*[DKP-RGD]-VA-PTX with

a similar system than **121**) was fully stable after 4-hour incubation in neutral (pH 7.4) and acidic (pH 5.5) buffers.[130]

3.3.3. Cell Proliferation Assays

In a preliminary analysis, *cyclo*[DKP-RGD]-PEG-4-NPV-PTX conjugate **121** was tested *in vitro* for its ability to inhibit the proliferation of 786-O renal cancer cell line in the presence or absence of elastase from human leucocytes. These assays were designed as a model to test the extracellular cleavage of the NPV linker by elastase and to evaluate whether the PTX metabolite can undergo subsequent passive diffusion into the cancer cell and display its anticancer activity. In the absence of elastase, 786-O cell line was incubated with increasing doses of free PTX, Pro-PTX **142** and SMDCs **121**, **123**-**124**. In one experimental set, elastase was added after treatment with PTX, Pro-PTX **142** and SMDCs **121**, **123**-**124**. After 96 hours, the cell viability was analyzed by Envision microplate reader using the CellTiter-Glo luciferase-based ATP detection assay (Table 7).

Table 7. Cytotoxicity assays of conjugates **121**, **123**, **124**, **142** and free PTX in 786-O renal cancer cell line (in presence or absence of elastase).

Cpd	Structure	IC_{50} (nM)[a]	
		ADDED ELASTASE	**–**
121	*cyclo*[DKP-RGD]-PEG-4-NPV-PTX	19.6 ± 4.1	> 5000
123	*cyclo*[DKP-RGD]-PEG-4-NP-[D]-V-PTX	> 5000	> 5000
124	*cyclo* [DKP-RGD]-uncleavable-PTX	> 5000	> 5000
142	Pro-PTX	208.9 ± 133.9	186.4 ± 6.5
20	PTX	35.8 ± 16.7	29.5 ± 7.6

[a] IC_{50} values were calculated as the concentration of compound required for 50% inhibition of cell viability in presence or absence of 50 nM of elastase. 786-O renal cancer cell line was treated with different concentrations of PTX and compounds **121**, **123**, **124**, **142** for 96 hours. The samples were measured in triplicate.

Under these conditions, in the absence of elastase from the cellular media, no activity is shown by SMDC **121** (IC_{50} > 5000 nM) – Table 7. Remarkably, the same SMDC **121** displayed a 256-fold increased activity (IC_{50} = 19.6 ± 4.1 nM), upon addition of elastase (Table 7), whereas the IC_{50} of free PTX was unaffected by the presence of the enzyme (IC_{50} = 29.5 ± 7.6 nM without elastase VS IC_{50} = 35.8 ± 16.7 nM with elastase). Notably, in the presence of elastase, the IC_{50} value of SMDC **121** decreases to a final concentration, comparable to the one of free PTX (IC_{50} = 19.6 ± 4.1 nM VS IC_{50} = 35.8 ± 16.7 nM, respectively), demonstrating the importance of the linker cleavage efficiency for the SMDC potency.

As for the control compounds, conjugates **123** (i.e. featuring a [D]-Val residue at the cleavage site) and **124** (the "uncleavable" version of **121**), showed no antiproliferative activity (IC_{50} > 5000 nM), regardless the presence or the absence of elastase. We were delighted to see that

the presence of [L]-Val at the cleavage site is crucial for the recognition of the tripeptide sequence by elastase and subsequent activity of the conjugate **121**. Moreover, the lack of activity of conjugate **124** further confirmed that the PTX payload is not active when it is not released from the targeting vehicle.

Finally, this experiment showed that Pro-PTX **142** was less active than the free toxin. This is in agreement with the slow cyclization process resulting in the PTX release, which may be even slower in the cell culture medium (this data is not available yet).

Such preliminary *in vitro* data proved that the release of the payload within the tumor stroma can be a valuable tool to raise the potency of our constructs. For this reason, conjugate **121** will be evaluated in *in vivo* anticancer therapy experiments, in order evaluate the payload accumulation at the tumor site mediated by the *cyclo*[DKP-RGD] ligand.

3.4. Results and Discussion

These preliminary results demonstrate that the approach used by SMDC **121**, relying in the extracellular release of the payload, can be more effective than the design of internalizing RGD-drug conjugates. Also in this case, the linker turned out to play a fundamental role for drug activity. In particular, the peptide sequence should be a preferential substrate of an extracellular enzyme, whose expression in the targeted tissue has to be validated.

The elastase-specific NPV linker was selected and evaluated in this Chapter. First of all, the binding ability to the purified $\alpha_v\beta_3$ integrin of the new RGD-PTX conjugates **121**, **123** and **124** was found to be comparable to the one of the free ligand **69** and of SMDCs developed in Chapter II (**97** and **102**-**105**).

Moreover, we observed that in the presence of elastase, the SMDC **121** is fully converted to the intermediate Pro-PTX **142** within 2 hours (Fig. 39B), confirming the two-step mechanism of PTX release described by Scheeren and co-workers.[173] In particular, we demonstrated that the NPV linker is cleaved by human elastase at the C-terminus, releasing the intermediate **144** (Fig. 42). The latter undergoes a fast 1,6-elimination of the aromatic *p*-aminobenzylcarbamate (PABC) spacer, leading to the formation of the metabolite Pro-PTX **142** (Fig. 42). Moreover, our cleavage experiments confirm that the cyclization of the diamine spacer is actually the rate-limiting step of the drug release.

While literature data indicate that the intermediate results in PTX release with a half-life of 47 min,[173] we observed release of free PTX within ~8 hours in a DMSO:PBS (1:1) mixture at physiological pH and temperature (i.e. pH 7.4 and 37 ºC, respectively).

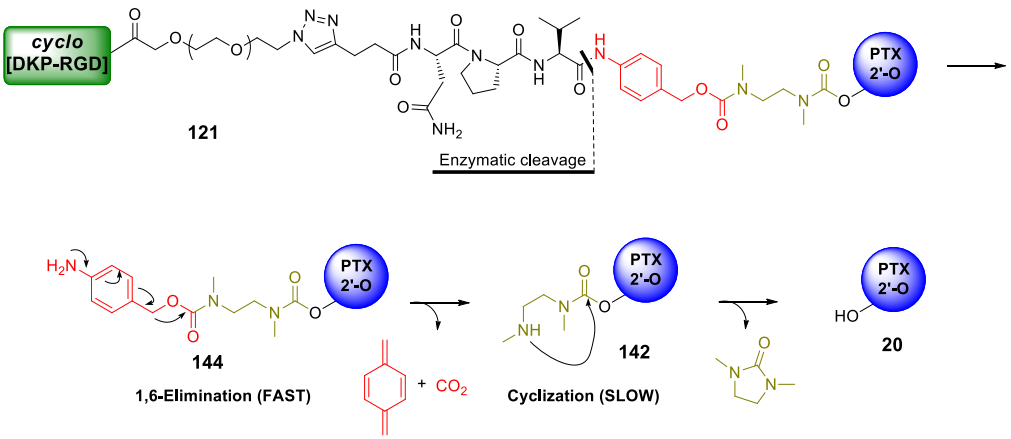

Figure 42. Enzymatic cleavage of conjugate **121** leading to the release of free paclitaxel.

Cell antiproliferative studies were performed in the absence or presence of elastase, aimed at the evaluation of SMDC **121** activity triggered by the enzyme in the cell medium. In the absence of elastase, no potency is shown by SMDC **121** (IC_{50} > 5000 nM) – Table 7. Remarkably, the same SMDC **121** displayed a 256-fold increased activity of (IC_{50} = 19.6 ± 4.1 nM) upon addition of elastase (Table 7). Remarkably, negative controls **123** and **124** showed to be inactive in presence or absence of elastase (IC_{50} > 5000 nM), proving the importance of the NPV linker in this system. This *in vitro* model experiment was already described for similar SMDCs: 1) Papot and co-workers incubated a SMDC with the targeted effector enzyme (i.e. β-Glucuronidase), observing a dramatic decrease of the IC_{50} values;[175] 2) Oliff and co-workers prepared a MMP-2 cleavable prodrug, which was treated with the protease and then added to the cell medium, unveiling the effect of the active metabolite.[176]

However, Pro-PTX **142** proved generally less potent than the free PTX toxin. While this is ascribed to the slow cyclization of the spacer, it is conceivable that the presence of a secondary amine moiety influences also on the ability of Pro-PTX to penetrate the cell membrane, eventually affecting the biological activity.[177] Overall, these data possibly indicate that PTX payload is not the best candidate for extracellular delivery, while this approach may be more attractive when the toxin is linked to the SMDC through a fast-eliminating spacer. For instance, compounds bearing an amino moiety (e.g. doxorubicin, dolastatin analogs, pyrrolobenzodiazepines etc.) could be considered for this application.

Finally, the selective release of payloads within the tumor microenvironment is gaining much interest in this field. Giving strength to this strategy, Neri and co-workers have been demonstrating that non-internalizing mAbs bearing an intracellularly-cleavable linker (e.g. Val-Cit and Val-Ala), can release the payload within the tumor stroma, observing therapeutic effects in mice.[178] Furthermore, this strategy has also been exploited for SMDCs bearing linkers as substrates of different extracellular tumor-associated enzymes: 1) Matrix Metalloproteinases-2 and -9,[117,176,179] 2) β-Galactosidase[21], 3) β-Glucuronidase,[175] and 4) Elastase.[171]

Chapter IV

cyclo[DKP-RGD]-MMAE/MMAF conjugates bearing Lysosomally and Extracellularly-Cleavable Linkers

cyclo[DKP-RGD]-MMAE/MMAF conjugates bearing Lysosomally and Extracellularly-Cleavable Linkers

4.1 Introduction

The research activity described so far has consisted in the development of *cyclo*[DKP-RGD]-PTX conjugates, showing remarkable results in terms of synthetic accessibility, affinity for $\alpha_v\beta_3$ integrin, stability and solubility properties. However, the biological evaluation of the *cyclo*[DKP-RGD]-VA-PTX (**77**) and *cyclo*[DKP-RGD]-PEG-4-VA-PTX (**97**) highlighted some important weaknesses of these compounds. As discussed in Chapter II and III, although conjugates **77** and **97** displayed promising targeting ability skills (TI = 39 - 533), the low potency showed by these conjugates in cell antiproliferative assays against $\alpha_v\beta_3$+/$\alpha_v\beta_3$− cells, represents a major drawback. These findings prompted the development of the extracellularly-cleavable SMDC *cyclo*[DKP-RGD]-PEG-4-NPV-PTX (**121**), which showed promising results in terms of PTX release in the proximity of tumor cells and subsequent passive drug uptake. In addition, the cell-antiproliferative properties of proper control compounds (i.e. uncleavable SMDCs **123** and **124**, see Chapter III) were evaluated, showing no activity in the presence of elastase.

While therapy studies on conjugate **121** will give important information about the feasibility of extracellular-cleavable linkers in our technology, the use of highly potent payloads represents a “more traditional” approach to increase the potency of targeted prodrugs. Accordingly, this Chapter focuses on the design of new *cyclo*[DKP-RGD]-auristatin conjugates. In particular, whereas PTX (**20**, Fig. 2, Chapter I) is still sold as first-line treatment of different types of cancer, the use of more potent tubulin poisons, such as maytansinoids and auristatins, was found to be the key for the clinical success of antibody-drug conjugates.[180] In particular, auristatins are synthetic peptide-like cytotoxic agents belonging to the family of dolastatins. Dolastatin 10 (**25**, Fig. 3, Chapter I) was the most cytotoxic component of a mixture extracted from cyanobacteria *Symploca hydnoides* and *Lyngbya majuscula*.[181] This compound entered phase I clinical trials in the 1990s[182] and successfully progressed to phase II trials. However,

these clinical trials were later stopped, as the drug exhibited insufficient activity and severe side effects when used as single agent.[183] Auristatins are synthetic analogs of dolastatin 10, lacking a thiazole ring and containing a terminal benzylamine moiety (Fig. 3, Chapter I).[184] These compounds act as potent microtubule-destabilizing agents, leading to apoptosis in dividing cells. Monomethyl auristatin-E (MMAE **29**, Fig. 3) and monomethyl auristatin-F (MMAF **26**, Fig. 3) are fully synthetic drugs, selected from SAR (structure-activity relationship) studies and then derivatized for their use as payloads in ADCs and SMDCs products. Designed to be exclusively used as payload for internalizing ADCs, MMAF differs from MMAE by the presence of a phenylalanine residue at the C-terminus. This structural modification substantially increases the hydrophilicity and thus reducing the membrane permeability, limiting off-target toxicities. Indeed, MMAE and MMAF were demonstrated to be similarly potent (IC_{50} in the subnanomolar range) when released intracellularly by ADCs.[185] On the other hand, such drugs display very different cytotoxicity properties when added, in the unconjugated form, to tumor cells. While MMAE still displays subnanomolar activity, MMAF shows submicromolar activity, as a result of its altered membrane permeability.[186,187]

Attracted by the unique structural and biological features of the payload pair MMAE/MMAF, we designed *cyclo*[DKP-RGD]-MMAE/MMAF conjugates bearing the lysosomally-cleavable linker Val-Ala (SMDCs **145** and **146**, Fig. 43) and their respective negative controls (**147**-**149**, Fig. 43). Compound **147** (with MMAE), devoid of the *cyclo*[DKP-RGD] ligand, was designed as negative control of **145** to evaluate the targeting ability of the RGD homing device.

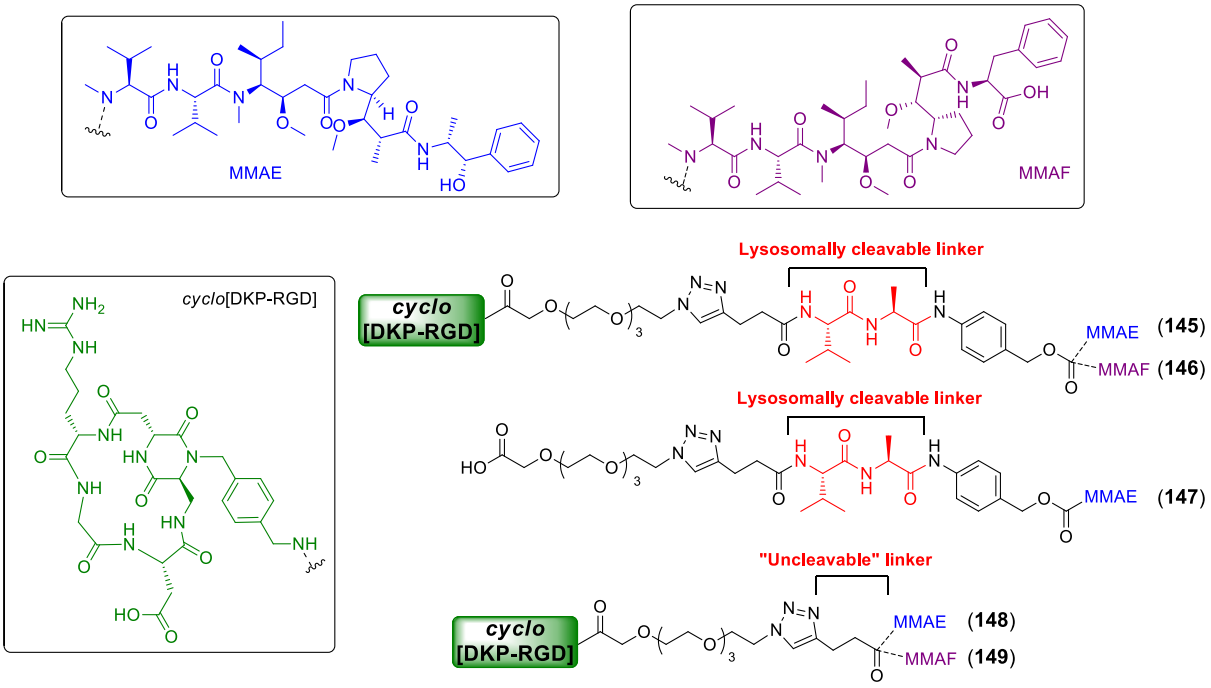

Figure 43. Molecular structures of designed lysosomally-cleavable *cyclo*[DKP-RGD]-PEG-4-VA-MMAE/MMAF conjugates (**145**-**146**) and their relative control compounds (**147** and **148**-**149**).

Given the poor internalization properties of the free payload MMAF, a RGD-lacking control compound relative to the *cyclo*[DKP-RGD]-MMAF conjugate **146**, was considered unnecessary and it was not prepared. SMDCs **148** and **149** represent the uncleavable versions of **145** and **146** (Fig. 43), respectively, and they were designed as reference for the evaluation of the antiproliferative performance of the cleavable conjugates.

Within this frame, another *cyclo*[DKP-RGD]-MMAE conjugate was prepared, endowed with the extracellularly-cleavable linker Asn-Pro-Val (SMDC **150**, Fig. 44). This compound represents a structural optimization of PTX-containing SMDC **121** described in Chapter III. This new conjugate represents an excellent candidate for *in vivo* applications, since MMAE has shown excellent antitumor properties, also when released in the extracellular tumor environment.[178,187]

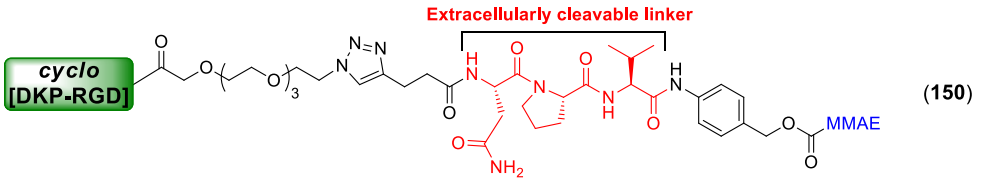

Figure 44. Molecular structure of the designed *cyclo*[DKP-RGD]-PEG-4-NPV-MMAE **150** conjugate. Structures of *cyclo*[DKP-RGD] and MMAE can be seen in Figure 43.

4.2. Synthesis of cyclo[DKP-RGD]-PEG-4-VA-MMAE Conjugate bearing a Lysosomally-Cleavable Linker

The *cyclo*[DKP-RGD] peptidomimetic was linked to MMAE via a self-immolative spacer, a cathepsin B-cleavable dipeptide linker (Val-Ala), a triazole linkage and a PEG-4 spacer, leading to SMDC **145** (Fig. 43). The secondary amine at the N-terminus of MMAE drug was used as anchoring point for the linker: this choice resulted in the formation of a stable carbamate bond between the drug and a *p*-aminobenzyl alcohol self-immolative spacer (Fig. 43). Unlike the PTX conjugates described in the previous Chapters, this layout allows the release of MMAE upon a single and fast 1,6-elimination step, avoiding the slow cyclization of the diamine spacer (the detailed mechanism is depicted in Fig. 42 on Chapter III). In analogy to the previous RGD-PTX conjugates described in Chapter II and III, the formation of a triazole ring between the linker-drug module and the ligand was chosen as the last conjugation step: this chemoselective methodology does not require specific protecting groups at the amino acid side chains and it is adaptable to several linker-drug combinations.

The synthesis of the *cyclo*[DKP-RGD]-PEG-4-VA-MMAE **145** is shown in Scheme 15. Similarly to what described by or group for SMDC **77**,[130] the Val-Ala dipeptide was coupled to *p*-aminobenzyl alcohol (**151**). The fast deprotection of the valine residue, followed by coupling

with 4-pentynoic acid, afforded the terminal alkyne-functionalized compound **152**. The latter was activated as 4-nitrophenyl carbonate (Scheme 15, compound **153**). MMAE was attached to the linker by reaction of its secondary amine with electrophile **153**, leading to carbamate **154**. The final conjugate **145** was obtained after copper-catalyzed azide-alkyne cycloaddition (CuAAC) between alkyne **154** and *cyclo*[DKP-RGD]-PEG-4-N_3 **86**, whose synthesis is described in Chapter II (Scheme 4). The latter reaction was also used to produce control compound **147** (devoid of the targeting ligand) by reacting alkyne **154** and HOOC-PEG-4-N_3 **91** (Scheme 4, Chapter II) through the same CuAAC "click reaction" (Scheme 15). Both products (**145** and **147**) were then purified by semi-preparative HPLC and lyophilized.

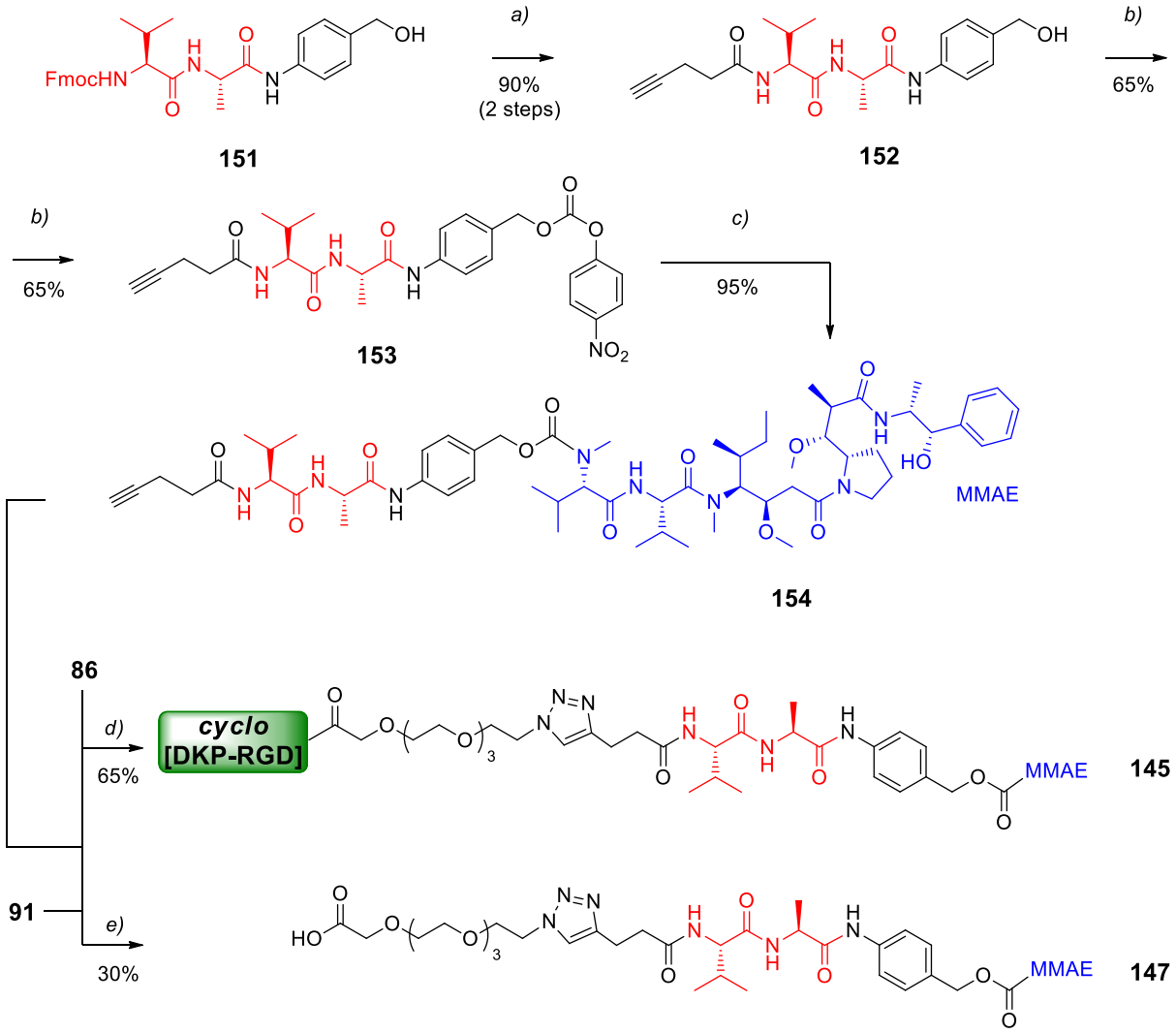

Scheme 15. Synthesis of *cyclo*[DKP-RGD]-PEG-4-VA-MMAE conjugate (**145**) and HOOC-PEG-4-VA-MMAE (**147**). Reagents and conditions: a) 1) piperidine, DMF, r.t., 2 h; 2) 4-pentynoic acid, HATU, HOAt, *i*Pr_2NEt, DMF, r.t., overnight; b) 4-nitrophenyl chloroformate, pyridine, r.t., THF, 2 h, c) MMAE, HOBt, *i*Pr_2NEt, r.t., DMF:pyridine (4:1), over-weekend; d) *cyclo*[DKP-RGD]-PEG-4-N_3 (**86**), $CuSO_4 \cdot 5H_2O$, NaAsc, DMF/H_2O (1:1), 35 ºC, overnight; e) HOOC-PEG-4-N_3 (**91**), $CuSO_4 \cdot 5H_2O$, NaAsc, DMF/H_2O (1:1), 35 ºC, overnight.

In addition to compounds **145** and **147**, a third conjugate (compound **148**, Fig 43) was prepared, in which the cleavable linker moiety (Val-Ala) is replaced by a tertiary amide bond.

Similarly to conjugate **124** (Chapter III, Fig.38), the synthesis of the RGD-MMAE conjugate featuring the "uncleavable" linker (**148**) is reported in Scheme 16.

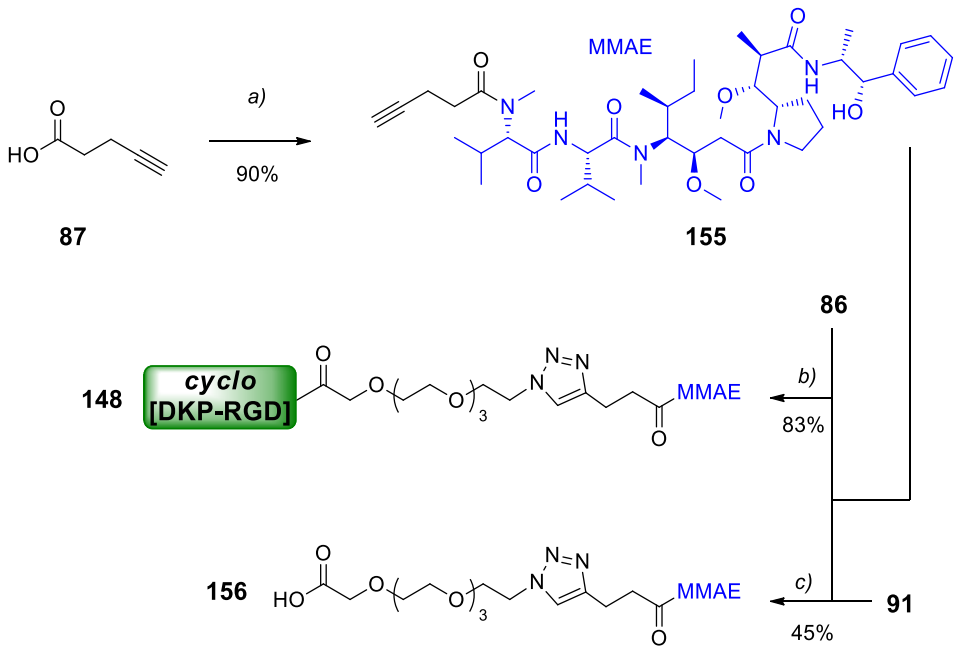

Scheme 16. Synthesis of *cyclo*[DKP-RGD]-Uncleavable-MMAE conjugate (**148**) and HOOC-Uncleavable-MMAE (**156**). Reagents and conditions: a) MMAE, HATU, HOAt, *i*Pr$_2$NEt, DMF, r.t., overnight; b) *cyclo*[DKP-RGD]-PEG-4-N$_3$ (**86**), CuSO$_4$·5H$_2$O, NaAsc, DMF/H$_2$O (1:1), 35 ºC, overnight; e) HOOC-PEG-4-N$_3$ (**91**), CuSO$_4$·5H$_2$O, NaAsc, DMF/H$_2$O (1:1), 35 ºC, overnight.

Herein, 4-pentynoic **87** acid was reacted with the secondary amine of MMAE affording tertiary amide **155**. Also in this case, a final CuAAC afforded *cyclo*[DKP-RGD]-uncleavable-MMAE (**148**). Finally, compound **156** was also prepared, consisting in an analog compound of uncleavable conjugate **148**, devoid of the targeting unit. This exhaustive panel of SMDC compounds and relative controls would facilitate the rationalization of *in vitro* data, providing important information for the determination of the mechanism of action of our RGD-MMAE conjugates.

4.3. Synthesis of cyclo[DKP-RGD]-PEG-4-VA-MMAF Conjugates bearing a Lysosomally-Cleavable Linker

As previously mentioned, another group of compounds was prepared, being structurally similar to *cyclo*[DKP-RGD]-MMAE-containing conjugates (**145** and **148**, Fig. 43), but possessing the MMAF cytotoxic payload (**146** and **149**, Fig. 43).[185]

According to the synthetic pathway used for the development of *cyclo*[DKP-RGD]-MMAE-containing conjugates, *cyclo*[DKP-RGD]-MMAF conjugates (**146** and **149**) were synthesized as it is described in Schemes 17 and 18.

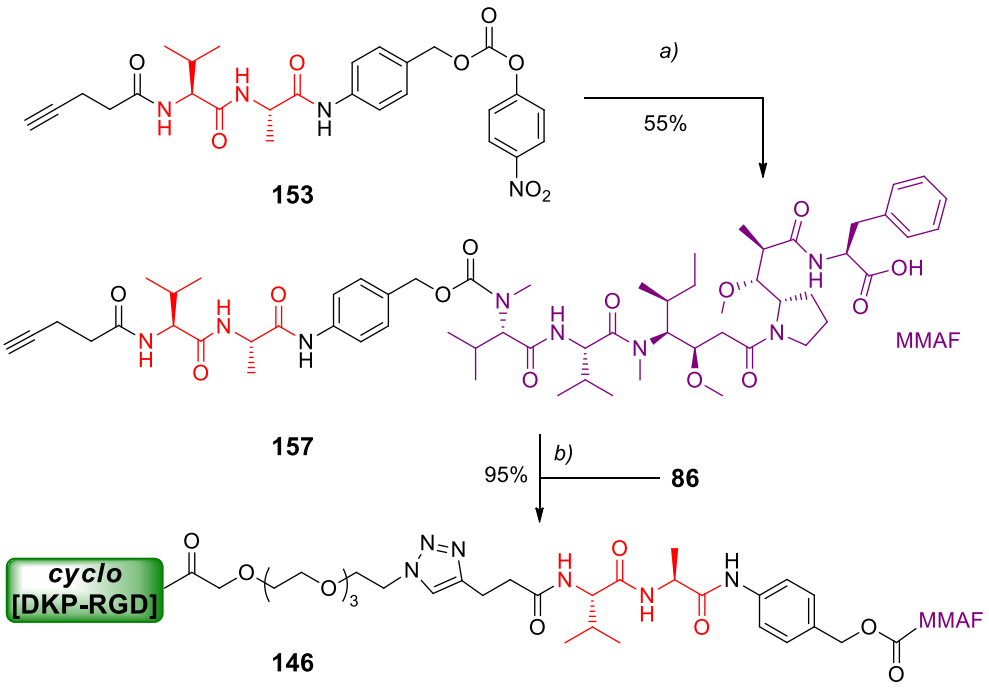

Scheme 17. Synthesis of *cyclo*[DKP-RGD]-PEG-4-VA-MMAF conjugate (**146**). Reagents and conditions: a) MMAF·TFA, HOBt, *i*Pr$_2$NEt, r.t., DMF:pyridine (4:1), over-weekend; b) *cyclo*[DKP-RGD]-PEG-4-N$_3$ **86**, $CuSO_4 \cdot 5H_2O$, NaAsc, DMF/H_2O (1:1), 35 ºC, overnight.

Likewise, the synthesis of *cyclo*[DKP-RGD]-PEG-4-VA-MMAE (**145**) was performed following the same pathway for the development of *cyclo*[DKP-RGD]-PEG-4-VA-MMAF (**146**). Carbamate **157** was prepared reacting carbonate **153** with the commercial TFA salt of MMAF, in the presence of 1-Hydroxybenzotriazole (HOBt) and excess of base. The resulting alkyne was reacted with azide **86** through the same CuAAC "click reaction" to give the final conjugate **146**, after purification by semi-preparative HPLC and lyophilization.

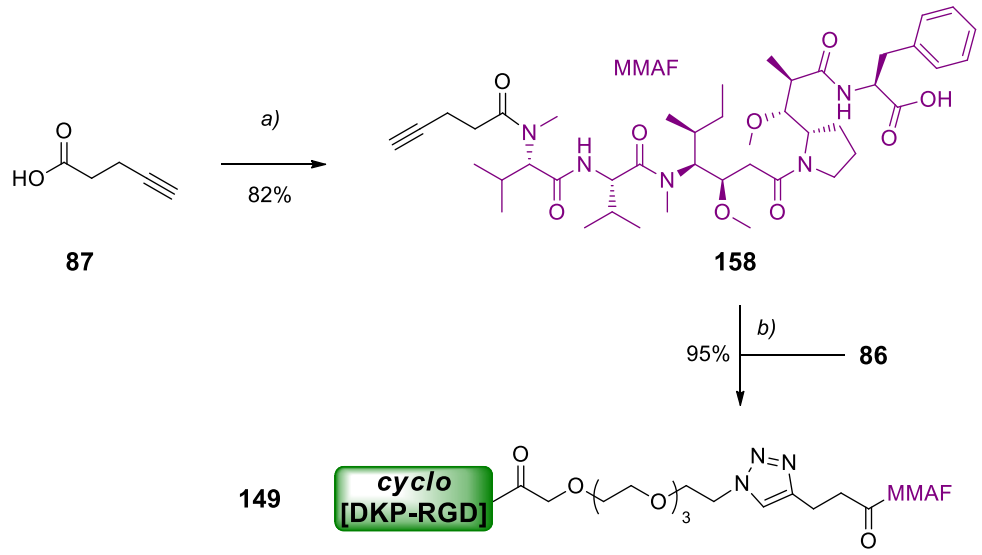

Scheme 18. Synthesis of *cyclo*[DKP-RGD]-Uncleavable-MMAF (**149**) conjugate. Reagents and conditions: a) MMAF·TFA, HATU, HOAt, *i*Pr$_2$NEt, DMF, r.t., overnight; b) *cyclo*[DKP-RGD]-PEG-4-N$_3$ **86**, $CuSO_4 \cdot 5H_2O$, NaAsc, DMF/H_2O (1:1), 35 ºC, overnight.

Furthermore, the synthesis of the uncleavable conjugate *cyclo*[DKP-RGD]-uncleavable-MMAF (**149**, Scheme 18) was performed in analogy to the one used for *cyclo*[DKP-RGD]-uncleavable-MMAE (**148**, Scheme 15). Conjugate **149** was successfully synthesized, purified by semi-preparative HPLC and freeze-dried.

4.4. Synthesis of cyclo[DKP-RGD]-PEG-4-NPV-MMAE Conjugate bearing an Extracellularly-Cleavable Linker

Conjugate **150** (Scheme 19) carrying the elastase-cleavable linker Asn-Pro-Val (NPV) represents an analog of conjugate **121** (Chapter III). Here, the $\alpha_v\beta_3$ integrin ligand *cyclo*[DKP-RGD] is connected to MMAE via a self-immolative spacer, an elastase-cleavable tripeptide linker (Asn-Pro-Val), a triazole linkage and a PEG-4 spacer. The synthesis of conjugate **150** is reported in Scheme 19.

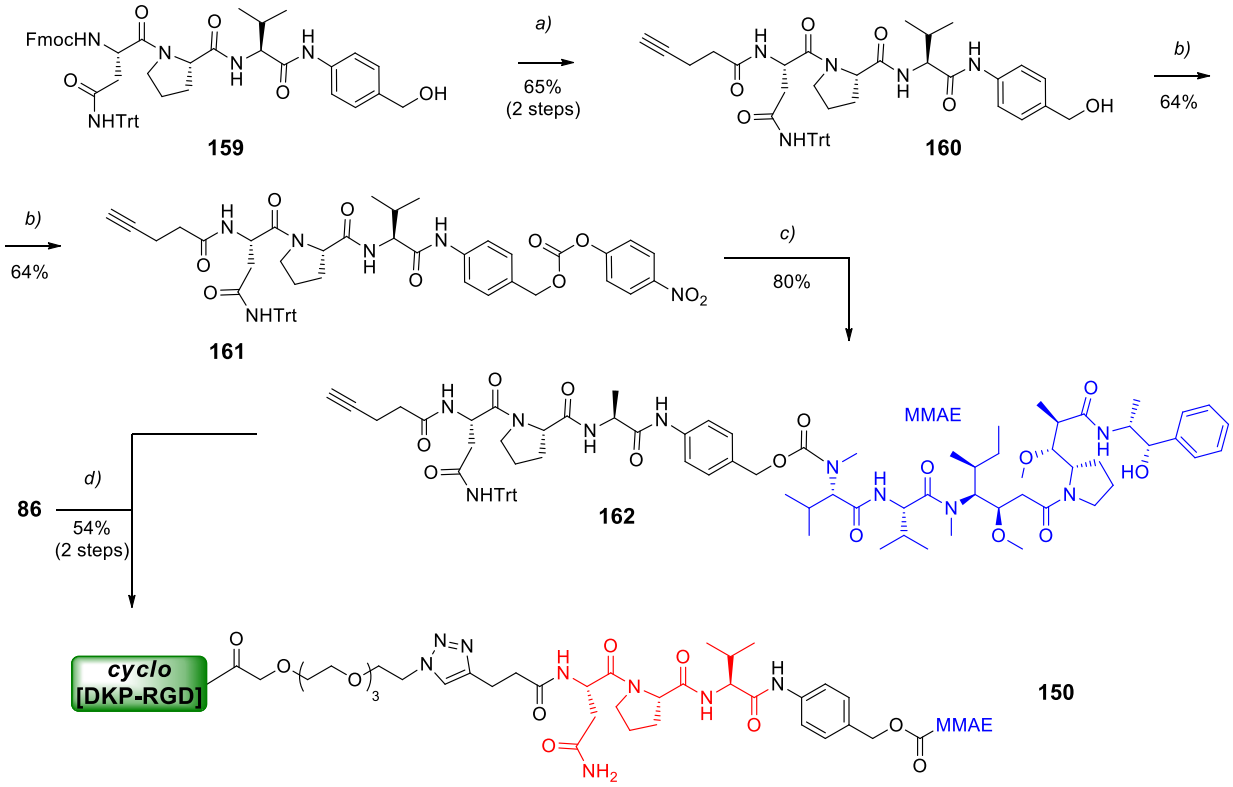

Scheme 19. Synthesis of *cyclo*[DKP-RGD]-PEG-4-NPV-MMAE (**150**). Reagents and conditions: a) 1) piperidine, DMF, r.t., 2 h; 2) 4-pentynoic acid, HATU, HOAt, *i*Pr$_2$NEt, DMF, r.t., overnight; b) 4-nitrophenyl chloroformate, pyridine, r.t., THF, 2 h; c) MMAE, HOBt, DIPEA, RT, DMF:pyridine (4:1), over-weekend; d) 1) TFA, Et$_3$SiH, CH$_2$Cl$_2$, r.t., 45'; 2) *cyclo*[DKP-RGD]-PEG-4-N$_3$ **86**, CuSO$_4$·5H$_2$O, NaAsc, DMF/H$_2$O (1:1), 35 ºC, overnight.

Intermediate **159**, previously synthesized for the development of conjugate **121**, was Fmoc-deprotected in the presence of piperidine and the resulting amine was treated with 4-pentynoic acid, leading to amide **160**. The latter was converted into the corresponding 4-nitrophenyl carbonate (**161**) and reacted with commercial MMAE, leading to carbamate **162.** Finally,

conjugate *cyclo*[DKP-RGD]-PEG-4-NPV-MMAE **150** was isolated after CuAAC reaction with *cyclo*[DKP-RGD]-PEG-4-N_3 **86**.

4.5. In vitro Biological Evaluation

4.5.1. Integrin Receptor Competitive Binding Assays

Also in this case, the newly synthesized *cyclo*[DKP-RGD]-MMAE/MMAF **145**, **148**, **146** and **149** conjugates were evaluated in competitive assays for the binding to the purified $\alpha_v\beta_3$ integrin, in the presence of biotinylated vitronectin. The IC_{50} values obtained are shown in Table 8.

Table 8. Inhibition of biotinylated vitronectin binding to isolated $\alpha_v\beta_3$ receptor.

Cpd	Structure	$\alpha_v\beta_3$ IC_{50} [nM][a]
145	*cyclo*[DKP-RGD]-PEG-4-VA-MMAE	58.5 ± 10.5
147	HOOC-PEG-4-VA-MMAE	3200 ± 2.4
148	*cyclo*[DKP-RGD]-Uncleavable-MMAE	40.0 ± 16.1
156	HOOC-Uncleavable-MMAE	> 10000
146	*cyclo*[DKP-RGD]-PEG-4-VA-MMAF	57.9 ± 17.9
149	*cyclo*[DKP-RGD]-Uncleavable-MMAF	30.3 ± 7.4

In the same frame to the SMDCs described in the previous Chapters, the results showed that despite their remarkable steric bulk, the conjugates' affinity for the purified $\alpha_v\beta_3$ receptor is comparable to that of the free ligand **69**. Remarkably, the high affinity observed towards the $\alpha_v\beta_3$ receptor (IC_{50} = 30.3-58.5 nM), demonstrates that the use of a new tripeptide sequence as cleavable linker in the presence of this type of constructs does not impair the binding to the integrin receptor. In addition, compounds **147** and **156** (devoid of the targeting ligand) did not show binding affinity to the isolated $\alpha_v\beta_3$ receptor (IC_{50} values in the micromolar range), proving the importance of the *cyclo*[DKP-RGD] targeting ligand for the binding avidity to $\alpha_v\beta_3$ integrin.

4.5.2. Cell Proliferation Assays

Preliminary cytotoxicity assays were performed in collaboration with Italfarmaco, Milan (Dr. Christian Steinkühler and Msc. Ana Martins). These assays were carried out in parallel with other four conjugates (**163**-**166**) synthesized by Prof. Umberto Piarulli's research group (University of Insubria, Como - Italy), bearing the *cyclo*[DKP-*iso*DGR] integrin ligand (Fig. 45). Such ligand was developed as analog of the well-known RGD-bearing peptidomimetics, in which the RGD sequence is substituted with an isoaspartate-glycine-arginine tripeptide (*iso*DGR). The latter is also recognized by integrins and the *cyclo*[DKP-*iso*DGR] was found to bind $\alpha_V\beta_3$ receptor with low nanomolar affinity.[133] The resulting *cyclo*[DKP-*iso*DGR]-MMAE/MMAF conjugates were structurally similar to the RGD-bearing analogs **145**-**146** and **148**-**149**. In particular, the ligand and the MMAE/MMAF cytotoxic payloads were connected through either a Val-Ala dipeptide or an uncleavable nonpeptide linker (in compound **163**-**164** and **165**-**166**, respectively) – Figure 45.

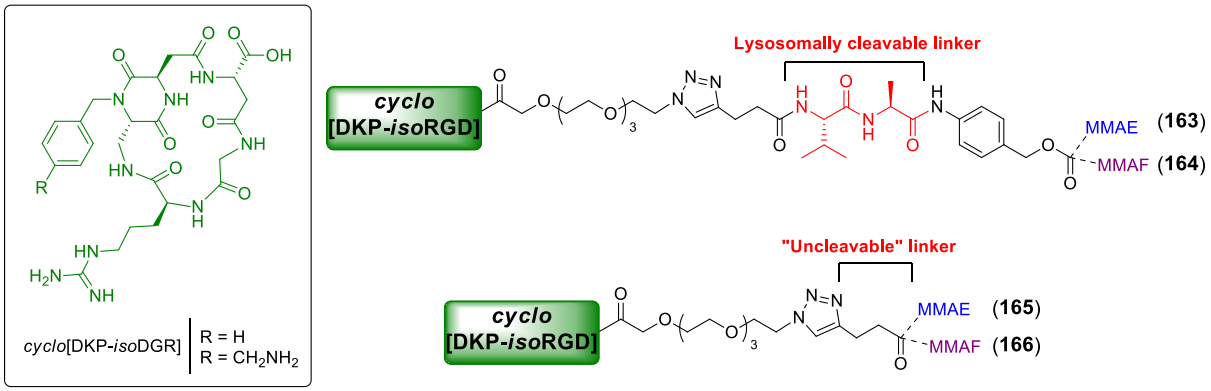

Figure 45. Structures of *cyclo*[DKP-*iso*DGR]-PEG-4-VA-MMAE (**163**), *cyclo*[DKP-*iso*DGR]-PEG-4-VA-MMAF (**164**), *cyclo*[DKP-*iso*DGR]-Uncleavable-MMAE (**165**) and *cyclo*[DKP-*iso*DGR]-Uncleavable-MMAF (**166**).

All synthesized compounds have been tested against $\alpha_v\beta_3$-expressing cell line (human glioblastoma cell line U87). In this experiment, $\alpha_v\beta_3$-negative cells were not included, in order to gain information on the integrin-targeting ability of (RGD / *iso*DGR)-MMAE/MMAF conjugates by comparing their anticancer activity with the one of their relative control compounds (devoid of the targeting ligand) against the same cancer cells.

In a first set of experiments, cells were incubated with increasing doses of free MMAE (**29**) and MMAE-containing compounds (**145**, **147**-**148**, **156**, **163** and **165**). After 72 hours, the cell viability was analyzed by MTT assay.

The measured IC_{50} values are shown in Table 9.

Table 9. Cytotoxicity assays of compounds **145**, **147**-**148**, **156**, **163** and **165** and free MMAE in U87 cell line.

Cpd	Structure	IC_{50} (nM)[a] U87 ($\alpha_v\beta_3$ +)
29	MMAE	0.076 ± 0.08
145	*cyclo*[DKP-RGD]-PEG-4-VA-MMAE	38.99 ± 0.11
147	HOOC-PEG-4-VA-MMAE	77.32 ± 0.07
148	*cyclo*[DKP-RGD]-Uncleavable-MMAE	571.80 ± 0.21
156	HOOC-Uncleavable-MMAE	> 10000
163	*cyclo*[DKP-*iso*DGR]-PEG-4-VA-MMAE	11.50 ± 0.13
165	*cyclo*[DKP-*iso*DGR]-Uncleavable-MMAE	685.50 ± 0.08

[a] IC_{50} values were calculated as the concentration of compound required for 50% inhibition of cell viability. U87 cell line was treated with different concentrations of MMAE and compounds **145**, **147**-**148**, **156**, **163** and **165** for 72 hours. The samples were measured in triplicate.

From these first set of *in vitro* assays arose that lysosomally-cleavable *cyclo*[DKP-RGD]-PEG-4-VA-MMAE (**145**) and *cyclo*[DKP-*iso*DGR]-PEG-4-VA-MMAE (**163**) conjugates show IC_{50} values 2-3 order of magnitude (100-1000) higher than MMAE **29**, Table 9. This could be ascribed by a non-efficient $\alpha_V\beta_3$-mediated endocytosis process. However, this test revealed the high absolute potency of conjugates **145** and **163** against U87 cells (IC_{50} in the low nanomolar range), resulting much more effective than its analog *cyclo*[DKP-RGD]-PEG-4-VA-PTX conjugate **97**, described in Chapter II. This expected result proved that the use of more potent cytotoxic payloads also increases the potency of the SMDC constructs, and conjugates **145** and **163** can be now considered a promising compound for further tests.

As for the control compounds, conjugates **148** and **165**, bearing an uncleavable linker, showed IC_{50} values 4 order of magnitude (~10000) higher than MMAE (IC_{50} = 571.80 nM and 685.50 nM, respectively), proving that the payload is not active when it is not released from the targeting vehicle. Furthermore, it can be observed that the absence of targeting ligand (**147**) led to a slightly less potent construct than conjugates **145** and **163** (IC_{50} = 77.32 nM VS IC_{50} = 38.99 nM and 11.50 nM, respectively). The high lipophilicity of compound **147** (especially when compared to **145** and **163**) may account for its significant anticancer activity: indeed, this compound may behave as a "non-targeted" prodrug, capable of penetrating the cell by passive diffusion and undergo intracellular linker cleavage. A more representative control compound is now being developed by our group (e.g. a cyclopeptide bearing the Arg-Ala-Asp "non-targeting" sequence or a more hydrophilic spacer such as peptidoglycan-based structure, see Figure 10 in Chapter I), in order to minimize non-specific internalization of the prodrug.

Later on, cells were incubated with increasing doses of free MMAF and conjugates (**146**, **149**, **164** and **166**). After 72 hours, the cell viability was analyzed by MTT assay.

The measured IC_{50} values are shown in Table 10.

Table 10. Cytotoxicity assays of compounds **146**, **149**, **164**, **166** and free MMAF in U87 cell line.

Cpd	Structure	IC_{50} (nM)[a] U87 ($\alpha_v\beta_3$ +)
26	MMAF	94.40 ± 0.06
146	*cyclo*[DKP-RGD]-PEG-4-VA-MMAF	385.90 ± 0.09
149	*cyclo*[DKP-RGD]-Uncleavable-MMAF	> 10000
164	*cyclo*[DKP-*iso*DGR]-PEG-4-VA-MMAF	165.90 ± 0.05
166	*cyclo*[DKP-*iso*DGR]-Uncleavable-MMAF	763.70 ± 0.08

[a] IC_{50} values were calculated as the concentration of compound required for 50% inhibition of cell viability. U87 cell line was treated with different concentrations of MMAF and compounds **146**, **149**, **164**, **166** for 72 hours. The samples were measured in triplicate.

Since free MMAF shows weak membrane diffusion properties, internalizing ligands would increase its anticancer activity. However, from the results presented in Table 10, it can be observed that the conjugates displayed reduced cytotoxicity when compared with the free drug MMAF, which can be ascribed to a non-efficient $\alpha_V\beta_3$-mediated endocytosis process. In particular, cleavable MMAF-conjugates (**146** and **164**) show IC_{50} values 2-4 times higher than MMAF, by means that there is no advantage with the conjugation. Finally, the *cyclo*[DKP-*iso*DGR]-PEG-4-VA-MMAF (**164**) conjugate proved slightly more potent (ca. 2 times) than the *cyclo*[DKP-RGD]-PEG-4-VA-MMAF (**146**), which may indicate that the internalization of the *iso*DGR could be more pronounced.

Additional *in vitro* cytotoxicity assays with MMAE-containing conjugates are now being handled in presence of an $\alpha_v\beta_3$-negative cell line, in order to gain insights into the targeting performance of these constructs.

Finally, the biological evaluation of conjugate *cyclo*[DKP-RGD]-PEG-4-NPV-MMAE (**145**), bearing the elastase-cleavable linker NPV, is still in progress.

Hopefully, with all data in our hands, it will be possible to rationalize the mechanism of action of our (RGD / *iso*DGR)-MMAE/MMAF conjugates. This will facilitate the choice of the most suitable linker (e.g. to mediate an intra- or extracellular drug release) to consider future *in vivo* antitumor applications.

Chapter V

Conclusions and Future Perspectives

Conclusions and Future Perspectives

The work presented in this thesis mainly focused on potentialities of the peptidomimetic *cyclo*[DKP-RGD] as targeting device, for specific release of payloads against integrin-expressing cancer cells. The chemical properties of such *cyclo*[DKP-RGD] ligand allowed its covalent connection to a wide range of chemical compounds and, due to the hydrophilic nature of the RGD peptide, the final constructs of these conjugation reactions exhibited better solubility in aqueous solutions compared to highly lipophilic anticancer drugs and peptide linkers. Generally, the attachment of the RGD peptidomimetic to the N-termini of such di- or tripeptide linkers was found to affect neither the affinity of the RGD moiety for the isolated $\alpha_v\beta_3$ receptor, nor the enzymatic cleavage at the linkers' C-termini. A previous SMDC developed in our group, the *cyclo*[DKP-RGD]-VA-PTX conjugate (**77**), showed a 66.9-fold higher cytotoxic activity against $\alpha_v\beta_3$+ cancer cells, compared to antigen-negative isogenic cells (TI = 9.0 shown by **77**, calculated considering the intrinsic selectivity of free PTX).[130] The present thesis describes the multimerization of conjugate **77**, representing a logical upgrade of the previous research activity and devised in order to increase the binding affinity and the TI of such SMDC against $\alpha_V\beta_3$-overexpressing cells. We synthesized three new multimeric (*cyclo*[DKP-RGD]-PEG-4)$_n$-VA-PTX conjugates (n = 2-4) and we compared them against two other monomeric analogs. Our new conjugates were tested for their ability to compete with biotinylated vitronectin for the binding to the purified $\alpha_v\beta_3$ integrin: it was observed that when the number of *cyclo*[DKP-RGD] units increases, the binding affinity raises to a plateau achieved by the trimeric (*cyclo*[DKP-RGD]-PEG-4)$_3$-VA-PTX conjugate **104** (IC_{50} $\alpha_v\beta_3$ = 1.2 ± 0.5 nM), which exhibits higher binding affinity than the free ligand *cyclo*[DKP3-RGD] (IC_{50} $\alpha_v\beta_3$ = 4.5 ± 0.1 nM). Later on, all conjugates (**77**, **97**, **102**-**105**) were subjected to cell viability assays against two non-isogenic cell lines: human colorectal adenocarcinoma cell line HT29 ($\alpha_v\beta_3$ −) and, the human glioblastoma cell line U87 ($\alpha_v\beta_3$ +). Unfortunately, while all conjugates showed reduced potency when compared to free PTX (for U87 and HT29 cell lines), we observed that the increase of the valency of the conjugates leads to a progressive loss of cytotoxic activity. This trend may be ascribed to the increased steric bulk around the linker system, which hinders the enzymatic cleavage. However, despite the potency issue, remarkable TI values were observed for monomeric conjugates **77** (TI = 43) and **94** (TI = 94-533). These results can be considered

as a valuable reference in the field of $\alpha_v\beta_3$-targeted chemotherapeutics. Furthermore, from our research activity two main issues emerged:

1) the central role of the biological system chosen to test and compare the synthesized compounds (e.g. isogenic or non-isogenic cell lines, integrin expressing or non-expressing cells etc.). The *in vitro* variability shown by **77** on CCRF-CEM cells[130] and U87 cells (Table 1 and Table 3, Chapter II) and then by **97** (Table 3 and Table 5, Chapter II), together with the different cytotoxic activity detected for the free payload itself, prompted our group to prepare different chemical tools as negative controls in biological investigations (i.e. nontargeting-RAD ligand or conjugates lacking the ligand moiety);
2) the significant reduced potency shown by our conjugates. This drawback limits substantially the escalation of our products to *in vivo* therapy experiments.

Thus, following efforts focused on the development of new SMDCs bearing extracellularly-cleavable linkers (Chapter III) and highly potent payloads (Chapter IV). The first project was devised to evaluate whether the extracellular release of PTX and its subsequent passive diffusion into the cancer cell would raise the potency of our SMDC system. Indeed, the *cyclo*[DKP-RGD]-NPV-PTX (**121**) was synthesized to be cleaved in the extracellular environment by the tumor-associated enzyme elastase at the C-terminus of NPV linker. Although the biological evaluation of this latter compound is still in progress, some interesting preliminary results emerged from the *in vitro* investigation of **121**. Besides showing good binding affinity for the $\alpha_v\beta_3$ isolated receptor, conjugate **121** displayed a 256-fold increment of antiproliferative activity (IC_{50} = 19.6 ± 4.1 nM) against 786-O renal cancer cell line, in the presence of elastase. By contrast, when elastase was not added to the cellular medium, the antiproliferative activity of **121** is substantially decreased (IC_{50} > 5000 nM). This result proved that the release of the payload within the tumor stroma can be a valuable tool to raise the potency of our constructs. Given that the enzyme effector is present at significantly high concentrations at the tumor site, conjugate **121** may be indicated as attractive candidate for *in vivo* anticancer applications, in order evaluate the payload accumulation at the tumor site mediated by the *cyclo*[DKP-RGD] ligand.

The last project consisted in the modification of the payload: we used the same construct system (i.e. same ligand and same linkers), replacing PTX with MMAE or MMAF. The conjugation of the *cyclo*[DKP-RGD] integrin ligand to ultrapotent cytotoxic agents represent a logical strategy to increase the potency of ADC and SMDC products. Several *cyclo*[DKP-RGD]-linker-drug conjugates were synthesized (i.e. combination between VA or NPV linkers and MMAE or MMAF drugs, Chapter IV) in order to evaluate their antiproliferative activity. Moreover, analog versions of such conjugates, lacking the homing device, were also synthesized as a negative control to assess the *cyclo*[DKP-RGD] targeting ability. While some

clear preliminary data were provided, cytotoxicity assays on $\alpha_v\beta_3$-overexpressing cells (U87) and $\alpha_v\beta_3$-nonexpressing cells (HT29) are currently still under evaluation.

In conclusion, the significant decrease of drug's potency displayed by our lysosomally-cleavable SMDCs revealed to be a major issue during this project, which was addressed both by modifications of the payload component and by forcing the extracellular payload release. The latter approach overcomes the need for antigen internalization. Moreover, it remains to be understood if our *cyclo*[DKP-RGD] ligand can mediate an effective integrin-mediated endocytosis and if literature data are confirmed (mentioning that the internalization process is stimulated by ligand multimerization), the development of 'theranostic' SMDCs or multimeric *cyclo*[DKP-RGD]-dyes can be a valuable tool to confirm that the loss of potency is related to ineffective internalization. This analysis, together with an exhaustive linker screening, might hopefully lead to a significant increase of the potency and selectivity of our constructs.

Chapter VI

Experimental Section

Experimental Section

General Remarks and Procedures

Materials and Methods

All manipulations requiring anhydrous conditions were carried out in flame-dried glassware, with magnetic stirring and under a nitrogen atmosphere. All commercially available reagents were used as received. Anhydrous solvents were purchased from commercial sources and withdrawn from the container by syringe, under a slight positive pressure of nitrogen. *cyclo*[DKP-RGD] (**75**),[127] azido-tetraethylene glycol-acid (**91**),[188] azido-tetraethylene glycol-*N*-hydroxysuccinimidyl ester (**92**),[188] Fmoc-Val-Ala-*N*-[4-[[[(N-(Boc)-*N*,*N*'-dimethylethylenediamine)carbonyl]oxy]methyl]phenyl] (**93**),[130] 2'-(4-nitrophenoxycarbonyl) paclitaxel (**95**),[130] 4-(Prop-2-yn-1-yloxy)benzoic acid (**109**)[189] and intermediates, Fmoc-Asn(Trt)-Pro-OH (**126**)[190] and Fmoc-[D]-Val-PABA (**132**)[191] were prepared according to literature procedures, and their analytical data were in agreement with those already published. Reactions were monitored by analytical thin-layer chromatography (TLC) using silica gel 60 F254 pre-coated glass plates (0.25 mm thickness). Visualization was accomplished by irradiation with a UV lamp and/or staining with a potassium permanganate alkaline solution or ninhydrin. Flash column chromatography was performed according to the method of Still and co-workers[192] using Chromagel 60 ACC (40-63 µm) silica gel. Proton NMR spectra were recorded on a spectrometer operating at 400.16 MHz. Proton chemical shifts are reported in ppm (δ) with the solvent reference relative to tetramethylsilane (TMS) employed as the internal standard ($CDCl_3$ δ = 7.26 ppm; CD_2Cl_2, δ = 5.32 ppm; D_2O, *δ* = 4.79 ppm; $[D]_6$DMSO, δ = 2.50 ppm; CD_3OD, δ = 3.33 ppm).[193] The following abbreviations are used to describe spin multiplicity: s = singlet, d = doublet, t = triplet, q = quartet, m = multiplet, bs = broad signal, dd = doublet of doublet, ddd = doublet of doublet of doublet, ddt = doublet of doublet of triplet. Carbon NMR spectra were recorded on a spectrometer operating at 100.63 MHz, with complete proton decoupling. Carbon chemical shifts are reported in ppm (*δ*) relative to TMS with the respective solvent resonance as the internal standard ($CDCl_3$, δ = 77.16 ppm; CD_2Cl_2, δ = 54.00 ppm; $[D]_6$DMSO, δ = 39.51 ppm; CD_3OD, δ = 49.05 ppm).

ESI-MS spectra were recorded on the ion trap mass spectrometer Finnigan LCQ Advantage or Micro Waters Q-Tof (ESI source). MALDI-TOF-MS spectra were recorded on the instrument Bruker Microflex™ LT, supporting the sample on the 2,5-dihydroxybenzoic acid (DHB), α-cyano-4-hydroxycinnamic acid (HCCA) and sinapinic acid (SIN) matrices. The peptide calibration standard (300-6000 Da range), which consisted of Angiotensin II, Angiotensin I, Substance P, Bombesin; ACTH clip 1-17, ACTH clip 18-39, Somatostatin 28, was purchased from Bruker Daltonics® and used to calibrate the MALDI-TOF-MS instrument. The sample was mixed in equal volumes with the matrix solution: a small amount (1 µL) of this mixture was spotted on the target surface. The target matrix was dried at room temperature and then analyzed.

High-resolution mass spectra (HRMS) were performed with a Fourier Transform Ion Cyclotron Resonance (FT-ICR) Mass Spectrometer APEX II & Xmass software (Bruker Daltonics) – 4.7 T Magnet (Magnex) equipped with ESI source, available at CIGA (Centro Interdipartimentale Grandi Apparecchiature), University of Milan.

HPLC purifications and HPLC traces of final products were performed on Dionex Ultimate 3000 equipped with Dionex RS Variable Wavelength Detector (column: Atlantis Prep T3 OBD™ 5 µm 19 × 100 mm; flow 15 mL/min unless stated otherwise). The crude reaction mixture was dissolved in H_2O or, if the compound was insoluble in water, adding first DMF, then diluting slowly with H_2O until reaching a 1:1 mixture DMF/H_2O (ultrasonic sonicator was used to assist the dissolution). The solution so obtained was filtered (polypropylene, 0.45 µm, 13 mm ø, PK/100) and injected in the HPLC, affording purified products. Purity analyses were carried on a Dionex Ultimate 3000 instrument equipped with a Dionex RS Variable Wavelength detector (column: Waters Atlantis® 5 µm 21 mm × 10 cm column). 1 mg of analyte was dissolved in 1 mL of H_2O and was injected using the same gradient used in the purification step. The analysis of the integrals and the relative percentage of purity was performed with the software Cromeleon 6.80 SR11 Build 3161.

Freeze-drying: The products were dissolved in water and frozen with dry ice. Later on, the freeze-drying was carried out at least for 48 h at -50 °C using the instrument 5Pascal Lio5P DGT.

General Procedures

GENERAL PROCEDURE FOR Boc DEPROTECTION REACTIONS:

GP1: To a 0.03 M CH_2Cl_2 solution of the *N*-Boc-protected compound half volume of TFA was added, and the reaction was stirred at r.t. for 1 h. The solvent was evaporated and then for two times CH_2Cl_2 was added to the residue followed by evaporation under vacuum, to afford the amine TFA salt.

GENERAL PROCEDURE FOR Fmoc DEPROTECTION REACTIONS:

GP2: A 0.01 M solution of the *N*-Fmoc-protected compound (1 equiv) in DMF was cooled to 0 °C under nitrogen atmosphere. Piperidine (5 equiv) was added and the reaction was stirred at room temperature for 2 h. The mixture was diluted with AcOEt (20 × volume of DMF) and washed twice with a saturated aqueous solution of $NaHCO_3$. The organic phase was dried over Na_2SO_4 and concentrated at rotavapor. CH_2Cl_2 was added to the residue and evaporated to afford a yellow solid. The crude was left under vacuum for 2 h and then used as starting material for the subsequent step.

GENERAL PROCEDURE FOR CuAAC ("click reaction") REACTIONS:

GP3: Alkyne (1 - 1.5 equiv) and azide (1 - 4.8 equiv) were dissolved in a degassed 1:1 mixture of H_2O/DMF (0.01 M) under a nitrogen atmosphere. Degassed aqueous solutions of $CuSO_4 \cdot 5H_2O$ (0.5 equiv per unit of alkyne) and sodium ascorbate (0.6 equiv per unit of alkyne) were added at room temperature and the mixture was stirred overnight at 35 ºC. The solvent was removed under vacuum, and the crude residue was purified by semipreparative HPLC [Waters Atlantis 21 mm x 10 cm column; gradient: 90% (H_2O+0.1% CF_3COOH)/10% (CH_3CN+0.1% CF_3COOH) to 100% (CH_3CN+0.1% CF_3COOH)]. After purification, the final product was then freeze-dried.

Biological Assays

SOLID-PHASE RECEPTOR BINDING ASSAY:

Recombinant human integrin $\alpha_v\beta_3$ receptor (R&D Systems, Minneapolis, MN, USA) was diluted to 0.5 µg/mL in coating buffer containing 20 mM Tris-HCl (pH 7.4), 150 mM NaCl, 1 mM $MnCl_2$, 2 mM $CaCl_2$, and 1 mM $MgCl_2$. An aliquot of diluted receptor (100 µL/well) was added to 96-well microtiter plates (Nunc MaxiSorp) and incubated overnight at 4 °C. The plates were then incubated with blocking solution (coating buffer plus 1% bovine serum albumin) for 2 h at r.t. to block nonspecific binding. After washing 2 times with blocking solution, plates were incubated shaking for 3 h at r.t., with various concentrations (10^{-5}-10^{-12} M) of test compounds in the presence of 1 µg/mL biotinylated vitronectin (Molecular Innovations, Novi, MI, USA). Biotinylation was performed using an EZ-Link Sulfo-NHS-Biotinylation kit (Pierce, Rockford, IL, USA). After washing 3 times, the plates were incubated shaking for 1 h at r.t., with streptavidin-biotinylated peroxidase complex (Amersham Biosciences, Uppsala, Sweden). After washing 3 times with blocking solution, plates were incubated with 100 µL/well of Substrate Reagent Solution (R&D Systems, Minneapolis, MN, USA) for 30 min, in the dark, with shaking. After stopping the reaction with the addition of 50 µL/well 2 N H_2SO_4, absorbance at λ = 415 nm was read in a SynergyTM HT Multi-Detection Microplate Reader (BioTek

Instruments, Inc.). Each data point represents the average of triplicate wells; data analysis was carried out by nonlinear regression analysis with GraphPad Prism software (GraphPad Prism, San Diego, CA, USA). Each experiment was repeated in duplicate.

DETERMINATION OF INTEGRIN $\alpha_v\beta_3$ RECEPTOR EXPRESSION BY FLUORESCENCE ACTIVATED CELL SORTER (FACS)

U87 and HT29 cells were seeded in T25 flasks with ventilation cap and incubated at 37 °C in a humidified atmosphere with 5% CO_2 for 48 h. Cells were harvested and fixed with 4% PFA (Paraformaldehyde). With 3% BSA (Bovine Serum Albumin) were blocked all possible non-specific binding sites on the cell, and cells were exposure with LM609 anti integrin $\alpha_V\beta_3$ antibody conjugated with FITC (Merck Millipore, Darmstadt, Germany). In control samples cells were not stained with antibody, and auto-fluorescence intensity of cells was measured. Fluorescent intensity of stained samples was measured by flow cytometer Beckman Coulter, and compared with auto-fluorescence intensity of control samples.

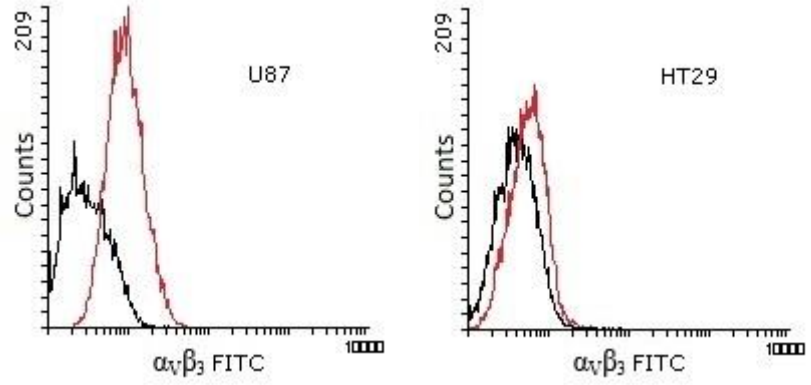

Figure 46. Flow cytometry analysis of integrin $\alpha_v\beta_3$ in U87 and HT29 cell lines. Black: auto-fluorescence of the cell; Red: fluorescence of $\alpha_V\beta_3$ integrin antibody.

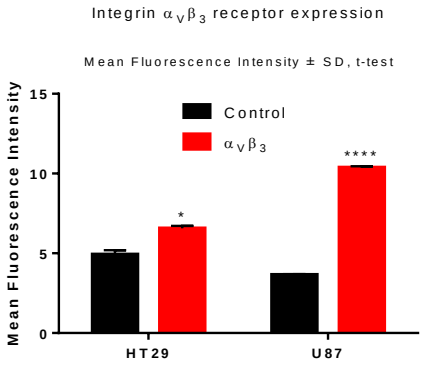

Figure 47. Mean fluorescence intensity of $\alpha_v\beta_3$ receptors expression in U87 and HT29 cell lines.

U87 AND HT29 CELL LINES AND CULTURE CONDITIONS:

U87 (human glioblastoma) and HT29 (human colorectal adenocarcinoma) cell lines obtained from ATCC and were cultured in sterile T25 flasks with ventilation cap (Sarstedt, Nümbrecht, Germany) at 37 °C in a humidified atmosphere with 5% CO_2. For U87 cells, DMEM medium (Dulbecco's Modified Eagle's Medium) (Lonza, Basel, Switzerland) containing 4500 mg·L^{-1} glucose and supplemented with 10% heat-inactivated and filtered FBS (Fetal Bovine Serum) (Lonza, Basel, Switzerland) and 1% Penicillin-Streptomycin (Lonza, Basel, Switzerland) was used. HT29 cells were grown in RPMI 1640 medium supplemented with 10% FBS and 1% Penicillin-Streptomycin.

ANTIPROLIFERATIVE ACTIVITY OF CONJUGATES **97**, **103**-**105**

Cell viability was determined by MTT assay (3-(4,5-dimethylthiazol-2-yl)-2,5-diphenyl-tetrazolium bromide) obtained from Sigma Aldrich (St. Louis, MO, USA). After standard trypsinization, cells were seeded at 3 × 10^3 cells (U87) and 4 × 10^3 cells (HT29) per well in a 96-well plate and incubated. After 24 h, cells were treated with various concentrations of conjugates **97**, **103**-**105** and free drug PTX (paclitaxel) and incubated in appropriate serum-containing growth medium for 96 h under standard growth conditions. Control wells were untreated. Subsequently, MTT assay was performed by adding 20 µL of MTT solution (5 mg·L^{-1} in PBS) to each well and after 4 h of incubation at 37 °C, the supernatant was removed. The formazan crystals were dissolved in 100 µL of a 1:1 solution of DMSO (Sigma Aldrich, St. Louis, MO, USA) and EtOH (Molar Chemicals Kft. Hungary) and the absorbance was measured after 15 min at λ = 570 nm by using a microplate reader (BIO-RAD, model 550). Average background absorbance of DMSO-EtOH only, was subtracted from absorbance values of control and treated wells, and cell viability was determined relative to untreated (control) wells where cell viability was arbitrarily set to 100%. Absorbance values of treated samples were normalized versus untreated control samples and interpolated by nonlinear regression analysis with GraphPad Prism software to generate dose-response curves. The 50% inhibitory concentration (IC_{50}) was determined from the dose-response curves by using sigmoidal interpolation curve fitting. The experiments were done in triplicate.

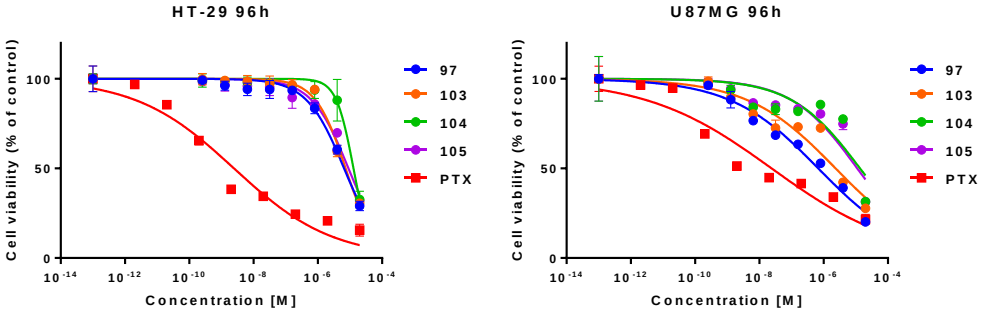

Figure 48. Dose-response curves of conjugates **97**, **103**-**105** and PTX.

DIGESTION OF **121** WITH ELASTASE AND LYSOSOMAL ENRICHED EXTRACT

100 µM solution of conjugate **121** was digested in PBS/ 10% CH_3CN at 37 °C for 2 h with 25 mUnits of Elastase from human leucocytes (ELANE, E-8140, Sigma-Aldrich).

0.2 mM solutions of conjugate **121** were digested in 200 mM sodium acetate (pH 5.5)/1 mM EDTA containing 1 mM cysteine at 37 °C for 2 h with 0.5 mg mL^{-1} of lysosomal enriched extract (prepared from a rat liver as previously described in the literature) in the presence or absence of 20 µM E-64 protease inhibitors (Enzo Life Sciences).

Control samples were prepared by diluting the compounds in the same reaction mixture acidified with TFA to inactivate elastase and the lysosomal enzymes.

All samples were analyzed by ESI-LC/MS on a PLRP-S column (Agilent Technologies; 2.1 × 150 mm, 8 µm, 1000 Å) with an Agilent 1100 HPLC system equipped with a diode array detector with an electrospray ion source. Mobile phase A was composed of 0.05% TFA in water, and mobile phase B was 0.05% TFA in CH_3CN. Samples (45 µM) were eluted at 0.25 mL min^{-1} by using a gradient from 20 to 50% B in 30 min, raised to 80% B and held at 80% B for 5 min; the UV signal was recorded at 220 and 280 nm, and MS detection was set in full-scan mode from 300–2000 amu.

PLASMA STABILITY OF CONJUGATE **121**

A 1 mM solution of conjugate **121** in DMSO was diluted to 5 µM with blank mouse plasma and incubated at 37 °C under mixing for 24 h. Aliquots of 20 µL were double collected at the time points 0, 0.25, 0.50, 1, 2, 4, 6 and 24 h and frozen up to analysis. Sample plasma proteins were precipitated by adding 180 mL of CH_3CN/MeOH (9:1) to the unfrozen aliquots. After mixing for 15 minutes, the aliquots were centrifuged for 5 minutes at 12000 rpm; the supernatants were collected and transferred into 96-well plate; the plate was further centrifuged for 5 minutes at 4000 rpm. The samples were analyzed against standard appropriately diluted for calibration line in CH_3CN /MeOH (9:1).

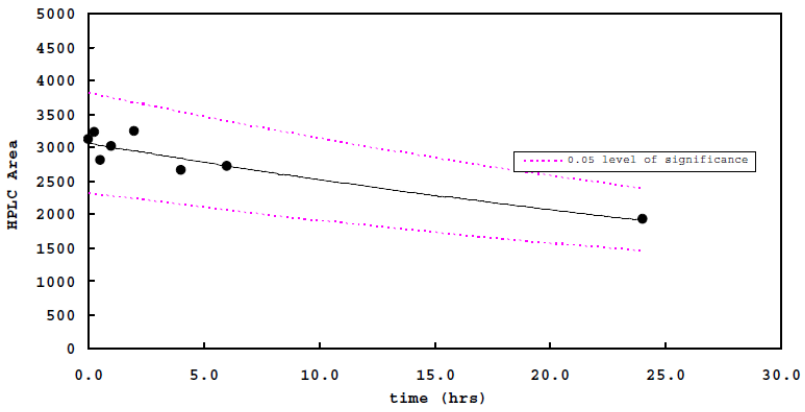

Figure 49. Plasma stability of conjugate **121**: the calculated half-life ($t_{1/2}$) is 35.27 hours.

All samples were analyzed by UPLC-LC-MS/MS on a BEH C18 column (Waters Acquity BSM; 2.1 × 50 mm, 1.7 µm) with an Waters UPLC system equipped with a diode array detector with an electrospray ion source. Mobile phase A was composed of 5% CH_3CN in 5 mM Ammonium Formate pH 3.5, and mobile phase B was 5% 5 mM Ammonium Formate pH 3.5 in CH_3CN; the UV signal was recorded at 220 and 280 nm, and MS detection was set in full-scan mode from 300–2000 amu. The software used to analyze all the data was Mass Lynx 4.1 SCN919. After linear regression analysis, the calculated half-life ($t_{1/2}$) is 35.27 hours.

STABILITY TEST OF PRO-PTX **142**

Paclitaxel drug release was investigated by incubation of Pro-PTX TFA salt **142** (250 µM) in DMSO:PBS (1:1), pH 7.5 at 37 ºC. Aliquots (100 µL) were taken at several time points and analyzed by HPLC after dilution with eluent (300 µL). HPLC conditions: analysis was carried out on a reverse-phase column (Waters Atlantis 21 mm x 10 cm column, gradient from 90% (H_2O + 0.1% CF_3COOH) / 10% (CH_3CN + 0.1% CF_3COOH) to 100% (CH_3CN + 0.1% CF_3COOH) in 20 min). The data were extracted from the software Cromeleon 6.80 SR11 Build 3161 and analyzed by Excel™ 2016.

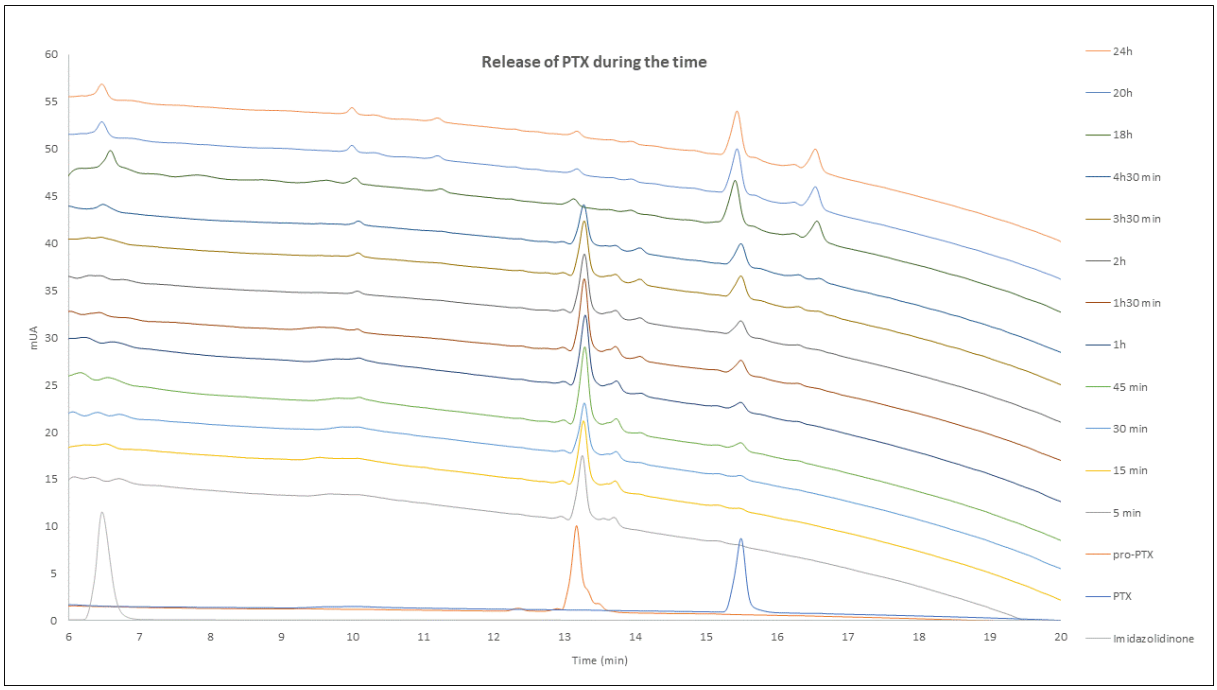

Figure 50. Pro-PTX **142** cyclization and PTX release during the time. A representative curve was treated for each HPLC run. X-axis shows the retention time of each specie; Y-axis shows the area of each peak.

ANTIPROLIFERATIVE ACTIVITY OF **121**-**124** AND **142**

786-O renal cancer cell line (NCI) was cultured in RPMI 1640 medium supplemented with 10% fetal calf serum (FCS) at 37°C and 5% CO_2. Cells were seeded at a density of 2000 cells/well (200 µl/well) in 96-well plates and, 24 hours after seeding. Cells were treated in duplicate with

serial dilutions of **121**-**124** in the range 5.0 μM - 9.8 nM and with serial dilutions of PTX and Pro-PTX **142** in the range 0.1 μM – 0.2 nM, in the presence or absence of Elastase from human leucocytes (ELANE, 324681, Millipore). In the case of presence of elastase, the latter was added immediately after compound treatment at a final concentration of 50 nM in half of replicates, then the plates were incubated for 96 hours at 37°C.

Cell viability was assessed with the CellTiter-Glo luciferase-based ATP detection assay (Promega) and Envision (PerkinElmer) microplate reader. Growth inhibitory activity was evaluated at the end of incubation by using GraphPad Prism software. Experimental data were normalized versus untreated control samples and interpolated by nonlinear regression analysis with GraphPad Prism software to generate dose-response curves. IC_{50} values were calculated by using sigmoidal interpolation curve fitting.

ANTIPROLIFERATIVE ACTIVITY OF RGD-MMAE/MMAF CONJUGATES (**145**-**149**, **156** and **163**-**166**)

To evaluate the cytotoxicity of (RGD/*iso*DGR)-MMAE/MMAF conjugates against U-87 MG glioblastoma cells obtained from American Type Culture Collection (ATCC, Bethesda, MD, USA). Cell viability was quantified by MTT (3-(4,5-dimethylthiazol-2-yl)-2,5-diphenyltetrazolium bromide) assay. Briefly, cells in EMEM supplemented with 10% FBS, 1% L-glutamine and 1% penicillin/streptomycin, were seeded in 96-well culture plates (5×10^4 cells/well) and incubated in a humidified, 37 °C, 5% CO_2 atmosphere overnight to allow adherence. The following day cells were treated with serial dilutions of each compound starting at 500 nM for MMAE or MMAF and 5000 nM for each conjugate, or 0.1% DMSO as a control, and incubated as described for 72h. At the end of treatment, 5 μL of MTT (5 mg/mL in deionized H_2O, Sigma #M5655) was added to each well. The cells were incubated for another 2 hours, and 100 μL of lysis buffer (10% SDS, 10 mM HCl) were added, and placed in the incubator overnight for the formazan crystal solubilization. Absorbance at 540 nm was measured and the growth inhibition ratio was calculated. Blank controls detecting cell-free media absorbance were performed in parallel. Three experimental replicates were used. The half-maximal inhibitory concentration values (IC_{50}) were obtained from viability curves using GraphPad Prism 6 (Figure 51). The cell viability was expressed as percentage relative to the respective control conditions (0.1% of DMSO).

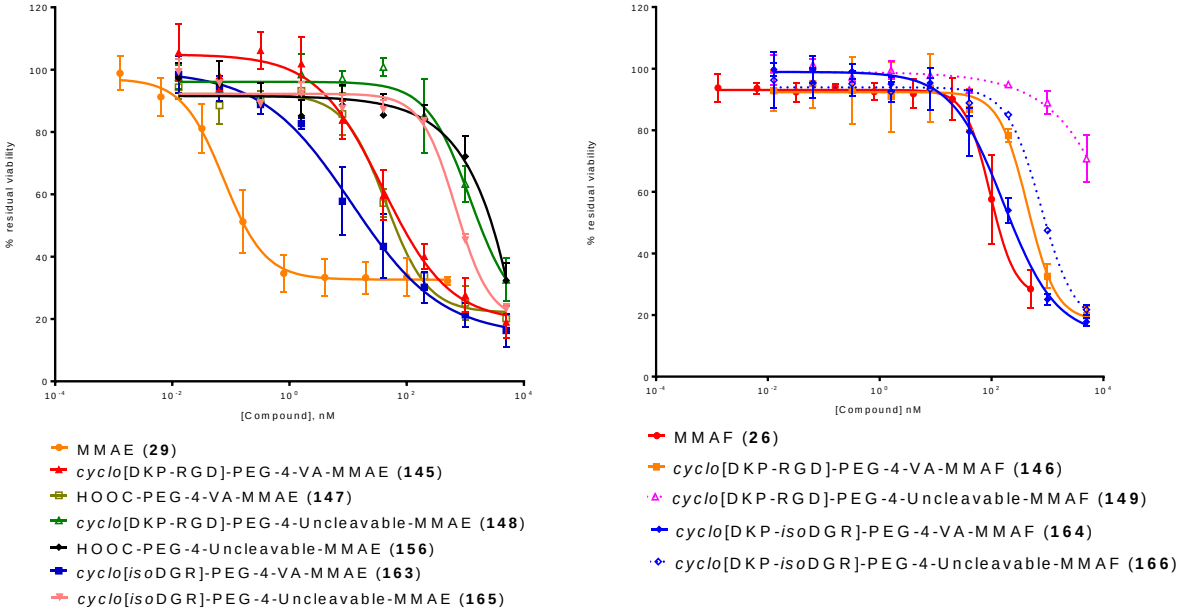

Figure 51. Dose-response curves of MMAE-containing compounds (left), MMAF-containing compounds (right), MMAE and MMAF.

Synthesis of cyclo[DKP-RGD]-Drug Conjugates

cyclo[DKP-RGD]-PEG-4-Azide (**86**)

14-Azido-3,6,9,12-tetraoxatetradecanoic acid (91)

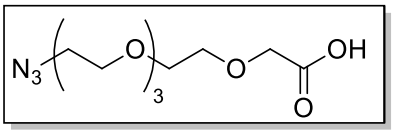

$C_{10}H_{19}N_3O_6$
MW: 277,28

Commercially available tetraethylene glycol (4.58 g, 23.6 mmol, 3 equiv) was dissolved in dry CH_2Cl_2 (80 mL) under inert atmosphere. Then DMAP (0.19 g, 1.58 mmol, 0.2 equiv) and Et_3N (3.3 mL, 23.6 mmol, 3 equiv) were added. The mixture was cooled at 0 °C and a solution of TsCl (1.5 g, 7.9 mmol, 1 equiv) in dry CH_2Cl_2 (40 mL) was added dropwise. The reaction was stirred at r.t. for 2 h. Hence, 100 mL of CH_2Cl_2 were added and the mixture was washed with a solution of HCl 1 M (2 × 40 mL) and brine (1 × 50 mL). The organic phase was dried over Na_2SO_4 and concentrated. Then the crude was dissolved in dry DMF (15 mL) and NaN_3 (1.03 g, 15.8 mmol, 2 equiv) was added under inert atmosphere. The suspension was stirred at 80 °C overnight. The solvent was removed and the crude was purified by flash chromatography on silica gel (gradient from 1% MeOH to 5% MeOH in AcOEt) affording the corresponding azide. Later on, to a suspension of NaH (0.6 g, 25 mmol, 5 equiv) in dry THF (25 mL), azido-tetraehtylene glycol (1.09 g, 5 mmol, 1 equiv) dissolved in dry THF (25 mL) was added dropwise over a period of 30 min under inert atmosphere. The reaction was stirred for 1 h more at room temperature. Later, a solution of bromoacetic acid (1.387 g, 10 mmol, 2 equiv) in dry THF (21 mL) was added dropwise over a period of 1 h and then the reaction was stirred overnight at r.t. After addition of cold water, THF was removed under vacuum and a solution of HCl 1 M was added until pH = 1. The mixture was extracted with AcOEt (5 × 80 mL) and the collected organic phases were washed with brine (1 × 150 mL). The organic phase was dried over Na_2SO_4 and concentrated, then the crude was purified by flash chromatography on silica gel (eluent: CH_2Cl_2/MeOH, 9:1 + 0.1% CH_3COOH) affording the corresponding carboxylic acid **91** as a pale-yellow oil (1.09 g, 79% yield).

R_f = 0.25 (9:1, CH_2Cl_2/MeOH + 0.1% CH_3COOH); ^{1}H NMR (400 MHz, CD_2Cl_2-d_2) δ 3.96 (s, 2H), 3.70-3.61 (m, 14H), 3.39 (t, J = 5.0 Hz, 2H).

Azido-tetraethylene glycol-*N*-hydroxysuccinimidyl ester (92)

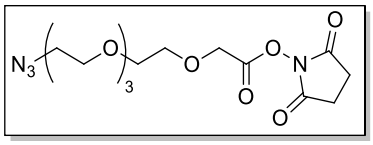

$C_{14}H_{22}N_4O_8$
MW: 374,35

Carboxylic acid **91** (77 mg, 0.28 mmol, 1 equiv) was dissolved in dry THF and cooled down to 0 °C under a nitrogen atmosphere. EDC·HCl (69 mg, 0.36 mmol, 1.3 equiv) and *N*-hydroxysuccinimide (41 mg, 0.36 mmol, 1.3 equiv) were added and the mixture was allowed to reach r.t. and stirred overnight. The solvent was removed and the crude was purified over a pad of silica [eluent: AcOEt/hexane, 8:2] affording ester **92** as a colorless oil (67 mg, 64% yield).

R_f = 0.43 (9:1, CH_2Cl_2/MeOH); ^{1}H NMR (400 MHz, CD_2Cl_2-d_2) δ 4.50 (s, 2H), 3.78-3.73 (m, 2H), 3.68-3.59 (m, 12H), 3.37 (t, *J* = 5.1 Hz, 2H), 2.83 (s, 4H); MS (ESI+): *m/z* calcd for $[C_{14}H_{22}N_4NaO_8]^+$: 397.13 [*M* + Na]$^+$; found: 397.19.

***cyclo*[DKP-RGD]-PEG-4-N_3 (86)**

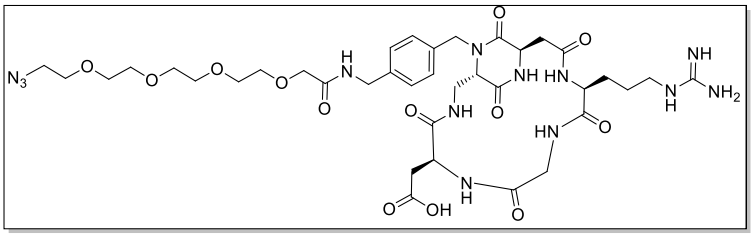

$C_{37}H_{55}N_{13}O_{13}$
MW: 889,91

To a solution of **92** (17 mg, 0.045 mmol, 1.3 equiv) in CH_3CN (2 mL) under a nitrogen atmosphere, *cyclo*[DKP-RGD] **75** (30 mg, 0.035 mmol, 1 equiv) dissolved in pH 7.5 PBS solution (1.5 mL) was added at 0 °C under a nitrogen atmosphere. The reaction mixture was allowed to reach r.t. and stirred overnight. During the first 3 h the pH value was kept close to 7.3-7.5 adding 0.2 M aqueous NaOH aq. when necessary. The crude was then purified by semipreparative-HPLC [Waters Atlantis 21 mm × 10 cm column, flow: 9 mL/min, gradient: 90% (H_2O + 0.1% CF_3COOH) / 10% (CH_3CN + 0.1% CF_3COOH) to 55% (H_2O + 0.1% CF_3COOH) / 45% (CH_3CN + 0.1% CF_3COOH) in 10 min; t_R (product): 8.3 min]. The purified product was then freeze-dried giving the desired **86** as a white solid (27 mg, 77% yield).

^{1}H NMR (400 MHz, D_2O) *δ* 7.36 (d, *J* = 8.1 Hz, 2H), 7.32 (d, *J* = 8.2 Hz, 2H), 5.12 (d, *J* = 15.4 Hz, 1H), 4.90 (t, *J* = 7.1 Hz, 1H), 4.59 (dd, *J* = 7.9, 5.4 Hz, 1H), 4.48 (s, 2H), 4.34 (d, *J* = 17.1 Hz, 1H), 4.22 (dd, *J* = 9.6, 5.2 Hz, 1H), 4.19-4.11 (m, 4H), 4.01 (d, *J* = 14.6 Hz, 1H), 3.80-3.75 (m, 3H), 3.75-3.69 (m, 3H), 3.69-3.59 (m, 10H), 3.47-3.43 (m, 2H), 3.25 (t, *J* = 6.8 Hz, 2H), 3.01-2.88 (m, 2H), 2.81 (dd, *J* = 16.9, 7.1 Hz, 1H), 2.67 (dd, *J* = 14.0, 5.4 Hz, 1H), 2.08-1.97 (m, 1H), 1.90-1.78 (m, 1H), 1.77-1.60 (m, 2H); ^{13}C NMR (101 MHz, D_2O) *δ* 174.1, 173.9, 173.1, 172.8, 172.7, 170.9, 170.1, 168.6, 156.8, 137.8, 134.1, 128.1, 127.8, 70.5, 69.5, 69.2, 59.3, 54.0, 52.1, 50.1, 49.4, 47.6, 42.5, 42.2, 40.6, 39.2, 38.0, 34.6, 25.8, 24.7; MS (ESI+) *m/z* calcd

for $[C_{37}H_{56}N_{13}O_{13}]^+$: 890.41 [*M* + H]$^+$; found: 890.47; *m/z* calcd $[C_{37}H_{55}N_{13}NaO_{13}]^+$: 912.39 [*M* + Na]$^+$; found: 912.45.

cyclo[DKP-RGD]-PEG-4-Val-Ala-PTX aliphatic scaffold (**97**)

Aliphatic alkyne-Val-Ala-PABC-*N*-(Boc)-*N*,*N'*-dimethylethylenediamine (94)

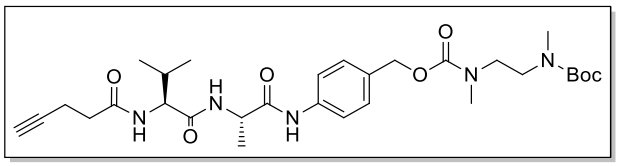

$C_{30}H_{45}N_5O_7$
MW: 587,71

N-Fmoc-protected compound **93** (150 mg, 0.206 mmol, 1 equiv) was deprotected following General Procedure GP2. A solution of commercial 4-pentynoic acid (31 mg, 0.31 mmol, 1.5 equiv) in dry DMF (7 mL) was cooled to 0 °C under a nitrogen atmosphere. HATU (134 mg, 0.35 mmol, 1.7 equiv), HOAt (48 mg, 0.35 mmol, 1.7 equiv) and *i*Pr$_2$NEt (145 µL, 0.83 mmol, 4 equiv) were added and the mixture was stirred for 20 min at 0 °C. A solution of **93-NH** (105 mg, 0.206 mmol, 1 equiv) in dry DMF (3 mL) was added to the stirred mixture. The reaction was allowed to slowly reach room temperature and stirred overnight. The mixture was diluted with an AcOEt/CH_2Cl_2, 4:1 mixture (100 mL) and washed with 1 M aqueous solution of $KHSO_4$ (2 × 15 mL), a saturated aqueous solution of $NaHCO_3$ (1 × 15 mL) and brine (1 × 20 mL). The organic phase was dried over Na_2SO_4 and concentrated. The solid was suspended in Et_2O. The product was collected by centrifugation and purified by flash chromatography [gradient: from 99:1 CH_2Cl_2/MeOH to 97:3 CH_2Cl_2/MeOH] to afford amide **94** as a white solid (106 mg, 88% yield over two steps).

R_f = 0.39 (9:1, CH_2Cl_2/MeOH); ^{1}H NMR (500 MHz, [D]$_6$DMSO) δ 9.71 (s, 1H), 7.93 (d, *J* = 7.2 Hz, 1H), 7.75 (d, *J* = 8.5 Hz, 1H), 7.58 (d, *J* = 8.5 Hz, 2H), 7.29 (d, *J* = 8.2 Hz, 2H), 5.00 (s, 2H), 4.44 (p, *J* = 7.0 Hz, 1H), 4.21 (dd, *J* = 8.4, 6.5 Hz, 1H), 3.38-3.29 (m, 4H), 2.87 (s, 3H), 2.75 (s, 3H), 2.62 (t, *J* = 2.4 Hz, 1H), 2.46-2.32 (m, 4H), 2.09-1.99 (m, 1H), 1.39 (s, 9H), 1.34 (d, *J* = 7.1 Hz, 3H), 0.90 (dd, *J* = 11.3, 6.8 Hz, 6H); ^{13}C NMR (126 MHz, [D]$_6$DMSO) δ 171.41, 171.23, 171.14, 155.93, 155.28, 139.02, 132.35, 128.64, 121.72, 120.36, 119.73, 84.25, 78.98, 71.33, 66.47, 58.45, 49.56, 34.73, 34.48, 30.77, 19.58, 18.53, 18.36, 14.79. MS (ESI+) *m/z* calcd for $[C_{30}H_{46}N_5O_7]^+$: 588.75 [*M* + H]$^+$; found: 588.77; *m/z* calcd $[C_{30}H_{45}NaN_5O_7]^+$: 610.72 [*M* + Na]$^+$; found: 610.70.

Aliphatic alkyne-Val-Ala-PTX (96)

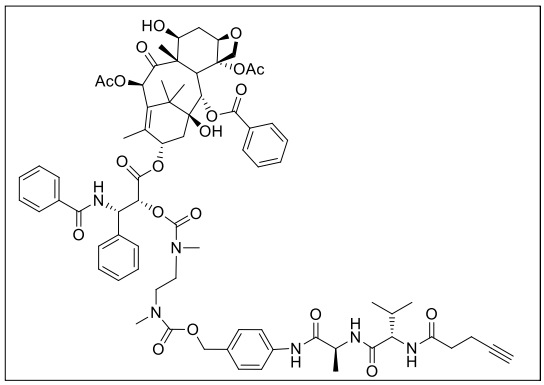

$C_{73}H_{86}N_6O_{20}$
MW: 1367,51

A solution of Boc-protected compound **94** (20 mg, 0.034 mmol, 1 equiv) was deprotected following General Procedure GP1. The obtained TFA salt was dissolved in dry DMF (500 μL) and *i*Pr_2NEt (25 μL, 0.136 mmol, 4 equiv). The resulting solution was added at 0 °C to a stirred solution of **95** (52 mg, 0.051 mmol, 1.5 equiv) in dry DMF (500 μL), under a nitrogen atmosphere. The reaction was then allowed to reach room temperature and stirred overnight. AcOEt (100 mL) was added and the solution was washed with a 1 M aqueous solution of $KHSO_4$ (2 × 10 mL) and brine (1 × 15 mL). The organic phase was dried over Na_2SO_4 and concentrated, then the crude was purified by flash chromatography [gradient: from 9:1 CH_2Cl_2/AcOEt to 7:3 CH_2Cl_2/AcOEt] to afford carbamate **96** as a white solid (30 mg, 66% yield). R_f = 0.33 (CH_2Cl_2/AcOEt, 9:1); MS (MALDI-TOF): *m/z* calcd for $[C_{73}H_{86}NaN_6O_{20}]^+$: 1389.98 [*M* + Na]$^+$; found: 1389.70 (HCCA matrix), 1390.08 (SA matrix); HRMS (ESI+): *m/z* calcd for $[C_{73}H_{86}NaN_6O_{20}]^+$: 1389.98 [*M* + Na]$^+$; found: 1389.57; *m/z* calcd for $[C_{73}H_{86}Na_2N_6O_{20}]^{2+}$: 706.14, [*M* + 2Na]$^{2+}$; found: 706.28.

***cyclo*[DKP-RGD]-PEG-4-Val-Ala-PTX aliphatic scaffold (97)**

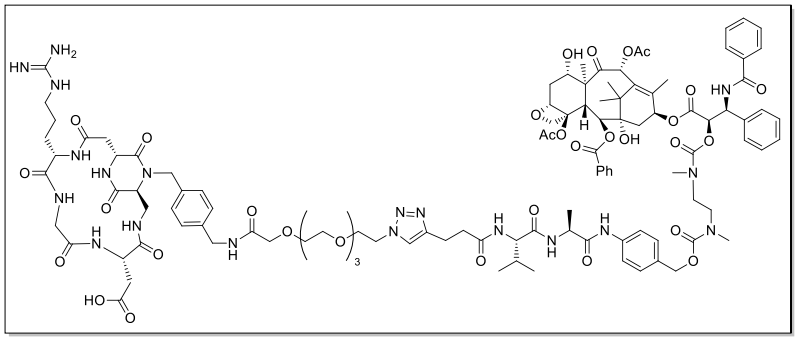

$C_{110}H_{141}N_{19}O_{33}$
MW: 2257,40

Alkyne **96** (10 mg, 0.0075 mmol, 1.5 equiv) and azide **86** (5 mg, 0.005 mmol, 1 equiv) were reacted following the General Procedure GP3. Crude was purified by semipreparative HPLC [Waters Atlantis 21 mm x 10 cm column; gradient: 90% (H_2O+0.1% CF_3COOH)/10% (CH_3CN+0.1% CF_3COOH) to 100% (CH_3CN+0.1% CF_3COOH) in 20 min; t_R (product)=11.9

min]. The purified product was then freeze-dried to give the desired compound **97** as a white solid (9 mg, 81% yield).

MS (MALDI-TOF): *m/z* calcd for $[C_{110}H_{142}N_{19}O_{33}]^+$: 2258.40 [*M* + H]$^+$; found: 2258.30 (HCCA matrix), 2258.34 (SA matrix); HRMS (ESI+): *m/z* calcd for $[C_{110}H_{140}Na_3N_{19}O_{33}]^{2+}$: 1161.90, [*M* + 3Na - H]$^{2+}$; found: 1161.97; *m/z* calcd for $[C_{110}H_{141}Na_2N_{19}O_{33}]^{2+}$: 1150.90, [*M* + 2Na]$^{2+}$ found: 1150.98.

cyclo[DKP-RGD]-PEG-4-Val-Ala-PTX aromatic scaffold (**102**)

Methyl 4-hydroxybenzoate (107)

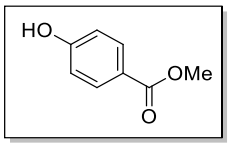

$C_8H_8O_3$
MW: 152,15

Commercial 4-hydroxybenzoic acid **106** (100 mg, 0.724 mmol, 1 equiv) was dissolved in MeOH (1.3 mL), and H_2SO_4 (19 µL, 0.362 mmol, 0.5 equiv) was added thereto, and stirred for 4 hours under reflux. The reaction mixture was concentrated, diluted in water, and extracted with EtOAc. The organic layer was washed with brine, dried over Na_2SO_4 and concentrated under reduced pressure. Then, the residue was purified by flash chromatography on silica gel (1:1 Et_2O/*n*-Hexane) affording the desired product **107** as a white solid (110 mg, yield: quantitative). R_f = 0.48 (1:1, Et_2O/*n*-Hexane); ^{1}H NMR (400 MHz, CD_2Cl_2-d_2) δ 7.98 (d, *J* = 8.8 Hz, 2H), 6.92 (d, *J* = 8.7 Hz, 2H), 5.90 (s, 1H), 3.90 (s, 3H); MS (ESI+) *m/z* calcd for $[C_8H_9O_3]^+$: 153.03 [*M* + H]$^+$; found: 153.08.

Methyl 4-(prop-2-yn-1-yloxy)benzoate (108)

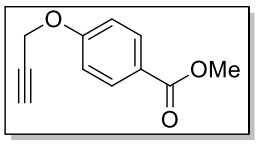

$C_{11}H_{10}O_3$
MW: 190,20

Compound **107** (110 mg, 0.723 mmol, 1 equiv) was dissolved in dry acetone (7 mL) under nitrogen atmosphere. The solution was cooled in an ice bath. Propargyl bromide (250 µL, 2.9 mmol, 4 equiv) and K_2CO_3 (400 mg, 2.9 mmol, 4 equiv) were added, and the mixture was stirred at room temperature for 24 h at 30 ºC. The mixture was concentrated, the crude was dissolved in AcOEt (70 mL) and washed with water (3 × 10 mL). The organic phase was dried over Na_2SO_4 and concentrated, affording the desired product **108** as an orange solid (135 mg, yield: 99%).

R_f = 0.77 (1:1, *n*-Hexane/EtOAc); ^{1}H NMR (400 MHz, CD_2Cl_2-d_2) δ 7.99 (d, *J* = 9.0 Hz, 2H), 7.01 (d, *J* = 8.9 Hz, 2H), 4.76 (d, *J* = 2.4 Hz, 2H), 3.86 (s, 3H), 2.61 (t, *J* = 2.4 Hz, 1H); MS (ESI+) *m/z* calcd for $[C_{11}H_{11}O_3]^+$: 191.06 [*M* + H]$^+$; found: 191.08.

4-(Prop-2-yn-1-yloxy)benzoic acid (109)

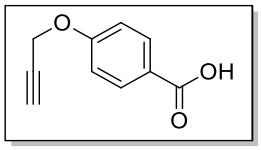

$C_{10}H_8O_3$
MW: 176,17

Compound **108** (135 mg, 0.710 mmol, 1 equiv) was dissolved in MeOH (6 mL) under a nitrogen atmosphere. The solution was cooled to 0 °C, then NaOH (142 mg, 3.6 mmol, 5 equiv) in H_2O (2 mL) was added. The mixture was stirred 5 h at room temperature. The mixture evaporated until the dryness under reduced pressure and later acidified to *ca.* pH = 1 with a 1 M $KHSO_4$ aqueous solution and extracted with EtOAc (4 × 20 mL). The organic phase was dried over Na_2SO_4 and concentrated, affording **109** as an orange solid (120 mg, yield: 98%).
R_f = 0.15 (3:2, *n*-Hexane/EtOAc); ^{1}H NMR (400 MHz, CD_3OD) δ 7.98 (d, *J* = 8.9 Hz, 2H), 7.05 (d, *J* = 8.9 Hz, 2H), 4.81 (d, *J* = 2.4 Hz, 2H), 2.99 (t, *J* = 2.4 Hz, 1H). MS (ESI+) *m/z* calcd for $[C_{10}H_9O_3]^+$: 177.05 [*M* + H]$^+$; found: 177.06; *m/z* calcd $[C_{10}H_8NaO_3]^+$: 199.39 [*M* + Na]$^+$; found: 199.45.

Aromatic alkyne-Val-Ala-PABC-*N*-(Boc)-*N*,*N*′-dimethylethylenediamine (118a)

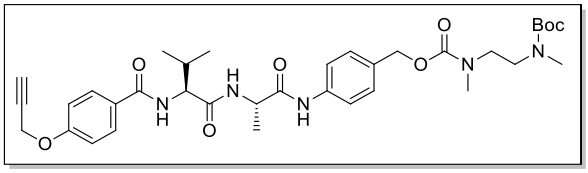

$C_{35}H_{47}N_5O_8$
MW: 665,78

N-Fmoc-protected compound **93** (70 mg, 0.096 mmol, 1 equiv) was deprotected following General Procedure GP2. A solution acid **109** (26 mg, 0.15 mmol, 1.5 equiv) in dry DMF (4 mL) was cooled to 0 °C under a nitrogen atmosphere. HATU (93 mg, 0.25 mmol, 1.7 equiv), HOAt (34 mg, 0.25 mmol, 1.7 equiv) and *i*Pr_2NEt (67 µL, 0.39 mmol, 4 equiv) were added and the mixture was stirred for 20 min at 0 °C. A solution of **93-NH** (49 mg, 0.096 mmol, 1 equiv) in dry DMF (2 mL) was added to the stirred mixture. The reaction was allowed to slowly reach room temperature and stirred overnight. The mixture was diluted with an AcOEt/CH_2Cl_2, 4:1 mixture (100 mL) and washed with 1 M aqueous solution of $KHSO_4$ (2 × 15 mL), a saturated aqueous solution of $NaHCO_3$ (1 × 15 mL) and brine (1 × 20 mL). The organic phase was dried over Na_2SO_4 and concentrated. The solid was solubilized in DCM/MeOH (95:5) and purified by flash chromatography [gradient: from 100% CH_2Cl_2 to 95:5 CH_2Cl_2/MeOH] to afford amide **118a** as a white solid (55 mg, 86% yield over two steps).
R_f = 0.35 (95:5, CH_2Cl_2/MeOH); ^{1}H NMR (400 MHz, CD_2Cl_2-d_2) δ 8.73 (s, 1H), 7.82 (d, *J* = 8.8 Hz, 2H), 7.58 (d, *J* = 8.1 Hz, 2H), 7.29 (d, *J* = 8.1 Hz, 2H), 7.13 (t, *J* = 6.4 Hz, 1H), 6.99 (d, *J* = 8.8 Hz, 2H), 6.90 (d, *J* = 7.7 Hz, 1H), 5.04 (s, 2H), 4.74 (d, *J* = 2.4 Hz, 2H), 4.66 (p, *J* = 7.1 Hz, 1H), 4.50 (t, *J* = 7.2 Hz, 1H), 3.38-3.27 (m, 4H), 2.91 (s, 3H), 2.76 (s, 3H), 2.61 (t, *J* = 2.4 Hz, 1H), 2.24 (q, *J* = 6.8 Hz, 1H), 1.43 (d, *J* = 11.8 Hz, 12H), 1.01 (dd, *J* = 6.8, 4.0 Hz, 6H). ^{13}C

NMR (101 MHz, CD_2Cl_2-d_2) δ 171.86, 170.91, 167.23, 160.23, 138.02, 132.73, 129.23, 128.66, 128.44, 127.08, 119.82, 114.50, 79.11, 77.96, 75.83, 66.59, 66.47, 59.13, 55.83, 49.66, 46.55, 38.37, 29.67, 28.08, 19.10, 18.50, 18.02. MS (ESI+) *m/z* calcd for $[C_{35}H_{48}N_5O_8]^+$: 666.34 [*M* + H]$^+$; found: 666.71; *m/z* calcd $[C_{35}H_{47}NaN_5O_8]^+$: 711.35 [*M* + Na]$^+$; found: 711.23.

Aromatic alkyne-Val-Ala-PTX (119a)

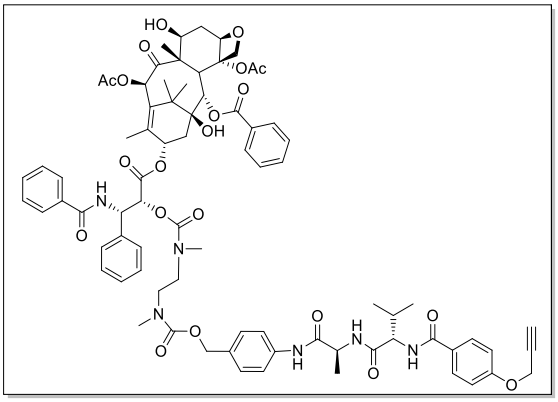

$C_{78}H_{88}N_6O_{21}$
MW: 1445,58

A solution of Boc-protected compound **118a** (20 mg, 0.03 mmol, 1 equiv) was deprotected following General Procedure GP1. The obtained TFA salt was dissolved in dry DMF (500 µL) and *i*Pr_2NEt (21 µL, 0.12 mmol, 4 equiv). The resulting solution was added at 0 °C to a stirred solution of **95** (46 mg, 0.045 mmol, 1.5 equiv) in dry DMF (500 µL), under a nitrogen atmosphere. The reaction was then allowed to reach room temperature and stirred overnight. AcOEt (100 mL) was added and the solution was washed with a 1 M aqueous solution of $KHSO_4$ (2 × 10 mL) and brine (1 × 15 mL). The organic phase was dried over Na_2SO_4 and concentrated, then the crude was purified by flash chromatography [eluent: 9:1 CH_2Cl_2/AcOEt] to afford carbamate **119a** as a white solid (39 mg, 93% yield).

R_f = 0.30 (9:1, CH_2Cl_2/AcOEt); MS (MALDI-TOF): *m/z* calcd for $[C_{78}H_{88}NaN_6O_{21}]^+$: 1467.99 [*M* + Na]$^+$; found: 1469.02 (HCCA matrix), 1469.09 (SA matrix); HRMS (ESI+): *m/z* calcd for $[C_{78}H_{88}NaN_6O_{21}]^+$: 1467.99, [*M* + Na]$^+$; found 1467.58; *m/z* calcd for $[C_{78}H_{88}Na_2N_6O_{21}]^{2+}$: 745.25, [*M* + 2Na]$^{2+}$; found: 745.28.

cyclo[DKP-RGD]-PEG-4-Val-Ala-PTX aromatic scaffold (102)

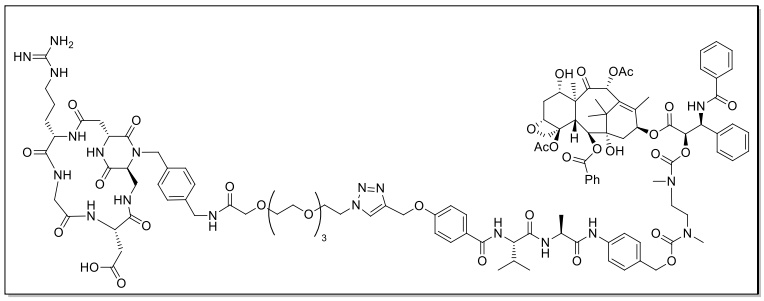

$C_{115}H_{143}N_{19}O_{34}$
MW: 2335,51

Alkyne **119a** (6.5 mg, 0.005 mmol, 1.5 equiv) and azide **86** (3 mg, 0.003 mmol, 1 equiv) were reacted following the General Procedure GP3. Crude residue was purified by semipreparative HPLC [Waters Atlantis 21 mm x 10 cm column; gradient: 90% (H_2O+0.1% CF_3COOH)/10% (CH_3CN+0.1% CF_3COOH) to 100% (CH_3CN+0.1% CF_3COOH) in 20 min; t_R (product)=12.9 min]. The purified product was then freeze-dried to give the desired compound **102** as a white solid (5 mg, 70% yield).

MS (MALDI-TOF): *m/z* calcd for $[C_{115}H_{144}N_{19}O_{34}]^+$: 2336.47 [*M* + H]$^+$; found: 2236.54 (HCCA matrix), 2236.09 (SA matrix); HRMS (ESI+): *m/z* calcd for $[C_{115}H_{144}NaN_{19}O_{34}]^{2+}$: 1178.98 [*M* + H + Na]$^{2+}$; found: 1179.00; *m/z* calcd for $[C_{115}H_{143}Na_2N_{19}O_{34}]^{2+}$: 1189.96 [*M* + 2Na]$^{2+}$; found: 1189.99; *m/z* calcd for $[C_{115}H_{142}Na_3N_{19}O_{34}]^{2+}$ 1200.86 [*M* + 3Na - H]$^{2+}$; found: 1200.98.

(*cyclo*[DKP-RGD]-PEG-4)$_2$-Val-Ala-PTX (**103**)

Methyl 3,5-bis(propynyloxy)phenyl acetate (111)

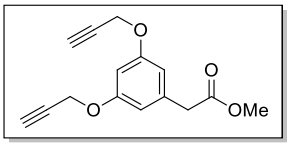

$C_{15}H_{14}O_4$
MW: 258,27

Commercial methyl 3,5-hydroxyphenyl acetate **110** (200 mg, 1.09 mmol, 1 equiv) was dissolved in dry acetone (11 mL) under nitrogen atmosphere. The solution was cooled in an ice bath. Propargyl bromide (760 µL, 8.8 mmol, 8 equiv) and K_2CO_3 (1.2 g, 8.8 mmol, 8 equiv) were added, and the mixture was stirred at room temperature 72 h. The mixture was concentrated, then the crude was dissolved in AcOEt (70 mL) and washed with water (3 × 10 mL). The organic phase was dried over Na_2SO_4 and concentrated. The crude residue was purified by a Grace Reveleris system (column: Reveleris Silica 12 g; dry load; flow rate: 30 mL min^{-1}; ramp: from 100% hexane to 100% AcOEt in 18 min) to afford **111** as a white solid (167 mg, yield: quantitative).

R_f = 0.58 (1:1, *n*-Hexane/AcOEt,); ^{1}H NMR (400 MHz, $CDCl_3$) δ 6.53 (bs, 3H), 4.65 (d, *J* = 2.4 Hz, 4H), 3.68 (s, 3H), 3.56 (s, 2H), 2.53 (t, *J* = 2.4 Hz, 2H). ^{13}C NMR (101 MHz, $CDCl_3$) δ 171.6, 158.7, 136.2, 109.1, 101.0, 78.4, 75.8, 55.9, 52.2, 41.4.

3,5-bis(Propynyloxy)phenyl acetic acid (88)

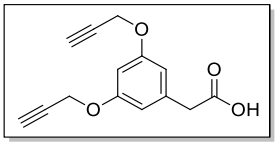

$C_{14}H_{12}O_4$
MW: 244,24

Compound **111** (165 mg, 0.64 mmol, 1 equiv) was dissolved in THF (20 mL) under a nitrogen atmosphere. The solution was cooled to 0 °C, then a solution of $LiOH{\cdot}H_2O$ (67 mg, 1.6 mmol, 2.5 equiv) in H_2O (10 mL) was added. The mixture was stirred 1.5 h at 0 °C. The mixture was acidified to *ca.* pH = 2 with a 1 M $KHSO_4$ aqueous solution and extracted with CH_2Cl_2 (4 × 20 mL). The organic phase was dried over Na_2SO_4 and concentrated, affording **88** as a white solid (158 mg, quantitative yield).

R_f = 0.36 (1:1, *n*-Hexane/AcOEt,); ^{1}H NMR (400 MHz, CD_3OD) δ 6.59-6.51 (m, 3H), 4.70 (d, *J* = 2.4 Hz, 4H), 3.54 (s, 2H), 2.92 (t, *J* = 2.4 Hz, 2H).

[3,5-bis(Propynyloxy)phenylacetyl]-Val–Ala-N-[4-[[[(N-(Boc)-*N*,*N*'-dimethylethylenediamine)carbonyl]oxy]methyl]phenyl] (118b)

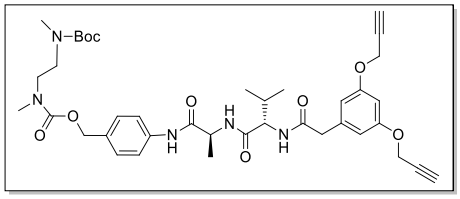

$C_{39}H_{51}N_5O_9$
MW: 733,85

N-Fmoc-protected compound **93** (160 mg, 0.219 mmol, 1 equiv) was deprotected following General Procedure GP2. A solution of acid **88** (68 mg, 0.28 mmol, 1.5 equiv) in dry DMF (2.3 mL) was cooled to 0 °C under a nitrogen atmosphere. HATU (114 mg, 0.3 mmol, 1.6 equiv), HOAt (41 mg, 0.3 mmol, 1.6 equiv) and *i*Pr_2NEt (100 µL, 0.57 mmol, 3 equiv) were added and the mixture was stirred for 20 min at 0 °C. A solution of **93-NH** (96 mg, 0.19 mmol, 1 equiv) in dry DMF (2.3 mL) was added to the stirred mixture. The reaction was allowed to slowly reach room temperature and stirred overnight. The mixture was diluted with a AcOEt/CH_2Cl_2, 4:1 mixture (100 mL) and washed with 1 M aqueous solution of $KHSO_4$ (2 × 15 mL), a saturated aqueous solution of $NaHCO_3$ (1 × 15 mL) and brine (1 × 20 mL). The organic phase was dried over Na_2SO_4 and concentrated. The solid was suspended in Et_2O. The product was collected by centrifugation and purified by flash chromatography [gradient: from 99:1 CH_2Cl_2/MeOH to 97:3 CH_2Cl_2/MeOH] to afford amide **118b** as a white solid (101 mg, 71% yield).

R_f = 0.3 (100 %, AcOEt); ^{1}H NMR (400 MHz, CD_3OD + $[D]_6$DMSO) δ 7.57 (m, 2H), 7.32 (m, 2H), 6.60 (d, *J* = 2.2 Hz, 2H), 6.53 (t, *J* = 2.2 Hz, 1H), 5.06 (s, 2H), 4.70 (d, *J* = 2.4 Hz, 4H), 4.46 (q, *J* = 7.1 Hz, 1H), 4.20 (d, *J* = 7.2 Hz, 1H), 3.56 (s, 1H), 3.41 (m, 4H), 3.03 (t, *J* = 2.4 Hz, 2H), 2.95 (m, rotamer A+B, 3H), 2.85 (bs, rotamer A, 3H), 2.75 (bs, rotamer B, 3H), 2.11 (m, 1H), 1.42 (m, 12H), 0.99 (d, *J* = 6.9 Hz, 3H), 0.97 (d, *J* = 6.9 Hz, 3H); ^{13}C NMR (101 MHz,

CD_3OD + $[D]_6DMSO$) δ 173.6, 173.3, 172.9, 160.2, 139.3, 130.0, 129.7, 121.0, 110.0, 101.8, 79.9, 77.2, 68.1, 67.9, 60.4, 56.7, 51.0, 43.6, 35.6, 35.3, 34.7, 31.9, 28.8, 19.8, 18.7, 18.1.

[3,5-bis(Propynyloxy)phenylacetyl]-Val–Ala-PTX (119b)

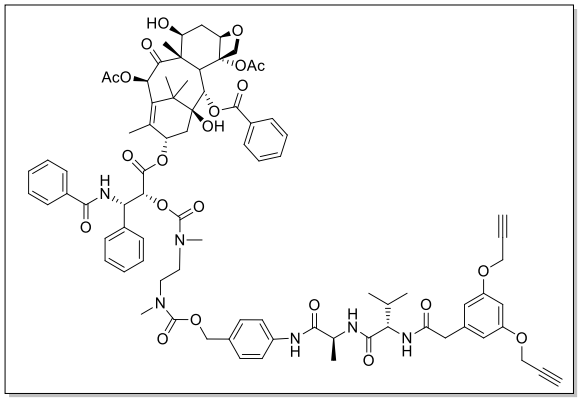

$C_{82}H_{92}N_6O_{22}$
MW: 1513,63

A solution of Boc-protected compound **118b** (75 mg, 0.1 mmol, 1 equiv) was deprotected following General Procedure GP1. The obtained TFA solid was dissolved in dry DMF (2 mL) and *i*Pr_2NEt (52 µL, 0.3 mmol, 3 equiv). The resulting solution was added at 0 °C to a stirred solution of **95** (204 mg, 0.2 mmol, 2 equiv) in dry DMF (1 mL), under a nitrogen atmosphere. The reaction was then allowed to reach room temperature and stirred overnight. AcOEt (100 mL) was added and the solution was washed with a 1 M aqueous solution of $KHSO_4$ (2 × 10 mL) and brine (1 × 15 mL). The organic phase was dried over Na_2SO_4 and concentrated, then the crude was purified by a Grace Reveleris system (column: Reveleris Silica HP 12 g, dry load, flow rate: 25 mL/min., ramp from 0% to 15% of MeOH in CH_2Cl_2 in 15 min) to afford carbamate **119b** as a white solid (116 mg, 77% yield).

R_f = 0.22 (100%, AcOEt); MS (ESI+) *m/z* calcd for $[C_{82}H_{92}N_6NaO_{22}]^+$: 1535.62 [*M* + Na]$^+$; found: 1535.89. MS (MALDI-TOF): *m/z* calcd for $[C_{82}H_{92}N_6NaO_{22}]^+$: 1535.62 [*M* + Na]$^+$; found: 1536.00 (HCCA matrix), 1536.08 (SA matrix); HRMS (ESI+): *m/z* calcd for $[C_{82}H_{92}N_6NaO_{22}]^+$: 1535.62, [*M* + Na]$^+$; found: 1535.68; *m/z* calcd for $[C_{82}H_{92}N_6Na_2O_{22}]^{2+}$: 779.01, [*M* + 2Na]$^{2+}$; found: 779.02.

(*cyclo*[DKP-RGD]-PEG-4)$_2$-Val-Ala-PTX (103)

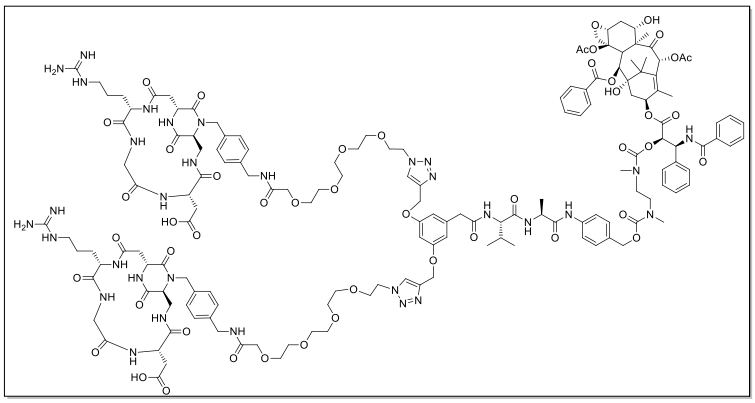

$C_{156}H_{202}N_{32}O_{48}$
MW: 3293,46

The bis-alkyne **119b** (5 mg, 33.2×10^{-2} mmol, 1 equiv) and azide **86** (10 mg, 99.6×10^{-2} mmol, 3 equiv) were reacted following the General Procedure GP3. The solvent was removed under vacuum, and the crude residue was purified by semipreparative HPLC [Waters Atlantis 21 mm x 10 cm column; gradient: 90% (H_2O+0.1% CF_3COOH)/10% (CH_3CN+0.1% CF_3COOH) to 100% (CH_3CN+0.1% CF_3COOH) in 26 min; t_R (product) = 14.9 min]. The purified product was then freeze-dried to give the desired compound **103** as a white solid (11 mg, quantitative yield). MS (ESI+): *m/z* calcd for $[C_{156}H_{204}N_{32}O_{48}]^{2+}$: 1646.73 $[M + 2H]^{2+}$; found: 1647.02; *m/z* calcd for $[C_{156}H_{203}N_{32}NaO_{48}]^{2+}$: 1657.72 $[M + H + Na]^{2+}$; found: 1658.01; MS (MALDI): *m/z* calcd for $[C_{156}H_{203}N_{32}O_{48}]^{+}$: 3294.47 $[M + H]^{+}$; found: 3291.00 (HCCA matrix), 3294.00 (SA matrix); HRMS (ESI+): *m/z* calcd for $[C_{156}H_{204}N_{32}O_{48}]^{2+}$: 1646.725 $[M + 2H]^{2+}$; found: 1646.726; *m/z* calcd for $[C_{156}H_{205}N_{32}O_{48}]^{3+}$; 1098.152 $[M + 3H]^{3+}$; found: 1098.148.

(*cyclo*[DKP-RGD]-PEG-4)$_3$-Val-Ala-PTX (**104**)

Methyl 2-(3,5-bis(2-((tert-butoxycarbonyl)amino)ethoxy)phenyl)acetate (112)

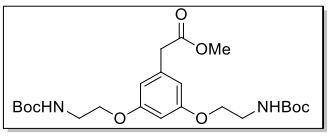

$C_{23}H_{36}N_2O_8$
MW: 468,55

Methyl 3,5-hydroxyphenyl acetate **110** (500 mg, 2.75 mmol, 1 equiv) was dissolved in dry acetone (20 mL) under nitrogen atmosphere. 2-(Boc-amino)ethyl bromide (3.7 g, 16.5 mmol, 6 equiv) in dry acetone (7 mL) was added to the starting material at 0 ºC together with K_2CO_3 (2.3 g, 16.5 mmol, 6 equiv), and the mixture was stirred under reflux, overnight. The mixture was concentrated, and later diluted in AcOEt (70 mL). The organic layer was washed with H_2O (2 × 30 mL) and brine (1 × 20 mL). The organic phase was dried over Na_2SO_4 and concentrated, then the crude was purified by flash chromatography [eluent: 9:1 CH_2Cl_2/AcOEt] to afford protected diamine **112** as a transparent oil (1.12 g, 87% yield).

R_f = 0.38 (9:1, CH_2Cl_2/AcOEt); ^{1}H NMR (400 MHz, $CDCl_3$) δ 6.42 (d, *J* = 2.2 Hz, 2H), 6.34 (t, *J* = 2.2 Hz, 1H), 4.99 (s, 2H), 3.97 (t, *J* = 5.1 Hz, 4H), 3.68 (s, 3H), 3.53 (s, 2H), 3.51-3.46 (m, 4H), 1.44 (s, 18H). ^{13}C NMR (101 MHz, $CDCl_3$) δ 171.62, 159.82, 155.86, 136.23, 108.31, 100.14, 67.26, 52.06, 41.30, 40.09, 28.39, 27.34.

Methyl 2-(3-(2-(2-(3,5-bis(prop-2-yn-1-yloxy)phenyl)acetamido)ethoxy)-5-(2-(4-(prop-2-yn-1-yloxy)benzamido)ethoxy)phenyl)acetate (116)

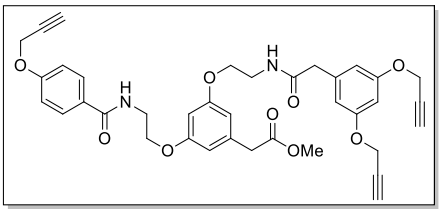

$C_{37}H_{36}N_2O_9$
MW: 652,69

A solution of Boc-protected compound **112** (550 mg, 2.05 mmol, 1 equiv) was deprotected following General Procedure GP1. The obtained solid (550 mg, 2.05 mmol, 5 equiv) was dissolved in a pre-flame dry flask with DMF (14 mL) and Et_3N (57 µL, 0.41 mmol, 1 equiv) and stirred about 20 min at r.t. Then, the acyl chloride **114** (110 mg, 0.410 mmol, 1 equiv) dissolved in DMF (5 mL) was slowly added (dropwise) to the TFA salt **113** at 0 ºC and the reaction mixture was stirred overnight at r.t. AcOEt (100 mL) was added and the solution was washed with $NaHCO_3$ (2 × 30 mL) and brine (1 × 15 mL). The organic phase was dried over Na_2SO_4 and concentrated, giving a yellow crude as amine **115** (MS (ESI+): m/z calcd for $[C_{27}H_{31}N_2O_7]^+$: 495.21 [*M* + H]$^+$; found: 495.25). Without isolation, the amine **115** was directly used in the next coupling. A solution of acid **109** (109 mg, 0.62 mmol, 1.5 equiv) in dry DMF (15 mL) was cooled to 0 °C under a nitrogen atmosphere. HATU (265 mg, 0.70 mmol, 1.7 equiv), HOAt (95 mg, 0.70 mmol, 1.7 equiv) and *i*Pr_2NEt (286 µL, 1.64 mmol, 4 equiv) were added and the mixture was stirred for 20 min at 0 °C. A solution of **115** (203 mg, 0.410 mmol, 1 equiv) in dry DMF (5 mL) was added to the stirred mixture. The reaction was allowed to slowly reach room temperature and stirred overnight. The mixture was diluted with AcOEt (200 mL) and washed with aqueous solution of $NaHCO_3$ sat. (2 × 30 mL), a saturated aqueous solution of K_2CO_3 (1 × 30 mL) and brine (2 × 20 mL). The organic phase was dried over Na_2SO_4 and concentrated. The crude was purified by flash chromatography [gradient: from 3:2 AcOEt/Petroleum Ether to 4:1 AcOEt/Petroleum Ether] to afford carbamate **116** as a light orange solid (80 mg, 30% yield over three steps).

R_f = 0.29 (25:75, Petroleum Ether/AcOEt); ^{1}H NMR (600 MHz, CD_2Cl_2-d_2) δ 7.77 (d, *J* = 8.8 Hz, 2H), 6.98 (d, *J* = 8.8 Hz, 2H), 6.87 (t, *J* = 5.5 Hz, 1H), 6.51 (d, *J* = 3.5 Hz, 3H), 6.43 (t, *J* = 1.8 Hz, 1H), 6.35 (dt, *J* = 13.6, 2.1 Hz, 2H), 6.28 (t, *J* = 5.3 Hz, 1H), 4.73 (d, *J* = 2.4 Hz, 2H), 4.62 (d, *J* = 2.5 Hz, 4H), 4.08 (t, *J* = 5.3 Hz, 2H), 3.95 (t, *J* = 5.3 Hz, 2H), 3.78 (q, *J* = 5.4 Hz, 2H), 3.66 (s, 3H), 3.55 (q, *J* = 5.6 Hz, 2H), 3.52 (s, 2H), 3.48 (s, 2H), 2.62 (t, *J* = 2.4 Hz, 1H),

2.58 (t, *J* = 2.5 Hz, 2H). ^{13}C NMR (151 MHz, CD_2Cl_2-d_2) δ 172.19, 171.03, 167.36, 160.54, 160.36, 160.27, 159.40, 138.15, 137.02, 129.34, 128.12, 115.07, 109.51, 109.01, 108.82, 101.42, 100.45, 78.91, 78.59, 76.34, 76.14, 67.36, 67.21, 56.40, 52.49, 44.15, 41.58, 39.92, 39.51, 38.92; MS (MALDI): *m/z* calcd for $[C_{37}H_{37}N_2O_9]^+$: 653.24 [*M* + H]$^+$; found: 653.27 (DHB matrix); *m/z* calcd for $[C_{37}H_{36}NaN_2O_9]^+$: 675.24 [*M* + Na]$^+$; found: 675.56 (DHB matrix).

2-(3-(2-(2-(3,5-bis(Prop-2-yn-1-yloxy)phenyl)acetamido)ethoxy)-5-(2-(4-(prop-2-yn-1-yloxy)benzamido)ethoxy)phenyl)acetic acid (89)

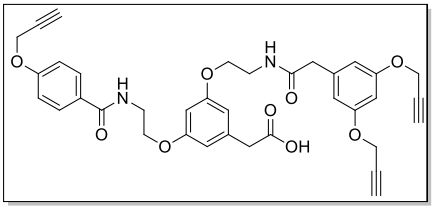

$C_{36}H_{34}N_2O_9$
MW: 638,67

Compound **116** (71 mg, 0.11 mmol, 1 equiv) was dissolved in THF (4 mL) under a nitrogen atmosphere. The solution was cooled to 0 °C, then a solution of $LiOH·H_2O$ (12 mg, 0.27 mmol, 2.5 equiv) in H_2O (2 mL) was added. The mixture was stirred 1.5 h at 0 °C. The mixture was acidified to *ca.* pH = 2 with a 1 M $KHSO_4$ aqueous solution and extracted with CH_2Cl_2 (4 × 20 mL). The organic phase was dried over Na_2SO_4 and concentrated, affording **89** as a white solid (158 mg, 99% yield).

R_f = 0.39 (9:1, CH_2Cl_2/MeOH); ^{1}H NMR (500 MHz, CD_3OD) δ 7.80 (d, *J* = 8.8 Hz, 2H), 7.01 (d, *J* = 8.9 Hz, 2H), 6.53 (d, *J* = 2.3 Hz, 2H), 6.50-6.46 (m, 2H), 6.44 (s, 1H), 6.41 (t, *J* = 2.3 Hz, 1H), 4.76 (d, *J* = 2.4 Hz, 2H), 4.61 (d, *J* = 2.5 Hz, 4H), 4.10 (t, *J* = 5.7 Hz, 2H), 3.97 (t, *J* = 5.2 Hz, 2H), 3.72 (t, *J* = 5.6 Hz, 2H), 3.52 (t, *J* = 6.1 Hz, 2H), 3.50 (s, 2H), 3.45 (s, 2H), 2.97 (t, *J* = 2.4 Hz, 1H), 2.90 (t, *J* = 2.4 Hz, 2H); ^{13}C-DEPT135 NMR (126 MHz, CD_3OD) δ 128.77, 114.29, 108.37, 108.23, 108.06, 100.52, 99.74, 78.34, 77.95, 75.87, 75.54, 66.13, 66.10, 55.32, 42.56, 40.93, 39.27, 38.88. MS (MALDI): *m/z* calcd for $[C_{36}H_{35}N_2O_9]^+$: 639.24 [*M* + H]$^+$; found: 639.27 (DHB matrix); *m/z* calcd for $[C_{36}H_{34}NaN_2O_9]^+$: 661.24 [*M* + Na]$^+$; found: 661.27 (DHB matrix); *m/z* calcd for $[C_{36}H_{34}KN_2O_9]^+$: 677.24 [*M* + K]$^+$; found: 677.27 (DHB matrix).

Tris-alkyne-Val-Ala-PABC-*N*-(Boc)-*N*,*N*′-dimethylethylenediamine (118c)

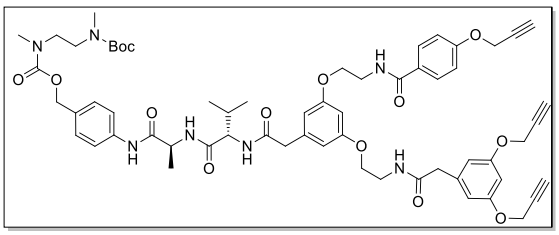

$C_{61}H_{73}N_7O_{14}$
MW: 1128,29

N-Fmoc-protected compound **93** (65 mg, 0.091 mmol, 1 equiv) was deprotected following General Procedure GP2. A solution of acid **89** (70 mg, 0.11 mmol, 1.2 equiv) in dry DMF (2 mL) was cooled to 0 °C under a nitrogen atmosphere. HATU (59 mg, 0.16 mmol, 1.7 equiv),

HOAt (22 mg, 0.16 mmol, 1.7 equiv) and *i*Pr_2NEt (64 µL, 0.364 mmol, 4 equiv) were added and the mixture was stirred for 20 min at 0 °C. A solution of **93-NH** (45 mg, 0.091 mmol, 1 equiv) in dry DMF (3 mL) was added to the stirred mixture. The reaction was allowed to slowly reach room temperature and stirred overnight. The mixture was diluted with AcOEt (100 mL) and washed with 1 M aqueous solution of $KHSO_4$ (2 × 15 mL), a saturated aqueous solution of $NaHCO_3$ (1 × 15 mL) and brine (1 × 20 mL). The organic phase was dried over Na_2SO_4 and concentrated. The crude was purified by flash chromatography [eluent: CH_2Cl_2/MeOH, 9:1] to afford amide **118c** as a light-yellow solid (73 mg, 80% yield over two steps).

R_f = 0.41 (9:1, CH_2Cl_2/MeOH); ^{1}H NMR (400 MHz, [D]$_6$DMSO) δ 9.77 (s, 1H), 8.39 (t, *J* = 5.5 Hz, 1H), 8.10-8.00 (m, 2H), 7.89-7.81 (m, 3H), 7.55 (d, *J* = 8.5 Hz, 2H), 7.27 (d, *J* = 8.3 Hz, 2H), 7.03 (d, *J* = 8.9 Hz, 2H), 6.53 (d, *J* = 2.2 Hz, 2H), 6.50 (d, *J* = 2.2 Hz, 2H), 6.48 (s, 1H), 6.40 (t, *J* = 2.3 Hz, 1H), 4.98 (s, 2H), 4.85 (d, *J* = 2.4 Hz, 2H), 4.72 (d, *J* = 2.4 Hz, 4H), 4.41 (p, *J* = 7.0 Hz, 1H), 4.20 (dd, *J* = 8.7, 6.6 Hz, 1H), 4.08 (t, *J* = 6.0 Hz, 2H), 3.97 (t, *J* = 5.8 Hz, 2H), 3.60 (q, *J* = 5.8 Hz, 2H), 3.51-3.45 (m, 2H), 3.44-3.37 (m, 7H), 3.32 (dd, *J* = 12.3, 4.7 Hz, 4H), 2.85 (s, 3H), 2.74 (s, 3H), 2.00 (h, *J* = 6.8 Hz, 1H), 1.37 (s, 9H), 1.30 (d, *J* = 7.1 Hz, 3H), 0.85 (dd, *J* = 9.5, 6.8 Hz, 6H); ^{13}C NMR (101 MHz, [D]$_6$DMSO) δ 170.73, 170.53, 169.74, 165.80, 159.27, 159.20, 159.12, 157.98, 155.18, 154.54, 138.44, 138.33, 138.26, 131.52, 128.68, 127.93, 127.23, 118.93, 114.18, 108.69, 107.95, 100.04, 99.41, 78.91, 78.64, 78.24, 77.95, 77.68, 66.19, 66.03, 65.75, 57.52, 55.44, 48.89, 45.92, 42.19, 38.66, 38.24, 33.73, 30.28, 28.67, 27.78, 18.86, 17.81, 17.60.

MS (MALDI): *m/z* calcd for $[C_{61}H_{74}N_7O_{14}]^+$: 1128.52 [*M* + H]$^+$; found: 1128.52 (DHB matrix); *m/z* calcd for $[C_{61}H_{73}NaN_7O_{14}]^+$: 1150.54 [*M* + Na]$^+$; found: 1150.55 (DHB matrix); *m/z* calcd for $[C_{61}H_{73}KN_7O_{14}]^+$: 1166.24 [*M* + K]$^+$; found: 1166.27 (DHB matrix).

Tris-alkyne–Val–Ala–PTX (119c)

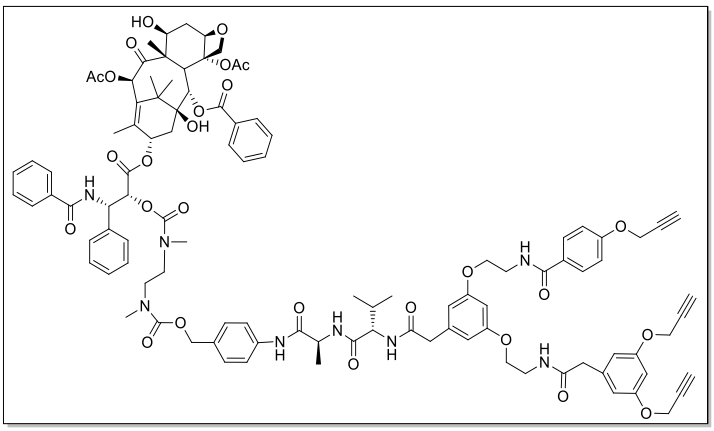

$C_{104}H_{114}N_8O_{27}$
MW: 1908,06

A solution of Boc-protected compound **118c** (40 mg, 0.035 mmol, 1 equiv) was deprotected following General Procedure GP1. The obtained TFA solid was dissolved in dry DMF (500 µL) and *i*Pr_2NEt (25 µL, 0.14 mmol, 4 equiv). The resulting solution was added at 0 °C to a stirred

solution of **95** (54 mg, 0.052 mmol, 1.5 equiv) in dry DMF (700 µL), under a nitrogen atmosphere. The reaction was then allowed to reach room temperature and stirred overnight. AcOEt (60 mL) was added and the solution was washed with a 1 M aqueous solution of $KHSO_4$ (2 × 10 mL) and brine (1 × 15 mL). The organic phase was dried over Na_2SO_4 and concentrated, then the crude was purified by a flash chromatography (eluent: CH_2Cl_2/MeOH from 100% to 95% of CH_2Cl_2) to afford carbamate **119c** as a white solid (44 mg, 69% yield over two steps).

R_f = 0.43 (9:1, CH_2Cl_2/MeOH); MS (ESI+): *m/z* calcd for $[C_{104}H_{114}NaN_8O_{27}]^+$: 1930.03 [*M* + Na]$^+$; found: 1930.04; MS (MALDI-TOF): *m/z* calcd for $[C_{104}H_{114}NaN_8O_{27}]^+$: 1930.03 [*M* + Na]$^+$; found: 1930.03 (DHB matrix); *m/z* calcd for $[C_{104}H_{114}KN_8O_{27}]^+$: 1946.07 [*M* + K]$^+$; found: 1946.09 (DHB matrix); HRMS (ESI+): *m/z* calcd for $[C_{104}H_{114}NaN_8O_{27}]^+$: 1930.03 [*M* + Na]$^+$; found: 1930.75; *m/z* calcd for $[C_{104}H_{114}Na_2N_8O_{27}]^{2+}$: 976.39 [*M* + 2Na]$^{2+}$; found: 976.38.

(cyclo[DKP-RGD]-PEG-4)$_3$-Val-Ala-PTX (104)

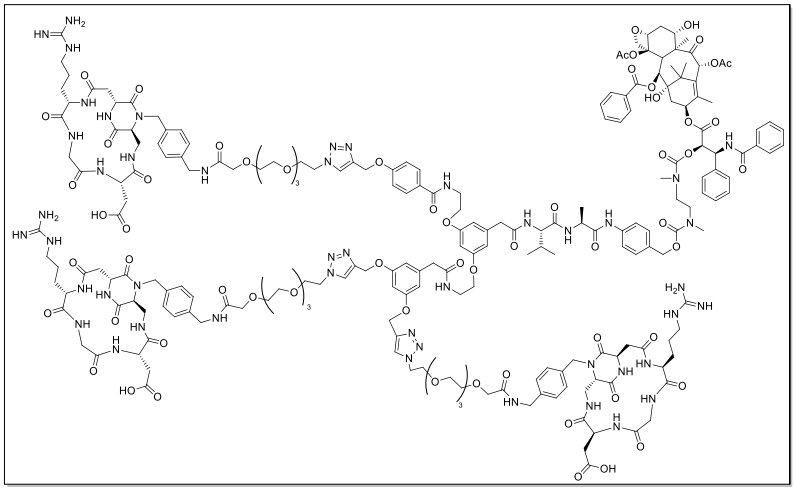

$C_{215}H_{279}N_{47}O_{66}$
MW: 4577.86

Tri-alkyne **119c** (5 mg, 0.0026 mmol, 1 equiv) and azide **86** (9.5 mg, 0.0094 mmol, 3.6 equiv) were reacted following the General Procedure GP3. The solvent was removed under vacuum, and the crude residue was purified by semipreparative HPLC [Waters Atlantis 21 mm x 10 cm column; gradient: 90% (H_2O+0.1% CF_3COOH)/10% (CH_3CN+0.1% CF_3COOH) to 100% (CH_3CN+0.1% CF_3COOH) in 20 min; t_R (product)=11.5 min]. The purified product was then freeze-dried to give the desired compound **104** as a white solid (6.9 mg, 62% yield).

MS (ESI+): *m/z* calcd for $[C_{215}H_{281}N_{47}O_{66}]^{2+}$: 2289.85, [*M* + 2H]$^{2+}$; found: 2289.89; *m/z* calcd for $[C_{215}H_{282}N_{47}O_{66}]^{3+}$: 1526.86 [*M* + 3H]$^{3+}$; found: 1527.00; *m/z* calcd for $[C_{215}H_{283}N_{47}O_{66}]^{4+}$: 1145.86 [*M* + 4H]$^{4+}$; found: 1145.51; *m/z* calcd for $[C_{215}H_{284}N_{47}O_{66}]^{5+}$: 916.23 [*M* + 5H]$^{5+}$; found: 916.61; MS (MALDI-TOF): *m/z* calcd for $[C_{215}H_{280}N_{47}O_{66}]^+$: 4577.01 [*M* + H]$^+$; found: 4582.01 (DHB matrix); HRMS (ESI+): *m/z* calcd for $[C_{215}H_{279}Na_3N_{47}O_{66}]^{3+}$: 1548.99 [*M* + 3Na]$^{3+}$; found: 1548.92; *m/z* calcd for $[C_{215}H_{279}Na_4N_{47}O_{66}]^{4+}$: 1167.43 [*M* + 4Na]$^{4+}$; found: 1167.24.

(*cyclo*[DKP-RGD]-PEG-4)$_4$-Val-Ala-PTX (**105**)

Methyl 2-(3,5-bis(2-(2-(3,5-bis(prop-2-yn-1-yloxy)phenyl)acetamido)ethoxy)phenyl) acetate (117)

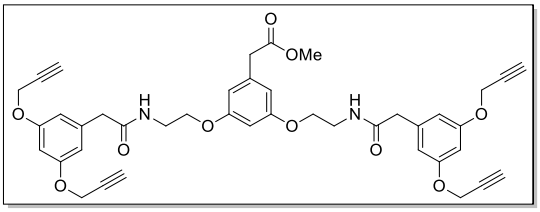

$C_{41}H_{40}N_2O_{10}$
MW: 720,78

A solution of Boc-protected compound **112** (200 mg, 0.43 mmol, 1 equiv) was deprotected following General Procedure GP1. Then, acid **88** (315 mg, 1.29 mmol, 3 equiv) was solubilized in dry DMF (15 mL) and cooled to 0 °C under a nitrogen atmosphere. HATU (556 mg, 1.46 mmol, 3.6 equiv), HOAt (199 mg, 1.46 mmol, 3.6 equiv) and *i*Pr$_2$NEt (449 µL, 2.58 mmol, 6 equiv) were added and the mixture was stirred for 20 min at 0 °C. Later, the salt **113** (200 mg, 0.43 mmol, 1 equiv) was dissolved in dry DMF (9 mL) and slowly added (dropwise) the reaction mixture that was stirred overnight at r.t. The mixture was diluted with AcOEt (100 mL) and washed with 1 M aqueous solution of $KHSO_4$ (2 × 15 mL), a saturated aqueous solution of $NaHCO_3$ (1 × 15 mL) and brine (1 × 20 mL). The organic phase was dried over Na_2SO_4 and concentrated. The crude was purified by flash chromatography [eluent: CH_2Cl_2/MeOH, 9:1] to afford diamide **117** as a light orange solid (238 mg, 77% yield over two steps).
R_f = 0.28 (99:1, CH_2Cl_2/MeOH); ^{1}H NMR (400 MHz, CD_2Cl_2-d_2) δ 6.50 (s, 6H), 6.37-6.34 (m, 2H), 6.27 (s, 1H), 6.02 (t, *J* = 5.7 Hz, 2H), 4.63 (d, *J* = 2.3 Hz, 8H), 3.96 (t, *J* = 5.2 Hz, 4H), 3.66 (s, 3H), 3.56 (q, *J* = 5.5 Hz, 4H), 3.52 (s, 2H), 3.48 (s, 4H), 2.56 (t, *J* = 2.5 Hz, 4H). ^{13}C NMR (101 MHz, CD_2Cl_2-d_2) δ 172.12, 170.86, 160.29, 159.47, 138.10, 137.11, 109.56, 108.93, 101.54, 100.53, 78.91, 76.11, 67.30, 56.46, 52.50, 44.28, 41.62, 39.54. MS (ESI+): *m/z* calcd for $[C_{41}H_{40}NaN_2O_{10}]^+$: 743.11 [*M* + Na]$^+$; found: 743.10.

2-(3,5-bis(2-(2-(3,5-bis(Prop-2-yn-1-yloxy)phenyl)acetamido)ethoxy)phenyl)acetic acid (90)

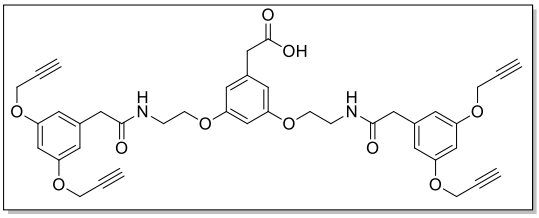

$C_{40}H_{38}N_2O_{10}$
MW: 706,75

Compound **117** (137 mg, 0.2 mmol, 1 equiv) was dissolved in THF (6.6 mL) under a nitrogen atmosphere. The solution was cooled to 0 °C, then a solution of $LiOH{\cdot}H_2O$ (21 mg, 0.5 mmol, 2.5 equiv) in H_2O (3.3 mL) was added. The mixture was stirred 1.5 h at 0 °C. The mixture was acidified to *ca.* pH = 2 with a 1 M $KHSO_4$ aqueous solution and extracted with CH_2Cl_2 (4 × 20 mL). The organic phase was dried over Na_2SO_4 and concentrated. The crude was purified by

flash chromatography [eluent: 9:1:0.1 CH_2Cl_2/MeOH/AcOH] affording **90** as a white solid (120 mg, 85% yield).

R_f = 0.2 (95:5, CH_2Cl_2/MeOH); ^{1}H NMR (400 MHz, CD_3OD) δ 6.56 (d, *J* = 2.3 Hz, 4H), 6.51 (t, *J* = 2.3 Hz, 2H), 6.47 (d, *J* = 2.2 Hz, 2H), 6.37 (d, *J* = 2.2 Hz, 1H), 4.64 (d, *J* = 2.4 Hz, 8H), 4.01 (t, *J* = 5.4 Hz, 4H), 3.56 (t, *J* = 5.3 Hz, 4H), 3.52 (s, 2H), 3.48 (s, 4H), 2.91 (t, *J* = 2.4 Hz, 4H). ^{13}C NMR (101 MHz, CD_3OD) δ 173.97, 161.21, 160.27, 139.04, 138.69, 109.77, 109.55, 108.51, 101.94, 101.07, 79.71, 76.87, 67.50, 56.72, 43.95, 42.75, 40.26. MS (ESI+): *m/z* calcd for $[C_{40}H_{38}NaN_2O_{10}]^+$: 729.42 [*M* +Na]$^+$; found: 729.45.

Tetra-alkyne-Val-Ala-PABC-*N*-(Boc)-*N*,*N'*-dimethylethylenediamine (118d)

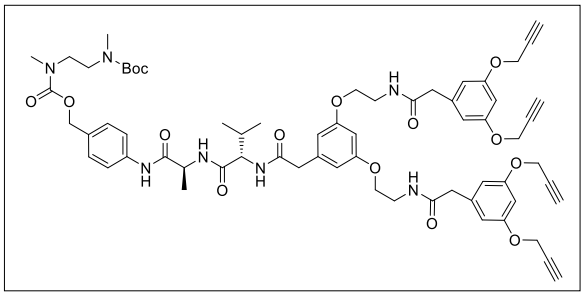

Chemical Formula: $C_{65}H_{77}N_7O_{15}$
Molecular Weight: 1196,37

N-Fmoc-protected compound **93** (35 mg, 0.047 mmol, 1 equiv) was deprotected following General Procedure GP2. A solution of acid **90** (50 mg, 0.071 mmol, 1.5 equiv) in dry DMF (1 mL) was cooled to 0 °C under a nitrogen atmosphere. HATU (31 mg, 0.08 mmol, 1.7 equiv), HOAt (11 mg, 0.08 mmol, 1.7 equiv) and *i*Pr_2NEt (33 µL, 0.189 mmol, 4 equiv) were added and the mixture was stirred for 20 min at 0 °C. A solution of **93-NH** (24 mg, 0.047 mmol, 1 equiv) in dry DMF (1.6 mL) was added to the stirred mixture. The reaction was allowed to slowly reach room temperature and stirred overnight. The mixture was diluted with AcOEt (100 mL) and washed with 1 M aqueous solution of $KHSO_4$ (2 × 15 mL), a saturated aqueous solution of $NaHCO_3$ (1 × 15 mL) and brine (1 × 20 mL). The organic phase was dried over Na_2SO_4 and concentrated. The crude was purified by flash chromatography [eluent: CH_2Cl_2/MeO, 95:5 H] to afford amide **118d** as a light-yellow solid (54 mg, 92% yield over two steps).

R_f = 0.27 (95:5, CH_2Cl_2/MeOH); ^{1}H NMR (400 MHz, [D]$_6$DMSO) δ 9.82 (s, 1H), 8.18-8.07 (m, 3H), 7.91 (d, *J* = 8.6 Hz, 1H), 7.56 (d, *J* = 8.5 Hz, 2H), 7.28 (d, *J* = 8.2 Hz, 2H), 6.54 (d, *J* = 2.3 Hz, 2H), 6.51 (t, *J* = 2.2 Hz, 5H), 6.49 (d, *J* = 2.3 Hz, 2H), 4.99 (s, 2H), 4.73 (d, *J* = 2.4 Hz, 8H), 4.41 (p, *J* = 6.9 Hz, 1H), 4.21 (dd, *J* = 8.7, 6.6 Hz, 1H), 3.97 (t, *J* = 5.9 Hz, 4H), 3.50-3.38 (m, 14H), 3.33 (dd, *J* = 12.1, 4.6 Hz, 4H), 2.86 (s, 3H), 2.74 (s, 3H), 2.01 (h, *J* = 6.7 Hz, 1H), 1.38 (s, 9H), 1.31 (d, *J* = 7.1 Hz, 3H), 0.86 (dd, *J* = 10.3, 6.8 Hz, 6H). ^{13}C NMR (101 MHz, [D]$_6$DMSO) δ 170.82, 170.61, 169.78, 159.29, 159.13, 158.00, 141.44, 138.52, 138.38, 138.31, 131.54, 128.03, 108.67, 108.25, 107.94, 107.69, 107.44, 100.00, 99.65, 99.36, 78.96, 78.28, 77.81, 66.21, 65.80, 57.45, 55.44, 48.91, 42.24, 40.42, 38.28, 30.41, 27.83, 18.93, 17.88, 17.68; MS

(MALDI-TOF): *m/z* calcd for $[C_{65}H_{77}NaN_7O_{15}]^+$: 1218.03 [*M* + Na]$^+$; found: 1218.2 (HCCA matrix).

Tetra–alkyne–Val–Ala-PTX (119d)

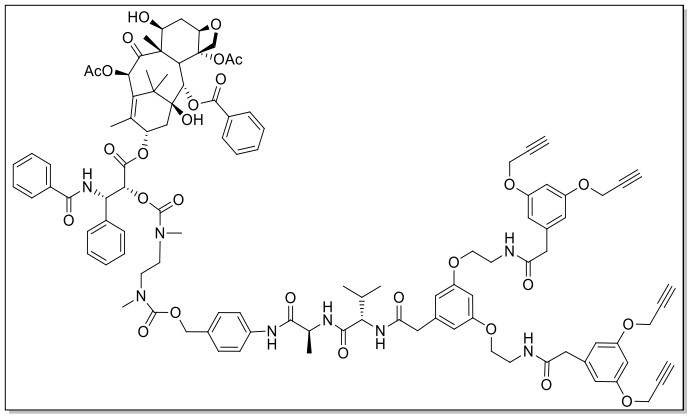

$C_{108}H_{118}N_8O_{28}$
MW: 1976,13

A solution of Boc-protected compound **118d** (40 mg, 0.033 mmol, 1 equiv) was deprotected following General Procedure GP1. The obtained TFA solid was dissolved in dry DMF (500 μL) and *i*Pr$_2$NEt (24 μL, 0.13 mmol, 4 equiv). The resulting solution was added at 0 °C to a stirred solution of **95** (51 mg, 0.05 mmol, 1.5 equiv) in dry DMF (500 μL), under a nitrogen atmosphere. The reaction was then allowed to reach room temperature and stirred overnight. AcOEt (60 mL) was added and the solution was washed with a 1 M aqueous solution of $KHSO_4$ (2 × 10 mL) and brine (1 × 15 mL). The organic phase was dried over Na_2SO_4 and concentrated, then the crude was purified by a flash chromatography (eluent: AcOEt/MeOH from 100% to 95% of AcOEt) to afford carbamate **119d** as a white solid (49 mg, 75% yield over two steps).
R_f = 0.25 (95:5, CH_2Cl_2/MeOH); MS (MALDI-TOF): *m/z* calcd for $[C_{108}H_{119}N_8O_{28}]^+$: 1976.01 [*M* + H]$^+$; found: 1976.2 (HCCA matrix); *m/z* calcd for $[C_{108}H_{118}NaN_8O_{28}]^+$: 1997.9 [*M* + Na]$^+$; found: 1998.02 (HCCA matrix); HRMS (ESI+): *m/z* calcd for $[C_{108}H_{118}NaN_8O_{28}]^+$: 1997.99, [*M* + Na]$^+$; found 1997.79; *m/z* calcd for $[C_{108}H_{118}Na_2N_8O_{28}]^{2+}$: 1010.31, [*M* + 2Na]$^{2+}$: found 1010.39.

(*cyclo*[DKP-RGD]-PEG-4)$_4$-Val-Ala-PTX (105)

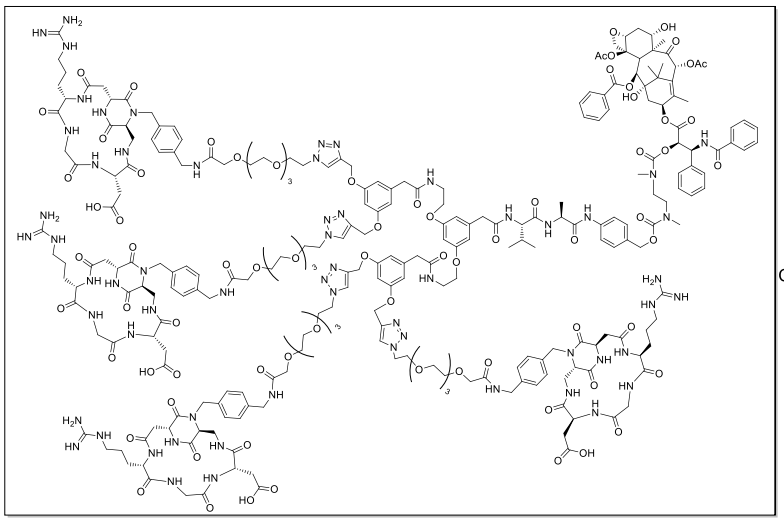

$C_{256}H_{338}N_{60}O_{80}$
MW: 5535.86

Tetra-alkyne **119d** (4 mg, 0.002 mmol, 1 equiv) and azide **86** (9.8 mg, 0.0097 mmol, 4.8 equiv) were reacted following the General Procedure GP3. The solvent was removed under vacuum, and the crude residue was purified by semipreparative HPLC [Waters Atlantis 21 mm x 10 cm column; gradient: 90% (H_2O + 0.1% CF_3COOH)/10% (CH_3CN + 0.1% CF_3COOH) to 100% (CH_3CN + 0.1% CF_3COOH) in 20 min; t_R (product)=10.9 min]. The purified product was then freeze-dried to give the desired compound **105** as a white solid (8 mg, 73% yield).

MS (MALDI-TOF): *m/z* calcd for $[C_{256}H_{339}N_{60}O_{80}]^+$: 5532.78 [*M* + H]$^+$; found: 5532.90 (HCCA matrix); HRMS (ESI+): *m/z* calcd for $[C_{256}H_{338}Na_4N_{60}O_{80}]^{4+}$: 1406.93 [*M* + 4Na]$^{4+}$; found: 1406.84; *m/z* calcd for $[C_{256}H_{338}Na_5N_{60}O_{80}]^{5+}$: 1130.14 [*M* + 5Na]$^{5+}$; found: 1130.07.

cyclo[DKP-RGD]-PEG-4-Asn-Pro-Val-PTX (**121**)

Fmoc-Asn(Trt)-Pro-OH (126)

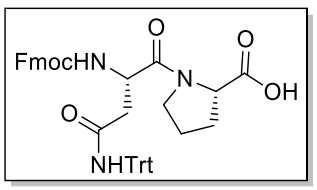

$C_{43}H_{39}N_3O_6$
MW: 693,79

Commercial Fmoc-Asn(Trt)-OH **125** (2 g, 3.35 mmol, 1 equiv) and EDC·HCl (1.9 g, 10.05 mmol, 3 equiv) were dissolved in dry CH_2Cl_2 (33 mL) under nitrogen atmosphere. *N*-hydroxysuccinimide (771 mg, 6.70 mmol, 2 equiv) was added thereto, and the mixture was stirred overnight at room temperature. The reaction mixture was diluted with CH_2Cl_2 (30 mL) and washed with HCl aq. 1 M (1 × 25 mL) and brine. The organic layer was washed with brine, dried over Na_2SO_4 and concentrated under reduced pressure. Then, the residue was purified by flash chromatography on a pad of silica gel (eluent: 8:2, CH_2Cl_2/AcOEt) affording the desired activated Fmoc-Asn(Trt)-OSu as a white solid. Later on, commercial H-Pro-OH (464 mg, 4.02

mmol, 1.2 equiv) was dissolved in H_2O (20 mL) and $NaHCO_3$ (563 mg, 6.70 mmol, 2 equiv) was added. The previously obtained Fmoc-Asn(Trt)-OSu was dissolved in THF (20 mL) and added to the stirred solution of H-Pro-OH and $NaHCO_3$. The mixture was stirred overnight at room temperature. The solvent was concentrated, followed by addition of a 1 M aqueous solution of $KHSO_4$ (40 mL). The suspension was extracted with CH_2Cl_2 (4 × 20 mL), and the collected organic phases were dried and concentrated. The crude was purified by flash chromatography [eluent: 8:2, CH_2Cl_2/AcOEt + 0.1% AcOH] affording Fmoc-Asn(Trt)-Pro-OH **126** (1.2 g, 52% yield).

R_f = 0.15 (8:2, CH_2Cl_2/AcOEt + 0.1% AcOH); ^{1}H NMR (500 MHz, CD_2Cl_2-d_2) δ 7.80 (d, *J* = 7.6 Hz, 2H), 7.60 (t, *J* = 8.7 Hz, 2H), 7.42 (t, *J* = 7.7 Hz, 2H), 7.34 – 7.18 (m, 18H), 6.08 (s, 1H), 4.83 – 4.74 (m, 1H), 4.37 (d, *J* = 7.0 Hz, 3H), 4.19 (t, *J* = 6.8 Hz, 1H), 3.64 – 3.53 (m, 1H), 3.43 (s, 1H), 2.84 (dd, *J* = 15.4, 7.3 Hz, 1H), 2.72 (dd, *J* = 15.4, 5.8 Hz, 1H), 2.19 – 2.04 (m, 2H), 1.95 – 1.82 (m, 2H); MS (MALDI-TOF): *m/z* calcd for $[C_{43}H_{40}N_3O_6]^+$: 694.79 [*M* + H]$^+$; found: 694.81; *m/z* calcd $[C_{43}H_{39}NaN_3O_6]^+$: 716.79 [*M* + Na]$^+$; found: 716.80 (DHB matrix).

Fmoc-Asn(Trt)-Pro-Val-OH (127)

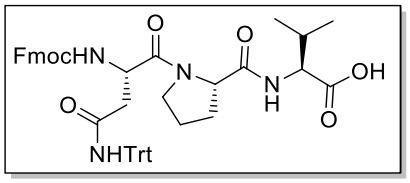

$C_{48}H_{48}N_4O_7$
MW: 792,92

Fmoc-Asn(Trt)-Pro-OH **126** (1.18 g, 1.70 mmol, 1 equiv) and EDC·HCl (977 mg, 5.10 mmol, 3 equiv) were dissolved in dry CH_2Cl_2 (17 mL) under nitrogen atmosphere. *N*-hydroxysuccinimide (400 mg, 3.40 mmol, 2 equiv) was added thereto, and the mixture was stirred overnight at room temperature. The reaction mixture was diluted with CH_2Cl_2 (20 mL) and washed with HCl aq. 1 M (1 × 15 mL) and brine. The organic layer was washed with brine, dried over Na_2SO_4 and concentrated under reduced pressure affording the desired activated Fmoc-Asn(Trt)-Pro-OSu as a white solid. Later, commercial H-Val-OH (240 mg, 2.04 mmol, 1.2 equiv) was dissolved in H_2O (11 mL) and $NaHCO_3$ (290 mg, 3.40 mmol, 2 equiv) was added. The previously obtained Fmoc-Asn(Trt)-Pro-OSu was dissolved in THF (11 mL) and added to the stirred solution of H-Val-OH and $NaHCO_3$. The mixture was stirred overnight at room temperature. The solvent was concentrated, followed by addition of a 1 M aqueous solution of $KHSO_4$ (20 mL). The suspension was extracted with CH_2Cl_2 (4 × 15 mL), then the collected organic phases were dried and concentrated. The crude was purified by flash chromatography [eluent: 95:5 CH_2Cl_2/MeOH + 0.1% AcOH] affording Fmoc-Asn(Trt)-Pro-Val-OH **127** (1.10 g, 82% yield).

R_f = 0.21 (95:5, CH_2Cl_2/MeOH + 0.1% AcOH); ^{1}H NMR (500 MHz, CD_2Cl_2-d_2) δ 7.85 (d, *J* = 8.2 Hz, 1H), 7.66 (d, *J* = 6.9 Hz, 2H), 7.51 – 7.41 (m, 3H), 7.27 (td, *J* = 7.3, 3.5 Hz, 2H), 7.20 -

7.05 (m, 17H), 6.60 (d, *J* = 8.4 Hz, 1H), 4.44 (td, *J* = 9.5, 3.6 Hz, 1H), 4.21 – 4.08 (m, 3H), 4.04 (t, *J* = 7.3 Hz, 1H), 3.85 (t, *J* = 8.3 Hz, 1H), 3.27 (q, *J* = 8.6 Hz, 1H), 2.95 – 2.82 (m, 1H), 2.71 – 2.64 (m, 1H), 2.61 (dd, *J* = 14.0, 3.7 Hz, 1H), 1.92 – 1.76 (m, 2H), 1.70 – 1.58 (m, 2H), 1.47 (p, *J* = 10.7, 9.8 Hz, 1H), 0.67 (d, *J* = 6.7 Hz, 3H), 0.44 (d, *J* = 6.6 Hz, 3H); ^{13}C-DEPT45 NMR (126 MHz, CD_2Cl_2-d_2) δ 128.87, 128.81, 127.99, 127.86, 127.80, 127.18, 127.05, 125.34, 125.33, 120.02, 67.24, 61.55, 59.26, 49.72, 47.60, 47.15, 40.58, 29.81, 29.56, 29.15, 24.70, 19.36, 18.87. MS (MALDI-TOF): *m/z* calcd for $[C_{48}H_{49}N_4O_7]^+$: 793.92 [*M* + H]$^+$; found: 793.99; *m/z* calcd $[C_{48}H_{48}NaN_4O_7]^+$: 815.92 [*M* + Na]$^+$; found: 816.01 (DHB matrix).

Fmoc-Asn(Trt)-Pro-Val-PABC-PNP (128)

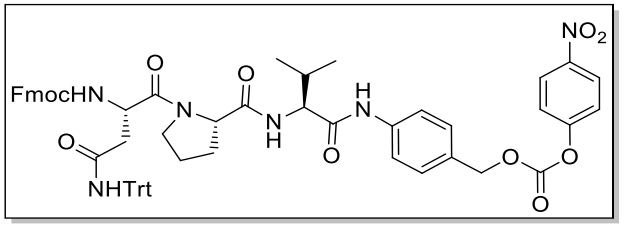

$C_{62}H_{58}N_6O_{11}$
MW: 1063,16

Compound **127** (880 mg, 1.11 mmol, 1 equiv) was dissolved in dry CH_2Cl_2/MeOH (2:1, 11 mL) under a nitrogen atmosphere. EEDQ (686 mg, 2.77 mmol, 2.5 equiv) and 4-aminobenzyl alcohol (273 mg, 2.22 mmol, 2 equiv) were added at 0 °C, under a nitrogen atmosphere. Then, the mixture was allowed to reach room temperature and stirred overnight under nitrogen atmosphere. The solvent was removed under reduced pressure affording a yellow solid. The crude was diluted in Et_2O (3 × 30 mL) and filtered in a fritz. The solid was purified by flash chromatography [gradient: from 0% MeOH / 100% CH_2Cl_2 to 5% MeOH / 95% CH_2Cl_2] to afford the Fmoc-Asn(Trt)-Pro-Val-PABA as a white solid (MS (MALDI-TOF): *m/z* calcd for $[C_{55}H_{55}NaN_5O_7]^+$: 921.05 [*M* + Na]$^+$; found: 921.23). Later on, a solution of Fmoc-Asn(Trt)-Pro-Val-PABA in a mixture of dry THF (65 mL) under nitrogen atmosphere was cooled to 0 °C. Pyridine (224 µL, 2.77 mmol, 2.5 equiv) and 4-nitrophenylchloroformate (448 mg, 2.22 mmol, 2 equiv) were added, then the mixture could reach room temperature and stirred for 2 h. The reaction mixture was concentrated under reduced pressure and AcOEt (150 mL) was added and the solution was washed with a 1 M aqueous solution of $KHSO_4$ (3 × 20 mL) and brine (20 mL). The organic phase was dried and concentrated, then the crude was purified by flash chromatography [eluent: 4:6, *n*-Hexane/EtOAc] affording compound **128** (640 mg, 54% yield) as a white solid.

R_f = 0.28 (4:6, *n*-Hexane/EtOAc); ^{1}H NMR (500 MHz, CD_2Cl_2-d_2) δ 8.57 (s, 1H), 8.28 (d, *J* = 8.9 Hz, 2H), 7.89 – 7.80 (m, 4H), 7.77 (d, *J* = 8.6 Hz, 1H), 7.62 (dd, *J* = 13.4, 7.5 Hz, 2H), 7.47 – 7.40 (m, 6H), 7.37 – 7.17 (m, 18H), 5.86 (d, *J* = 8.4 Hz, 1H), 5.31 (s, 2H), 4.48 (t, *J* = 10.1 Hz, 1H), 4.43 – 4.35 (m, 3H), 4.22 (t, *J* = 6.9 Hz, 1H), 4.10 (t, *J* = 8.2 Hz, 1H), 3.41 (q, *J* = 8.5 Hz, 1H), 3.00 (t, *J* = 12.6 Hz, 1H), 2.73 – 2.66 (m, 1H), 2.62 (dd, *J* = 13.8, 3.0 Hz, 1H), 2.22 –

2.13 (m, 1H), 2.00 – 1.92 (m, 1H), 1.90 – 1.75 (m, 2H), 1.62 – 1.53 (m, 1H), 0.80 (d, *J* = 6.7 Hz, 3H), 0.44 (d, *J* = 6.6 Hz, 3H). ^{13}C-APT NMR (151 MHz, CD_2Cl_2-d_2) δ 171.61, 171.25, 169.93, 168.88, 155.64, 155.36, 152.49, 145.38, 143.83, 143.78, 143.69, 141.28, 141.24, 139.61, 129.48, 128.59, 127.95, 127.73, 127.07, 127.02, 125.18, 124.97, 121.90, 120.04, 119.98, 70.83, 70.77, 66.99, 61.85, 60.01, 49.41, 49.31, 47.62, 47.11, 40.68, 29.85, 29.67, 28.45, 28.11, 24.62, 19.56, 19.05. MS (MALDI-TOF): *m/z* calcd for $[C_{62}H_{58}NaN_6O_{11}]^+$: 1086.92 [*M* + Na]$^+$; found: 1087.03 (DHB matrix).

Fmoc-Asn(Trt)-Pro-Val-PABC-*N*-(Boc)-*N*,*N*′-dimethylethylenediamine (129)

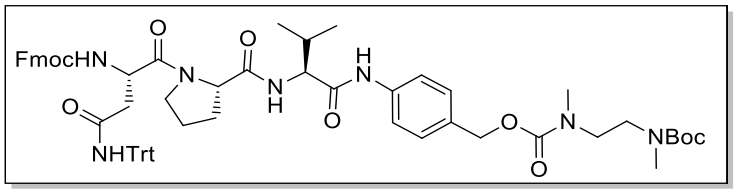

$C_{65}H_{73}N_7O_{10}$
MW: 1112,32

A solution of commercial *N*-(Boc)-*N*,*N*′-dimethylethylenediamine (208 µL, 1.03 mmol, 2 equiv) in dry THF (7 mL) and *i*Pr_2NEt (250 mg, 1.38 mmol, 2.5 equiv) were added under nitrogen to a solution of **128** (587 mg, 0.552 mmol, 1 equiv) in dry THF (15 mL) kept at 0 ºC. The mixture was stirred overnight at room temperature, then the solvent was removed at the rotavapor. AcOEt (100 mL) was added and the solution was washed with 1 M aqueous solution of $KHSO_4$ (3 × 20 mL), a saturated aqueous solution of $NaHCO_3$ (2 × 20 mL) and brine (20 mL). The organic phase was dried and concentrated. The crude was purified by flash chromatography (gradient: 3:2, AcOEt/*n*-Hexane to 4:1, AcOEt/*n*-Hexane), affording **129** (490 mg, 80% yield) as white solid.

R_f = 0.19 (1:4, *n*-Hexane/EtOAc); ^{1}H NMR (500 MHz, CD_2Cl_2-d_2) δ 8.47 (d, *J* = 11.0 Hz, 1H), 7.86 – 7.76 (m, 4H), 7.72 (d, *J* = 7.0 Hz, 1H), 7.65 – 7.58 (m, 2H), 7.43 (s, 2H), 7.38 – 7.06 (m, 21H), 5.11 (s, 2H), 4.48 (t, *J* = 10.2 Hz, 1H), 4.41 – 4.34 (m, 3H), 4.25 – 4.21 (m, 1H), 4.16 – 4.06 (m, 1H), 3.51 – 3.25 (m, 5H), 3.06 – 2.93 (m, 4H), 2.86 (s, 2H), 2.75 (s, 1H), 2.70 – 2.62 (m, 2H), 2.19 – 2.12 (m, 1H), 1.97 – 1.93 (m, 1H), 1.91 – 1.76 (m, 2H), 1.58 – 1.55 (m, 1H), 1.46 (s, 9H), 0.77 (d, *J* = 6.8 Hz, 3H), 0.41 (d, *J* = 6.8 Hz, 3H). ^{13}C NMR (151 MHz, CD_2Cl_2-d_2) δ 171.53, 171.33, 171.24, 169.72, 168.94, 156.21, 155.97, 155.41, 143.80, 143.74, 141.27, 141.24, 138.71, 138.58, 132.31, 132.19, 128.60, 127.93, 127.72, 127.04, 125.01, 119.96, 119.77, 79.31, 70.74, 67.01, 66.72, 66.53, 61.85, 59.90, 59.68, 49.40, 47.57, 47.10, 46.98, 46.68, 46.42, 40.70, 35.00, 34.46, 34.22, 29.87, 29.67, 28.59, 28.13, 24.61, 19.59, 18.98, 18.90. MS (MALDI-TOF): *m/z* calcd for $[C_{65}H_{74}N_7O_{10}]^+$: 1113.32 [*M* + H]$^+$; found: 1113.87; calcd for $[C_{65}H_{73}NaN_7O_{10}]^+$: 1135.32 [*M* + Na]$^+$; found: 1135.75 (DHB matrix).

4-pentynamido-Asn(Trt)-Pro-Val-PABC-*N*-(Boc)-*N*,*N'*-dimethylethylenediamine (130)

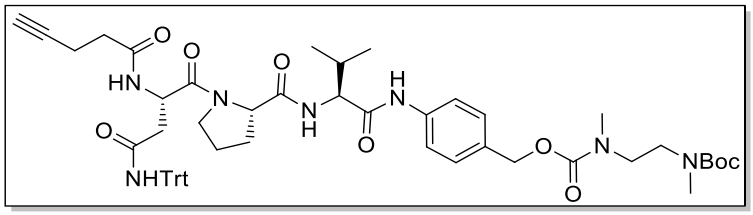

$C_{55}H_{67}N_7O_9$
MW: 970,16

N-Fmoc-protected compound **129** (90 mg, 0.081 mmol, 1 equiv) was deprotected following General Procedure GP2. Commercial 4-pentynoic acid (12 mg, 0.122 mmol, 1.5 equiv) in dry DMF (1.5 mL) was cooled to 0 °C under a nitrogen atmosphere. HATU (51 mg, 0.134 mmol, 1.7 equiv), HOAt (18 mg, 0.134 mmol, 1.7 equiv) and *i*Pr_2NEt (56 µL, 0.324 mmol, 4 equiv) were added and the mixture was stirred for 20 min at 0 °C. A solution of **129-NH** in dry DMF (3 mL) was added to the stirred mixture. The reaction was allowed to slowly reach room temperature and stirred overnight. The mixture was diluted with an AcOEt/CH_2Cl_2, 4:1 mixture (100 mL) and washed with 1 M aqueous solution of $KHSO_4$ (2 × 15 mL), a saturated aqueous solution of $NaHCO_3$ (1 × 15 mL) and brine (1 × 20 mL). The organic phase was dried over Na_2SO_4 and concentrated. The solid was purified by flash chromatography [gradient: from CH_2Cl_2 100% to 99:1 CH_2Cl_2/MeOH] to afford amide **130** as a white solid (70 mg, 90% yield over two steps).

R_f = 0.30 (95:5, CH_2Cl_2/MeOH); ^{1}H NMR (400 MHz, CD_2Cl_2-d_2) δ 8.46 (s, 1H), 7.84 – 7.69 (m, 3H), 7.57 (s, 1H), 7.37 – 7.14 (m, 17H), 6.84 (s, 1H), 5.10 (s, 2H), 4.74 (t, *J* = 9.7 Hz, 1H), 4.33 (dd, *J* = 9.0, 3.8 Hz, 1H), 4.09 (t, *J* = 8.8 Hz, 1H), 3.52 – 3.27 (m, 5H), 3.09 – 2.92 (m, 4H), 2.81 – 2.66 (m, 5H), 2.56 – 2.35 (m, 4H), 2.23 – 2.09 (m, 1H), 2.03 (t, *J* = 2.7 Hz, 1H), 1.94 (p, *J* = 6.0, 5.4 Hz, 1H), 1.86 – 1.75 (m, 2H), 1.65 – 1.53 (m, 1H), 1.47 (s, 9H), 0.76 (d, *J* = 6.7 Hz, 3H), 0.43 (d, *J* = 6.5 Hz, 3H); ^{13}C NMR (101 MHz, CD_2Cl_2-d_2) δ 171.57, 171.33, 170.32, 169.76, 169.21, 143.85, 138.67, 138.53, 132.26, 132.17, 128.63, 128.07, 127.88, 127.77, 126.99, 119.74, 82.86, 79.33, 79.08, 70.69, 68.98, 66.77, 66.63, 61.87, 60.09, 59.87, 47.75, 47.57, 47.04, 46.68, 46.44, 40.33, 38.36, 34.98, 34.66, 34.46, 34.29, 29.91, 29.68, 28.68, 28.15, 24.63, 19.59, 19.08, 14.47. MS (MALDI-TOF): *m/z* calcd for $[C_{55}H_{67}NaN_7O_9]^+$: 993.16 [*M* + Na]$^+$; found: 993.47.

Aliphatic alkyne-Asn-Pro-Val-PTX (122)

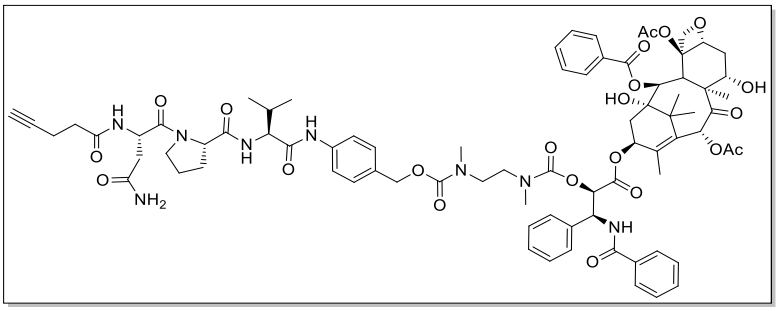

$C_{79}H_{94}N_8O_{22}$
MW: 1507,63

A solution of Boc-protected compound **130** (58 mg, 0.060 mmol, 1 equiv) was deprotected following General Procedure GP1. The obtained TFA salt was dissolved in dry DMF (900 μL) and *i*Pr_2NEt (42 μL, 0.240 mmol, 4 equiv). The resulting solution was added at 0 °C to a stirred solution of **95** (68 mg, 0.066 mmol, 1.1 equiv) in dry DMF (900 μL), under a nitrogen atmosphere. The reaction was then allowed to reach room temperature and stirred overnight. AcOEt (50 mL) was added and the solution was washed with a 1 M aqueous solution of $KHSO_4$ (2 × 10 mL) and brine (1 × 15 mL). The organic phase was dried over Na_2SO_4 and concentrated, then the crude was purified by flash chromatography [gradient: from 99:1 CH_2Cl_2/MeOH to 95:5 CH_2Cl_2/MeOH] to afford carbamate **122** as a white solid (63 mg, 71% yield over two steps).

R_f = 0.28 (CH_2Cl_2/MeOH, 9:1); MS (MALDI-TOF): *m/z* calcd for $[C_{79}H_{94}NaN_8O_{22}]^+$: 1530.63 [*M* + Na]$^+$; found: 1530.03 (HCCA matrix), 1532.08 (SA matrix); HRMS (ESI+): *m/z* calcd for $[C_{79}H_{94}NaN_8O_{22}]^+$: 1529.64 [*M* + Na]$^+$; found: 1529.63; *m/z* calcd for $[C_{79}H_{94}Na_2N_8O_{22}]^{2+}$: 776.31 [*M* + 2Na]$^{2+}$; found: 776.31.

***cyclo*[DKP-RGD]-PEG-4-Asn-Pro-Val-PTX (121)**

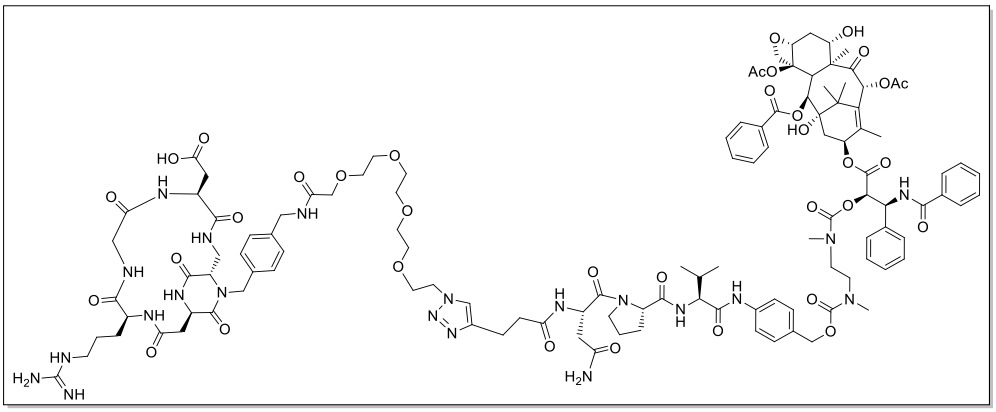

$C_{116}H_{149}N_{21}O_{35}$
MW: 2397,54

Alkyne **122** (7.8 mg, 0.0052 mmol, 1.3 equiv) and azide **86** (4 mg, 0.004 mmol, 1 equiv) were reacted following General Procedure GP3. The solvent was removed under vacuum, and the crude residue was purified by semipreparative HPLC [Waters Atlantis 21 mm x 10 cm column; gradient: 90% (H_2O+0.1% CF_3COOH)/10% (CH_3CN+0.1% CF_3COOH) to 100% (CH_3CN+0.1% CF_3COOH) in 20 min; t_R (product)=12.5 min]. The purified product was then freeze-dried to give the desired compound **122** as a white solid (9 mg, 94% yield).

MS (MALDI-TOF): *m/z* calcd for $[C_{116}H_{150}N_{21}O_{35}]^+$: 2398.54 [*M* + H]$^+$; found: 2398.99 (HCCA matrix), 2399.52 (SA matrix); HRMS (ESI+): *m/z* calcd for $[C_{116}H_{149}Na_2N_{21}O_{35}]^{2+}$: 1221.01 [*M* + 2Na]$^{2+}$; found: 1221.51.

cyclo[DKP-RGD]-PEG-4-Asn-Pro-[D]-Val-PTX (**123**)

Fmoc-[D]-Val-PABA (132)

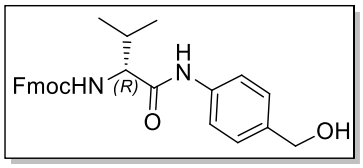

$C_{27}H_{28}N_2O_4$
MW: 444,52

Commercial Fmoc-[D]-Valine-OH **131** (150 mg, 0.442 mmol, 1 equiv) was dissolved in dry CH_2Cl_2/MeOH (2:1, 6 mL) under a nitrogen atmosphere. EEDQ and 4-aminobenzyl alcohol were added at 0 °C, under a nitrogen atmosphere. Then, the mixture was allowed to reach room temperature and stirred overnight under nitrogen atmosphere. The solvent was removed under reduced pressure affording a yellow solid. The crude was diluted in Et_2O (3 × 25 mL) and filtered in a fritz affording compound **132** as white solid (165 mg, 84% yield).

R_f = 0.18 (98:2, CH_2Cl_2/MeOH + 0.1% AcOH); ^{1}H NMR (400 MHz, MeOD-d_4) δ 7.79 (d, J = 7.6 Hz, 2H), 7.67 (t, J = 7.4 Hz, 2H), 7.54 (d, J = 8.4 Hz, 2H), 7.37 (t, J = 7.5 Hz, 2H), 7.34 – 7.26 (m, 4H), 4.56 (s, 2H), 4.45 – 4.33 (m, 2H), 4.23 (t, J = 6.8 Hz, 1H), 4.03 (d, J = 7.6 Hz, 1H), 2.10 (dq, J = 13.9, 6.9 Hz, 1H), 1.00 (d, J = 6.8 Hz, 3H); MS (ESI+) *m/z* calcd for $[C_{27}H_{29}N_2O_4]^+$: 445.20 [M + H]$^+$; found: 445.34; *m/z* calcd for $[C_{27}H_{28}NaN_2O_4]^+$: 467.52 [M + Na]$^+$; found: 467.71.

Fmoc-Asn(Trt)-Pro-[D]-Val-PABC-PNP (135)

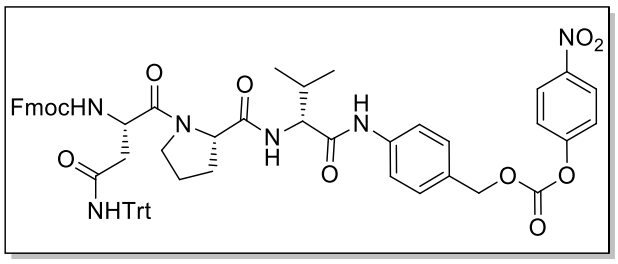

$C_{62}H_{58}N_6O_{11}$
MW: 1063,16

N-Fmoc-protected compound **132** (163 mg, 0.367 mmol, 1 equiv) was deprotected following General Procedure GP2. The remaining crude was directly used at the next step. A solution commercial Fmoc-L-Proline-OH (186 mg, 0.550 mmol, 1.5 equiv) in dry DMF (5 mL) was cooled to 0 °C under a nitrogen atmosphere. HATU (238 mg, 0.624 mmol, 1.7 equiv), HOAt (85 mg, 0.624 mmol, 1.7 equiv) and *i*Pr_2NEt (256 µL, 1.47 mmol, 4 equiv) were added and the mixture was stirred for 20 min at 0 °C. A solution of **132-NH** (82 mg, 0.367 mmol, 1 equiv) in dry DMF (2 mL) was added to the stirred mixture. The reaction was allowed to slowly reach room temperature and stirred overnight. The solvent was evaporated at rotavapor and the crude was purified by flash chromatography [gradient: from CH_2Cl_2 99:1 to 99:3 CH_2Cl_2/MeOH] to afford intermediate **133**, of which isolation was not possible. Similar procedure was used to afford intermediate **134**. A solution of Fmoc-Asn(Trt)-Pro-[D]-Val-PABA **134** in a mixture of dry

THF (21 mL) under nitrogen atmosphere was cooled to 0 °C. Pyridine (74 µL, 0.918 mmol, 2.5 equiv) and 4-nitrophenylchloroformate (148 mg, 0.734 mmol, 2 equiv) were added, then the mixture could reach room temperature and stirred for 2 h. AcOEt (200 mL) was added and the solution was washed with a 1 M aqueous solution of $KHSO_4$ (3 × 20 mL) and brine (20 mL). The organic phase was dried and concentrated, then the crude was purified by flash chromatography [gradient: from AcOEt/Hexane 1:1 to 7:3] affording compound **135** (185 mg, 47% yield, after five steps).

R_f = 0.36 (2:8, *n*-Hexane/EtOAc); ^{1}H NMR (400 MHz, CD_2Cl_2-d_2) δ 8.40 (s, 1H), 8.24 (d, *J* = 9.2 Hz, 2H), 7.77 (d, *J* = 7.6 Hz, 2H), 7.56 (d, *J* = 7.4 Hz, 2H), 7.47 – 7.12 (m, 27H), 5.93 (s, 1H), 5.22 (s, 2H), 4.65 (s, 1H), 4.50 – 4.28 (m, 3H), 4.19 (t, *J* = 6.7 Hz, 1H), 3.89 (d, *J* = 8.3 Hz, 1H), 3.49 (d, *J* = 8.9 Hz, 1H), 3.13 (s, 1H), 2.97 (t, *J* = 11.3 Hz, 1H), 2.63 (d, *J* = 14.0 Hz, 1H), 2.14 – 2.01 (m, 2H), 1.91 – 1.70 (m, 3H), 0.80 (dd, *J* = 15.9, 6.6 Hz, 6H). ^{13}C NMR (101 MHz, CD_2Cl_2-d_2) δ 171.67, 170.38, 169.87, 168.97, 155.61, 152.45, 145.41, 143.93, 143.72, 141.27, 138.92, 129.80, 129.39, 128.59, 127.94, 127.73, 127.09, 125.20, 125.06, 121.86, 120.11, 119.96, 70.82, 70.68, 67.14, 61.00, 60.24, 50.08, 47.39, 47.10, 40.21, 29.67, 28.91, 24.75, 19.35, 18.65. MS (MALDI-TOF): *m/z* calcd for $[C_{62}H_{59}N_6O_{11}]^+$: 1064.16 [*M* + H]$^+$; found: 1064.22 (HCCA matrix), 1065.25 (SA matrix).

Fmoc-Asn(Trt)-Pro-[D]-Val-PABC-*N*-(Boc)-*N*,*N*′-dimethylethylenediamine (136)

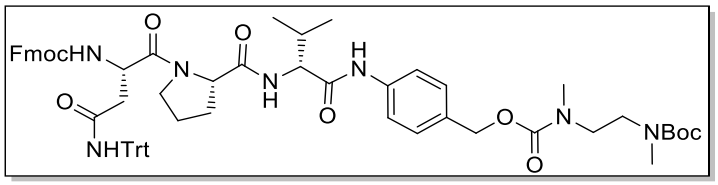

$C_{65}H_{73}N_7O_{10}$
MW: 1112,32

A solution of *N*-(Boc)-*N*,*N*′-dimethylethylenediamine (64 µL, 0.339 mmol, 2 equiv) in dry THF (2 mL) and *i*Pr_2NEt (74 µL, 0.423 mmol, 2.5 equiv) were added under nitrogen to a solution of **135** (180 mg, 0.169 mmol, 1 equiv) in dry THF (5 mL) kept at 0 ºC. The mixture was stirred overnight at room temperature, then the solvent was removed at the rotavapor. AcOEt (50 mL) was added and the solution was washed with 1 M aqueous solution of $KHSO_4$ (3 × 20 mL), a saturated aqueous solution of $NaHCO_3$ (2 × 20 mL) and brine (20 mL). The organic phase was dried and concentrated. The crude was purified by flash chromatography (8:2, AcOEt/*n*-Hexane), affording **136** (140 mg, 87% yield) as a white solid.

R_f = 0.19 (8:2 AcOEt/*n*-Hexane); ^{1}H NMR (400 MHz, MeOD-d_4) δ 7.80 (d, *J* = 7.6 Hz, 2H), 7.65 (t, *J* = 7.2 Hz, 4H), 7.39 (t, *J* = 7.6 Hz, 2H), 7.33 – 7.16 (m, 19H), 5.05 (s, 2H), 4.61 (t, *J* = 7.0 Hz, 1H), 4.51 – 4.32 (m, 3H), 4.24 – 4.15 (m, 2H), 3.63 (q, *J* = 6.9, 6.1 Hz, 1H), 3.42 – 3.35 (m, 4H), 3.29 – 3.18 (m, 1H), 2.91 (s, 3H), 2.85 (s, 2H), 2.77 – 2.71 (m, 3H), 2.18 – 2.04 (m, 2H), 2.01 – 1.85 (m, 3H), 1.42 (s, 9H), 0.91 (d, *J* = 5.9 Hz, 6H). ^{13}C NMR (101 MHz, MeOD-d_4) δ 173.23, 171.26, 170.46, 169.59, 156.66, 156.03, 144.33, 143.75, 141.19, 138.15, 138.03,

132.42, 132.20, 128.64, 128.27, 127.42, 127.34, 126.82, 126.38, 124.77, 124.74, 120.08, 119.56, 79.79, 79.50, 70.32, 66.88, 66.67, 60.68, 59.66, 50.09, 46.56, 46.15, 38.08, 34.18, 33.87, 33.23, 29.43, 29.34, 29.14, 27.32, 24.54, 18.44, 17.34. MS (MALDI-TOF): *m/z* calcd for $[C_{65}H_{74}N_7O_{10}]^+$: 1113.32 [*M* + H]$^+$; found: 1113.54 (HCCA matrix), 1113.55 (SA matrix).

4-pentynamido-Asn(Trt)-Pro-[D]-Val-PABC-*N*-(Boc)-*N*,*N′*-dimethylethylenediamine (137)

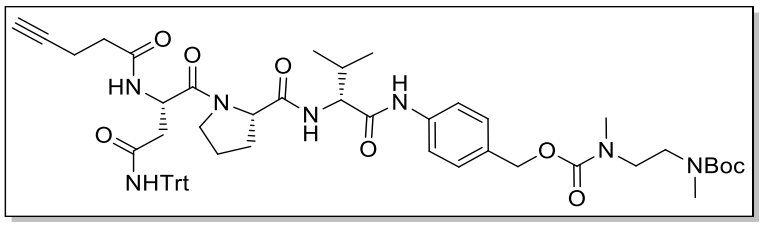

$C_{55}H_{67}N_7O_9$
MW: 970,16

N-Fmoc-protected compound **136** (153 mg, 0.138 mmol, 1 equiv) was deprotected following General Procedure GP2. Commercial 4-pentynoic acid (25 mg, 0.235 mmol, 1.5 equiv) in dry DMF (2 mL) was cooled to 0 °C under a nitrogen atmosphere. HATU (80 mg, 0.207 mmol, 1.7 equiv), HOAt (30 mg, 0.207 mmol, 1.7 equiv) and *i*Pr$_2$NEt (97 µL, 0.552 mmol, 4 equiv) were added and the mixture was stirred for 20 min at 0 °C. A solution of **136-NH** (123 mg, 0.138 mmol, 1 equiv) in dry DMF (5 mL) was added to the stirred mixture. The reaction was allowed to slowly reach room temperature and stirred overnight. The mixture was diluted with an AcOEt/CH_2Cl_2, 4:1 mixture (100 mL) and washed with 1 M aqueous solution of $KHSO_4$ (2 × 15 mL), a saturated aqueous solution of $NaHCO_3$ (1 × 15 mL) and brine (1 × 20 mL). The organic phase was dried over Na_2SO_4 and concentrated. The solid was purified by flash chromatography [gradient: from CH_2Cl_2 100% to 97:3 CH_2Cl_2/MeOH] to afford amide **137** as fade white solid (125 mg, 94% yield over two steps).

R_f = 0.37 (95:5, CH_2Cl_2/MeOH); ^{1}H NMR (400 MHz, CD_2Cl_2-d_2) δ 8.26 – 8.16 (m, 1H), 7.62 – 7.46 (m, 1H), 7.35 (s, 2H), 7.28 – 7.15 (m, 18H), 6.72 (s, 1H), 5.03 (s, 2H), 4.83 (td, *J* = 7.8, 3.7 Hz, 1H), 4.46 (dd, *J* = 8.4, 3.4 Hz, 1H), 3.83 (s, 1H), 3.45 (s, 1H), 3.39 – 3.26 (m, 4H), 3.06 (s, 1H), 2.91 (s, 4H), 2.83 (s, 2H), 2.75 (s, 1H), 2.70 (dd, *J* = 14.1, 3.7 Hz, 1H), 2.46 (td, *J* = 7.6, 6.6, 2.4 Hz, 2H), 2.40 – 2.30 (m, 2H), 2.17 – 2.06 (m, 1H), 2.05 – 1.98 (m, 1H), 1.97 (t, *J* = 2.6 Hz, 1H), 1.88 – 1.76 (m, 2H), 1.71 (s, 1H), 1.42 (s, 9H), 0.79 (dd, *J* = 16.8, 6.6 Hz, 6H); ^{13}C NMR (101 MHz, CD_2Cl_2-d_2) δ 171.59, 170.42, 170.30, 169.58, 169.01, 144.01, 138.08, 132.47, 128.62, 128.37, 127.88, 127.01, 120.01, 70.70, 69.00, 66.68, 66.55, 60.98, 48.42, 47.32, 40.10, 34.84, 28.95, 28.57, 28.11, 24.66, 19.49, 18.72, 14.44. MS (MALDI-TOF): *m/z* calcd for $[C_{55}H_{67}NaN_7O_9]^+$: 993.16 [*M* + Na]$^+$; found: 993.20 (HCCA matrix), 993.22 (SA matrix).

Aliphatic alkyne-Asn-Pro-[D]-Val-PTX (138)

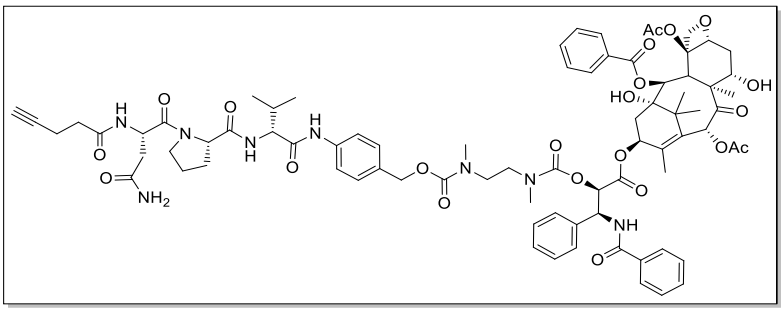

$C_{79}H_{94}N_8O_{22}$
MW: 1507,63

A solution of Boc-protected compound **137** (50 mg, 0.052 mmol, 1 equiv) in dry CH_2Cl_2 (1.8 mL) was cooled to 0 °C under a nitrogen atmosphere and TFA (900 µL) was added. The mixture was then allowed to reach room temperature and stirred for 15 min. The solvent was removed affording the corresponding trifluoroacetate salt, without further purifications. The solid was dissolved in dry DMF (800 µL) and *i*Pr_2NEt (37 µL, 0.208 mmol, 4 equiv). The resulting solution was added at 0 °C to a stirred solution of **95** (55 mg, 0.057 mmol, 1.1 equiv) in dry DMF (800 µL), under a nitrogen atmosphere. The reaction was then allowed to reach room temperature and stirred overnight. AcOEt (100 mL) was added and the solution was washed with a 1 M aqueous solution of $KHSO_4$ (2 × 10 mL) and brine (1 × 15 mL). The organic phase was dried over Na_2SO_4 and concentrated, then the crude was purified by flash chromatography [gradient: from CH_2Cl_2 100% to 95:5 CH_2Cl_2/MeOH] to afford carbamate **138** as a light-yellow solid (41 mg, 54% yield over two steps).

R_f = 0.19 (95:5, CH_2Cl_2/MeOH); MS (MALDI-TOF): *m/z* calcd for $[C_{79}H_{94}NaN_8O_{22}]^+$: 1530.65 [*M* + Na]$^+$; found: 1530.08 (HCCA matrix), 1530.52 (SA matrix); HRMS (ESI+): *m/z* calcd for $[C_{79}H_{94}NaN_8O_{22}]^+$: 1529.64 [*M* + Na]$^+$: found 1529.63.

***cyclo*[DKP-RGD]-PEG-4-Asn-Pro-[D]-Val-PTX conjugate (123)**

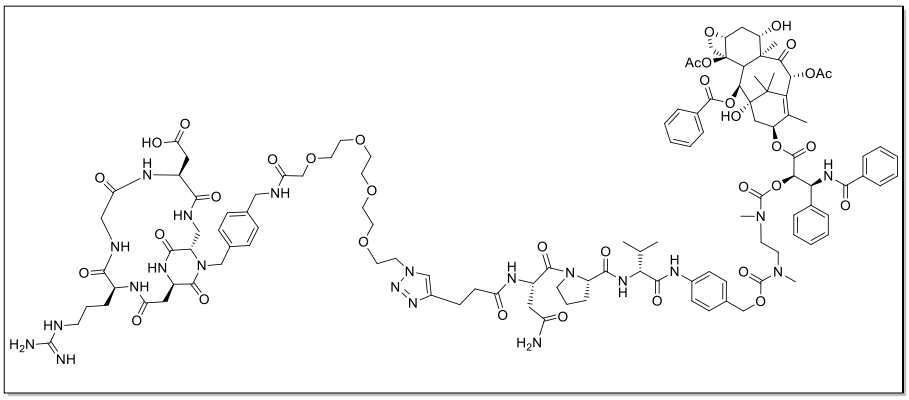

$C_{116}H_{149}N_{21}O_{35}$
MW: 2397,54

Alkyne **138** (5.6 mg, 0.0036 mmol, 1.2 equiv) and azide **86** (3 mg, 0.003 mmol, 1 equiv) were reacted following General Procedure GP3. The solvent was removed under vacuum, and the crude residue was purified by semipreparative HPLC [Waters Atlantis 21 mm x 10 cm column; gradient: 90% (H_2O+0.1% CF_3COOH)/10% (CH_3CN+0.1% CF_3COOH) to 100% (CH_3CN+0.1%

CF_3COOH) in 20 min; t_R (product)=12.2 min]. The purified product was then freeze-dried to give the desired compound **123** as a white solid (5 mg, 70% yield).

MS (MALDI-TOF): *m/z* calcd for $[C_{116}H_{150}N_{21}O_{35}]^+$: 2398.52 [*M* + H]$^+$; found: 2398.29 (HCCA matrix), 2399.52 (SA matrix); *m/z* calcd for $[C_{116}H_{149}NaN_{21}O_{35}]^+$: 2420.22 [*M* + Na]$^+$; found: 2420.32 (HCCA matrix), 2420.52 (SA matrix); HRMS (ESI+): *m/z* calcd for $[C_{116}H_{150}NaN_{21}O_{35}]^{2+}$: 1210.02 [*M* + H + Na]$^{2+}$; found: 1210.03; *m/z* calcd for $[C_{116}H_{150}Na_2N_{21}O_{35}]^{3+}$: 814.34 [*M* + H + 2Na]$^{3+}$; found: 814.35.

cyclo[DKP-RGD]-Uncleavable-PTX (**124**)

***tert*-butyl methyl(2-(*N*-methylpent-4-ynamido)ethyl)carbamate (140)**

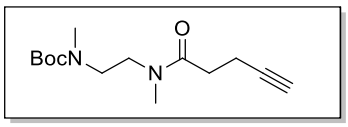

$C_{14}H_{24}N_2O_3$
MW: 268,35

Commercial 4-pentynoic acid (78 mg, 0.796 mmol, 1.5 equiv) in dry DMF (4 mL) was cooled to 0 °C under a nitrogen atmosphere. HATU (343 mg, 0.902 mmol, 1.7 equiv), HOAt (123 mg, 0.902 mmol, 1.7 equiv) and *i*Pr_2NEt (370 µL, 2.124 mmol, 4 equiv) were added and the mixture was stirred for 20 min at 0 °C. A solution of *N*-(Boc)-*N*,*N'*-dimethylethylenediamine **139** (100 mg, 0.531 mmol, 1 equiv) in dry DMF (5 mL) was added to the stirred mixture. The reaction was allowed to slowly reach room temperature and stirred overnight. The mixture was diluted with an AcOEt/CH_2Cl_2, 4:1 mixture (100 mL) and washed with 1 M aqueous solution of $KHSO_4$ (2 × 15 mL), a saturated aqueous solution of $NaHCO_3$ (1 × 15 mL) and brine (1 × 20 mL). The organic phase was dried over Na_2SO_4 and concentrated. The solid was purified by flash chromatography [eluent: CH_2Cl_2 100%] to afford amide **140** as dark yellow oil (140 mg, 98%). R_f = 0.46 (95:5, CH_2Cl_2/MeOH); ^{1}H NMR (400 MHz, CD_2Cl_2-d_2) δ 3.43 – 3.31 (m, 2H), 3.24 (t, *J* = 6.2 Hz, 2H), 2.91 (s, rotamer A, 3H), 2.83 (s, rotamer B, 3H), 2.75 (s, rotamer A + B, 3H), 2.49 – 2.36 (m, 4H), 1.90 (q, *J* = 2.2 Hz, 1H), 1.35 (s, rotamer A + B, 9H); ^{13}C NMR (101 MHz, CD_2Cl_2-d_2) δ 171.14, 156.27, 84.35, 79.57, 68.74, 48.30 (rotamer A), 48.09 (rotamer B), 47.72, 46.95 (rotamer A), 46.60 (rotamer B), 46.22 (rotamer A), 45.72 (rotamer B), 36.35 (rotamer A), 35.05, 34.24 (rotamer B), 33.08 (rotamer A), 32.20 (rotamer B), 28.71, 15.04 (rotamer A), 14.76 (rotamer B). MS (ESI +): *m/z* calcd for $[C_{14}H_{25}N_2O_3]^+$: 269.10 [*M* + H]$^+$; found: 269.09.

Aliphatic alkyne-PTX (141)

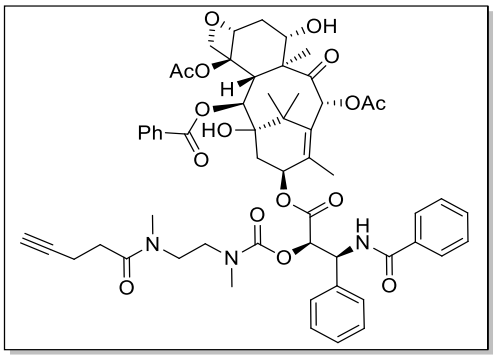

$C_{57}H_{65}N_3O_{16}$
MW: 1048,14

A solution of Boc-protected compound **140** (67 mg, 0.249 mmol, 1 equiv) was deprotected following General Procedure GP1. The resulting dark yellow oil was dissolved in dry DMF (0.5 mL) and *i*Pr_2NEt (87 µL, 0.5 mmol, 10 equiv). The resulting solution was added at 0 °C to a stirred solution of **95** (50 mg, 0.05 mmol, 1 equiv) in dry DMF (1 mL), under a nitrogen atmosphere. The reaction was then allowed to reach room temperature and stirred overnight. AcOEt (50 mL) was added and the solution was washed with a 1 M aqueous solution of $KHSO_4$ (2 × 5 mL) and brine (1 × 5 mL). The organic phase was dried over Na_2SO_4 and concentrated, then the crude was purified by flash chromatography [gradient: from AcOEt/*n*-Hexane 1:1 to 4:1] to afford carbamate **141** as a white solid (41 mg, 84% yield over two steps).

R_f = 0.31 (4:1, AcOEt/*n*-Hexane 1:1); ^{1}H NMR (400 MHz, $CDCl_3$-*d*) δ 8.71 (d, *J* = 9.8 Hz, 1H), 8.21 – 8.15 (m, 2H), 7.87 – 7.79 (m, 2H), 7.61 – 7.55 (m, 1H), 7.54 – 7.46 (m, 5H), 7.44 – 7.34 (m, 5H), 7.33 – 7.27 (m, 2H), 6.35 – 6.28 (m, 2H), 6.19 (dd, *J* = 9.8, 3.0 Hz, 1H), 5.69 (d, *J* = 7.3 Hz, 1H), 5.45 (d, *J* = 3.0 Hz, 1H), 5.00 (dd, *J* = 10.0, 2.3 Hz, 1H), 4.47 (td, *J* = 6.8, 3.3 Hz, 1H), 4.35 – 4.29 (m, 1H), 4.24 (dd, *J* = 8.4, 1.0 Hz, 1H), 4.00 – 3.89 (m, 1H), 3.84 (d, *J* = 7.1 Hz, 1H), 3.64 – 3.54 (m, 1H), 3.12 – 3.06 (m, 1H), 3.05 – 2.98 (m, 4H), 2.98 – 2.94 (m, 2H), 2.90 (s, 3H), 2.63 – 2.52 (m, 5H), 2.51 – 2.46 (m, 3H), 2.24 – 2.21 (m, 3H), 1.99 (d, *J* = 1.4 Hz, 3H), 1.93 (t, *J* = 2.6 Hz, 2H), 1.69 (s, 3H), 1.23 (s, 3H), 1.13 (s, 3H); ^{13}C NMR (101 MHz, $CDCl_3$-*d*) δ 133.56, 131.28, 130.31, 128.75, 128.67, 127.97, 127.95, 127.75, 126.81, 84.51, 83.14, 77.22, 76.48, 75.82, 75.71, 75.24, 72.14, 71.35, 52.73, 46.76, 45.80, 45.57, 36.78, 35.81, 35.55, 35.52, 32.34, 30.32, 29.69, 26.78, 22.79, 22.69, 22.35, 20.82, 14.88, 14.25, 14.11, 9.66. MS (MALDI-TOF): *m/z* calcd for $[C_{57}H_{66}N_3O_{16}]^+$: 1049.14 [*M* + H]$^+$; found: 1049.22 (HCCA matrix); *m/z* calcd for $[C_{57}H_{65}NaN_3O_{16}]^+$: 1071.14 [*M* + Na]$^+$; found: 1071.26.

***cyclo*[DKP-RGD]-Uncleavable-PTX (124)**

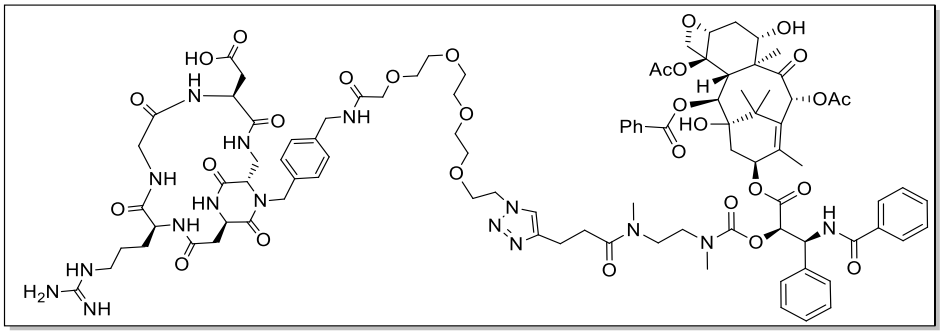

$C_{94}H_{120}N_{16}O_{29}$
MW: 1938,05

Alkyne **141** (7 mg, 0.0065 mmol, 1.3 equiv) and azide **86** (5 mg, 0.005 mmol, 1 equiv) were reacted following General Procedure GP3. The solvent was removed under vacuum, and the crude residue was purified by semipreparative HPLC [Waters Atlantis 21 mm x 10 cm column; gradient: 90% (H_2O+0.1% CF_3COOH)/10% (CH_3CN+0.1% CF_3COOH) to 100% (CH_3CN+0.1% CF_3COOH) in 20 min; t_R (product)=12.1 min]. The purified product was then freeze-dried to give the desired compound **124** as a white solid (9.7 mg, 100% yield).

MS (MALDI-TOF): *m/z* calcd for $[C_{94}H_{121}N_{16}O_{29}]^+$: 1939.05 [*M* + H]$^+$; found: 1939.70 (HCCA matrix); HRMS (ESI+): *m/z* calcd for $[C_{94}H_{121}N_{16}O_{29}]^+$: 1937.85, [*M* + H]$^+$; found 1937.85; *m/z* calcd for $[C_{94}H_{120}NaN_{16}O_{29}]^+$: 1959.83 [*M* + Na]$^+$; found 1959.83; *m/z* calcd for $[C_{94}H_{120}Na_2N_{16}O_{29}]^{2+}$: 991.41 [*M* + 2Na]$^{2+}$ found: 991.41; *m/z* calcd for $[C_{94}H_{121}NaN_{16}O_{29}]^{2+}$: 980.41 [*M* + H + Na]$^{2+}$; found: 980.42; *m/z* calcd for $[C_{94}H_{120}Na_3N_{16}O_{29}]^{2+}$: 1002.40 [*M* + 3Na]$^{2+}$; found: 1002.41.

Pro-PTX (**142**)

PTX-*N*-(Boc)-*N*,*N*′-dimethylethylenediamine (143)

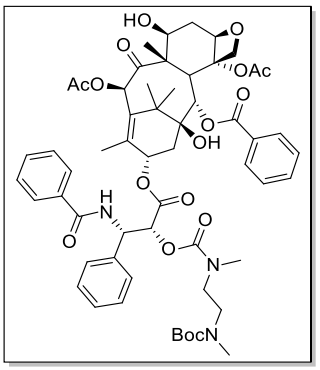

$C_{57}H_{69}N_3O_{17}$
MW: 1068,17

Compound **95** (10 mg, 0.01 mmol, 1 equiv) was solubilized in dry DMF (150 µL) under nitrogen. A mixture of *N*-(Boc)-*N*,*N*′-dimethylethylenediamine **139** (3 mg, 0.015 mmol, 1.5 equiv) in dry DMF (150 µL mL) and *i*Pr_2NEt (6 µL, 0.03 mmol, 3 equiv) were added to **95** at 0 ºC under nitrogen. The mixture was stirred overnight at room temperature. AcOEt (20 mL) was added and the solution was washed with 1 M aqueous solution of $KHSO_4$ (2 × 10 mL) and brine (20

mL). The organic phase was dried and concentrated. The crude was purified by preparative TLC (gradient: 65:35 AcOEt/*n*-Hexane), affording **143** (10 mg, 95% yield) as a fade white solid. R_f = 0.29 (3:2 AcOEt/*n*-Hexane); ^{1}H NMR (400 MHz, CD_2Cl_2-d_2) δ 8.65 (d, *J* = 9.7 Hz, 1H), 8.21 – 8.09 (m, 2H), 7.82 – 7.73 (m, 2H), 7.63 (t, *J* = 7.2 Hz, 1H), 7.55 (q, *J* = 8.1, 7.6 Hz, 4H), 7.47 – 7.25 (m, 6H), 6.31 – 6.20 (m, 2H), 6.13 (dd, *J* = 9.9, 2.8 Hz, 1H), 5.64 (d, *J* = 7.1 Hz, 1H), 5.31 (dd, *J* = 10.2, 2.3 Hz, 1H), 5.00 (dd, *J* = 9.8, 2.3 Hz, 1H), 4.46 (dd, *J* = 11.1, 6.6 Hz, 1H), 4.33 – 4.26 (m, 1H), 4.22 – 4.13 (m, 1H), 4.11 – 4.00 (m, 1H), 3.80 (dd, *J* = 15.0, 7.0 Hz, 1H), 3.64 – 3.46 (m, 2H), 2.88 (d, *J* = 8.3 Hz, 6H), 2.59 (s, 3H), 2.55 – 2.49 (m, 1H), 2.41 (t, *J* = 7.5 Hz, 1H), 2.20 (s, 3H), 2.12 (dd, *J* = 15.5, 9.2 Hz, 1H), 1.96 (s, 3H), 1.89 (s, 2H), 1.81 (ddd, *J* = 14.0, 10.8, 2.3 Hz, 2H), 1.63 (s, 3H), 1.27 (s, 9H), 1.19 (s, 3H), 1.10 (s, 3H); ^{13}C NMR (101 MHz, CD_2Cl_2-d_2) δ 204.57, 171.92, 170.62, 169.58, 168.77, 167.34, 156.24, 155.40, 143.96, 138.24, 135.14, 134.22, 134.10, 133.05, 131.71, 130.78, 130.07, 129.26, 129.08, 128.68, 128.33, 127.63, 84.90, 81.49, 80.49, 79.64, 76.87, 76.53, 76.27, 75.74, 72.75, 72.18, 71.85, 59.00, 53.36, 46.92, 46.77, 46.25, 43.71, 36.32, 36.25, 36.14, 35.81, 30.26, 28.54, 27.10, 23.34, 22.62, 21.21, 15.15, 10.02. MS (MALDI-TOF): *m/z* calcd for $[C_{57}H_{70}N_3O_{17}]^+$: 1069.17 [*M* + H]$^+$; found: 1069.00 (HCCA matrix); *m/z* calcd for $[C_{57}H_{69}NaN_3O_{17}]^+$: 1091.17 [*M* + Na]$^+$; found: 1091.36 (HCCA matrix).

Pro-PTX·TFA (142)

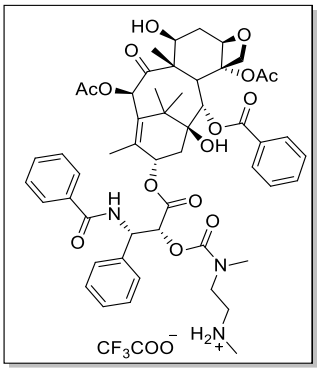

$C_{54}H_{62}F_3N_3O_{17}$
MW: 1082,08

To a solution of CH_2Cl_2/TFA (1:1, 300 µL), compound **143** (10 mg, 0.0095 mmol, 1 equiv) in dry CH_2Cl_2 (200 µL) was added, under nitrogen, at 0 ºC. The mixture was stirred for 20 minutes at room temperature. The solvent was removed under reduced pressure and the crude was purified by semipreparative HPLC [Waters Atlantis 21 mm x 10 cm column; gradient: 90% (H_2O+0.1% CF_3COOH)/10% (CH_3CN+0.1% CF_3COOH) to 100% (CH_3CN+0.1% CF_3COOH) in 20 min; t_R (product)=13 min]. The purified product was then freeze-dried to give the desired compound **142** as a white solid (7 mg, 68% yield).

MS (MALDI-TOF): *m/z* calcd for $[C_{52}H_{62}N_3O_{15}]^+$: 969.05 [*M* + H]$^+$; found: 969.20 (HCCA matrix); *m/z* calcd for $[C_{52}H_{61}NaN_3O_{15}]^+$: 991.05 [*M* + Na]$^+$; found: 991.23; HRMS (ESI+): *m/z* calcd for $[C_{52}H_{62}N_3O_{15}]^+$: 968.41 [*M* + H]$^+$; found: 968.42.

cyclo[DKP-RGD]-PEG-4-Val-Ala-MMAE (**145**)

Aliphatic alkyne-Val-Ala-PABA (152)

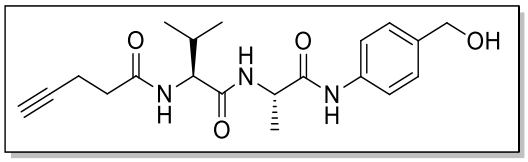

$C_{20}H_{27}N_3O_4$
MW: 373,45

The previously synthesized Fmoc-Val-Ala-PABA **151**[130] (800 mg, 1.55 mmol, 1 equiv) was deprotected following General Procedure GP2. Commercial 4-pentynoic acid (228 mg, 2.325 mmol, 1.5 equiv) in dry DMF (5 mL) was cooled to 0 °C under a nitrogen atmosphere. HATU (999 mg, 2.635 mmol, 1.7 equiv), HOAt (359 mg, 2.635 mmol, 1.7 equiv) and *i*Pr_2NEt (1.1 mL, 6.20 mmol, 4 equiv) were added and the mixture was stirred for 20 min at 0 °C. A solution of **151-NH** in dry DMF (15 mL) was added to the stirred mixture. The reaction was allowed to slowly reach room temperature and stirred overnight. The mixture was dried at rotavapor under reduced pressure. The remained oil was purified by flash chromatography [gradient: from CH_2Cl_2/MeOH (98:2) to CH_2Cl_2/MeOH (90:10)] to afford amide **152** as a white solid (550 mg, 90% yield over two steps).

R_f = 0.21 (9:1, CH_2Cl_2/AcOEt); ^{1}H NMR (400 MHz, MeOD-d_4) δ 7.55 (d, *J* = 8.5 Hz, 2H), 7.30 (d, *J* = 8.5 Hz, 2H), 4.55 (s, 2H), 4.48 (q, *J* = 7.1 Hz, 1H), 4.21 (d, *J* = 7.0 Hz, 1H), 2.58 – 2.42 (m, 4H), 2.26 (t, *J* = 2.5 Hz, 1H), 2.09 (hept, *J* = 6.8 Hz, 1H), 1.43 (d, *J* = 7.1 Hz, 3H), 0.99 (d, *J* = 7.0 Hz, 3H), 0.97 (d, *J* = 6.6 Hz, 3H); ^{13}C NMR (101 MHz, MeOD-d_4) δ 174.37, 173.57, 172.93, 138.73, 138.65, 128.58, 121.17, 83.65, 70.39, 64.83, 60.39, 51.06, 35.76, 31.81, 19.72, 18.71, 18.00, 15.64. MS (ESI+): *m/z* calcd for $[C_{20}H_{28}N_3O_4]^+$: 373.20 $[M + H]^+$: found: 373.41.

Aliphatic alkyne-Val-Ala-PABC-PNP (153)

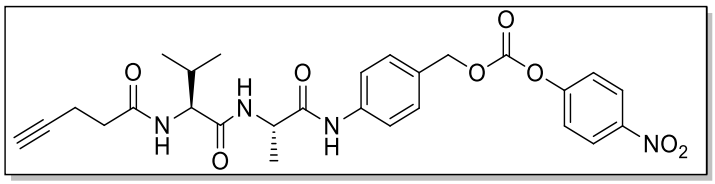

$C_{27}H_{30}N_4O_8$
MW: 538,55

A solution of compound **152** in a mixture of dry THF (78 mL) under nitrogen atmosphere was cooled to 0 °C. Pyridine (270 µL, 3.33 mmol, 2.5 equiv) and 4-nitrophenylchloroformate (537 mg, 2.66 mmol, 2 equiv) were added, then the mixture could reach room temperature and stirred for 2 h. The reaction mixture was concentrated under reduced pressure and AcOEt (50 mL) was added and the solution was washed with a 1 M aqueous solution of $KHSO_4$ (3 × 20 mL) and brine (20 mL). The organic phase was dried and concentrated, then the crude was purified by flash chromatography [eluent: 2:8, *n*-Hexane/EtOAc] affording compound **153** (460 mg, 65% yield) as a white solid.

R_f = 0.19 (2:8, *n*-Hexane/EtOAc); ^{1}H NMR (400 MHz, DMSO-d_6) δ 9.99 (s, 1H), 8.31 (d, *J* = 9.1 Hz, 2H), 8.21 (d, *J* = 6.9 Hz, 1H), 7.94 (d, *J* = 8.6 Hz, 1H), 7.64 (d, *J* = 8.5 Hz, 2H), 7.57 (d, *J* = 9.1 Hz, 2H), 7.41 (d, *J* = 8.7 Hz, 2H), 5.24 (s, 2H), 4.39 (p, *J* = 7.0 Hz, 1H), 4.21 (dd, *J* = 8.6, 6.7 Hz, 1H), 2.74 (t, *J* = 2.2 Hz, 1H), 2.48 – 2.30 (m, 4H), 1.97 (h, *J* = 6.8 Hz, 1H), 1.31 (d, *J* = 7.1 Hz, 3H), 0.87 (dd, *J* = 15.7, 6.7 Hz, 6H); ^{13}C NMR (101 MHz, DMSO-d_6) δ 171.23, 170.86, 170.52, 155.26, 151.91, 145.15, 139.42, 129.44, 125.37, 122.58, 119.00, 83.78, 71.21, 70.23, 57.53, 49.06, 33.96, 30.49, 19.14, 18.13, 17.82, 14.25. MS (ESI+): *m/z* calcd for $[C_{27}H_{31}N_4O_8]^+$: 538.21 [*M* + H]$^+$; found: 538.22.

Aliphatic alkyne-Val-Ala-PABC-MMAE (154)

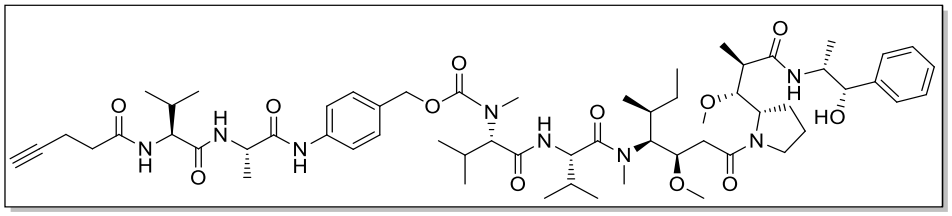

$C_{60}H_{92}N_8O_{12}$
MW: 1117,42

Compound **153** (20 mg, 0.037 mmol, 1 equiv) and HOBt (3 mg, 0.019 mmol, 0.5 equiv) were dissolved in dry DMF under argon atmosphere. Commercial MMAE (32 mg, 0.044 mmol, 1.2 equiv) was solubilized in dry DMF:Pyridine (4:1, 600 µL, reaction total volume) and DIPEA (6 µL, 0.033 mmol, 0.9 equiv) and added to the starting material solution at 0 ºC, under argon atmosphere. Then, the mixture was allowed to reach room temperature and stirred over weekend under argon atmosphere. The reaction mixture was diluted with AcOEt (150 mL) the solution was washed with a 1 M aqueous solution of $KHSO_4$ (3 × 20 mL) and brine (20 mL). The organic phase was dried with Na_2SO_4 and concentrated, then the crude was purified by flash chromatography [gradient: from 99:1, CH_2Cl_2/MeOH to 95:5, CH_2Cl_2/MeOH] affording compound **154** (40 mg, 95% yield) as a white solid.

R_f = 0.35 (95:5, CH_2Cl_2/MeOH); MS (ESI+): *m/z* calcd for $[C_{60}H_{93}N_8O_{12}]^+$: 1117.68 [*M* + H]$^+$; found: 1118.01. HRMS (ESI+): *m/z* calcd for $[C_{60}H_{92}NaN_8O_{12}]^+$: 1139.67 [*M* + Na]$^+$; found 1139.67.

***cyclo*[DKP-RGD]-PEG-4-Val-Ala-MMAE (145)**

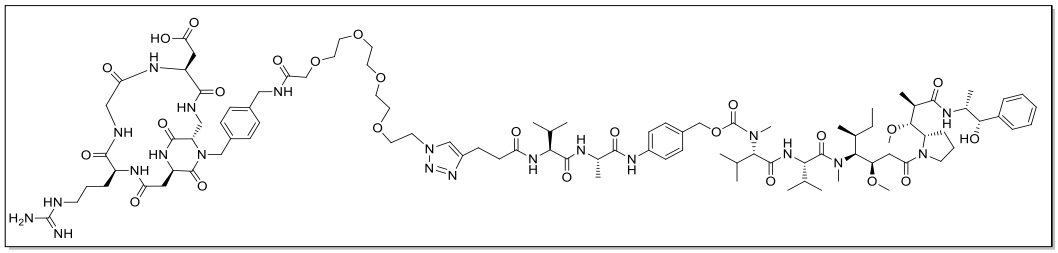

$C_{97}H_{147}N_{21}O_{25}$
MW: 2007,33

Alkyne **154** (7 mg, 0.006 mmol, 1.2 equiv) and azide **86** (5 mg, 0.005 mmol, 1 equiv) were reacted following General Procedure GP3. The solvent was removed under vacuum, and the

crude residue was purified by semipreparative HPLC [Waters Atlantis 21 mm x 10 cm column; gradient: 90% (H_2O+0.1% CF_3COOH)/10% (CH_3CN+0.1% CF_3COOH) to 100% (CH_3CN+0.1% CF_3COOH) in 20 min; t_R (product)=12 min]. The purified product was then freeze-dried to give the desired compound **145**as a white solid (6.7 mg, 65% yield).

MS (MALDI-TOF): *m/z* calcd for $[C_{97}H_{148}N_{21}O_{25}]^+$: 2007.33 [*M* + H]$^+$; found: 2007.77; (HCCA matrix), 2009.6 (SA matrix); HRMS (ESI+): *m/z* calcd for $[C_{97}H_{148}N_{21}O_{25}]^+$: 2007.096 [*M* + H]$^+$; found: 2007.093; *m/z* calcd for $[C_{97}H_{148}NaN_{21}O_{25}]^{2+}$: 1015.045 [*M* + H + Na]$^{2+}$; found 1015.042; *m/z* calcd for $[C_{97}H_{148}Na_2N_{21}O_{25}]^{3+}$: 684.363 [*M* + H + 2Na]$^{3+}$; found: 684.360.

HOOC-PEG-4-Val-Ala-MMAE (147)

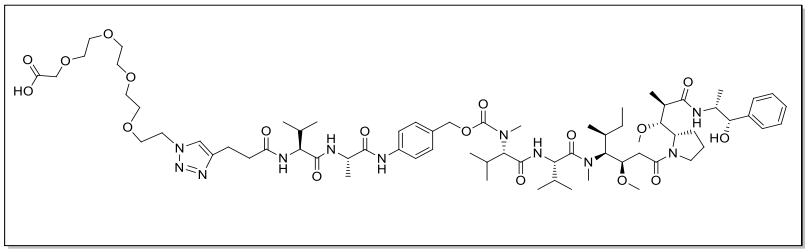

$C_{70}H_{111}N_{11}O_{18}$
MW: 1394,69

Alkyne **154** (5 mg, 0.006 mmol, 1 equiv) and azide-COOH **91** (1.7 mg, 0.006 mmol, 1 equiv) were reacted following General Procedure GP3. The solvent was removed under vacuum, and the crude residue was purified by semipreparative HPLC [Waters Atlantis 21 mm x 10 cm column; gradient: 90% (H_2O+0.1% CF_3COOH)/10% (CH_3CN+0.1% CF_3COOH) to 100% (CH_3CN+0.1% CF_3COOH) in 20 min; t_R (product)=13 min]. The purified product was then freeze-dried to give the desired compound **147** as a white solid (2.6 mg, 30% yield).

MS (MALDI-TOF): *m/z* calcd for $[C_{70}H_{112}N_{11}O_{18}]^+$: 1395.69 [*M* + H]$^+$; found: 1395.70; (HCCA matrix), 1395.85 (SA matrix); HRMS (ESI+): *m/z* calcd for $[C_{70}H_{112}N_{11}O_{18}]^+$: 1394.82 [*M* + H]$^+$; found 1394.82; *m/z* calcd for $[C_{70}H_{111}Na_2N_{11}O_{18}]^{2+}$: 719.91 [*M* + 2Na]$^{2+}$; found: 719.89; *m/z* calcd for $[C_{70}H_{110}Na_3N_{11}O_{18}]^{2+}$: 730.90 [*M* + 3Na - H]$^{2+}$; found: 730.88.

cyclo[DKP-RGD]-Uncleavable-MMAE (**148**)

Aliphatic alkyne-MMAE (155)

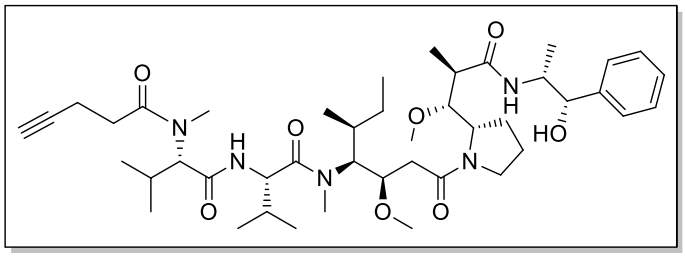

$C_{44}H_{71}N_5O_8$
MW: 798,06

Commercial 4-pentynoic acid (4.2 mg, 0.042 mmol, 1.5 equiv) in dry DMF (0.5 mL) was cooled to 0 °C under a nitrogen atmosphere. HATU (19 mg, 0.048 mmol, 1.7 equiv), HOAt (7 mg, 0.048 mmol, 1.7 equiv) and *i*Pr_2NEt (20 µL, 0.112 mmol, 4 equiv) were added and the mixture

was stirred for 20 min at 0 °C. A solution of commercial MMAE in dry DMF (1 mL) was added to the stirred mixture. The reaction was allowed to slowly reach room temperature and stirred overnight. The mixture was diluted with AcOEt (30 mL), washed with 1 M aqueous solution of $KHSO_4$ (2 × 10 mL) and brine (1 × 20 mL). The organic phase was dried over Na_2SO_4 and concentrated. The solid was purified by flash chromatography [gradient: from CH_2Cl_2/MeOH 97:2 to 97:] to afford amide **155** as white solid (20 mg, 90% yield).

R_f = 0.30 (97:3, CH_2Cl_2/MeOH); MS (ESI+) *m/z* calcd for $[C_{44}H_{72}N_5O_8]^+$: 798.06 [*M* + H]$^+$; found: 798.09; HRMS (ESI+): *m/z* calcd for $[C_{44}H_{71}NaN_5O_8]^+$: 820.52 [*M* + Na]$^+$; found: 820.51.

cyclo[DKP-RGD]-Uncleavable-MMAE (148)

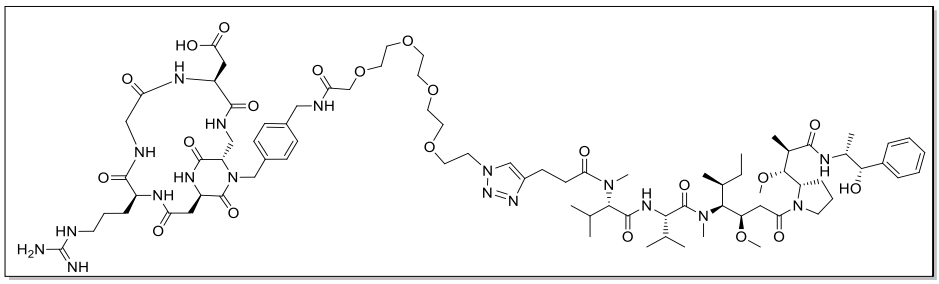

$C_{81}H_{126}N_{18}O_{21}$
MW: 1687,98

Alkyne **155** (4 mg, 0.004 mmol, 1.2 equiv) and azide **86** (5 mg, 0.004 mmol, 1 equiv) were reacted following the General Procedure GP3. The solvent was removed under vacuum, and the crude residue was purified by semipreparative HPLC [Waters Atlantis 21 mm x 10 cm column; gradient: 90% (H_2O+0.1% CF_3COOH)/10% (CH_3CN+0.1% CF_3COOH) to 100% (CH_3CN+0.1% CF_3COOH) in 20 min; t_R (product)=10.8 min]. The purified product was then freeze-dried to give the desired compound **148** as a white solid (5.5 mg, 83% yield).

MS (MALDI-TOF): *m/z* calcd for $[C_{81}H_{127}N_{18}O_{21}]^+$: 1688.98 [*M* + H]$^+$; found: 1688.90; (SA matrix), 1688.00 (HCCA matrix); HRMS (ESI+): *m/z* calcd for $[C_{81}H_{127}N_{18}O_{21}]^+$: 1687.94 [*M* + H]$^+$; found: 1687.94; *m/z* calcd for $[C_{81}H_{127}NaN_{18}O_{21}]^{2+}$: 855.47 [*M* + Na + H]$^{2+}$; found: 855.46.

HOOC-Uncleavable-MMAE (156)

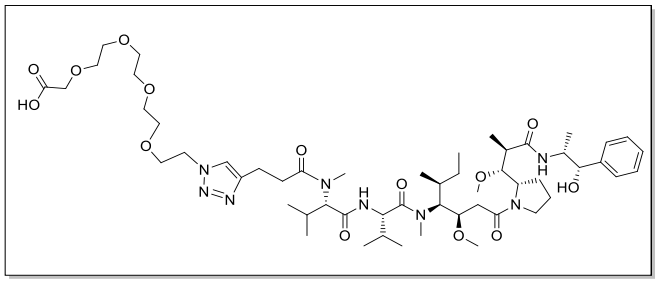

$C_{54}H_{90}N_8O_{14}$
MW: 1075,34

Alkyne **155** (4 mg, 0.005 mmol, 1 equiv) and azide-COOH **91** (1.4 mg, 0.004 mmol, 1 equiv) were reacted following the General Procedure GP3. The solvent was removed under vacuum, and the crude residue was purified by semipreparative HPLC [Waters Atlantis 21 mm x 10 cm column; gradient: 90% (H_2O+0.1% CF_3COOH)/10% (CH_3CN+0.1% CF_3COOH) to 100%

(CH_3CN+0.1% CF_3COOH) in 20 min; t_R (product)=12 min]. The purified product was then freeze-dried to give the desired compound **156** as a white solid (2.4 mg, 45% yield).
MS (MALDI-TOF): *m/z* calcd for $[C_{54}H_{91}N_8O_{14}]^+$: 1075.34 $[M + H]^+$; found: 1075.35; (SA matrix), 1075.55 (HCCA matrix); HRMS (ESI+): *m/z* calcd for $[C_{54}H_{91}N_8O_{14}]^+$: 1075.670 $[M + H]^+$; found: 1075.665; *m/z* calcd for $[C_{54}H_{90}NaN_8O_{14}]^+$: 1097.65 $[M + Na]^+$; found: 1097.64; *m/z* calcd for $[C_{54}H_{90}Na_2N_8O_{14}]^{2+}$: 560.33 $[M + 2Na]^{2+}$; found: 560.32.

cyclo[DKP-RGD]-PEG-4-Val-Ala-MMAF (**146**)

Aliphatic alkyne-Val-Ala-PABC-MMAF (157)

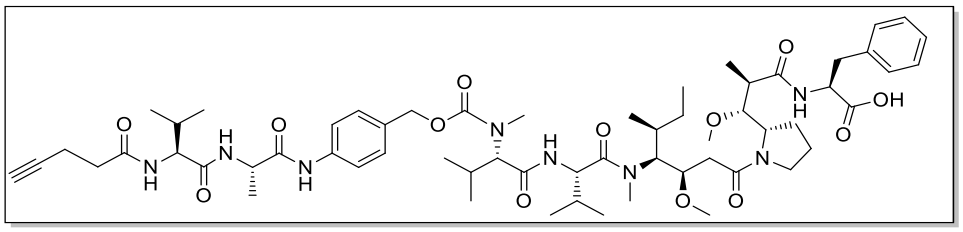

$C_{60}H_{90}N_8O_{13}$
MW: 1131,40

Compound **153** (20 mg, 0.037 mmol, 1 equiv) and HOBt (3 mg, 0.019 mmol, 0.5 equiv) were dissolved in dry DMF under argon atmosphere. Commercial MMAF·TFA (37 mg, 0.044 mmol, 1.2 equiv) is solubilized in dry DMF:Pyridine (4:1, 600 µL, reaction total volume) and DIPEA (12 µL, 0.066 mmol, 1.8 equiv) and added to the starting material solution at 0 ºC, under argon atmosphere. Then, the mixture was allowed to reach room temperature and stirred over weekend under argon atmosphere. The reaction mixture was concentrated at the rotavapor and the crude residue was purified by semipreparative HPLC [Waters Atlantis 21 mm x 10 cm column; gradient: 90% (H_2O+0.1% CF_3COOH)/10% (CH_3CN+0.1% CF_3COOH) to 100% (CH_3CN+0.1% CF_3COOH) in 20 min; t_R (product)=10.0 min]. The purified product was then freeze-dried to give the desired compound **157** as a white solid (23 mg, 55% yield).
MS (MALDI-TOF): *m/z* calcd for $[C_{60}H_{91}N_8O_{13}]^+$: 1131.40 $[M + H]^+$; found: 1132.00; (SA matrix), 1132.01 (HCCA matrix); *m/z* calcd for $[C_{60}H_{90}N_8O_{13}]^+$: 1153.02 $[M + Na]^+$; found: 1153.00; (SA matrix), 1153.01 (HCCA matrix).

cyclo[DKP-RGD]-PEG-4-Val-Ala-MMAF (146)

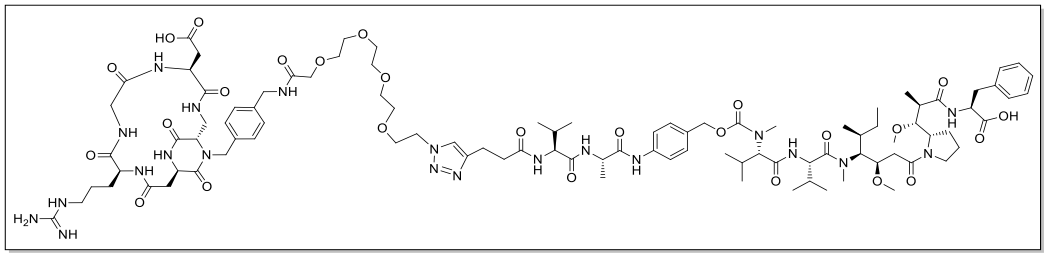

$C_{97}H_{145}N_{21}O_{26}$
MW: 2021,31

Alkyne **157** (5.5 mg, 0.0048 mmol, 1.2 equiv) and azide **86** (4 mg, 0.004 mmol, 1 equiv) were reacted according General Procedure GP3. The solvent was removed under vacuum, and the

crude residue was purified by semipreparative HPLC [Waters Atlantis 21 mm x 10 cm column; gradient: 90% (H_2O+0.1% CF_3COOH)/10% (CH_3CN+0.1% CF_3COOH) to 100% (CH_3CN+0.1% CF_3COOH) in 20 min; t_R (product)=12 min]. The purified product was then freeze-dried to give the desired compound **146** as a white solid (7.6 mg, 95% yield).

MS (MALDI-TOF): *m/z* calcd for $[C_{97}H_{146}N_{21}O_{26}]^+$: 2022.31 [*M* + H]$^+$; found: 2022.35; (SA matrix), 2022.85 (HCCA matrix); HRMS (ESI+): *m/z* calcd for $[C_{97}H_{146}N_{21}O_{26}]^+$: 2021.07 [*M* + H]$^+$; found: 2021.07; *m/z* calcd for $[C_{97}H_{146}NaN_{21}O_{26}]^{2+}$: 1022.04 [*M* + Na + H]$^{2+}$; found: 1022.03.

cyclo[DKP-RGD]-Uncleavable-MMAF (**149**)

Aliphatic alkyne-MMAF (158)

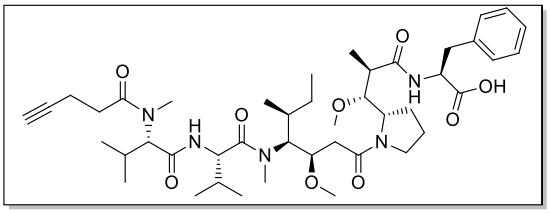

$C_{44}H_{69}N_5O_9$
MW: 812,05

Commercial 4-pentynoic acid (3.5 mg, 0.036 mmol, 1.5 equiv) in dry DMF (0.4 mL) was cooled to 0 °C under a nitrogen atmosphere. HATU (16 mg, 0.041 mmol, 1.7 equiv), HOAt (6 mg, 0.041 mmol, 1.7 equiv) and *i*Pr_2NEt (21 µL, 0.120 mmol, 5 equiv) were added and the mixture was stirred for 20 min at 0 °C. A solution of commercial MMAF·TFA in dry DMF (1 mL) was added to the stirred mixture. The reaction was allowed to slowly reach room temperature and stirred overnight. The reaction mixture was concentrated at the rotavapor and the crude residue was purified by semipreparative HPLC [Waters Atlantis 21 mm x 10 cm column; gradient: 90% (H_2O+0.1% CF_3COOH)/10% (CH_3CN+0.1% CF_3COOH) to 100% (CH_3CN+0.1% CF_3COOH) in 20 min; t_R (product)=10.2 min]. The purified product was then freeze-dried to give the desired compound **158** as a white solid (16 mg, 82% yield).

MS (MALDI-TOF): *m/z* calcd for $[C_{44}H_{70}N_5O_9]^+$: 812.05 [*M* + H]$^+$; found: 812.05; (SA matrix), 812.05 (HCCA matrix); *m/z* calcd for $[C_{44}H_{69}NaN_5O_9]^+$: 835.05 [*M* + Na]$^+$; found: 835.20; (SA matrix), 835.18 (HCCA matrix).

cyclo[DKP-RGD]-Uncleavable-MMAF (149)

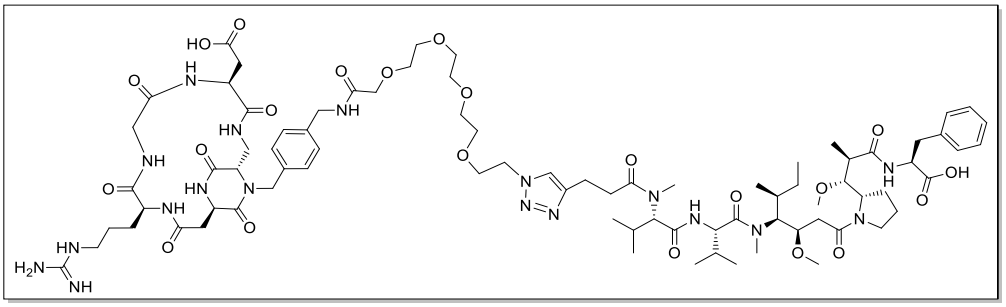

$C_{81}H_{124}N_{18}O_{22}$
MW: 1701,96

Alkyne **158** (4 mg, 0.0048 mmol, 1.2 equiv) and azide **86** (4 mg, 0.004 mmol, 1 equiv) were reacted following General Procedure GP3. The solvent was removed under vacuum, and the crude residue was purified by semipreparative HPLC [Waters Atlantis 21 mm x 10 cm column; gradient: 90% (H_2O+0.1% CF_3COOH)/10% (CH_3CN+0.1% CF_3COOH) to 100% (CH_3CN+0.1% CF_3COOH) in 20 min; t_R (product)=11.0 min]. The purified product was then freeze-dried to give the desired compound **149** as a white solid (6.3 mg, 95% yield).

MS (MALDI-TOF): *m/z* calcd for $[C_{81}H_{125}N_{18}O_{22}]^+$: 1701.96 [*M* + H]$^+$; found: 1702.01; (SA matrix), 1701.91; HRMS (ESI+): *m/z* calcd for $[C_{81}H_{125}N_{18}O_{22}]^+$: 1701.92 [*M* + H]$^+$; found: 1701.92; *m/z* calcd for $[C_{81}H_{125}NaN_{18}O_{22}]^{2+}$: 862.95 [*M* + Na + H]$^{2+}$; found: 862.96.

cyclo[DKP-RGD]-PEG-4-Asn-Pro-Val-MMAE (**150**)

Aliphatic alkyne-Asn(Trt)-Pro-Val-PABA (160)

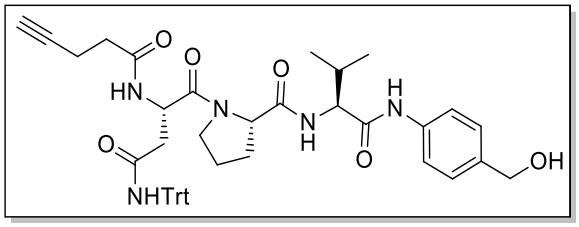

$C_{45}H_{49}N_5O_6$
MW: 755,90

Fmoc-Asn(Trt)-Pro-Val-PABA **159** (425 mg, 0.473 mmol, 1 equiv) was deprotected following General Procedure GP2. Commercial 4-pentynoic acid (70 mg, 0.709 mmol, 1.5 equiv) in dry DMF (4 mL) was cooled to 0 °C under a nitrogen atmosphere. HATU (310 mg, 0.804 mmol, 1.7 equiv), HOAt (110 mg, 0.804 mmol, 1.7 equiv) and *i*Pr_2NEt (330 µL, 1.892 mmol, 4 equiv) were added and the mixture was stirred for 20 min at 0 °C. A solution of **159-NH** in dry DMF (8 mL) was added to the stirred mixture. The reaction was allowed to slowly reach room temperature and stirred overnight. The mixture was dried at rotavapor under reduced pressure. The remained oil was purified by flash chromatography (gradient: from CH_2Cl_2 100% to CH_2Cl_2/MeOH, 95:5) to afford amide **160** as fade white solid (227 mg, 65% yield over two steps). R_f = 0.26 (97:3, CH_2Cl_2/MeOH); ^{1}H NMR (400 MHz, CD_2Cl_2-*d*$_2$) δ 8.62 (s, 1H), 7.90 (d, *J* = 8.5 Hz, 2H), 7.74 (s, 1H), 7.43 (d, *J* = 8.0 Hz, 2H), 7.33 – 7.16 (m, 18H), 4.61 – 4.49 (m, 2H), 4.43 (td, *J* = 11.4, 7.9 Hz, 1H), 4.27 (dd, *J* = 9.1, 3.5 Hz, 1H), 3.97 (t, *J* = 8.7 Hz, 1H), 3.25 (q, *J* = 8.7 Hz, 1H), 2.76 (t, *J* = 13.0 Hz, 1H), 2.50 (td, *J* = 10.1, 8.9, 3.4 Hz, 1H), 2.46 – 2.39 (m, 2H), 2.33 – 2.20 (m, 3H), 2.14 – 2.04 (m, 1H), 1.99 (t, *J* = 2.6 Hz, 1H), 1.92 – 1.80 (m, 2H), 1.78 – 1.69 (m, 1H), 1.51 – 1.40 (m, 1H), 0.78 (d, *J* = 6.6 Hz, 3H), 0.38 (d, *J* = 6.6 Hz, 3H); ^{13}C NMR (101 MHz, CD_2Cl_2-*d*$_2$) δ 172.85, 171.93, 170.88, 170.38, 169.71, 144.56, 138.31, 137.76, 129.33, 128.51, 128.45, 127.52, 121.16, 71.33, 69.52, 65.41, 62.30, 60.58, 48.00, 47.88, 40.27, 35.25, 30.40, 30.26, 28.09, 25.13, 20.18, 19.44, 14.86. MS (MALDI-TOF): *m/z* calcd for $[C_{45}H_{49}NaN_5O_6]^+$: 778.90 [*M* + Na]$^+$: found 778.30.

Aliphatic alkyne-Asn(Trt)-Pro-Val-PABC-PNP (161)

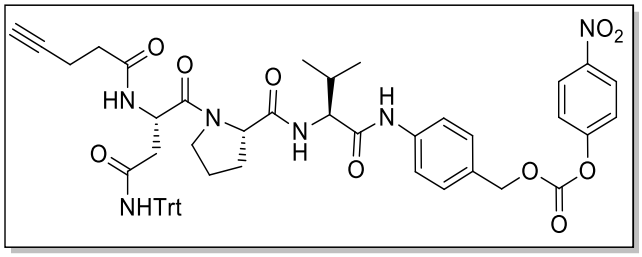

$C_{52}H_{52}N_6O_{10}$
MW: 921,00

A solution of compound **160** (210 mg, 0.278 mmol, 1 equiv) in dry THF (16 mL) under nitrogen atmosphere was cooled to 0 °C. Pyridine (60 µL, 0.695 mmol, 2.5 equiv) and 4-nitrophenylchloroformate (115 mg, 0.556 mmol, 2 equiv) were added, then the mixture could reach room temperature and stirred for 2 h. The reaction mixture was concentrated under reduced pressure and AcOEt (100 mL) was added and the solution was washed with a 1 M aqueous solution of $KHSO_4$ (3 × 30 mL) and brine (20 mL). The organic phase was dried and concentrated, then the crude was purified by flash chromatography (eluent: 1:9, *n*-Hexane/EtOAc) affording compound **161** (160 mg, 64% yield) as a white solid.

R_f = 0.29 (1:9, *n*-Hexane/EtOAc); ^{1}H NMR (400 MHz, CD_2Cl_2-d_2) δ 8.45 (s, 1H), 8.25 (d, *J* = 9.2 Hz, 2H), 7.78 – 7.71 (m, 3H), 7.43 – 7.36 (m, 4H), 7.29 (s, 1H), 7.27 – 7.20 (m, 9H), 7.18 – 7.13 (m, 6H), 6.58 (d, *J* = 8.0 Hz, 1H), 5.24 (d, *J* = 2.0 Hz, 2H), 4.72 (ddd, *J* = 11.3, 8.1, 3.0 Hz, 1H), 4.13 (dd, *J* = 8.7, 3.8 Hz, 1H), 3.93 (t, *J* = 8.1 Hz, 1H), 3.29 (q, *J* = 8.6 Hz, 1H), 2.97 (d, *J* = 13.7 Hz, 1H), 2.65 (dd, *J* = 13.7, 2.8 Hz, 1H), 2.61 – 2.53 (m, 1H), 2.49 – 2.44 (m, 2H), 2.43 – 2.38 (m, 2H), 1.98 (t, *J* = 2.5 Hz, 1H), 1.78 – 1.63 (m, 4H), 1.51 – 1.39 (m, 1H), 0.71 (d, *J* = 6.8 Hz, 3H), 0.40 (d, *J* = 6.6 Hz, 3H); ^{13}C NMR (101 MHz, CD_2Cl_2-d_2) δ 172.40, 171.69, 170.98, 170.92, 169.63, 156.16, 153.09, 146.03, 144.28, 139.84, 130.21, 130.14, 129.13, 128.51, 127.66, 125.80, 122.54, 120.40, 83.43, 71.35, 71.29, 69.57, 62.26, 61.20, 48.32, 48.14, 41.17, 35.25, 30.26, 29.42, 25.12, 19.96, 19.91, 15.00; MS (MALDI-TOF): *m/z* calcd for $[C_{52}H_{52}NaN_6O_{10}]^+$: 944.00 $[M + Na]^+$: found 944.21.

Aliphatic alkyne-Asn(Trt)-Pro-Val-PABC-MMAE (162)

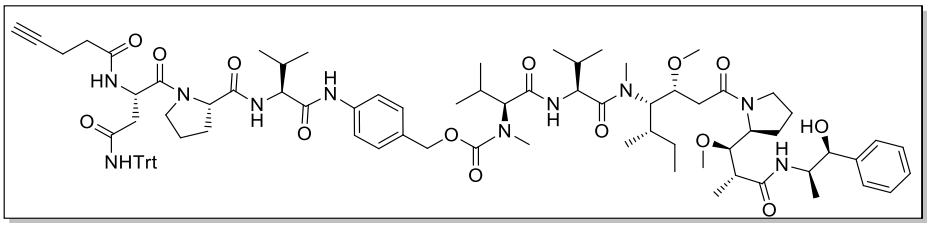

$C_{85}H_{114}N_{10}O_{14}$
MW: 1499,87

Compound **161** (20 mg, 0.022 mmol, 1 equiv) and HOBt (2 mg, 0.011 mmol, 0.5 equiv) were dissolved in dry DMF under argon atmosphere. Commercial MMAE (19 mg, 0.026 mmol, 1.2 equiv) was solubilized in dry DMF:Pyridine (4:1, 400 µL, reaction total volume) and DIPEA (4 µL, 0.020 mmol, 0.9 equiv) and added to the starting material solution at 0 ºC, under argon atmosphere. Then, the mixture was allowed to reach room temperature and stirred over

weekend under argon atmosphere. The reaction mixture was diluted with AcOEt (100 mL) the solution was washed with a 1 M aqueous solution of $KHSO_4$ (3 × 20 mL) and brine (20 mL). The organic phase was dried with Na_2SO_4 and concentrated, then the crude was purified by flash chromatography [gradient: from 98:2, CH_2Cl_2/MeOH to 95:5, CH_2Cl_2/MeOH] affording compound **162** (26 mg, 80% yield) as a white solid.

R_f = 0.30 (95:5, CH_2Cl_2/MeOH); MS (ESI+): *m/z* calcd for $[C_{85}H_{115}N_{10}O_{14}]^+$: 1499.85 [*M* + H]$^+$; found: 1499.75; HRMS (ESI+): *m/z* calcd for $[C_{85}H_{114}NaN_{10}O_{14}]^+$: 1521.84 [*M* + Na]$^+$; found: 1521.84; *m/z* calcd for $[C_{85}H_{114}Na_2N_{10}O_{14}]^{2+}$: 772.41 [*M* + 2Na]$^{2+}$; found: 772.41.

***cyclo*[DKP-RGD]-PEG-4-Asn-Pro-Val-MMAE (150)**

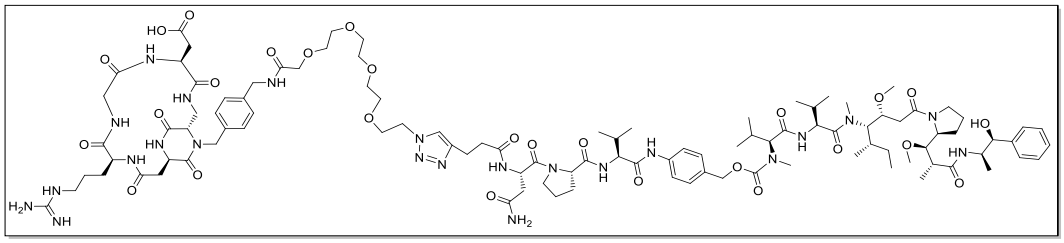

Alkyne **162** (15 mg, 0.01 mmol, 1 equiv) was solubilized in dry CH_2Cl_2 (0.75 mL) under nitrogen atmosphere. Et_3SiH (75 µL) and TFA (375 µL) were added at 0 ºC. The reaction mixture stirred for 45 min at room temperature and then CH_2Cl_2 (10 mL) was added. The organic layer was washed with H_2O (5 mL) and dried with Na_2SO_4. The CH_2Cl_2 was evaporated at rotavapor affording a white solid, which was used directly without purification. Resulting alkyne (13 mg, 0.00952 mmol, 1.4 equiv) and azide **86** (6.9 mg, 0.0068 mmol, 1 equiv) were reacted following General Procedure GP3. The solvent was removed under vacuum, and the crude residue was purified by semipreparative HPLC [Waters Atlantis 21 mm x 10 cm column; gradient: 90% (H_2O+0.1% CF_3COOH)/10% (CH_3CN+0.1% CF_3COOH) to 100% (CH_3CN+0.1% CF_3COOH) in 20 min; t_R (product)=11.5 min]. The purified product was then freeze-dried to give the desired compound **150** as a white solid (9.5 mg, 45% yield).

MS (MALDI-TOF): *m/z* calcd for $[C_{103}H_{156}N_{23}O_{27}]^+$: 2148.45 [*M* + H]$^+$; found: 2148.44; (SA matrix), 2148.51; HRMS (ESI+): *m/z* calcd for $[C_{103}H_{156}N_{23}O_{27}]^+$: 2147.15 [*M* + H]$^+$; found: 2147.15; *m/z* calcd for $[C_{103}H_{156}NaN_{23}O_{27}]^{2+}$: 1085.08 [*M* + Na + H]$^{2+}$; found: 1085.07; *m/z* calcd for $[C_{103}H_{156}Na_2N_{23}O_{27}]^{3+}$: 731.05 [*M* + 2Na + H]$^{3+}$; found: 731.04.

HPLC Traces of the Final Products

***cyclo*[DKP-RGD]-PEG-4-Val-Ala-PTX aliphatic scaffold (97)**

Waters Atlantis 21 mm × 10 cm column, gradient from 90% (H_2O + 0.1% CF_3COOH) / 10% (CH_3CN + 0.1% CF_3COOH) to 100% (CH_3CN + 0.1% CF_3COOH) in 20 min. Purity: 98%

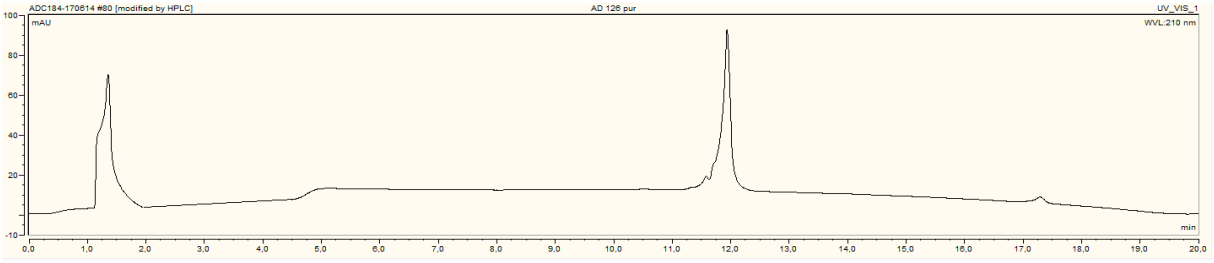

***cyclo*[DKP-RGD]-PEG-4-Val-Ala-PTX aromatic scaffold (102)**

Waters Atlantis 21 mm × 10 cm column, gradient from 90% (H_2O + 0.1% CF_3COOH) / 10% (CH_3CN + 0.1% CF_3COOH) to 100% (CH_3CN + 0.1% CF_3COOH) in 20 min. Purity: 98%

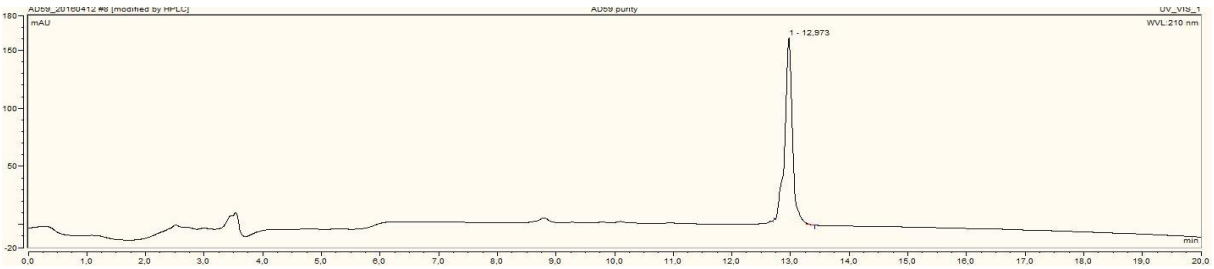

(*cyclo*[DKP-RGD]-PEG-4)$_2$-Val-Ala-PTX (103)

Waters Atlantis 21 mm × 10 cm column, gradient from 90% (H_2O + 0.1% CF_3COOH) / 10% (CH_3CN + 0.1% CF_3COOH) to 100% (CH_3CN + 0.1% CF_3COOH) in 26 min. Purity: >99%

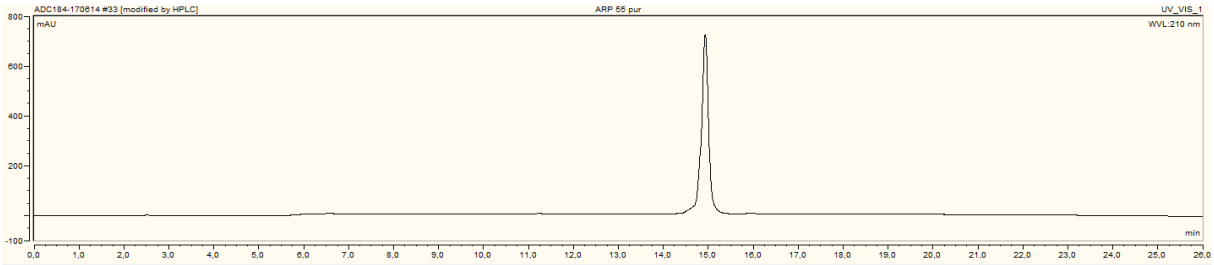

(*cyclo*[DKP-RGD]-PEG-4)$_3$-Val-Ala-PTX (104)

Waters Atlantis 21 mm × 10 cm column, gradient from 90% (H_2O + 0.1% CF_3COOH) / 10% (CH_3CN + 0.1% CF_3COOH) to 100% (CH_3CN + 0.1% CF_3COOH) in 20 min. Purity: >99%

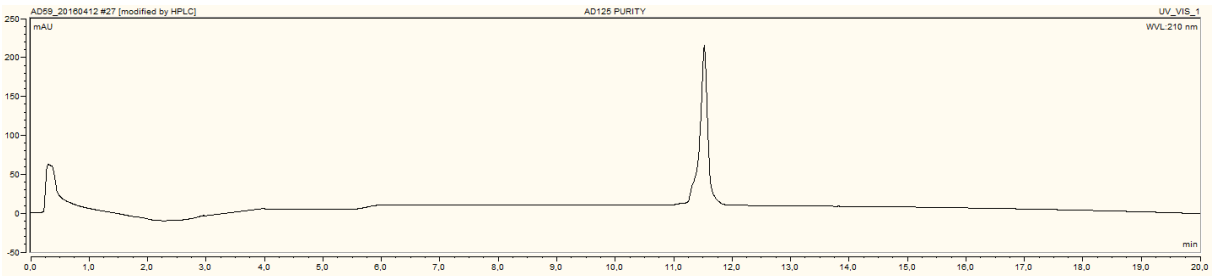

(*cyclo*[DKP-RGD]-PEG-4)$_4$-Val-Ala-PTX (105)

Waters Atlantis 21 mm × 10 cm column, gradient from 90% (H_2O + 0.1% CF_3COOH) / 10% (CH_3CN + 0.1% CF_3COOH) to 100% (CH_3CN + 0.1% CF_3COOH) in 20 min. Purity: >99%

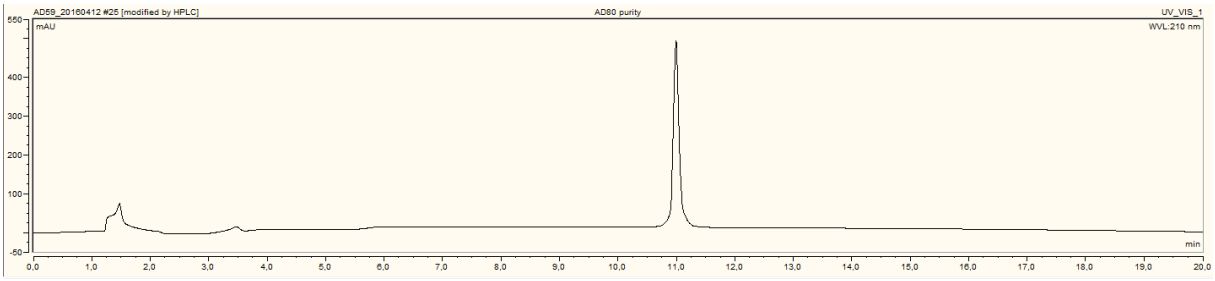

cyclo[DKP-RGD]-PEG-4-Asn-Pro-Val-PTX (121)

Waters Atlantis 21 mm × 10 cm column, gradient from 90% (H_2O + 0.1% CF_3COOH) / 10% (CH_3CN + 0.1% CF_3COOH) to 100% (CH_3CN + 0.1% CF_3COOH) in 20 min. Purity: 98%

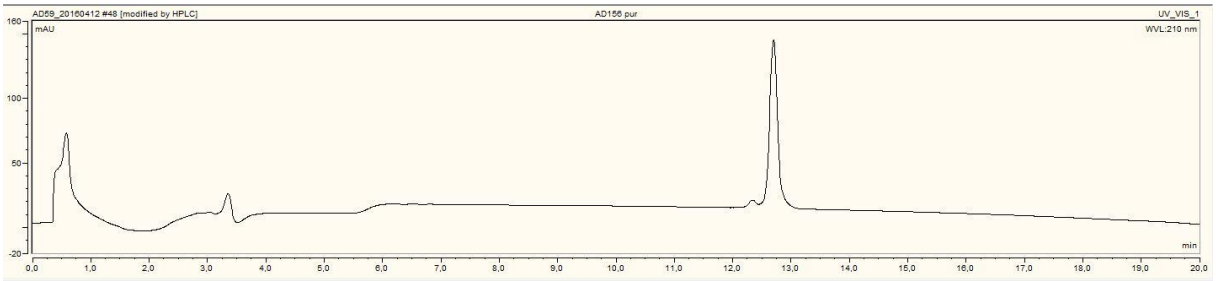

cyclo[DKP-RGD]-PEG-4-Asn-Pro-[D]-Val-PTX (123)

Waters Atlantis 21 mm × 10 cm column, gradient from 90% (H_2O + 0.1% CF_3COOH) / 10% (CH_3CN + 0.1% CF_3COOH) to 100% (CH_3CN + 0.1% CF_3COOH) in 20 min. Purity: >99%

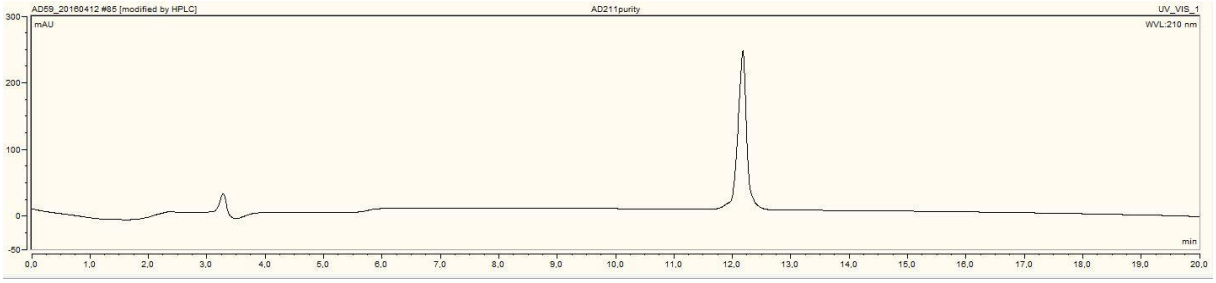

cyclo[DKP-RGD]-Uncleavable-PTX (124)

Waters Atlantis 21 mm × 10 cm column, gradient from 90% (H_2O + 0.1% CF_3COOH) / 10% (CH_3CN + 0.1% CF_3COOH) to 100% (CH_3CN + 0.1% CF_3COOH) in 20 min. Purity: 96%

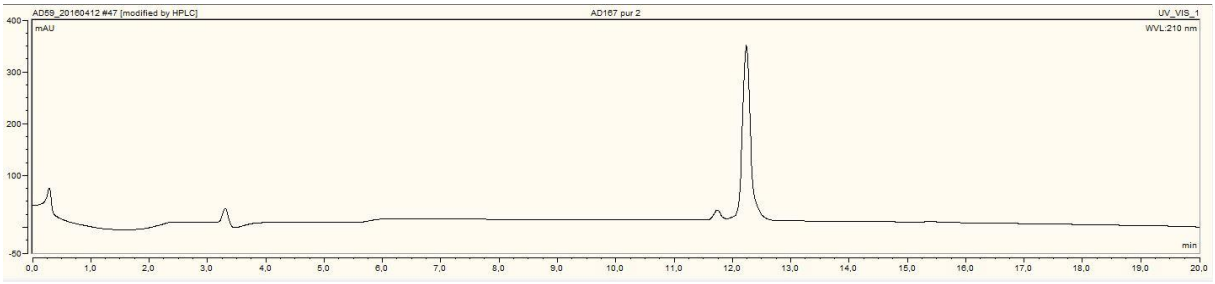

Pro-PTX (142)

Waters Atlantis 21 mm × 10 cm column, gradient from 90% (H_2O + 0.1% CF_3COOH) / 10% (CH_3CN + 0.1% CF_3COOH) to 100% (CH_3CN + 0.1% CF_3COOH) in 20 min. Purity: >99%

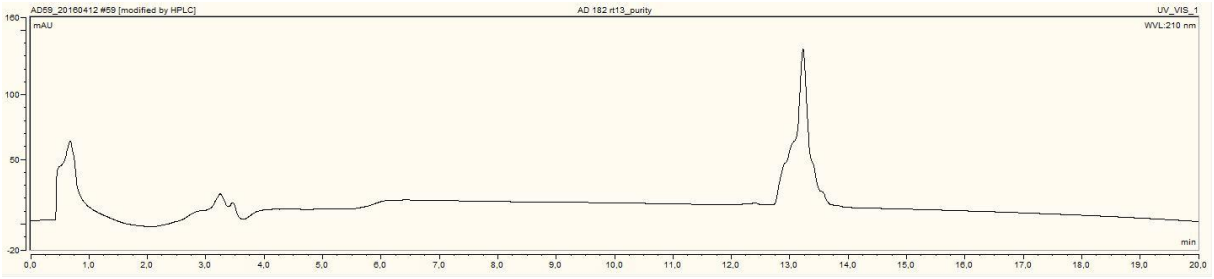

***cyclo*[DKP-RGD]-PEG-4-Val-Ala-MMAE (145)**

Waters Atlantis 21 mm × 10 cm column, gradient from 90% (H_2O + 0.1% CF_3COOH) / 10% (CH_3CN + 0.1% CF_3COOH) to 100% (CH_3CN + 0.1% CF_3COOH) in 20 min. Purity: >99%

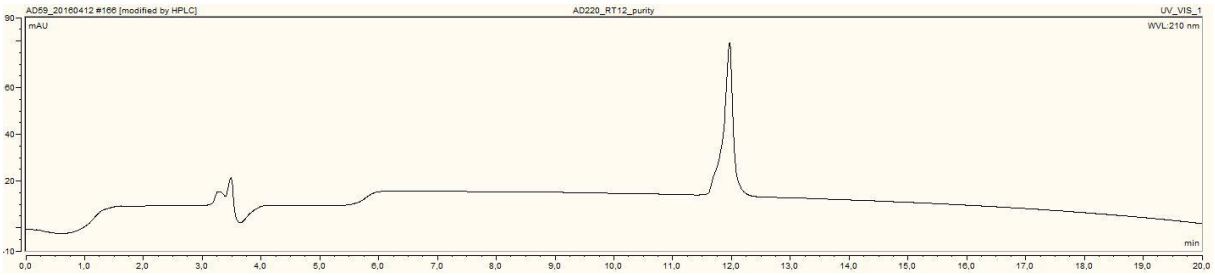

HOOC-PEG-4-Val-Ala-MMAE (147)

Waters Atlantis 21 mm × 10 cm column, gradient from 90% (H_2O + 0.1% CF_3COOH) / 10% (CH_3CN + 0.1% CF_3COOH) to 100% (CH_3CN + 0.1% CF_3COOH) in 20 min. Purity: >99%

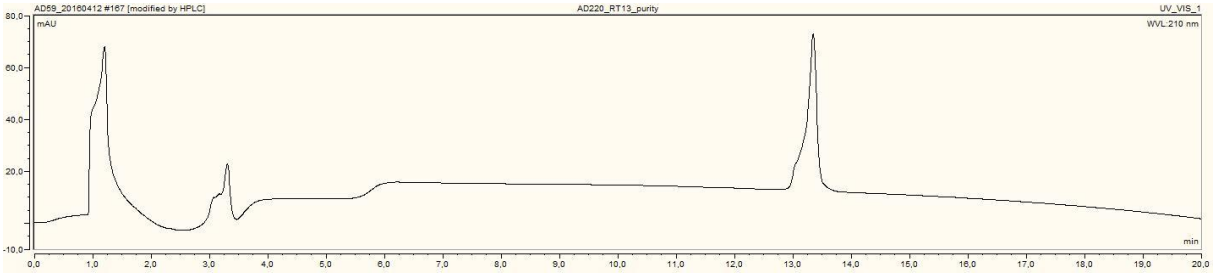

***cyclo*[DKP-RGD]-Uncleavable-MMAE (148)**

Waters Atlantis 21 mm × 10 cm column, gradient from 90% (H_2O + 0.1% CF_3COOH) / 10% (CH_3CN + 0.1% CF_3COOH) to 100% (CH_3CN + 0.1% CF_3COOH) in 20 min. Purity: >99%

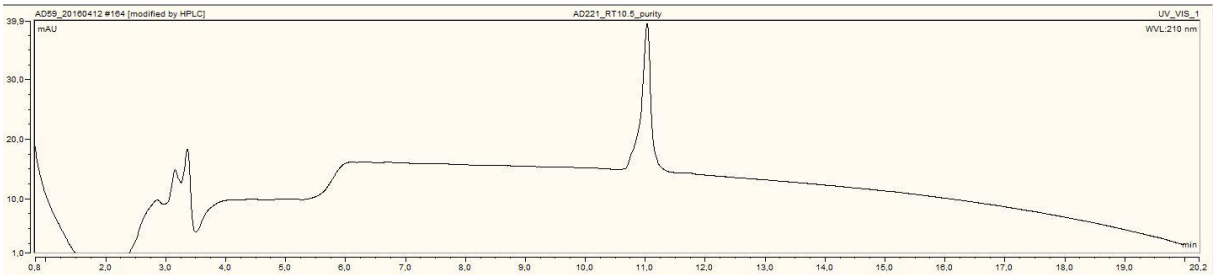

HOOC-Uncleavable-MMAE (156)

Waters Atlantis 21 mm × 10 cm column, gradient from 90% (H_2O + 0.1% CF_3COOH) / 10% (CH_3CN + 0.1% CF_3COOH) to 100% (CH_3CN + 0.1% CF_3COOH) in 20 min. Purity: >99%

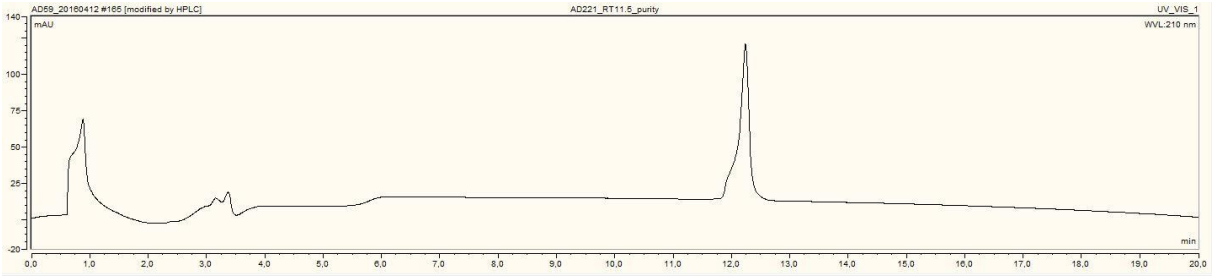

cyclo[DKP-RGD]-PEG-4-Val-Ala-MMAF (146)

Waters Atlantis 21 mm × 10 cm column, gradient from 90% (H_2O + 0.1% CF_3COOH) / 10% (CH_3CN + 0.1% CF_3COOH) to 100% (CH_3CN + 0.1% CF_3COOH) in 20 min. Purity: >99%

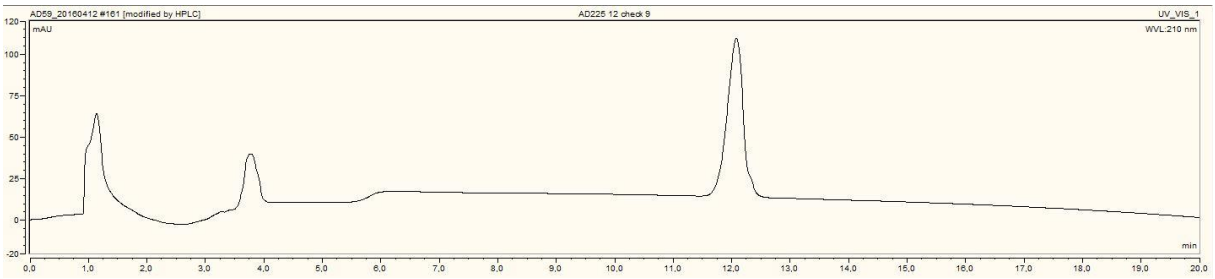

cyclo[DKP-RGD]-Uncleavable-MMAF (149)

Waters Atlantis 21 mm × 10 cm column, gradient from 90% (H_2O + 0.1% CF_3COOH) / 10% (CH_3CN + 0.1% CF_3COOH) to 100% (CH_3CN + 0.1% CF_3COOH) in 20 min. Purity: 97%

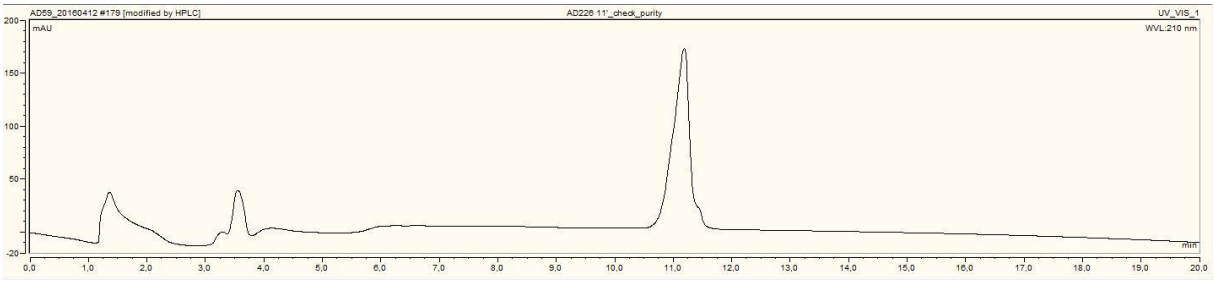

cyclo[DKP-RGD]-PEG-4-Asn-Pro-Val-MMAE (150)

Waters Atlantis 21 mm × 10 cm column, gradient from 90% (H_2O + 0.1% CF_3COOH) / 10% (CH_3CN + 0.1% CF_3COOH) to 100% (CH_3CN + 0.1% CF_3COOH) in 20 min. Purity: >99%

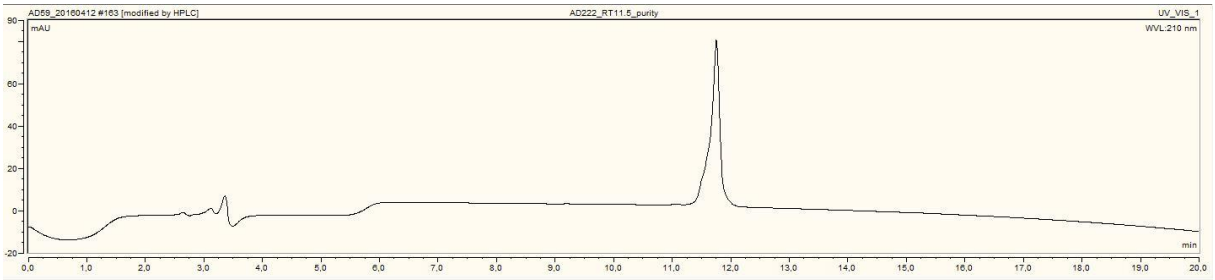

Appendix of NMR Data

14-Azido-3,6,9,12-tetraoxatetradecanoic acid (91)

^{1}H NMR (400 MHz, CD_2Cl_2-d_2)

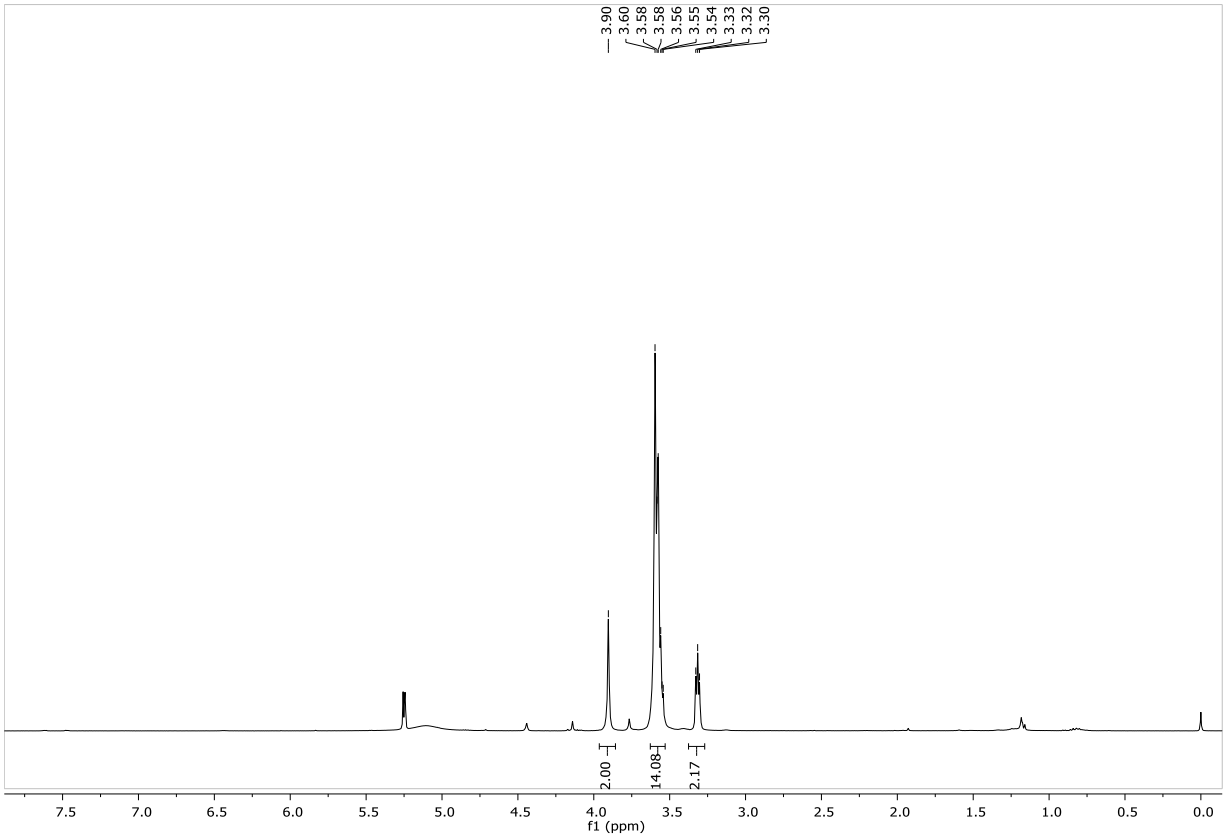

Azido-tetraethylene glycol-*N*-hydroxysuccinimidyl ester (92)

^{1}H NMR (400 MHz, CD_2Cl_2-d_2)

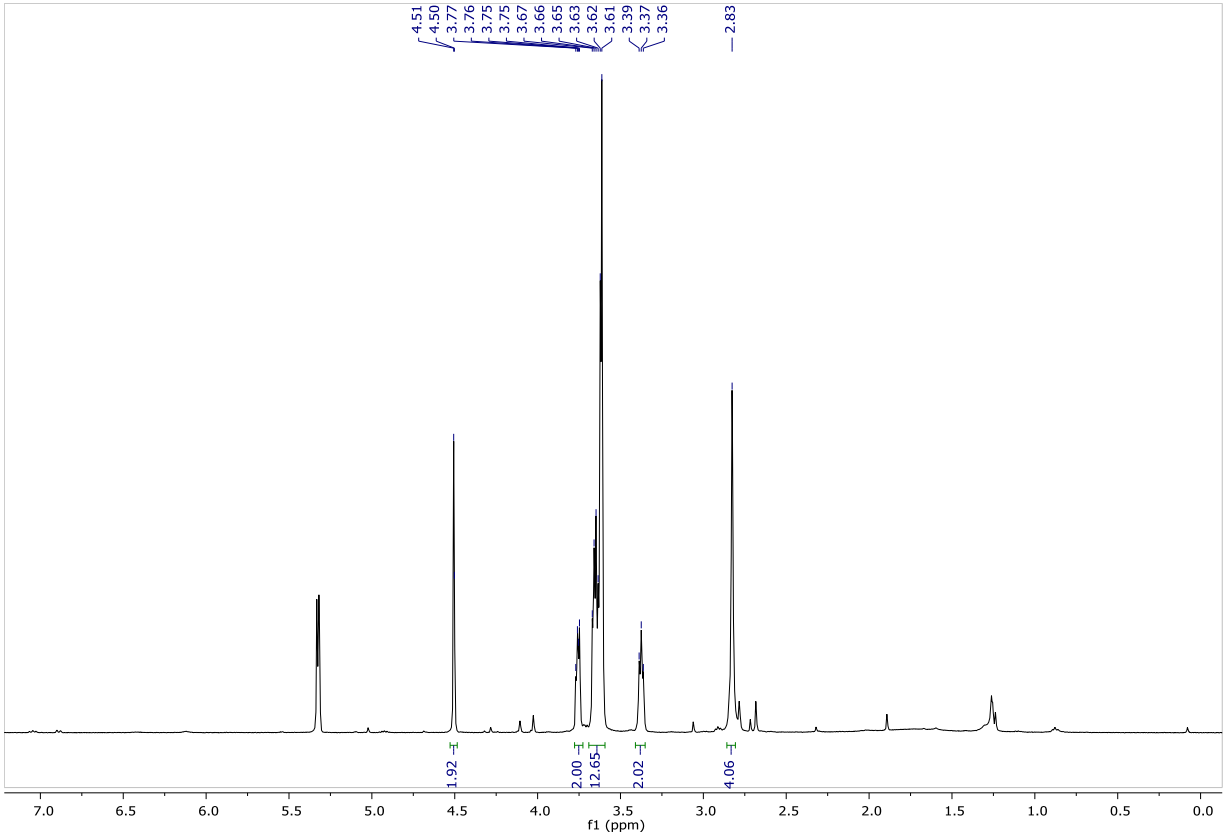

cyclo[DKP-RGD]-PEG-4-N_3 (86)

^{1}H NMR (400 MHz, D_2O)

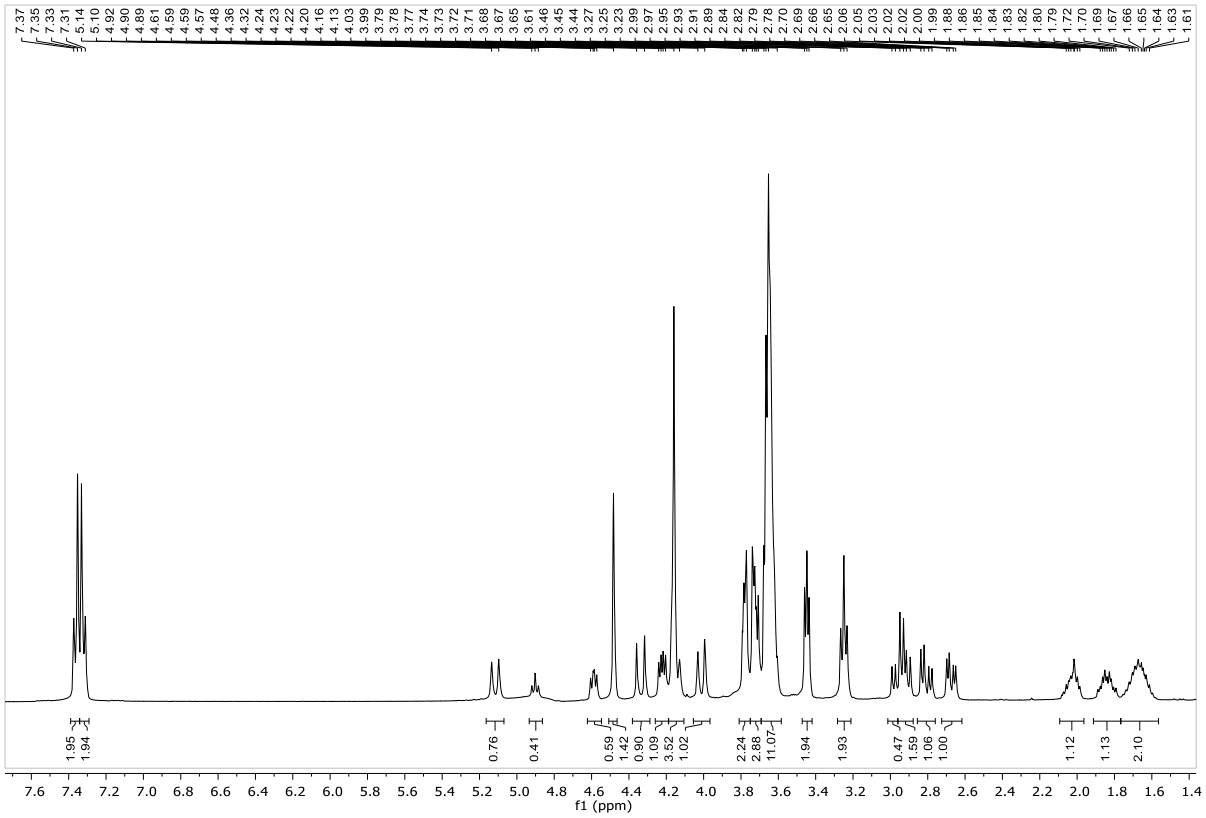

^{13}C NMR (101 MHz, D_2O)

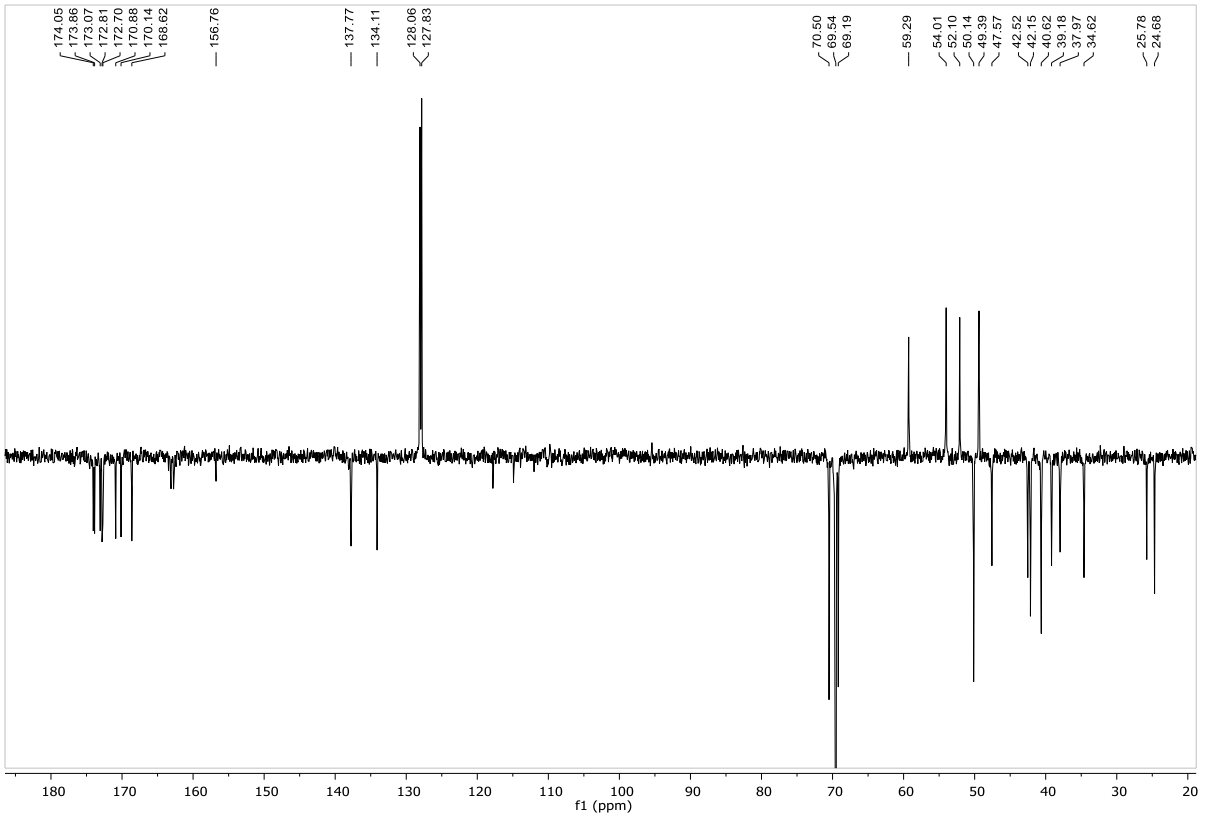

Aliphatic alkyne-Val-Ala-PABC-*N*-(Boc)-*N*,*N*′-dimethylethylenediamine (94)

^{1}H NMR (500 MHz, [D]$_6$DMSO), T= 70º C

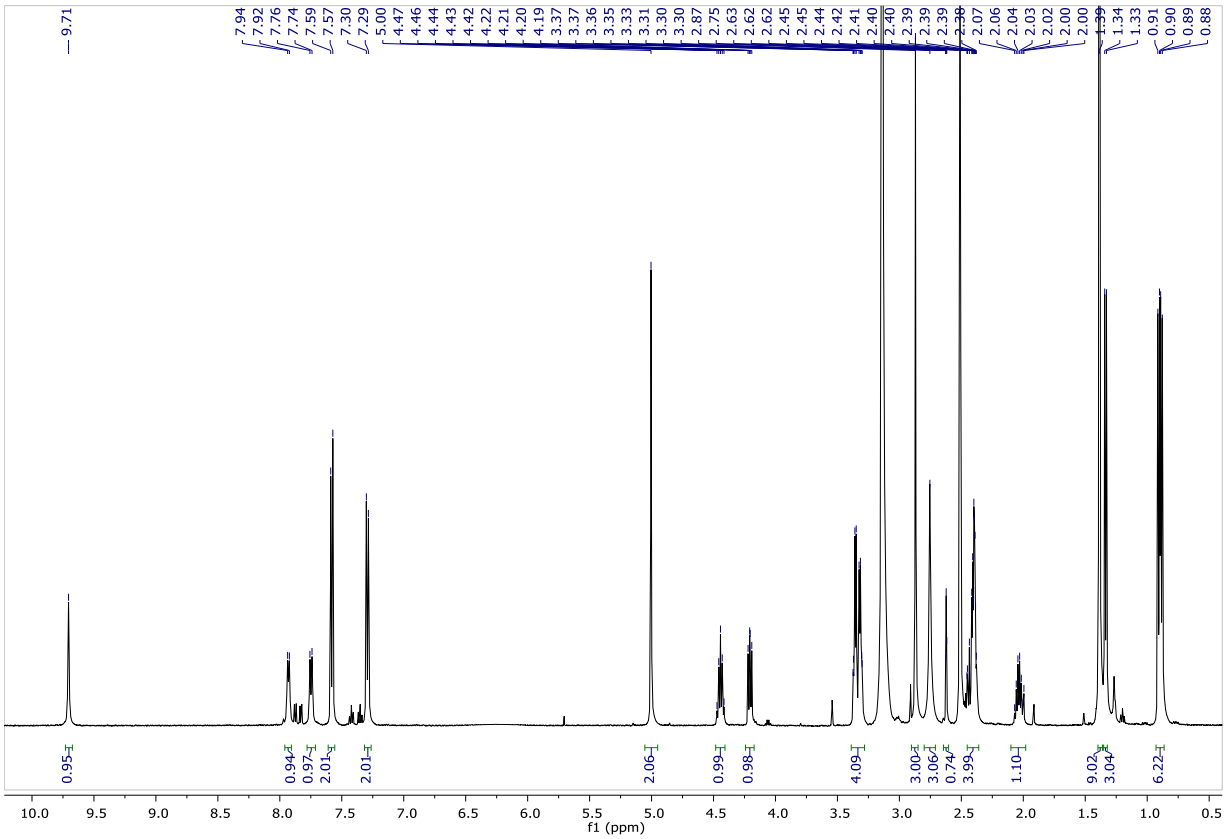

^{13}C NMR (126 MHz, [D]$_6$DMSO), T = 70 ºC

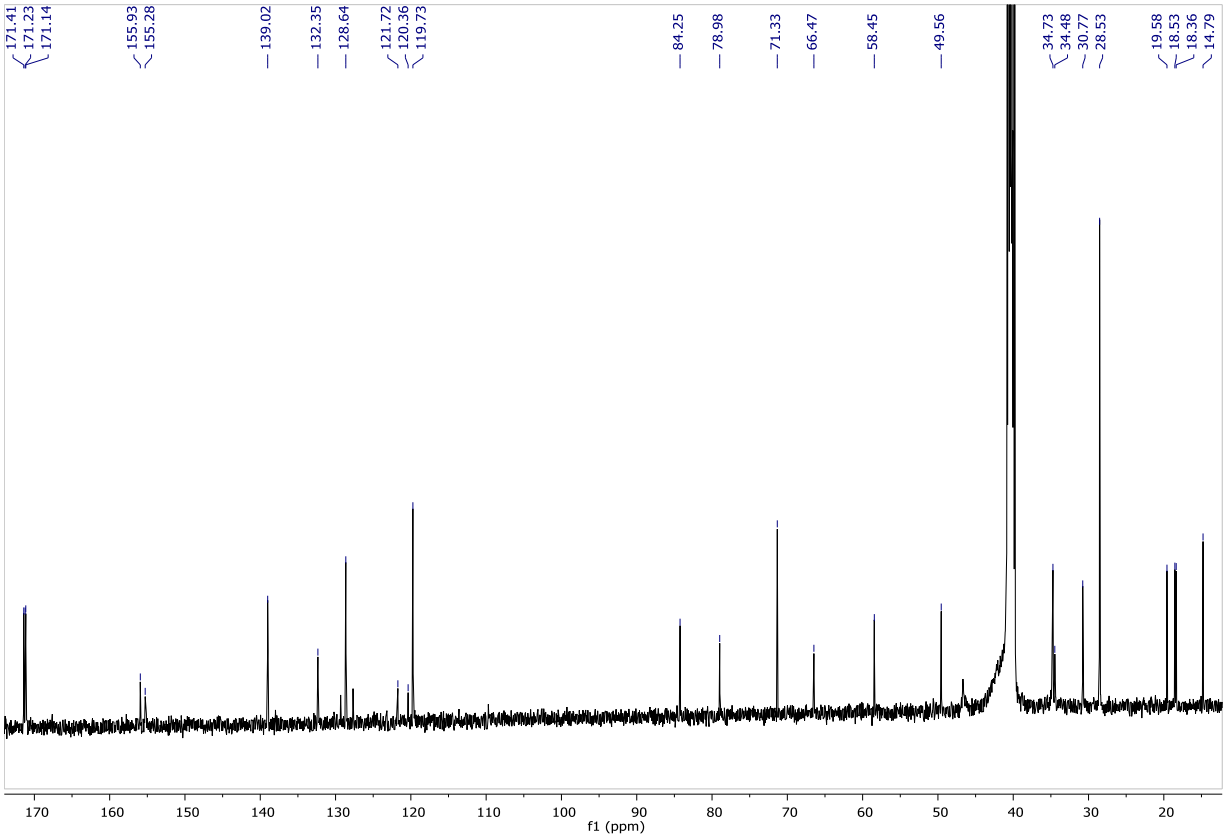

Methyl 4-hydroxybenzoate (107)

^{1}H NMR (400 MHz, CD_2Cl_2-d_2)

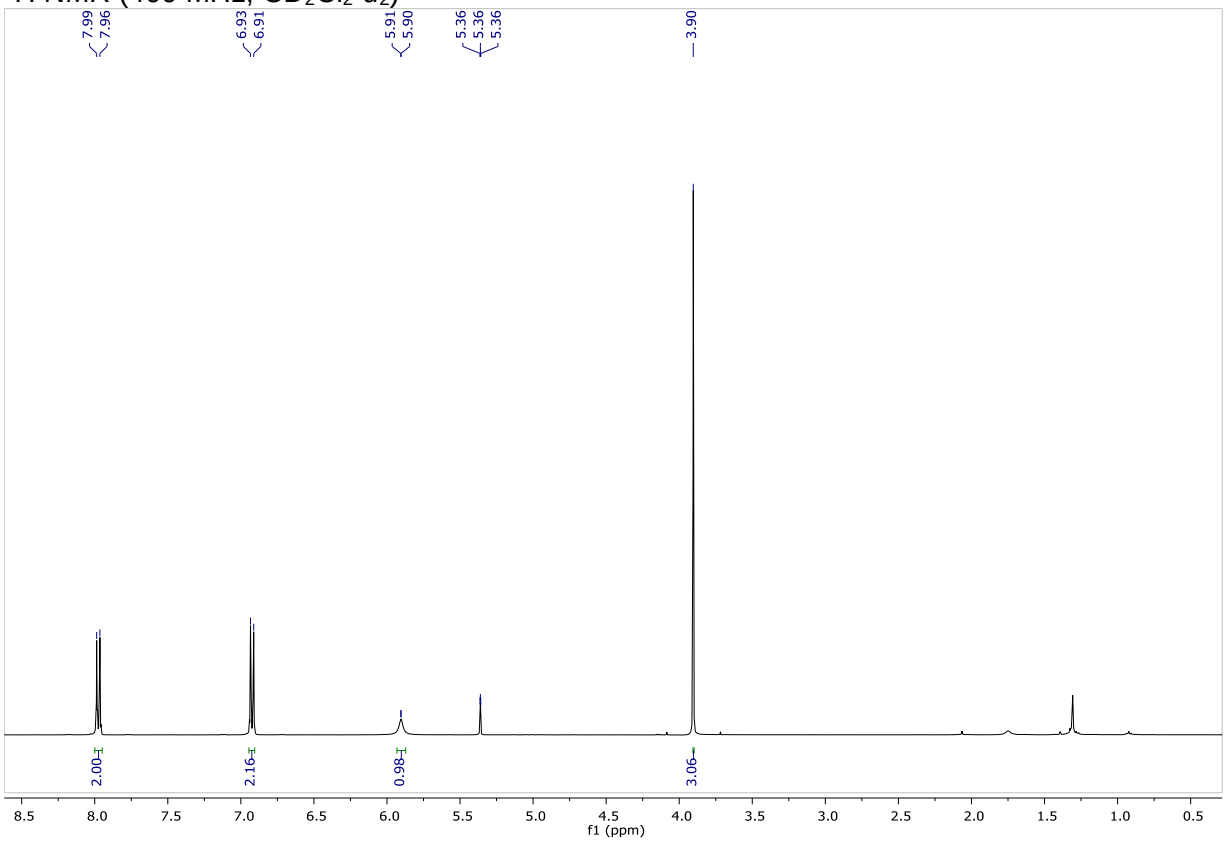

Methyl 4-(prop-2-yn-1-yloxy)benzoate (108)

^{1}H NMR (400 MHz, CD_2Cl_2-d_2)

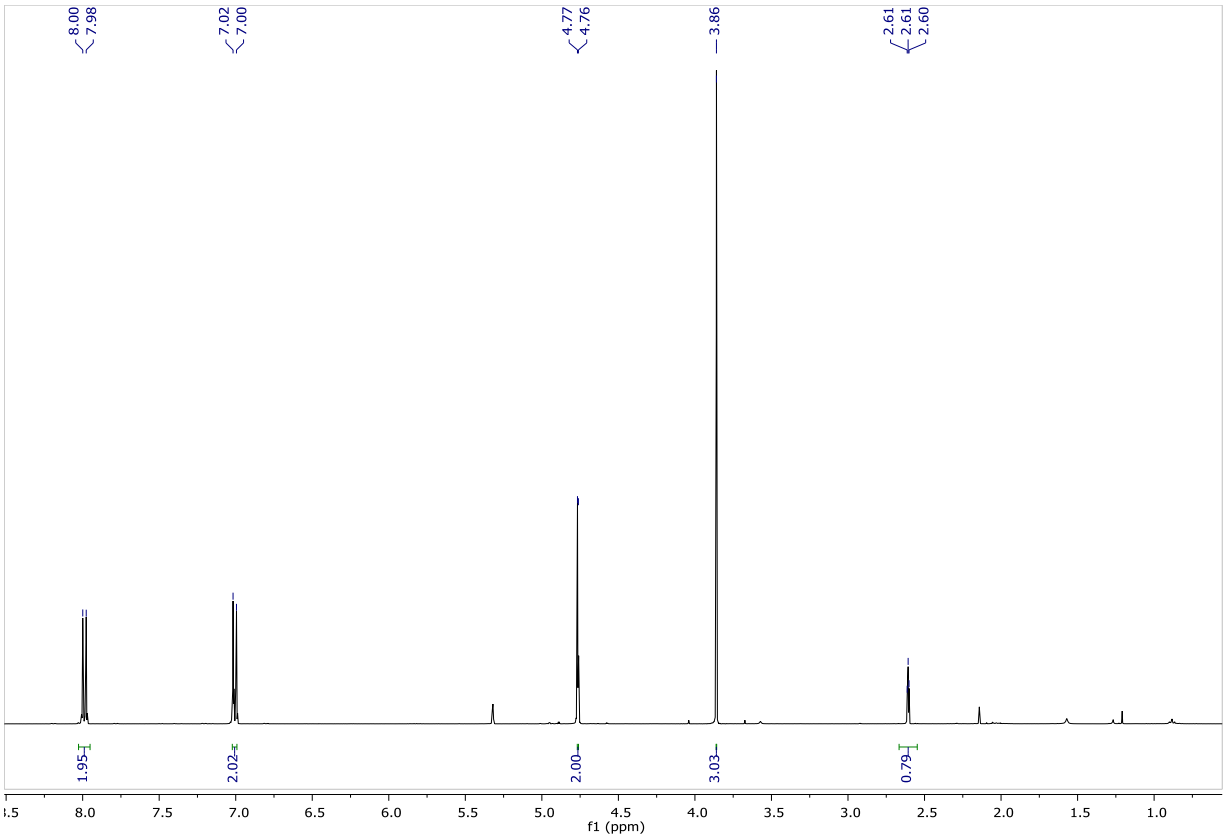

4-(Prop-2-yn-1-yloxy)benzoic acid (109)

^{1}H NMR (400 MHz, CD_3OD)

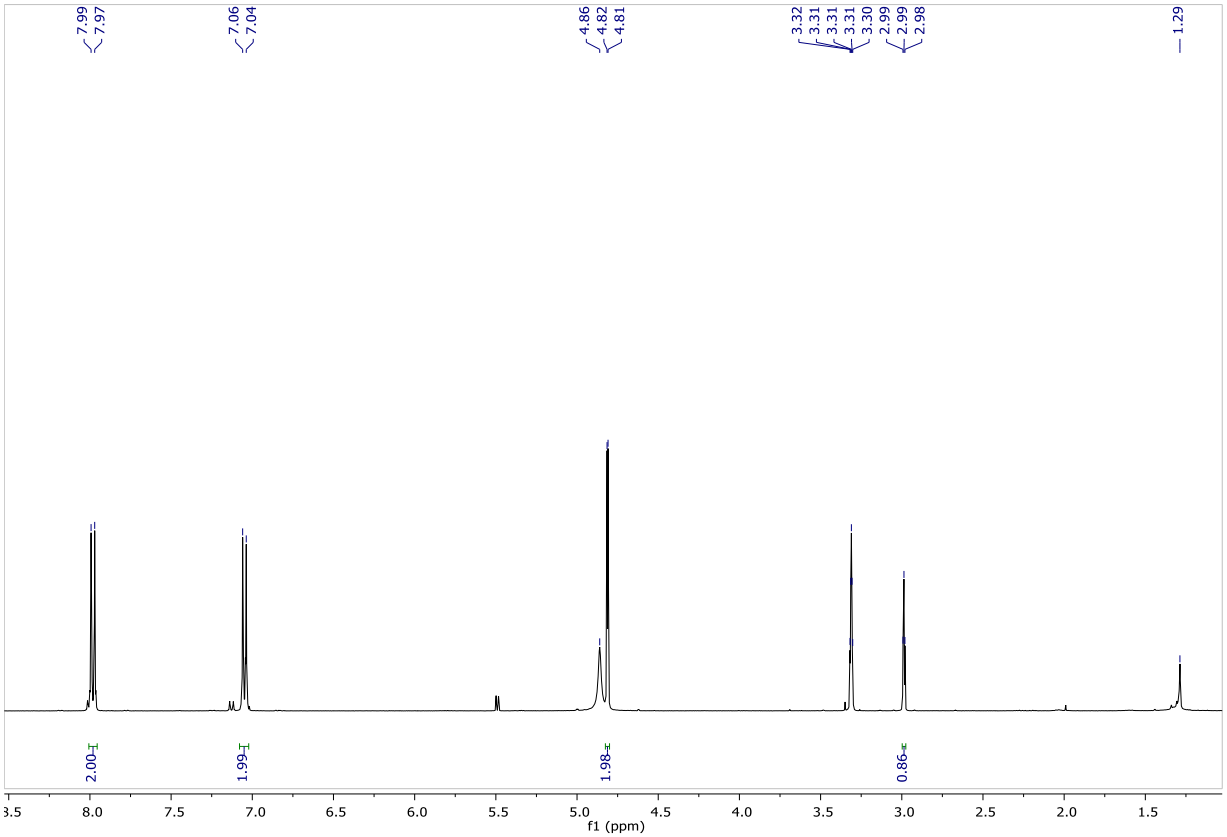

Aromatic alkyne-Val-Ala-PABC-*N*-(Boc)-*N*,*N*′-dimethylethylenediamine (118a)

^{1}H NMR (400 MHz, CD_2Cl_2-d_2)

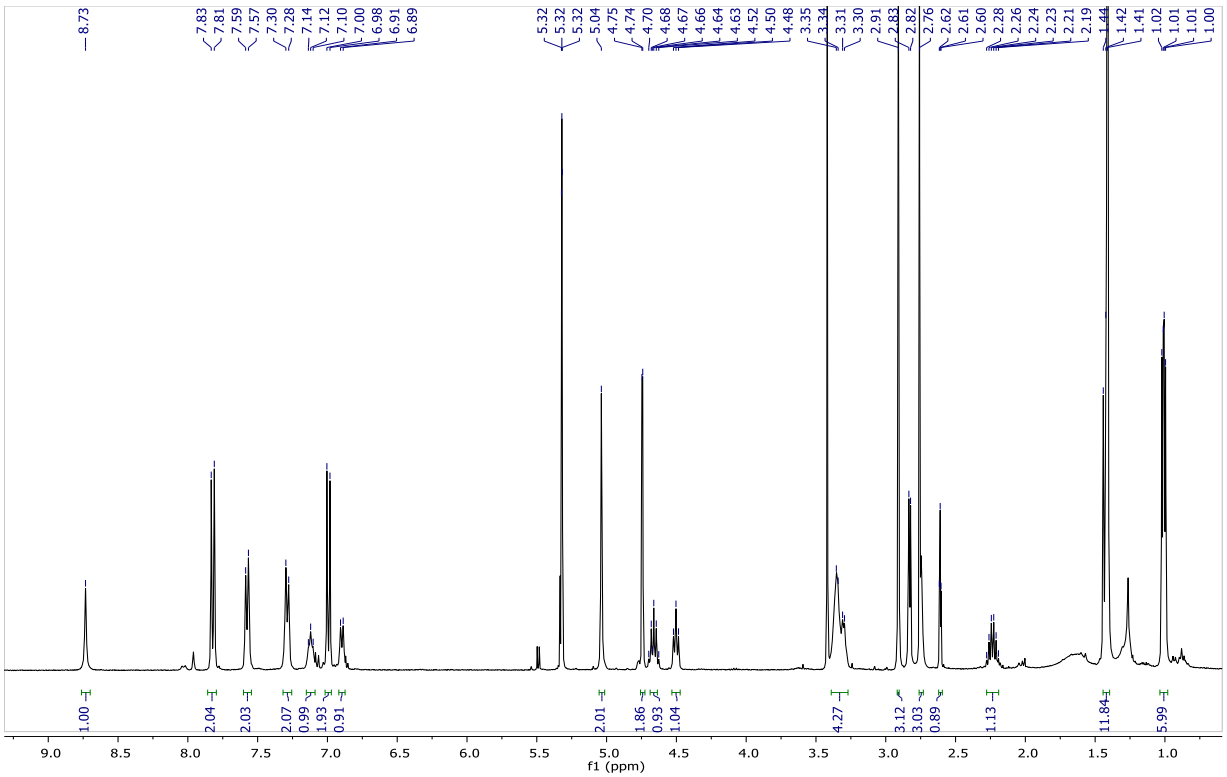

^{13}C NMR (101 MHz, CD_2Cl_2-d_2)

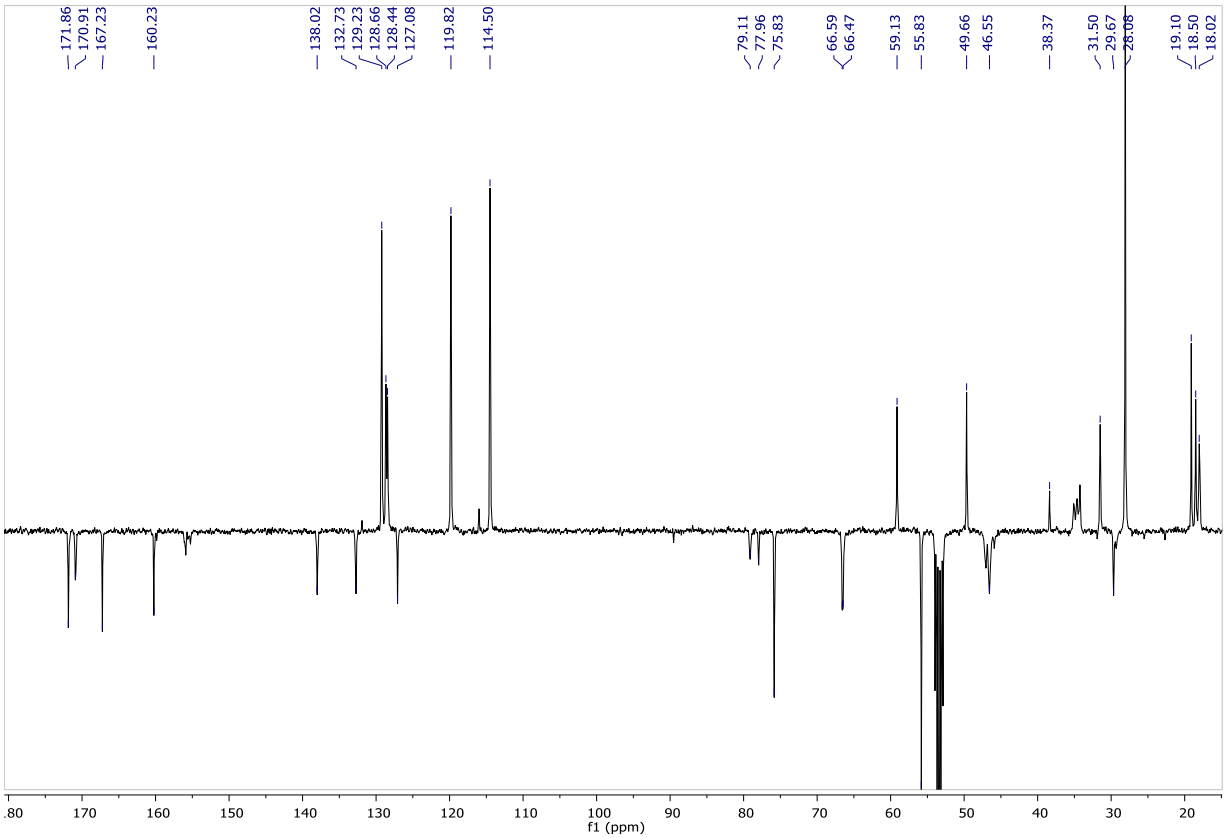

Methyl 3,5-bis(propynyloxy)phenyl acetate (111)

^{1}H NMR (400 MHz, $CDCl_3$)

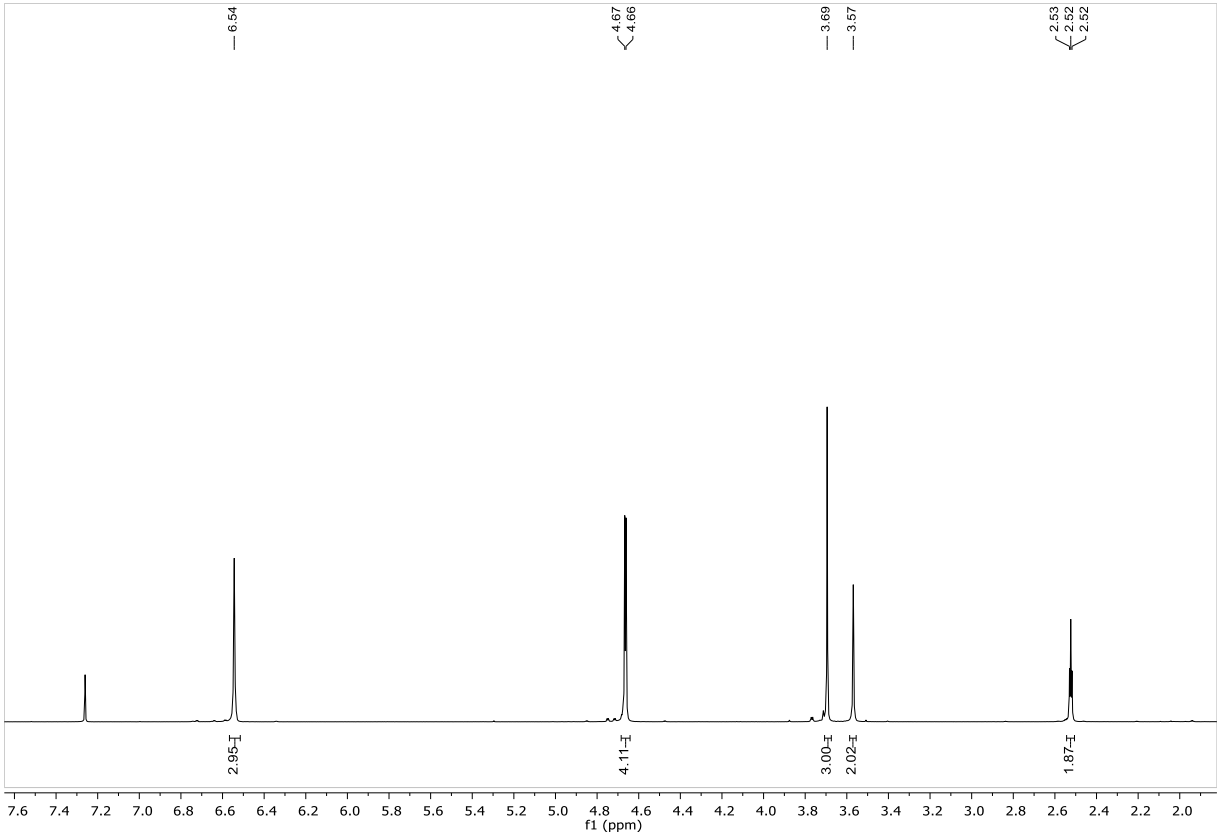

^{13}C NMR (101 MHz, $CDCl_3$)

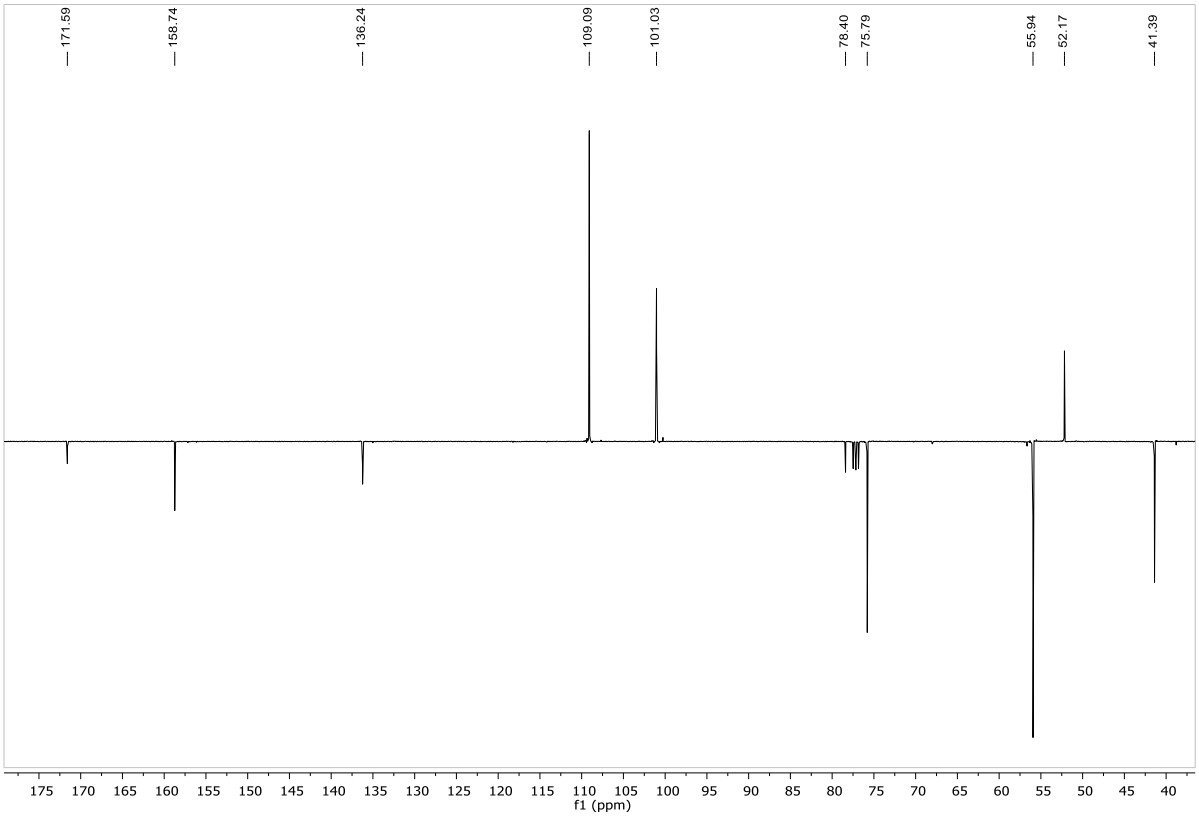

3,5-bis(Propynyloxy)phenyl acetic acid (88)

^{1}H NMR (400 MHz, CD_3OD)

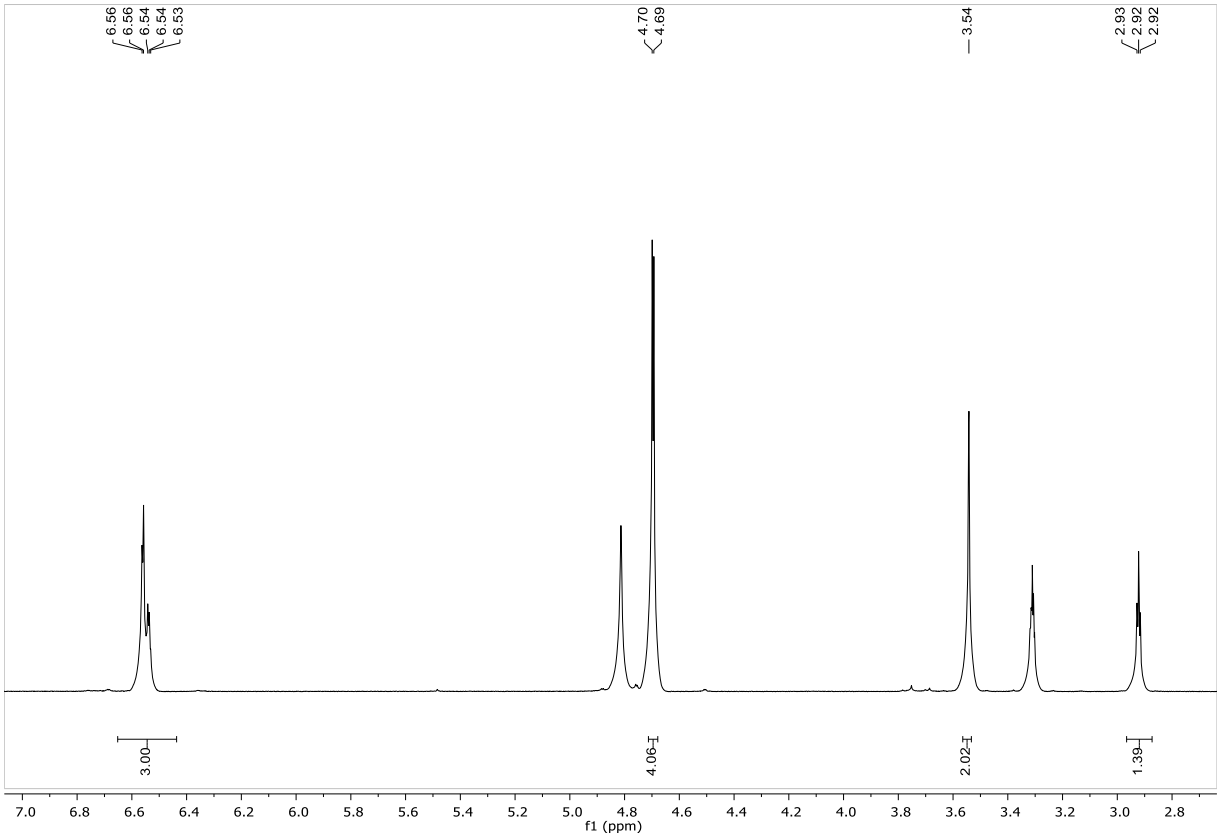

Bis-alkyne-Val-Ala-PABC-*N*-(Boc)-*N*,*N*′-dimethylethylenediamine (118b)

^{1}H NMR (400 MHz, CD_3OD + $[D]_6DMSO$)

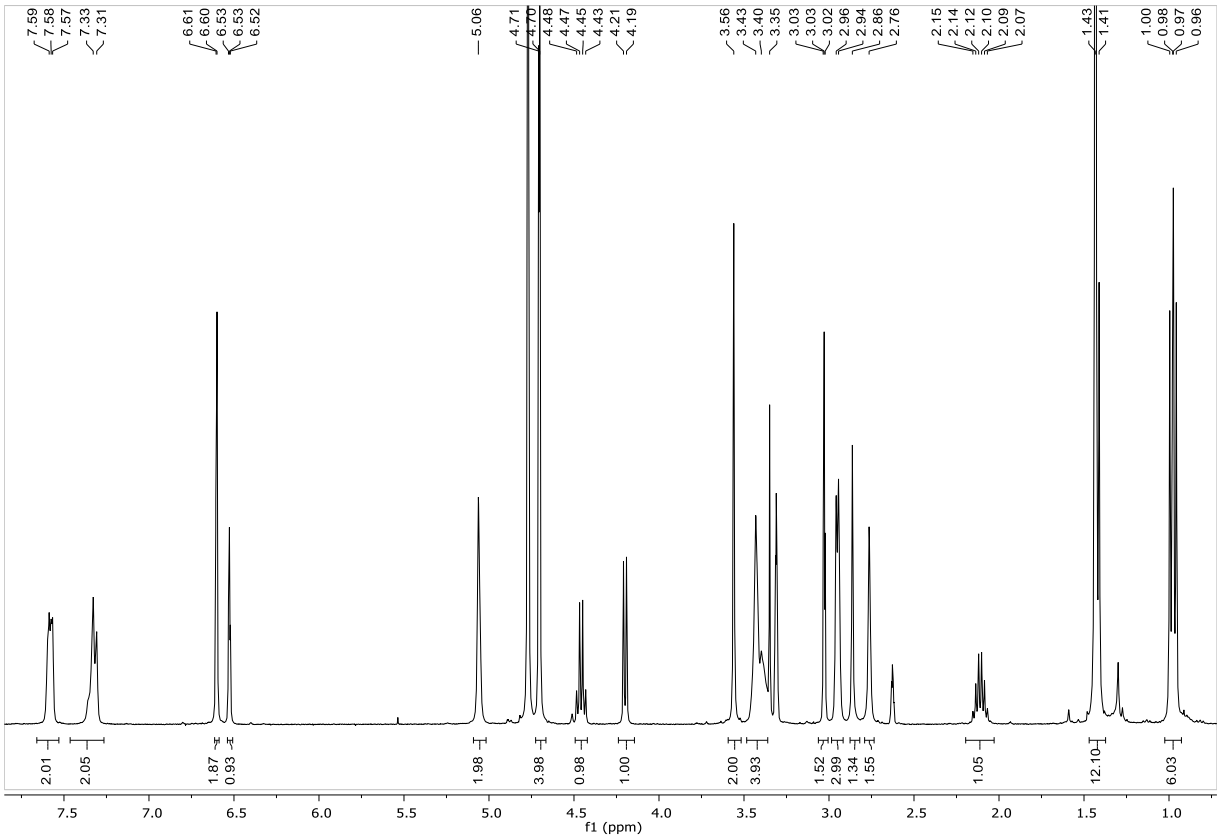

^{13}C NMR (101 MHz, CD_3OD + $[D]_6DMSO$)

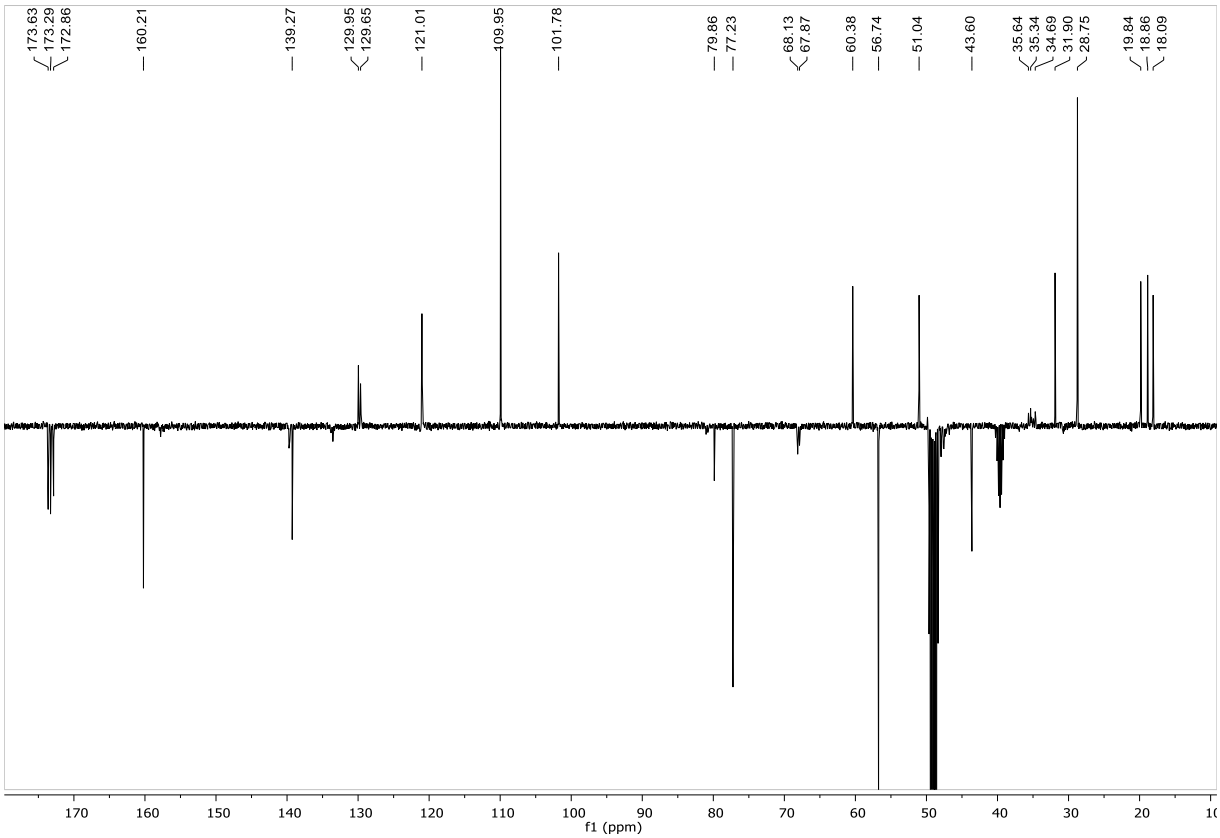

Methyl 2-(3,5-bis(2-((tert-butoxycarbonyl)amino)ethoxy)phenyl)acetate (112)

^{1}H NMR (400 MHz, $CDCl_3$)

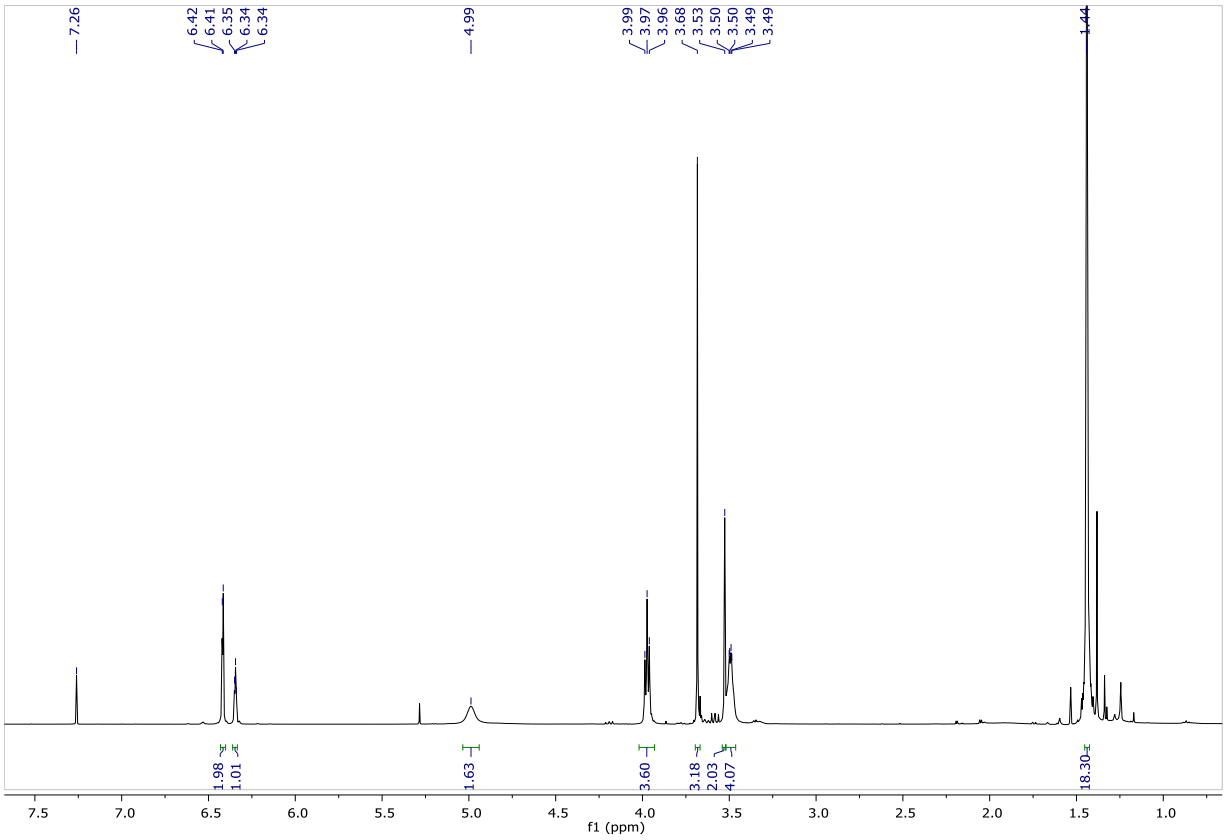

^{13}C NMR (101 MHz, $CDCl_3$)

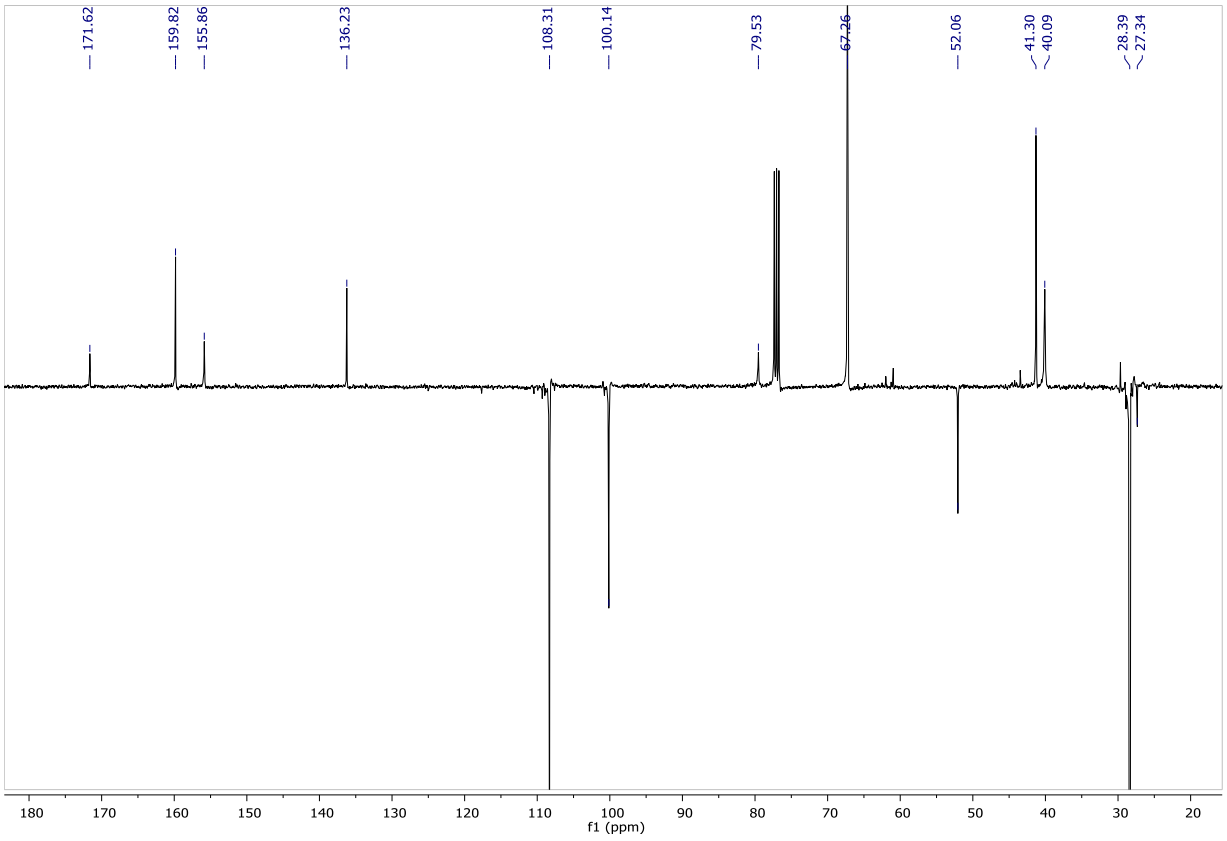

Methyl 2-(3-(2-(2-(3,5-bis(prop-2-yn-1-yloxy)phenyl)acetamido)ethoxy)-5-(2-(4-(prop-2-yn-1-yloxy)benzamido)ethoxy)phenyl)acetate (116)

^{1}H NMR (600 MHz, CD_2Cl_2-d_2)

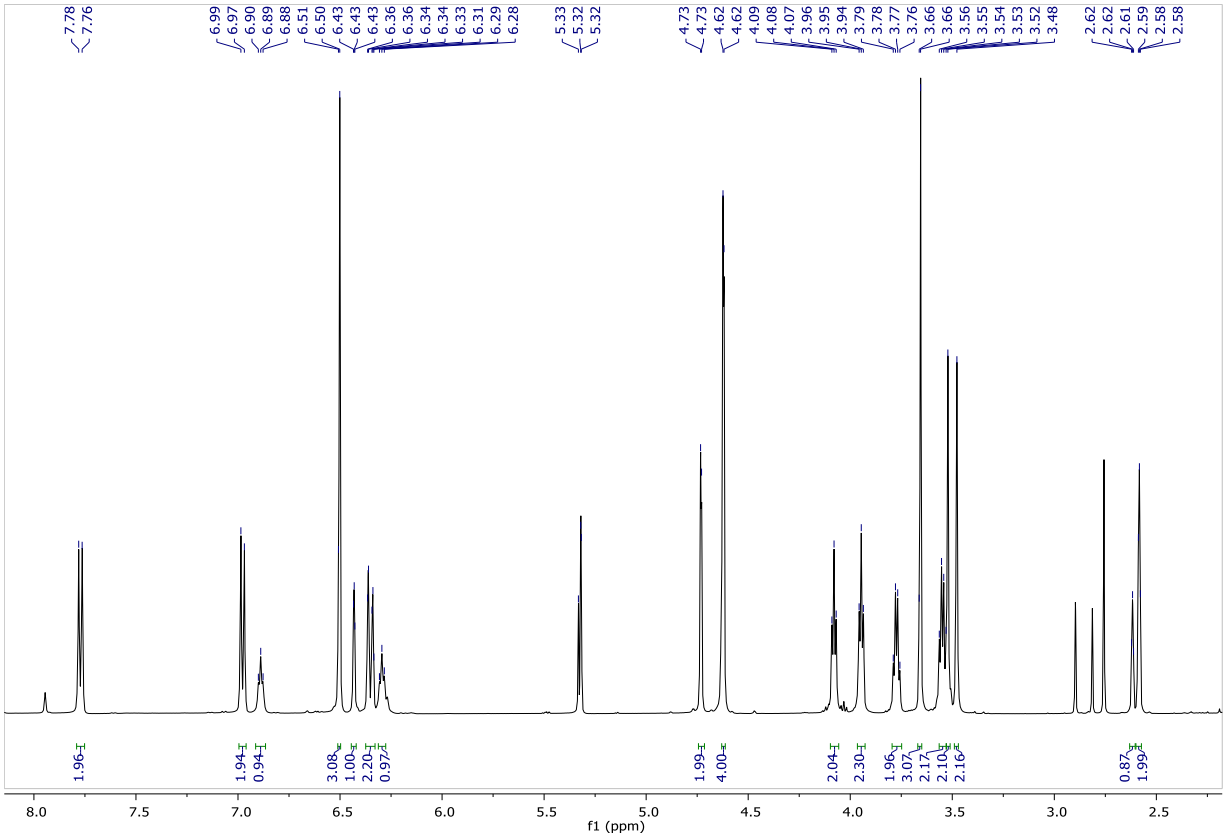

^{13}C NMR (151 MHz, CD_2Cl_2-d_2)

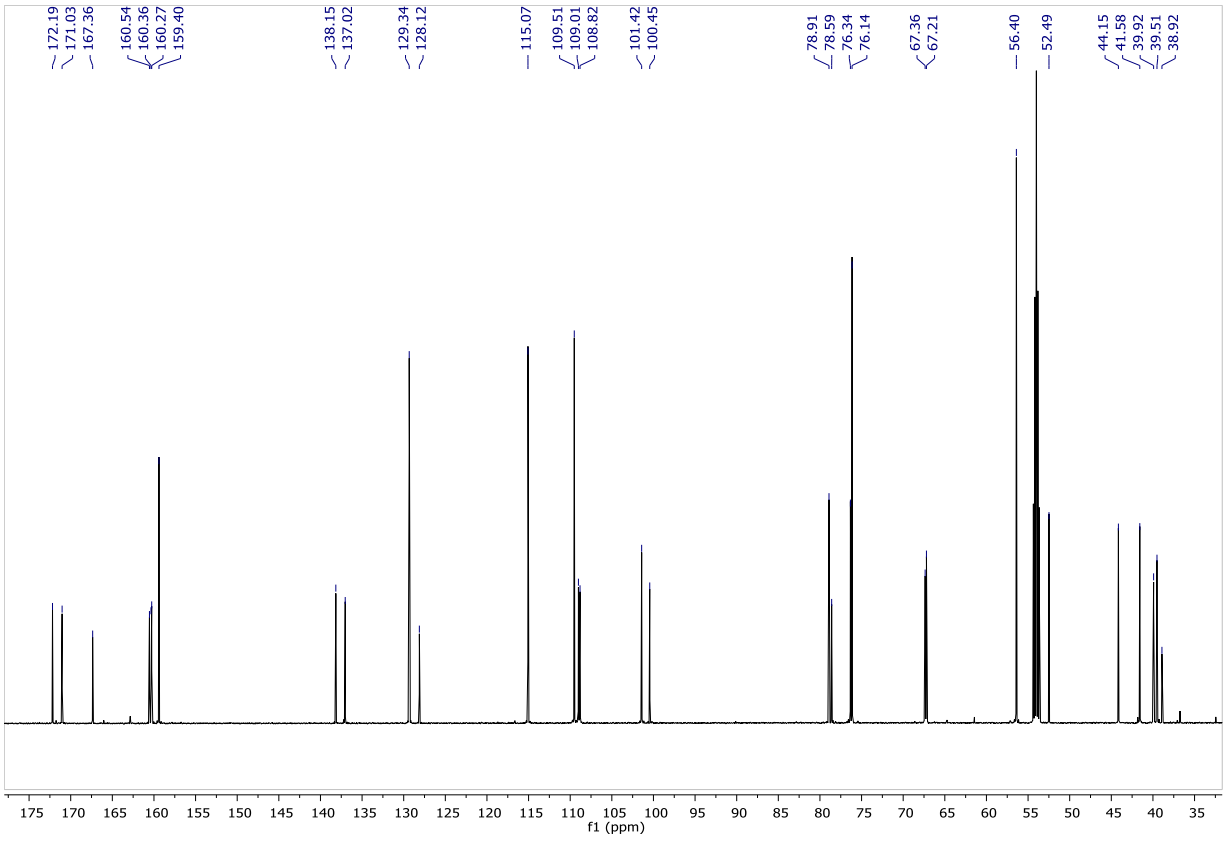

2-(3-(2-(2-(3,5-bis(Prop-2-yn-1-yloxy)phenyl)acetamido)ethoxy)-5-(2-(4-(prop-2-yn-1-yloxy)benzamido)ethoxy)phenyl)acetic acid (89)

^{1}H NMR (500 MHz, CD_3OD)

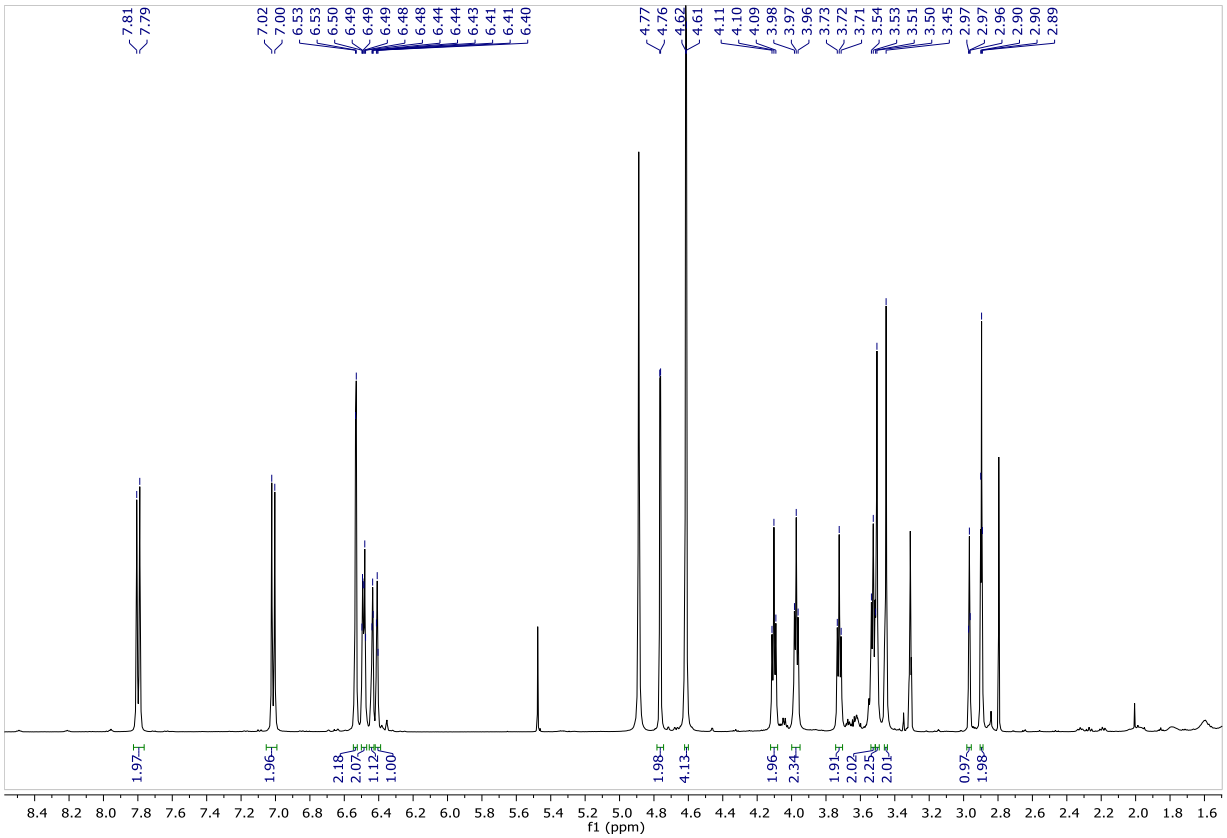

NMR (126 MHz, CD_3OD), ^{13}C-DEPT135

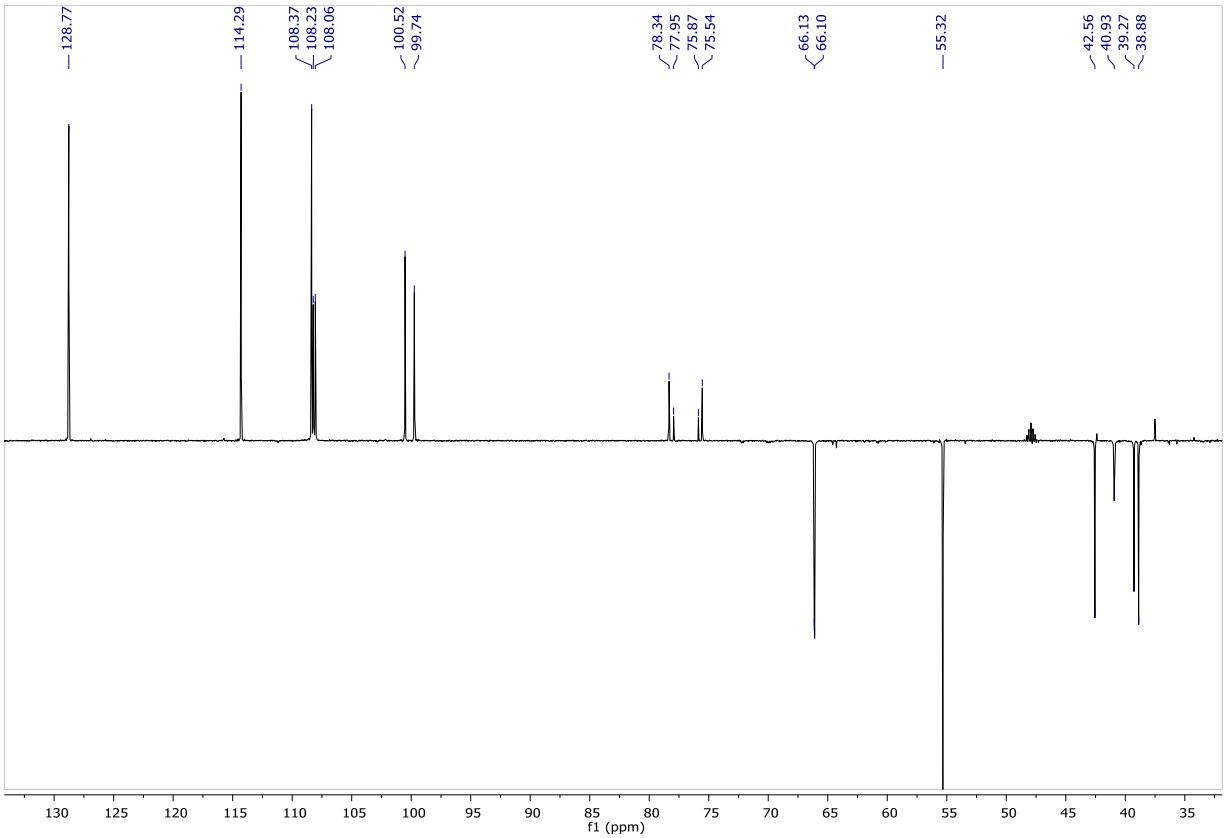

Tris-alkyne-Val-Ala-PABC-*N*-(Boc)-*N*,*N*'-dimethylethylenediamine (118c)

^{1}H NMR (400 MHz, [D]$_6$DMSO)

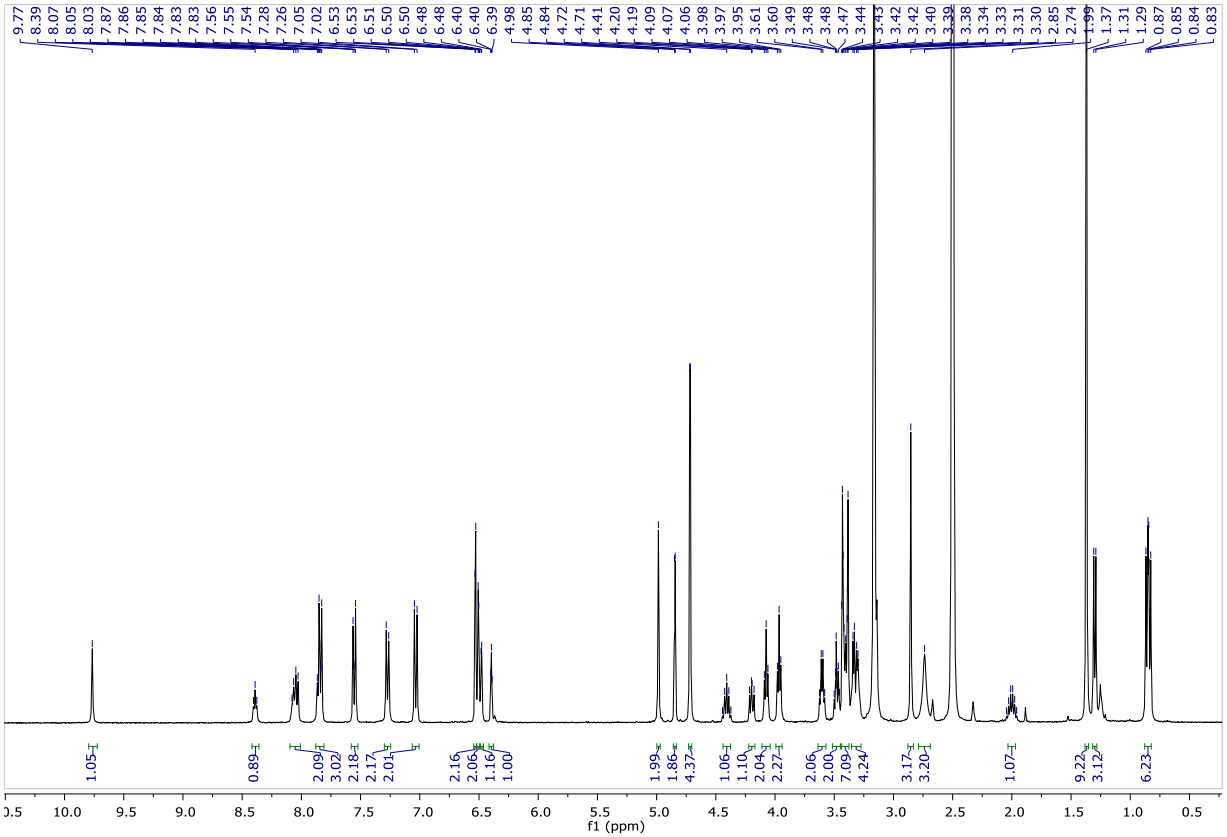

^{13}C NMR (101 MHz, [D]$_6$DMSO)

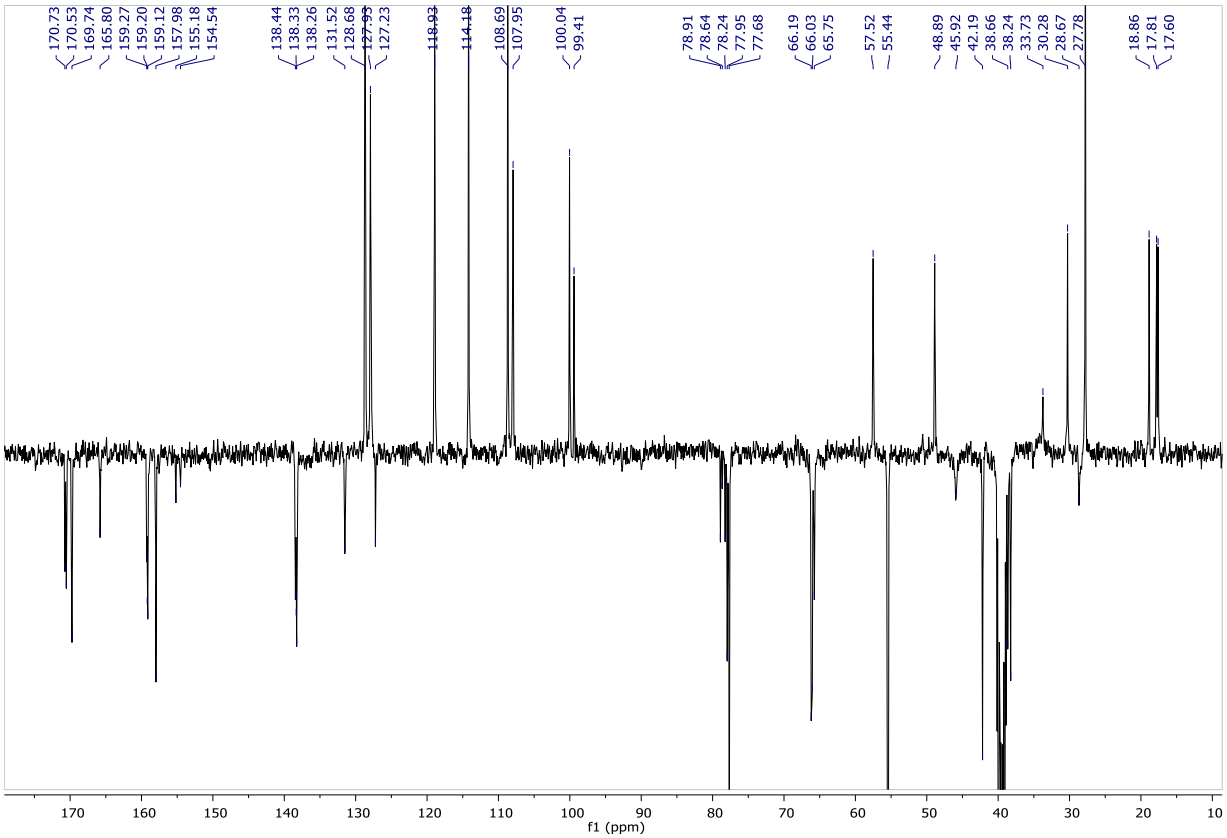

Methyl 2-(3,5-bis(2-(2-(3,5-bis(prop-2-yn-1-yloxy)phenyl)acetamido)ethoxy)phenyl) acetate (117)

^{1}H NMR (400 MHz, CD_2Cl_2-d_2)

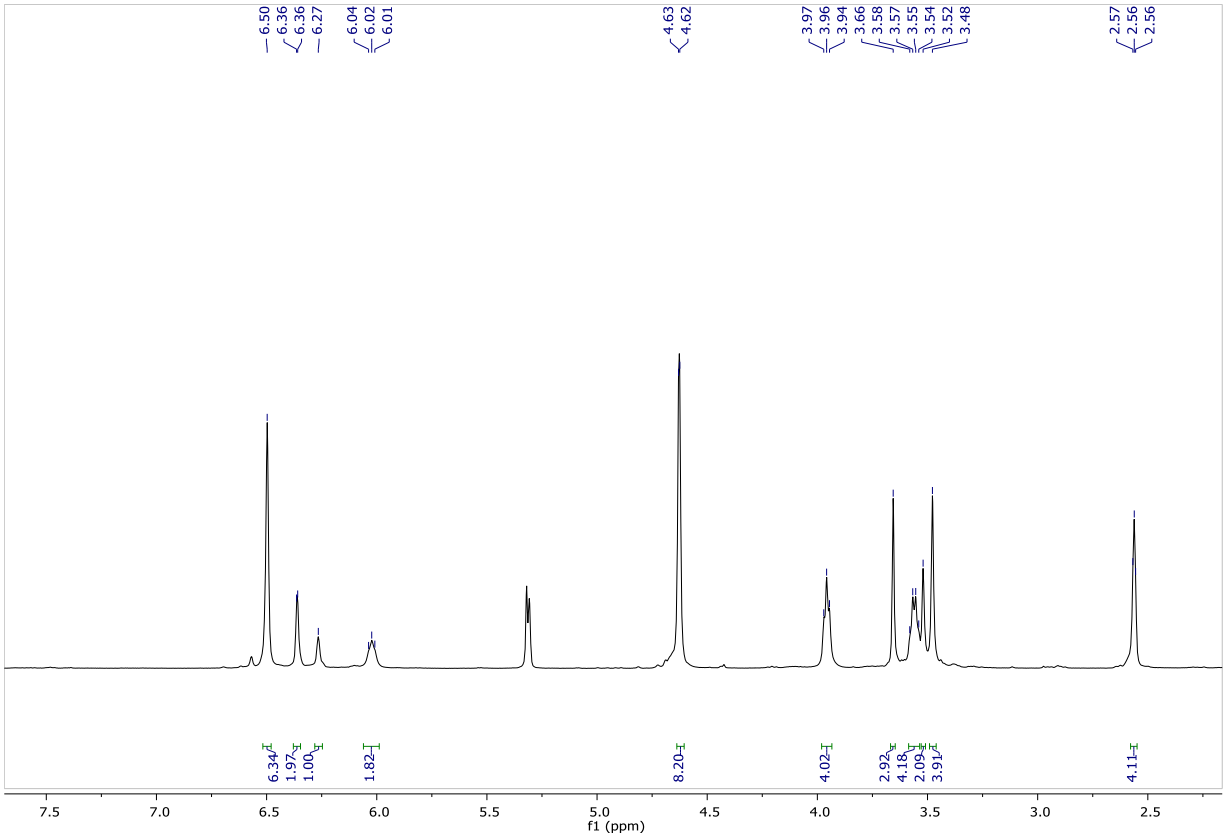

^{13}C NMR (101 MHz, CD_2Cl_2-d_2)

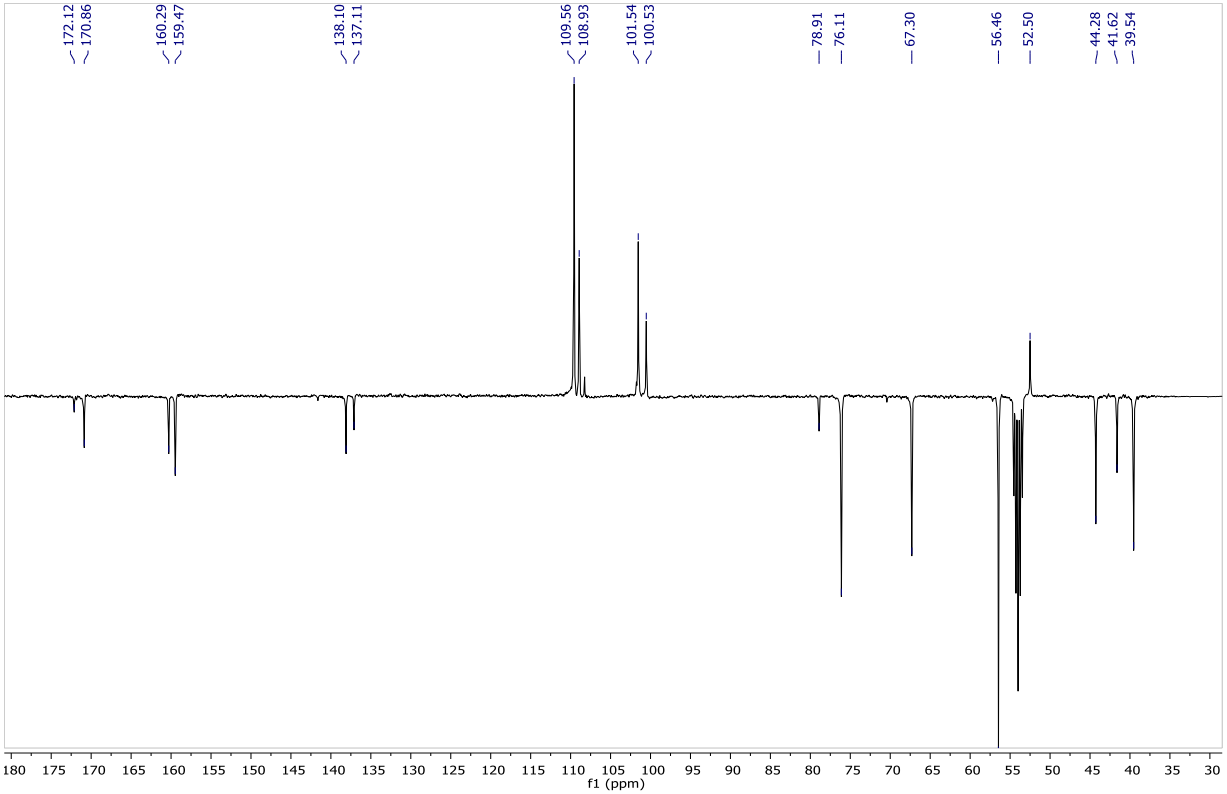

2-(3,5-bis(2-(2-(3,5-bis(Prop-2-yn-1-yloxy)phenyl)acetamido)ethoxy)phenyl)acetic acid (90)

^{1}H NMR (400 MHz, CD_3OD)

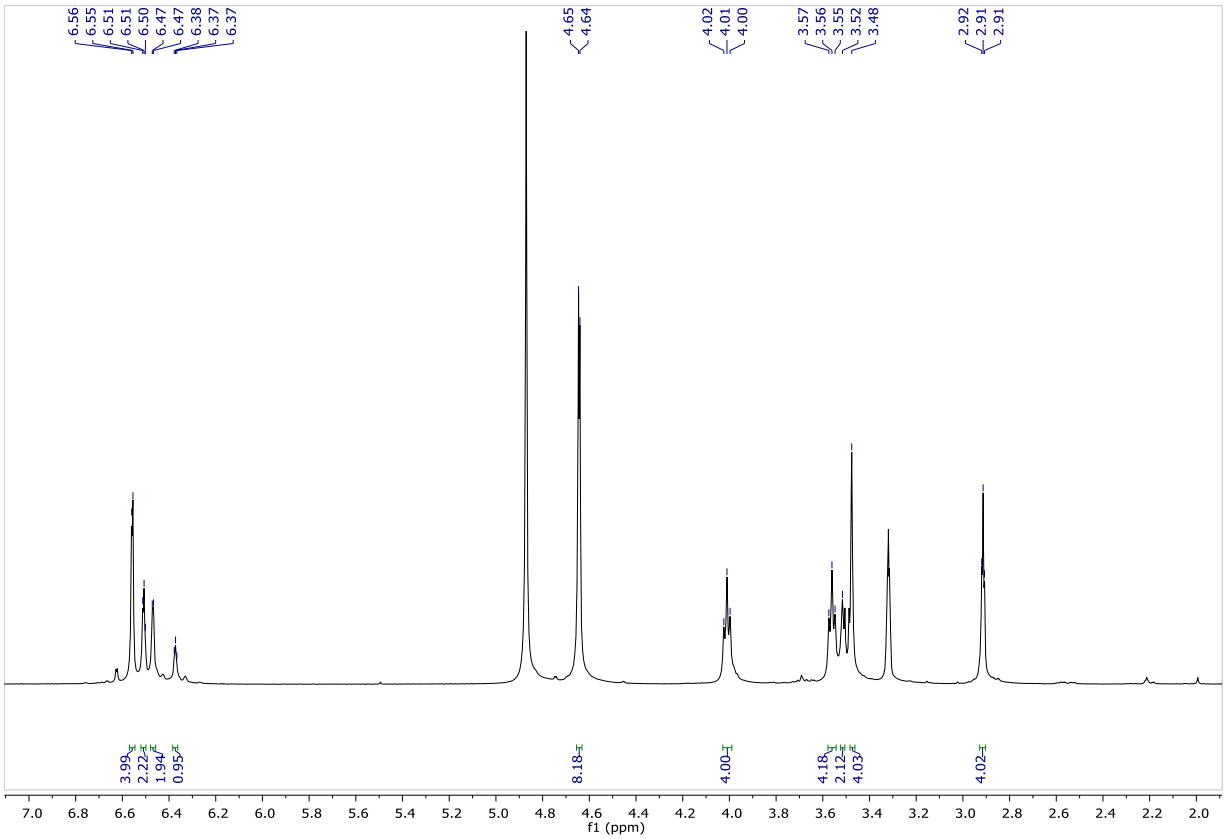

^{13}C NMR (101 MHz, CD_3OD)

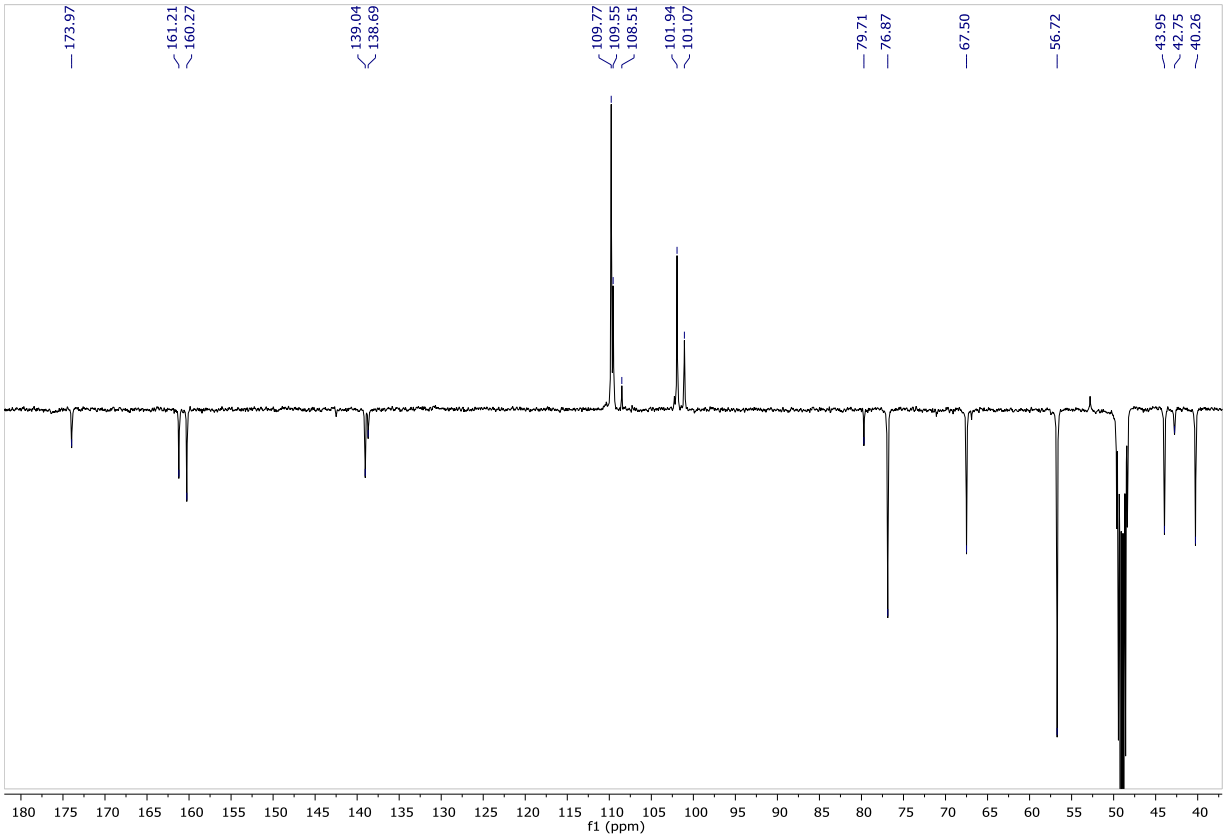

Tetra-alkyne-Val-Ala-PABC-*N*-(Boc)-*N*,*N*′-dimethylethylenediamine (118d)

^{1}H NMR (400 MHz, [D]$_6$DMSO)

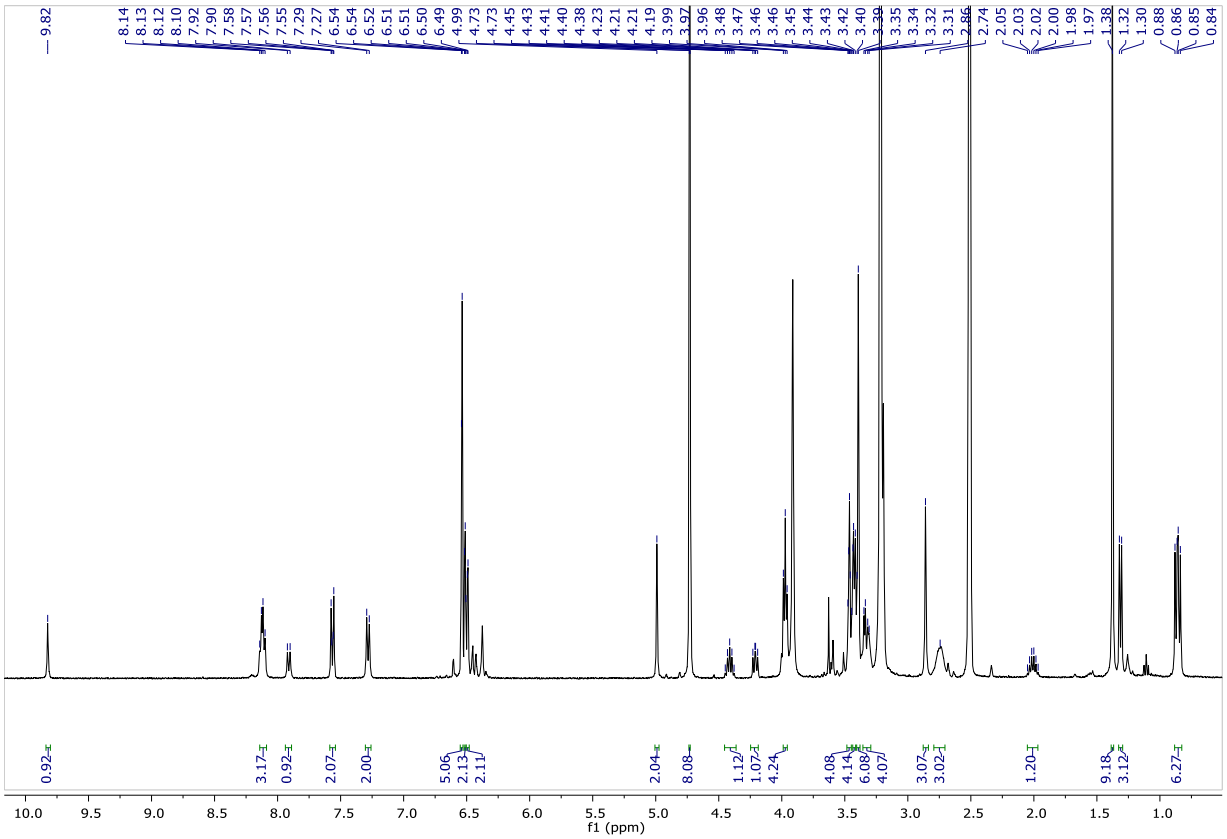

^{13}C NMR (101 MHz, [D]$_6$DMSO)

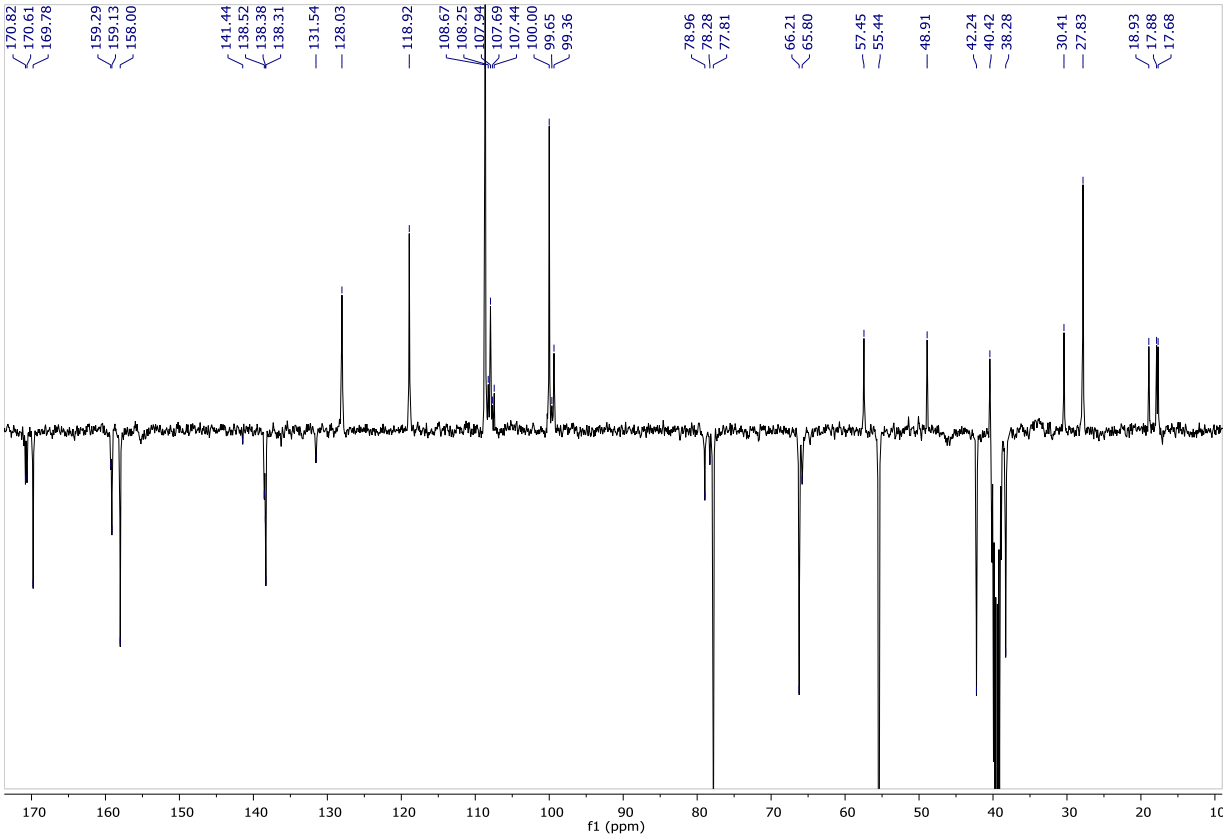

Fmoc-Asn(Trt)-Pro-OH (126)

^{1}H NMR (500 MHz, CD_2Cl_2-d_2)

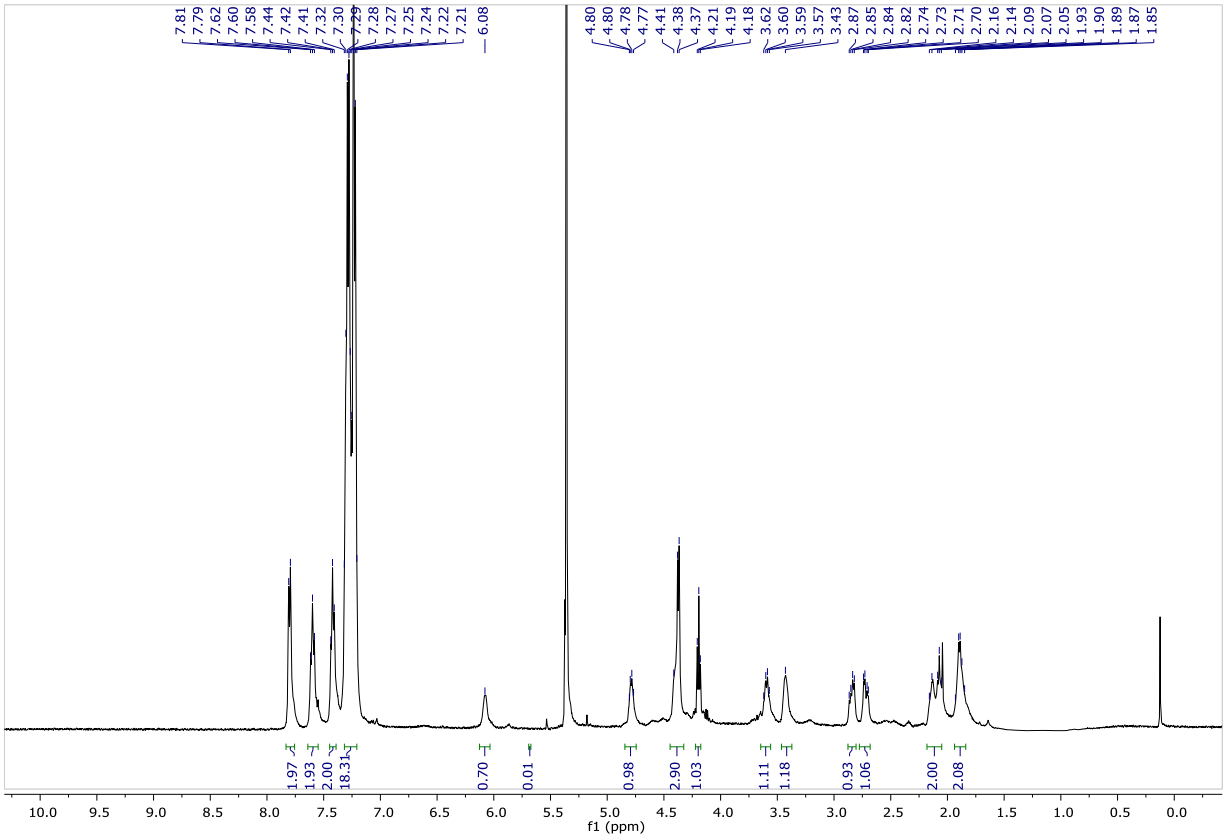

Fmoc-Asn(Trt)-Pro-Val-OH (127)

^{1}H NMR (500 MHz, CD_2Cl_2-d_2)

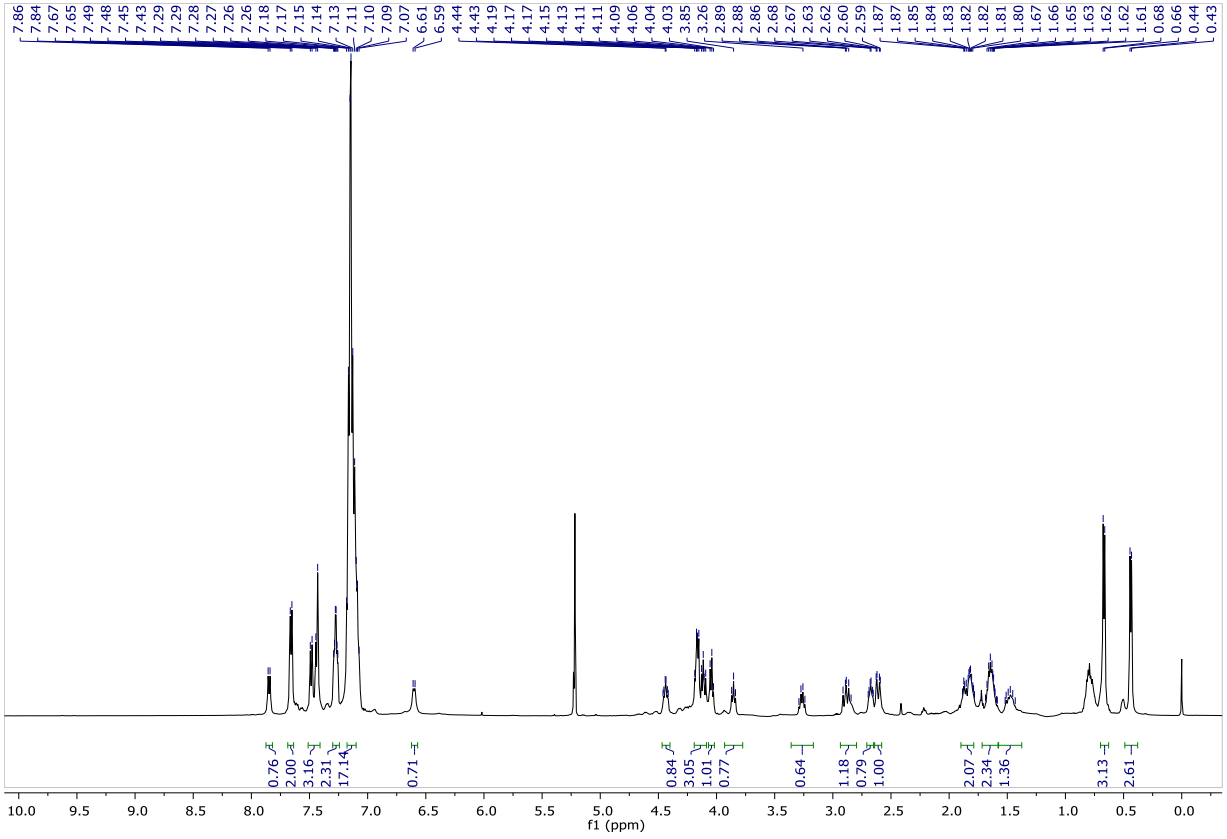

^{13}C-DEPT45 NMR (126 MHz, CD_2Cl_2-d_2)

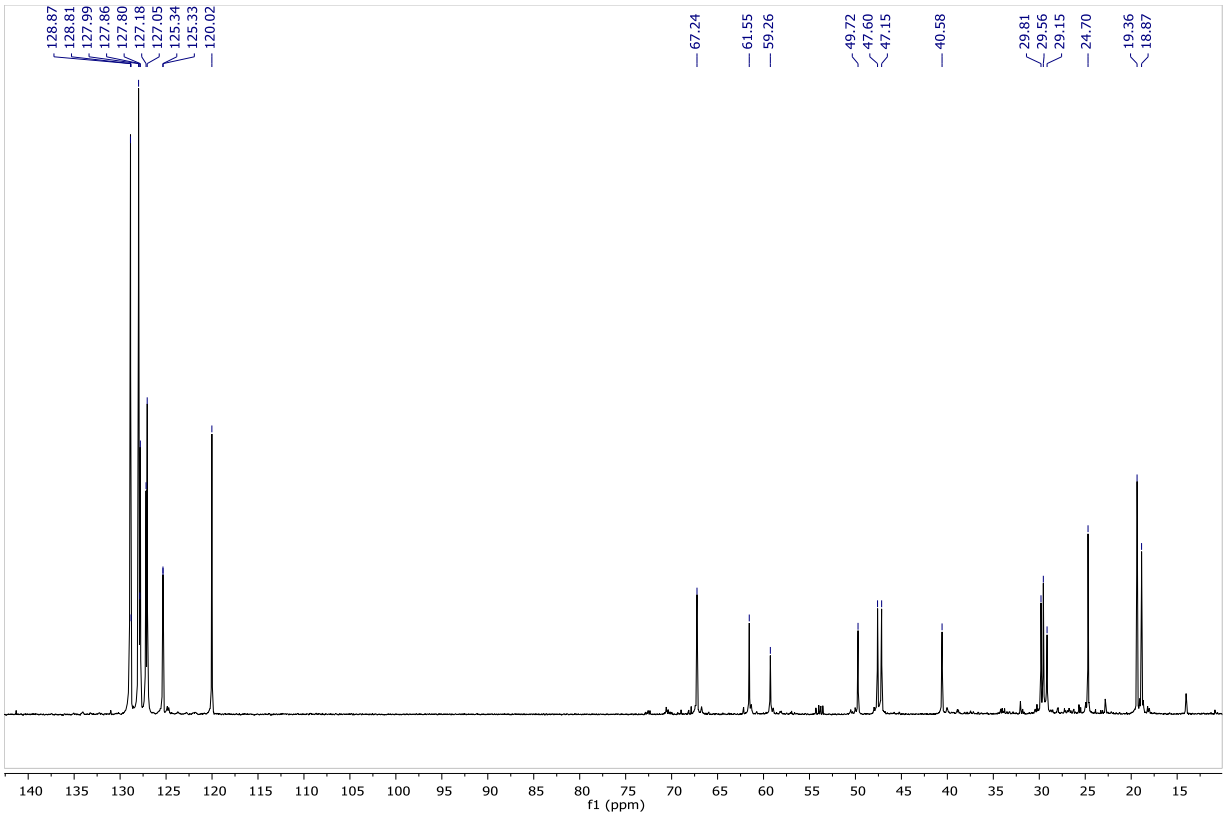

Fmoc-Asn(Trt)-Pro-Val-PABC-PNP (128)

^{1}H NMR (500 MHz, CD_2Cl_2-d_2)

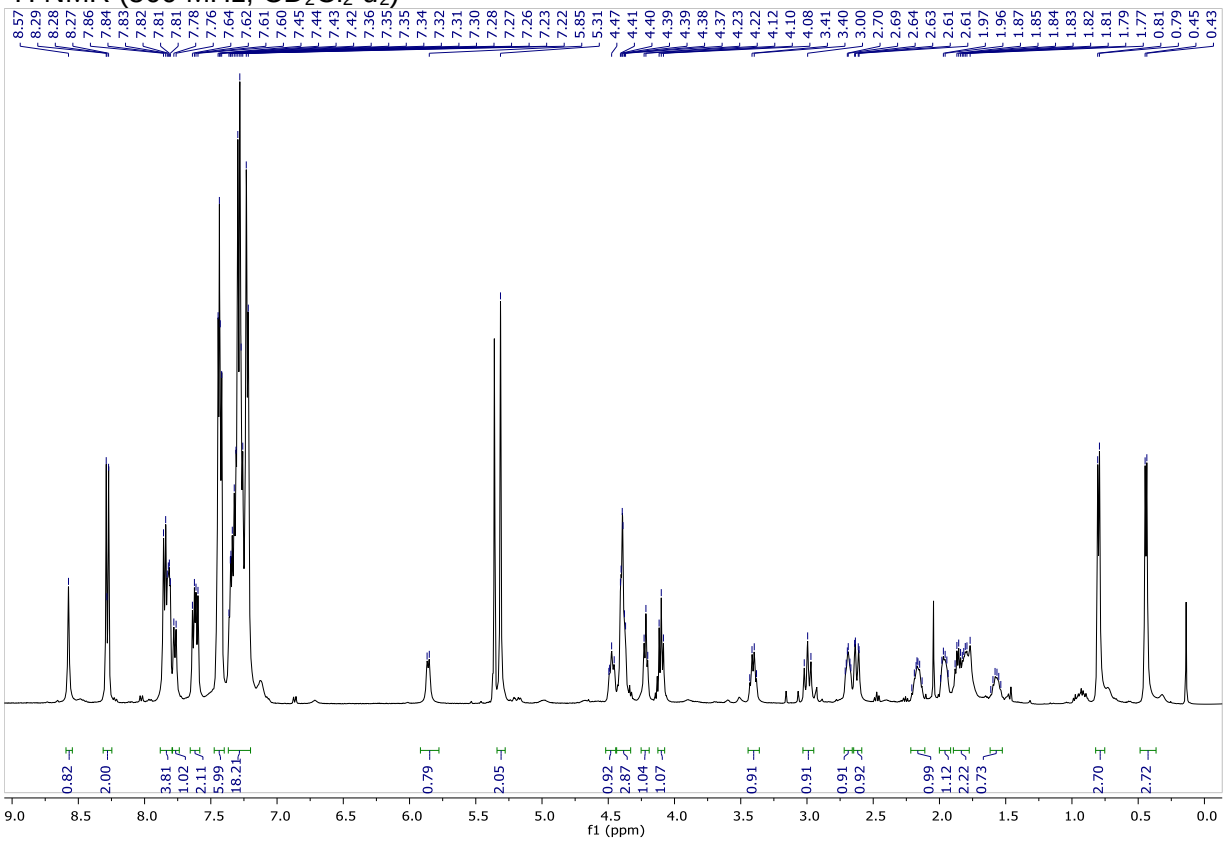

^{13}C-APT NMR (126 MHz, CD_2Cl_2-d_2)

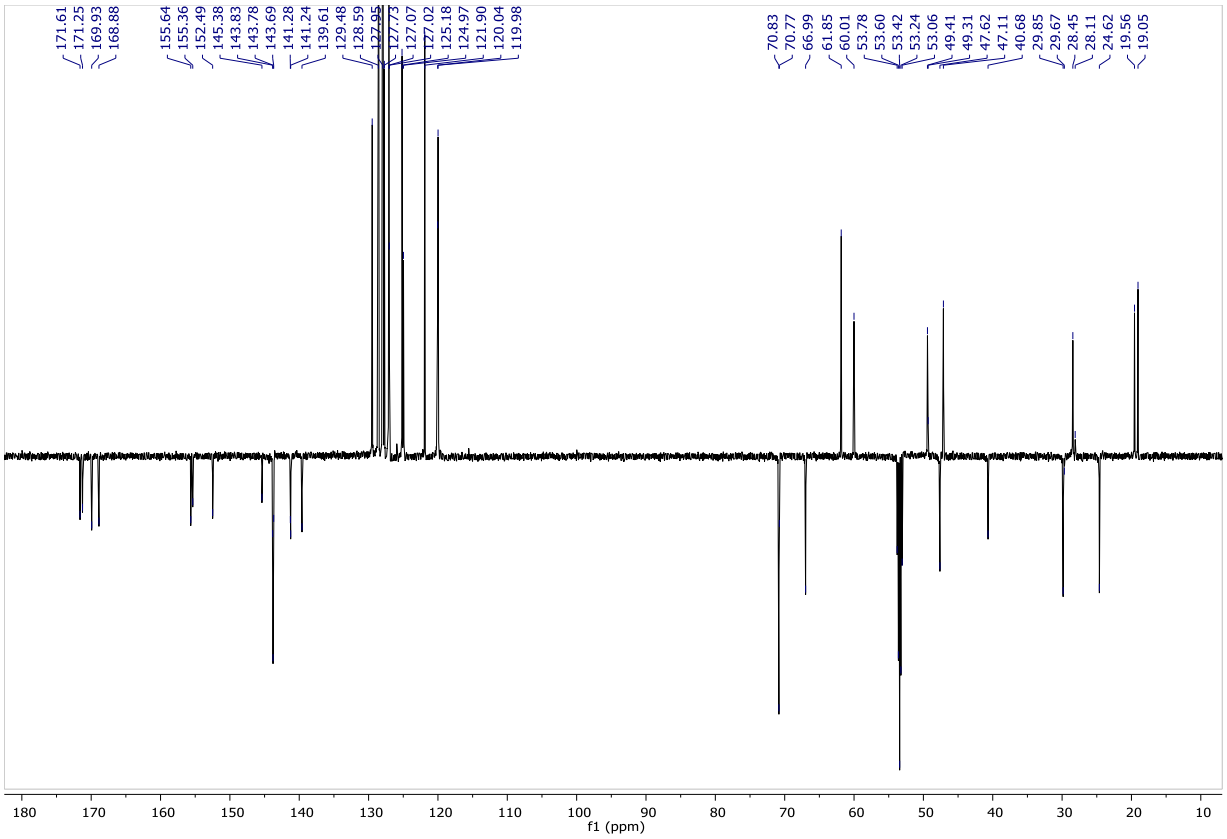

Fmoc-Asn(Trt)-Pro-Val-PABC-*N*-(Boc)-*N*,*N*′-dimethylethylenediamine (129)

^{1}H NMR (500 MHz, CD_2Cl_2-d_2)

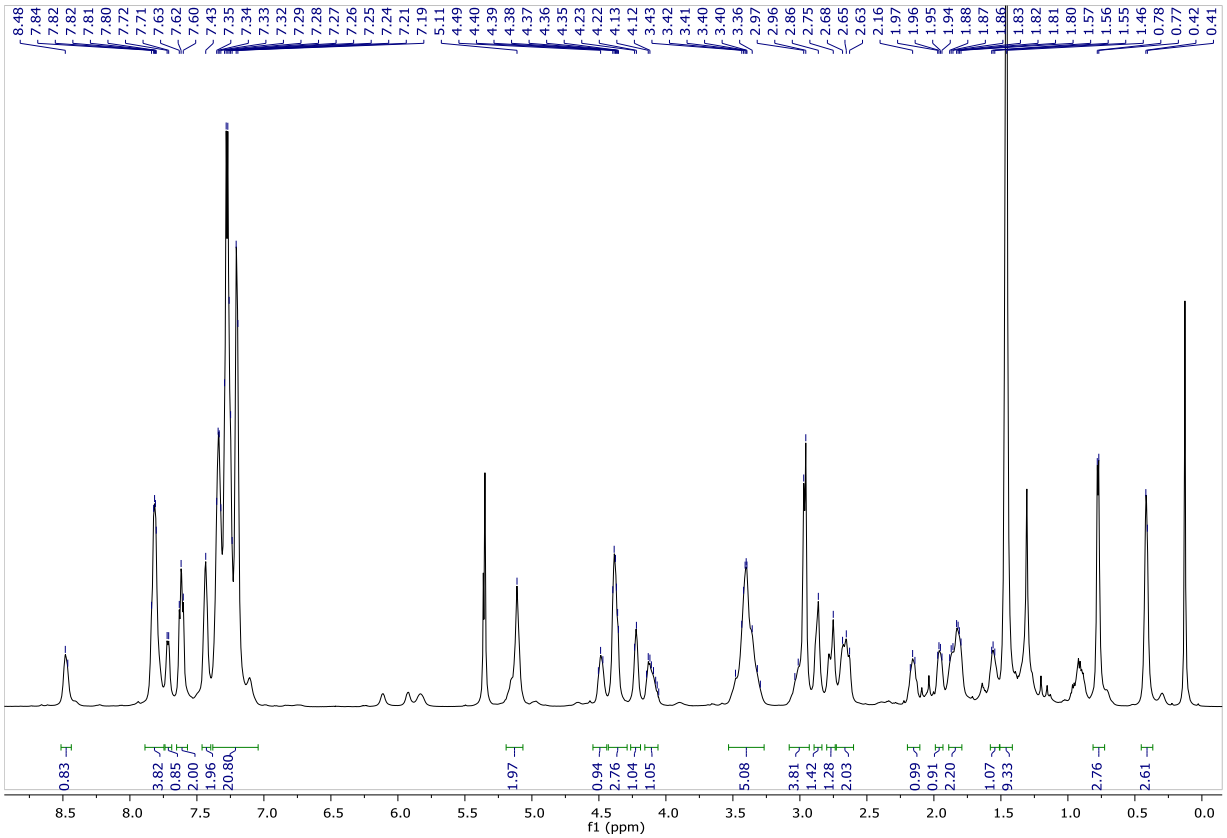

^{13}C-APT NMR (126 MHz, CD_2Cl_2-d_2)

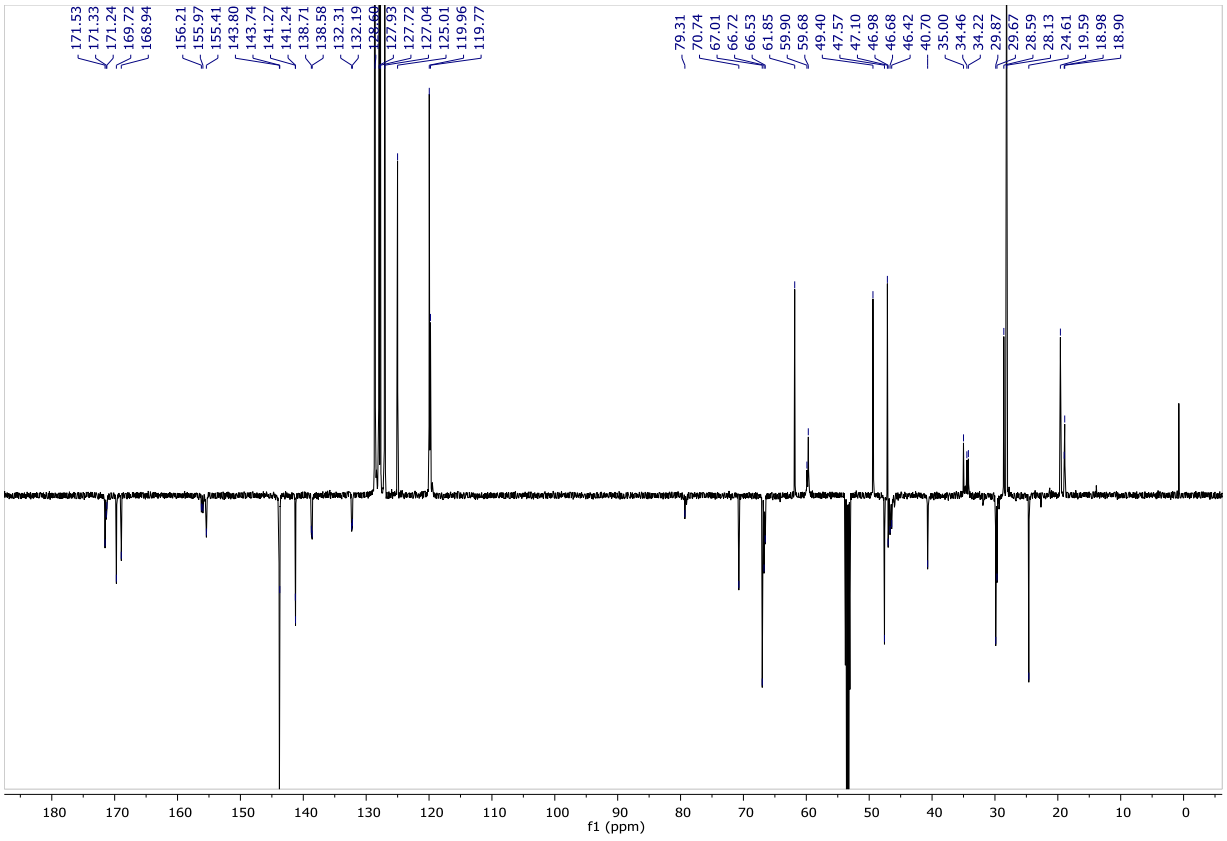

4-pentynamido-Asn(Trt)-Pro-Val-PABC-*N*-(Boc)-*N*,*N*′-dimethylethylenediamine (130)

^{1}H NMR (500 MHz, CD_2Cl_2-d_2)

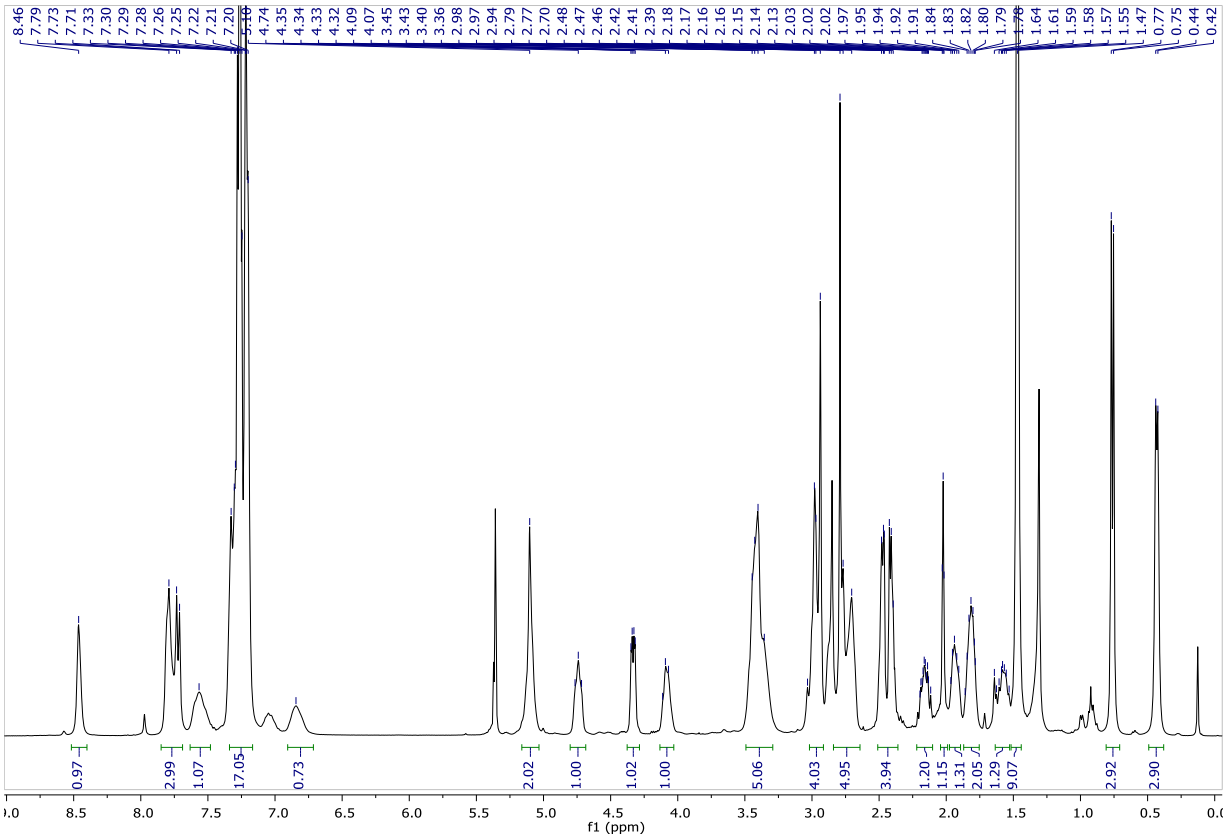

^{13}C-APT NMR (126 MHz, CD_2Cl_2-d_2)

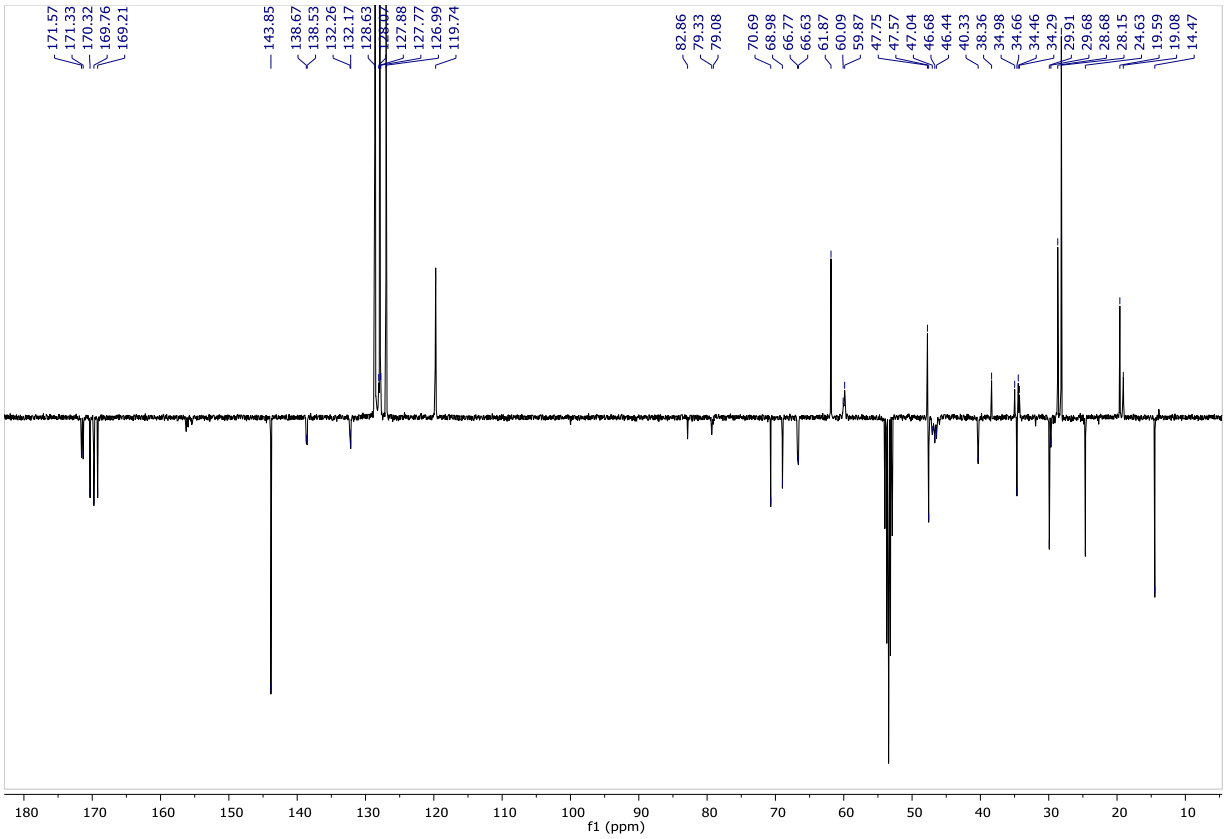

Fmoc-[D]-Val-PABA (132)

^{1}H NMR (400 MHz, MeOD-d_4)

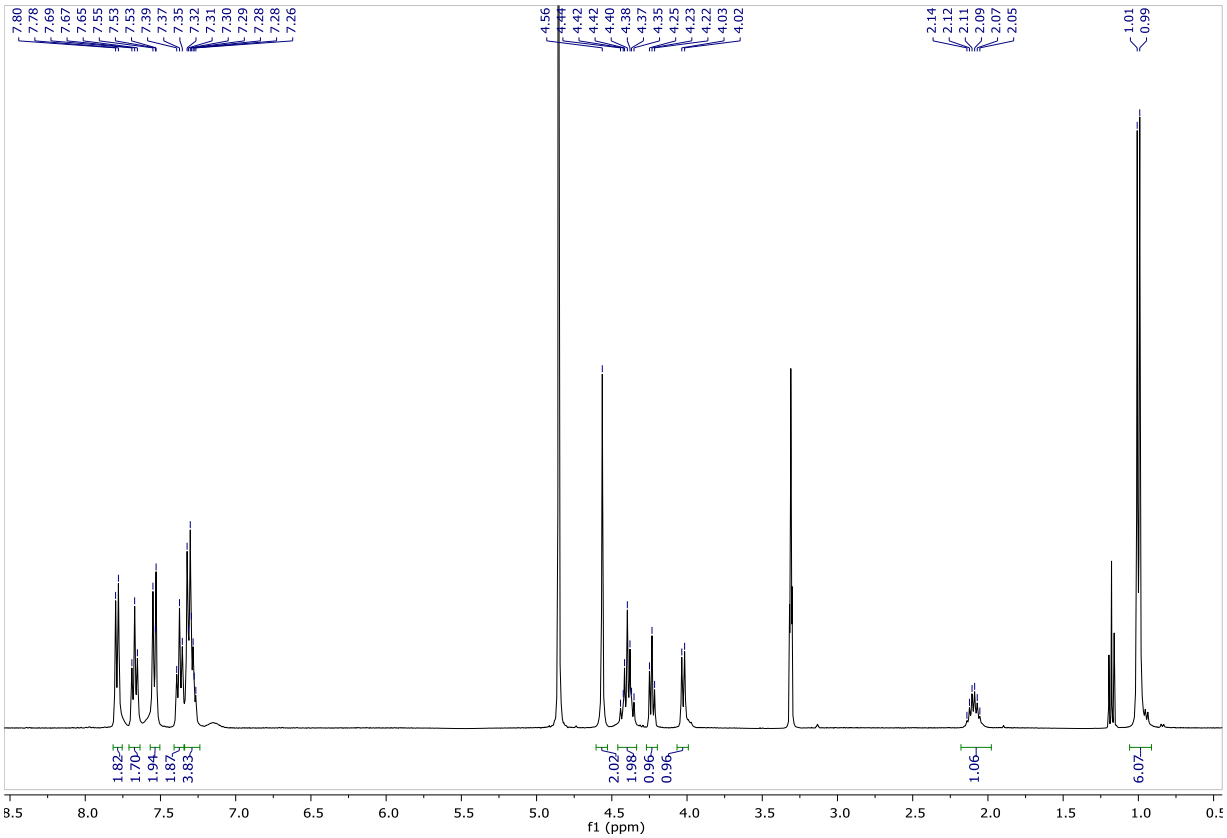

Fmoc-Asn(Trt)-Pro-[D]-Val-PABC-PNP (135)

^{1}H NMR (400 MHz, CD_2Cl_2-d_2)

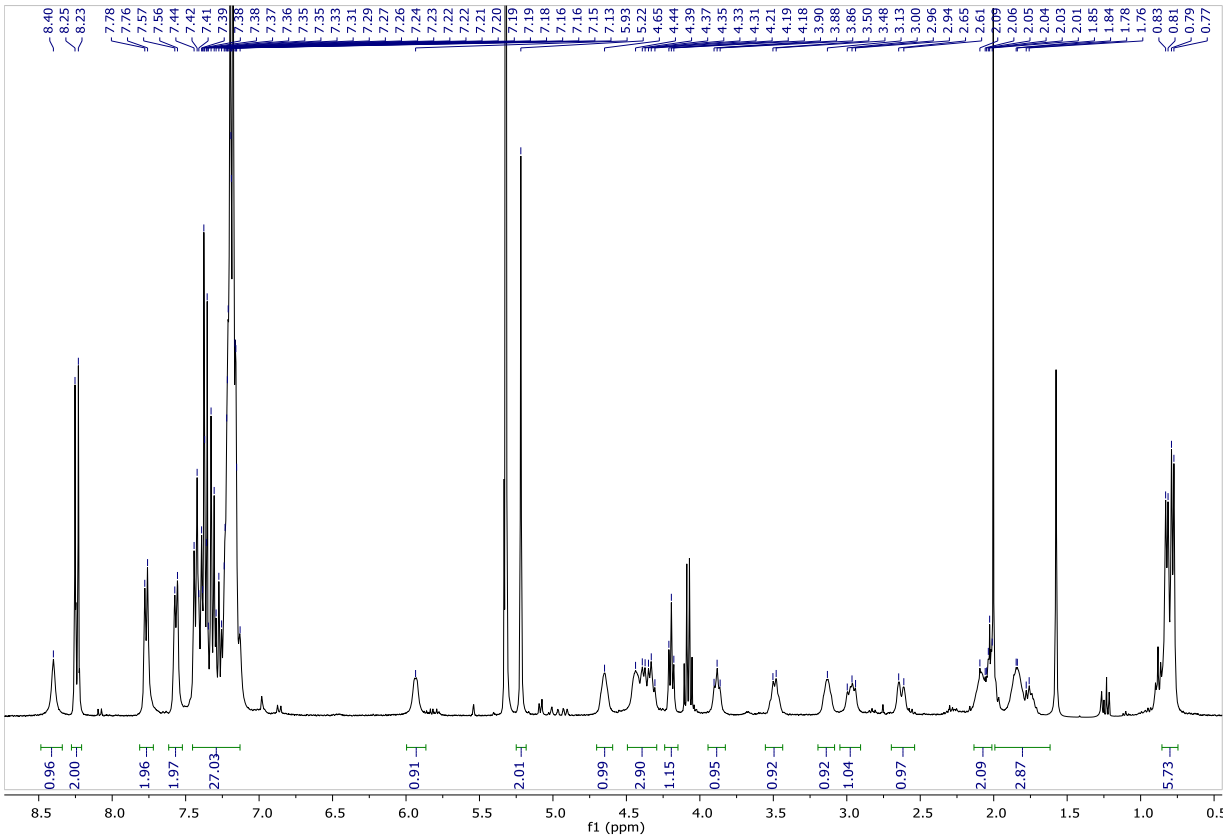

^{13}C-APT NMR (101 MHz, CD_2Cl_2-d_2)

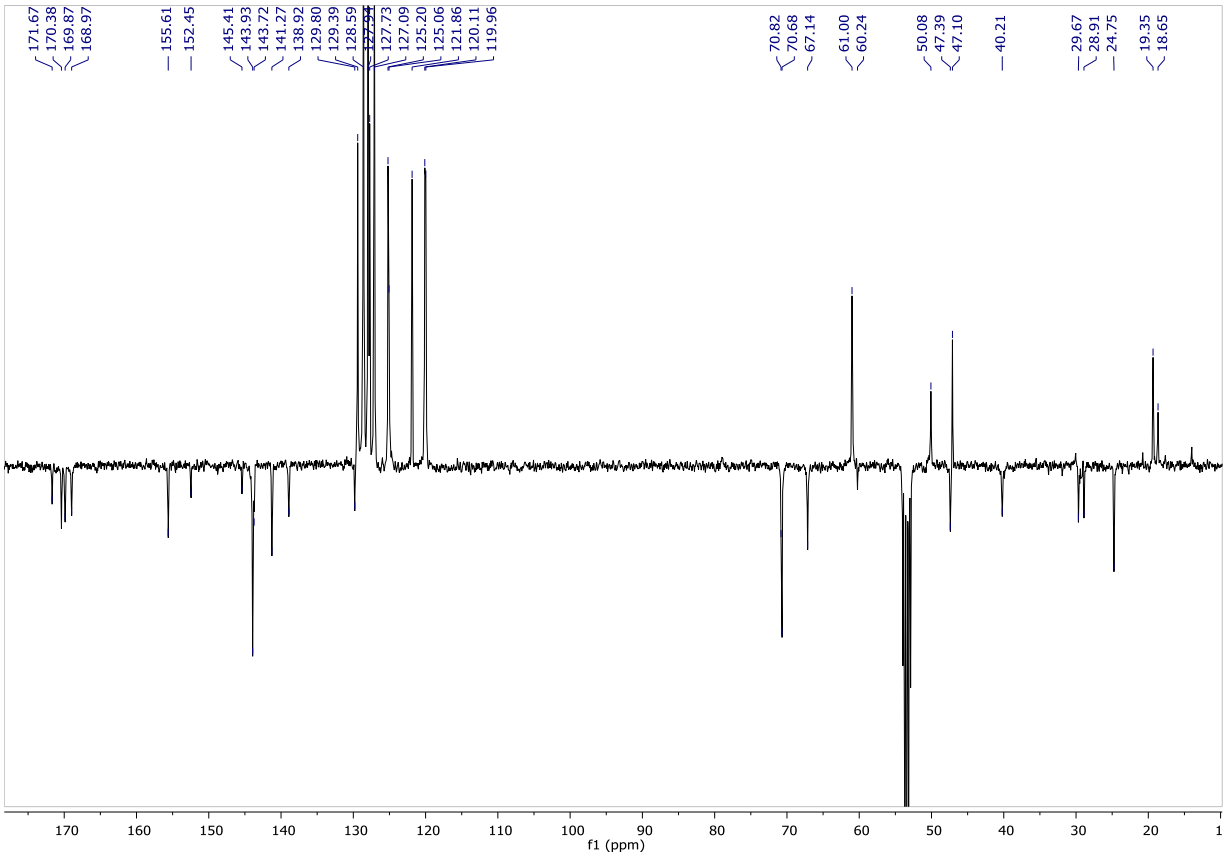

Fmoc-Asn(Trt)-Pro-[D]-Val-PABC-*N*-(Boc)-*N*,*N*'-dimethylethylenediamine (136)

^{1}H NMR (400 MHz, MeOD-d_4)

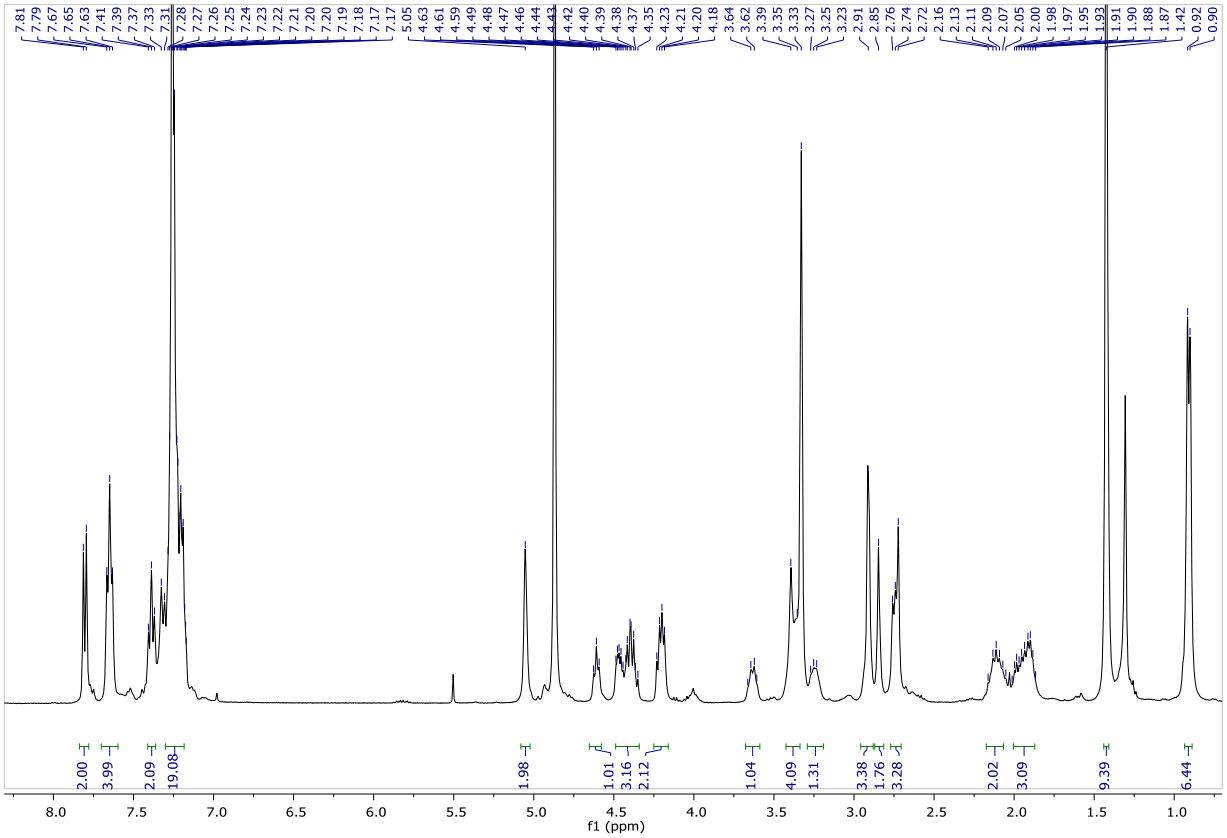

^{13}C-APT NMR (101 MHz, MeOD-d_4)

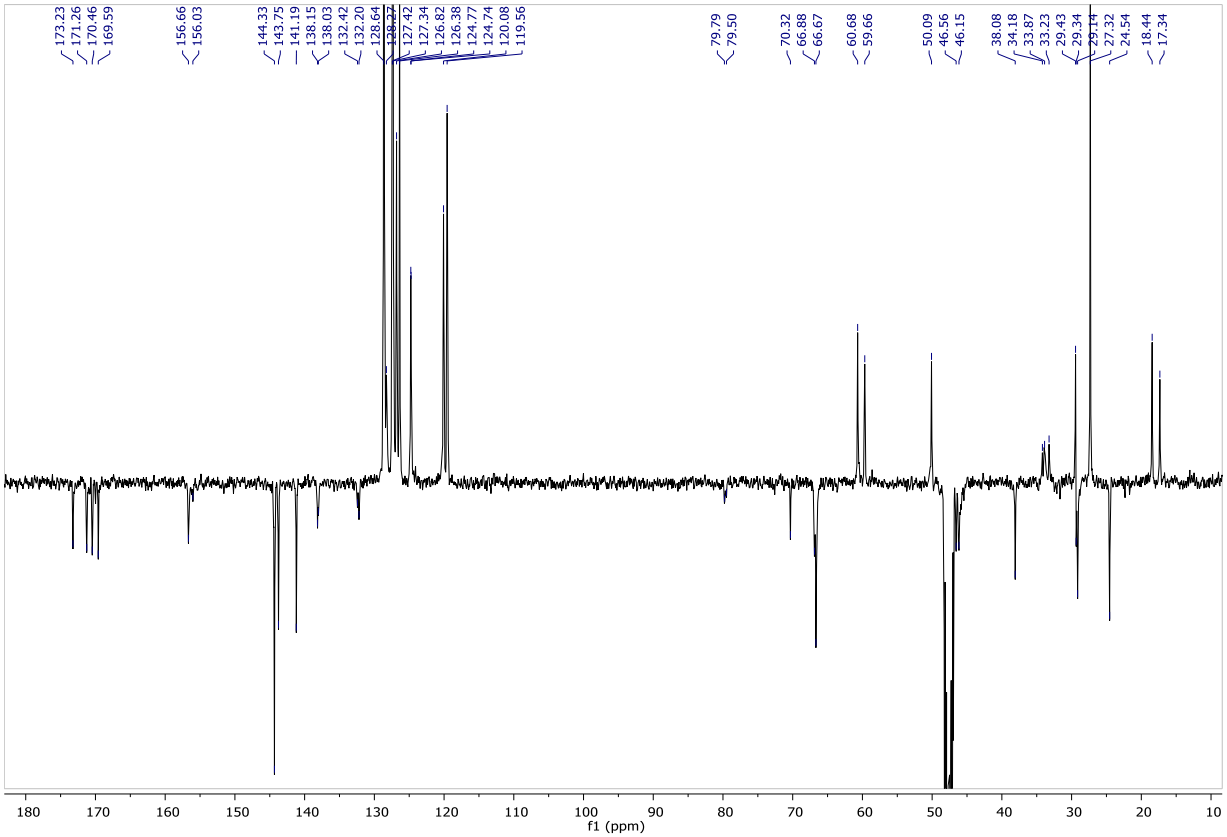

4-pentynamido-Asn(Trt)-Pro-[D]-Val-PABC-*N*-(Boc)-*N*,*N*′-dimethylethylenediamine (137)

^{1}H NMR (400 MHz, CD_2Cl_2-d_2)

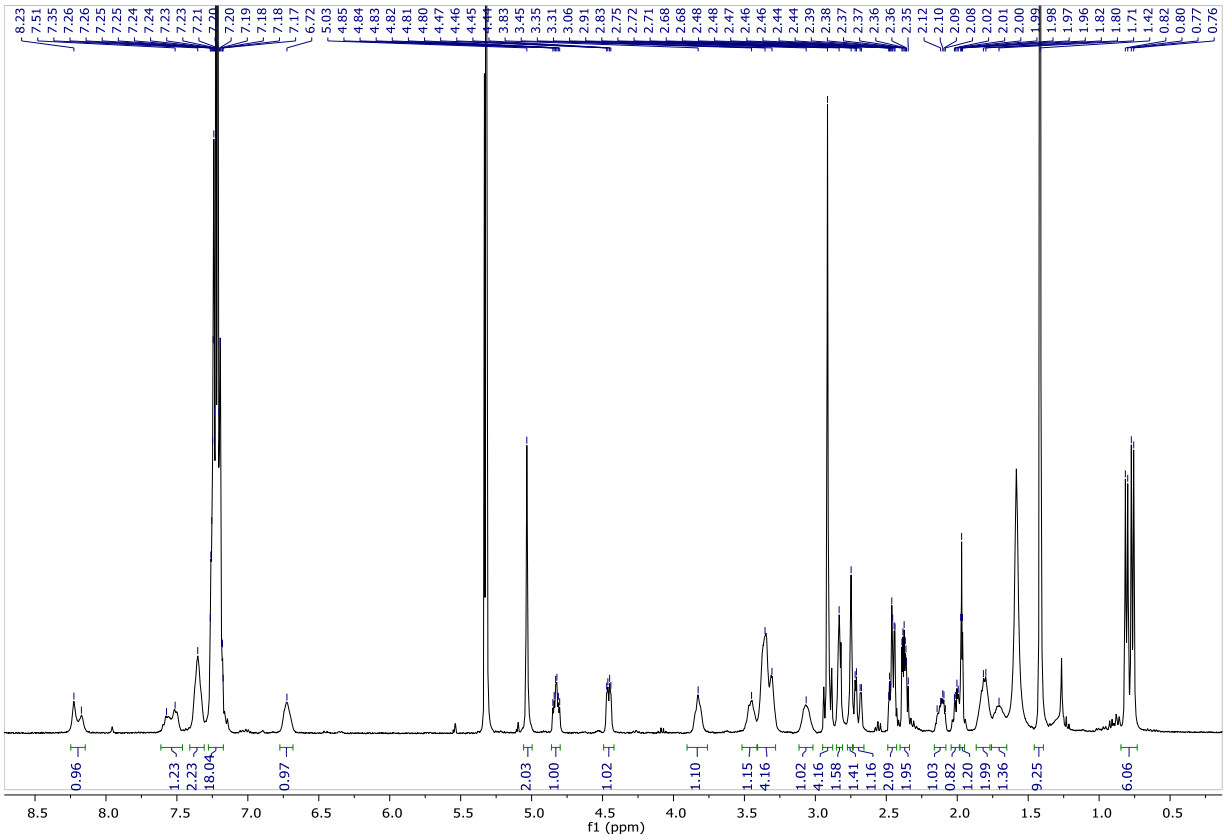

^{13}C-APT NMR (101 MHz, CD_2Cl_2-d_2)

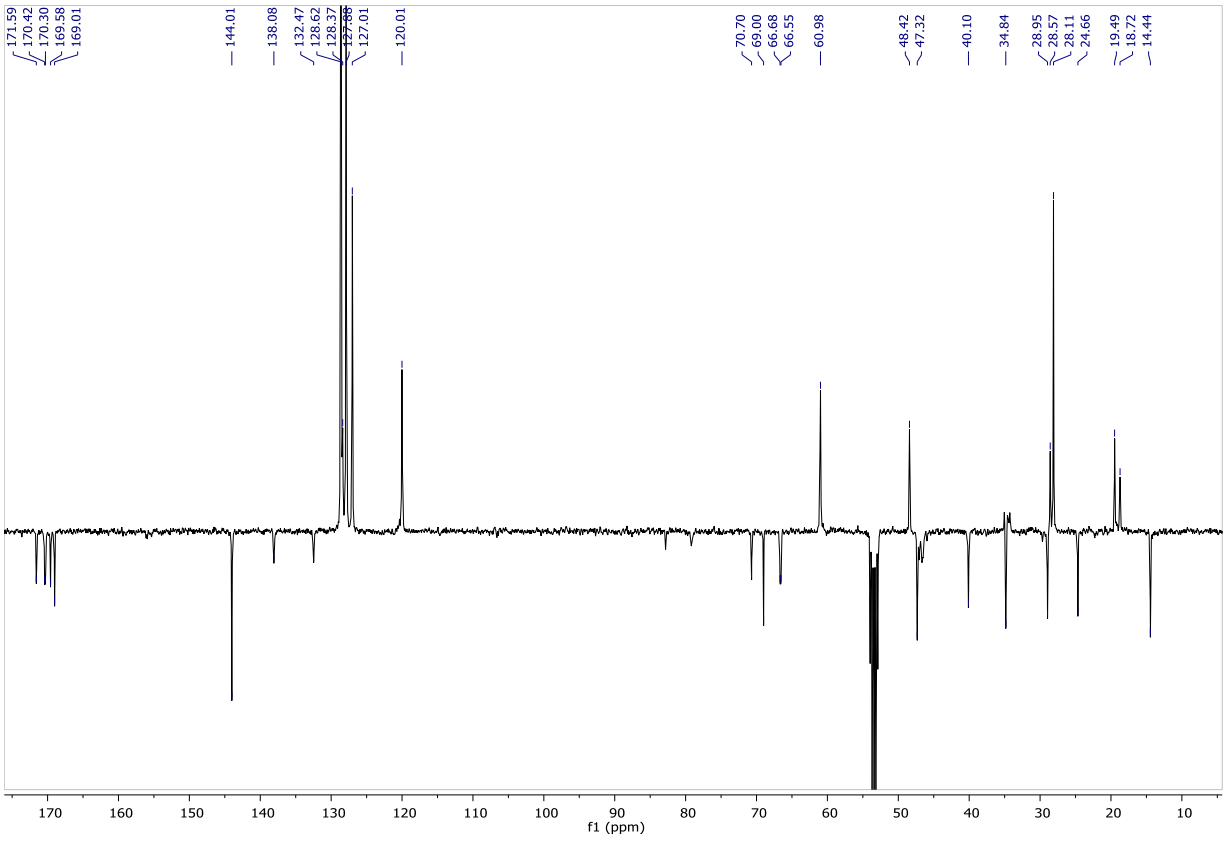

tert-Butyl methyl(2-(*N*-methylpent-4-ynamido)ethyl)carbamate (140)

^{1}H NMR (400 MHz, CD_2Cl_2-d_2)

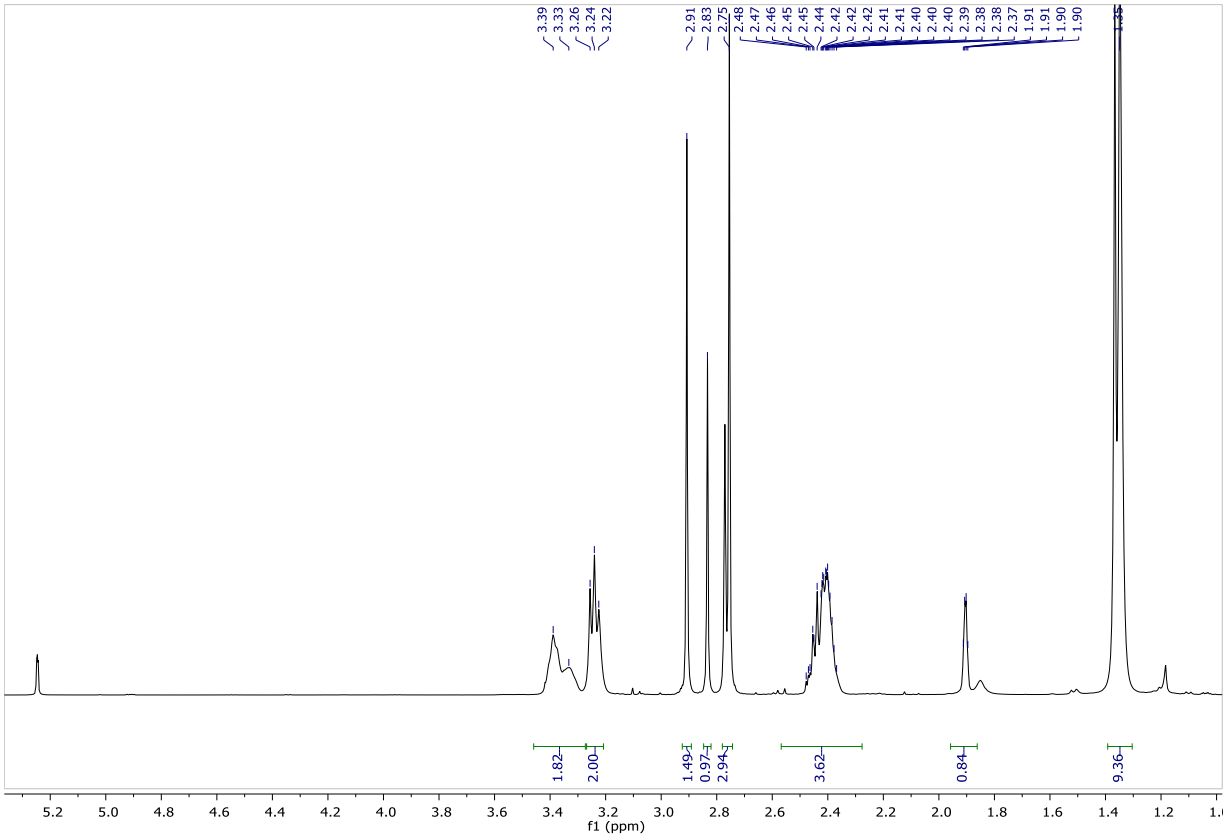

^{13}C-APT NMR (101 MHz, CD_2Cl_2-d_2)

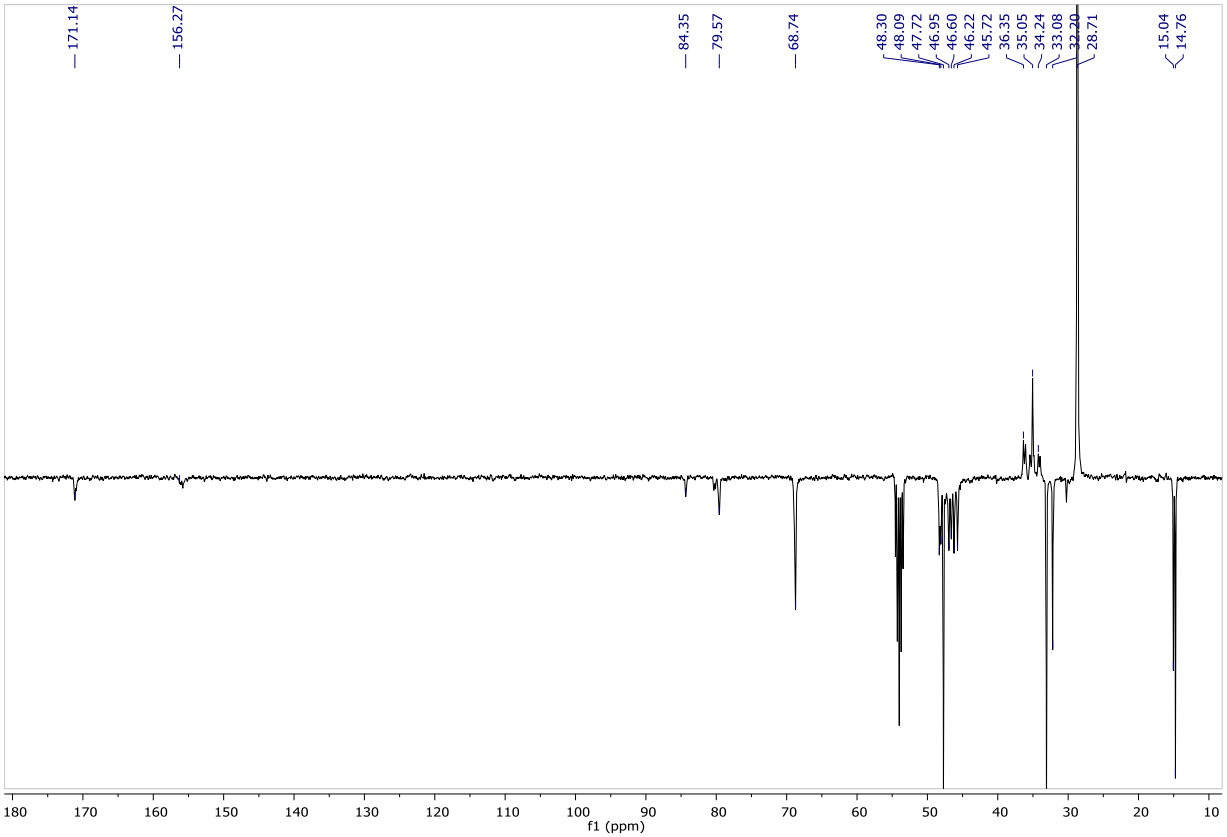

Aliphatic alkyne-PTX (141)

^{1}H NMR (400 MHz, $CDCl_3$-*d*)

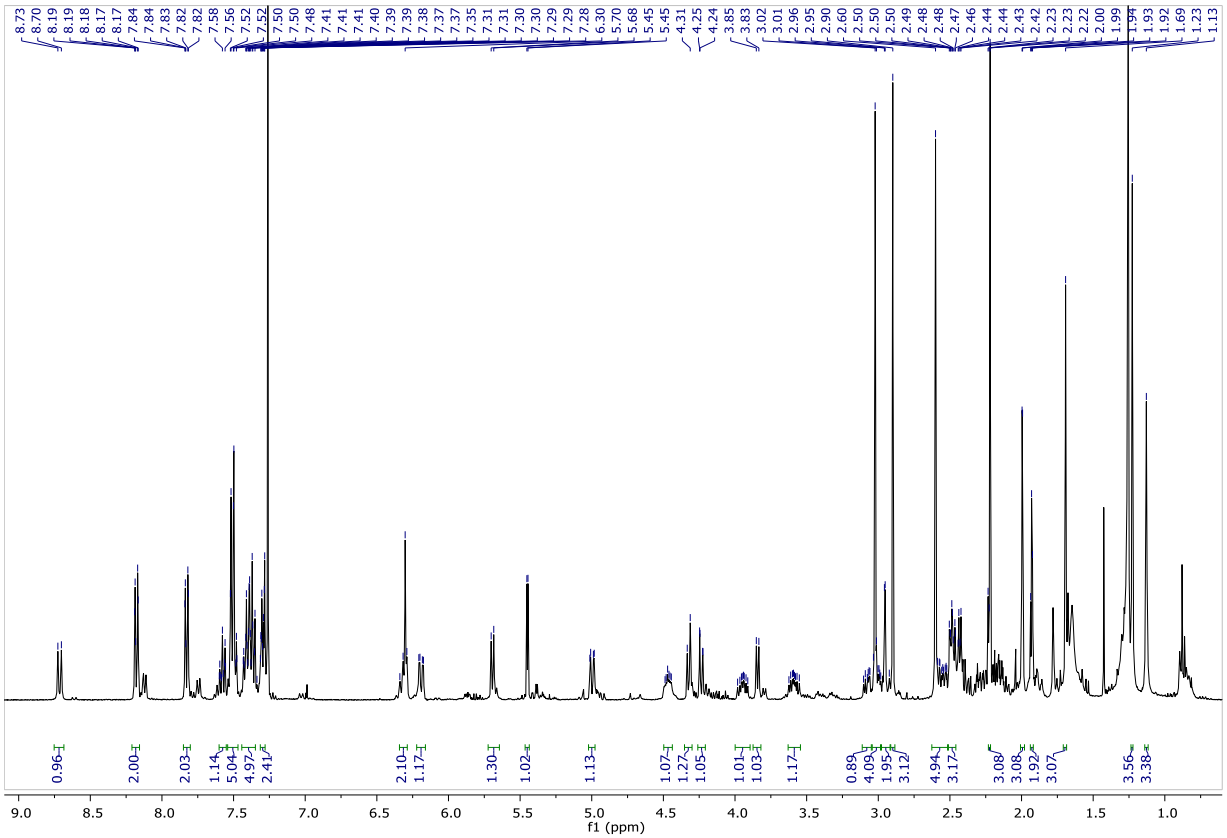

^{13}C-APT NMR (101 MHz, CD_2Cl_2-d_2)

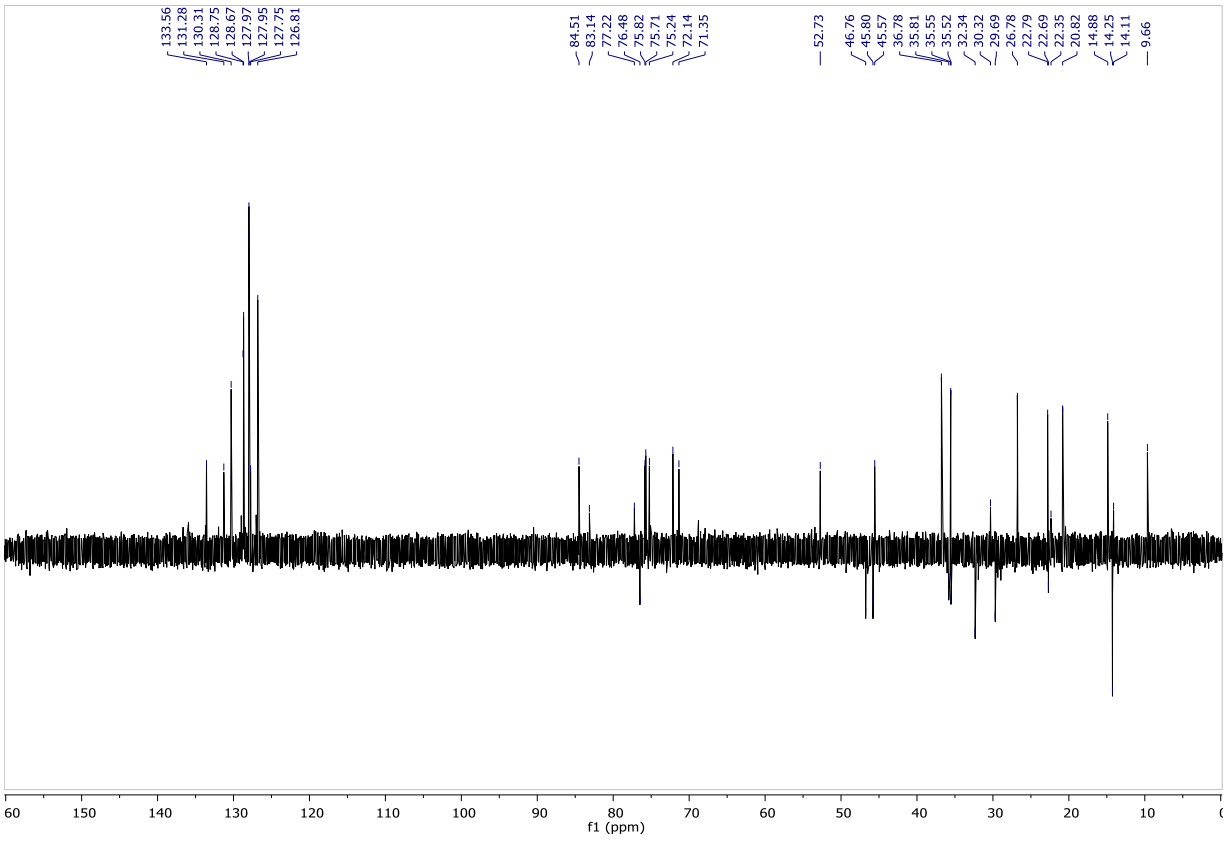

PTX-*N*-(Boc)-*N*,*N*′-dimethylethylenediamine (143)

^{1}H NMR (400 MHz, CD_2Cl_2-d_2)

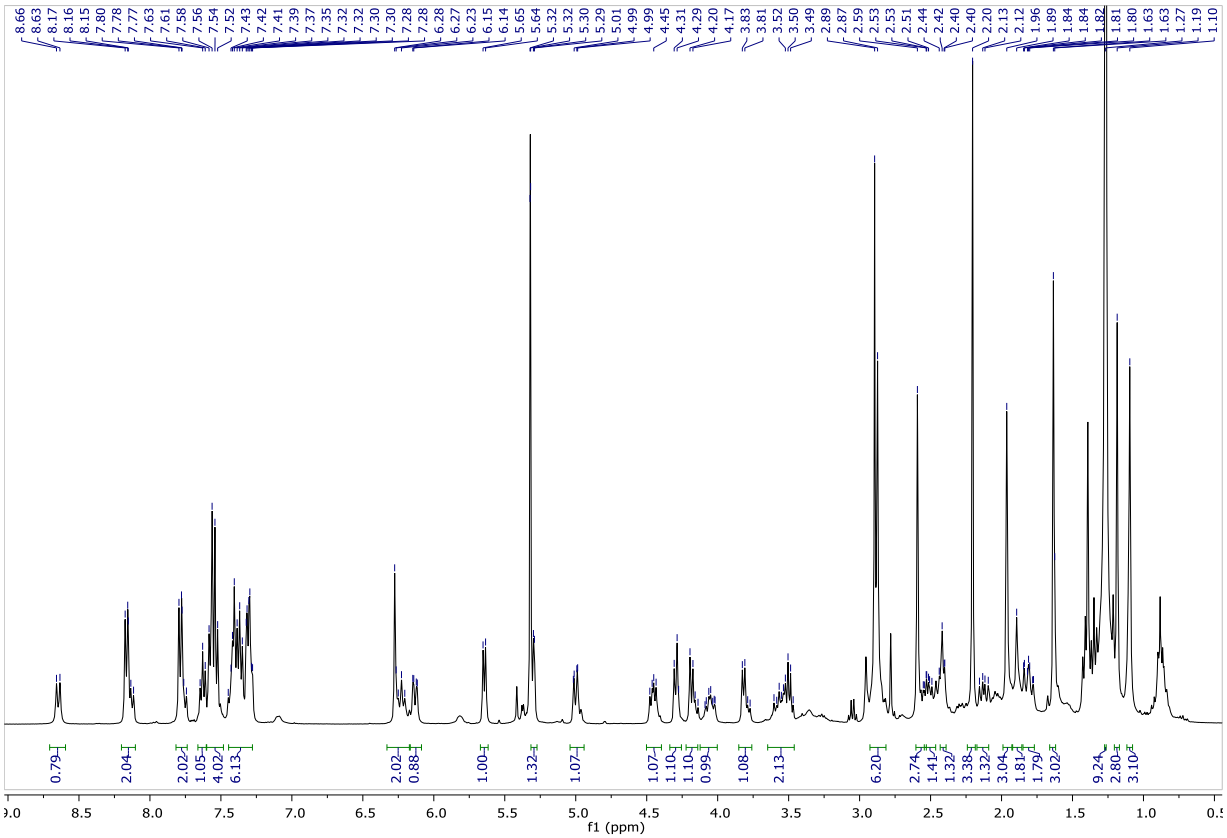

^{13}C-APT NMR (101 MHz, CD_2Cl_2-d_2)

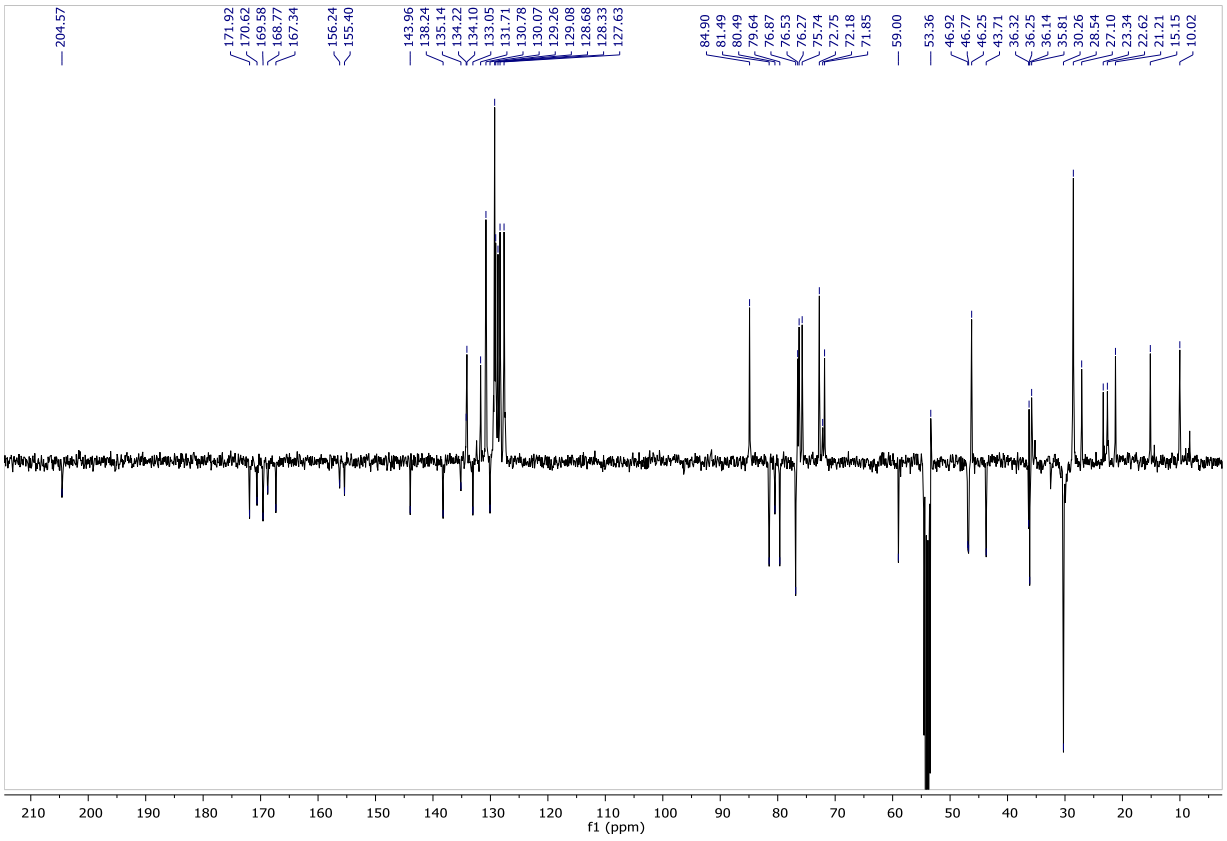

Aliphatic alkyne-Val-Ala-PABA (152)

^{1}H NMR (400 MHz, MeOD-d_4)

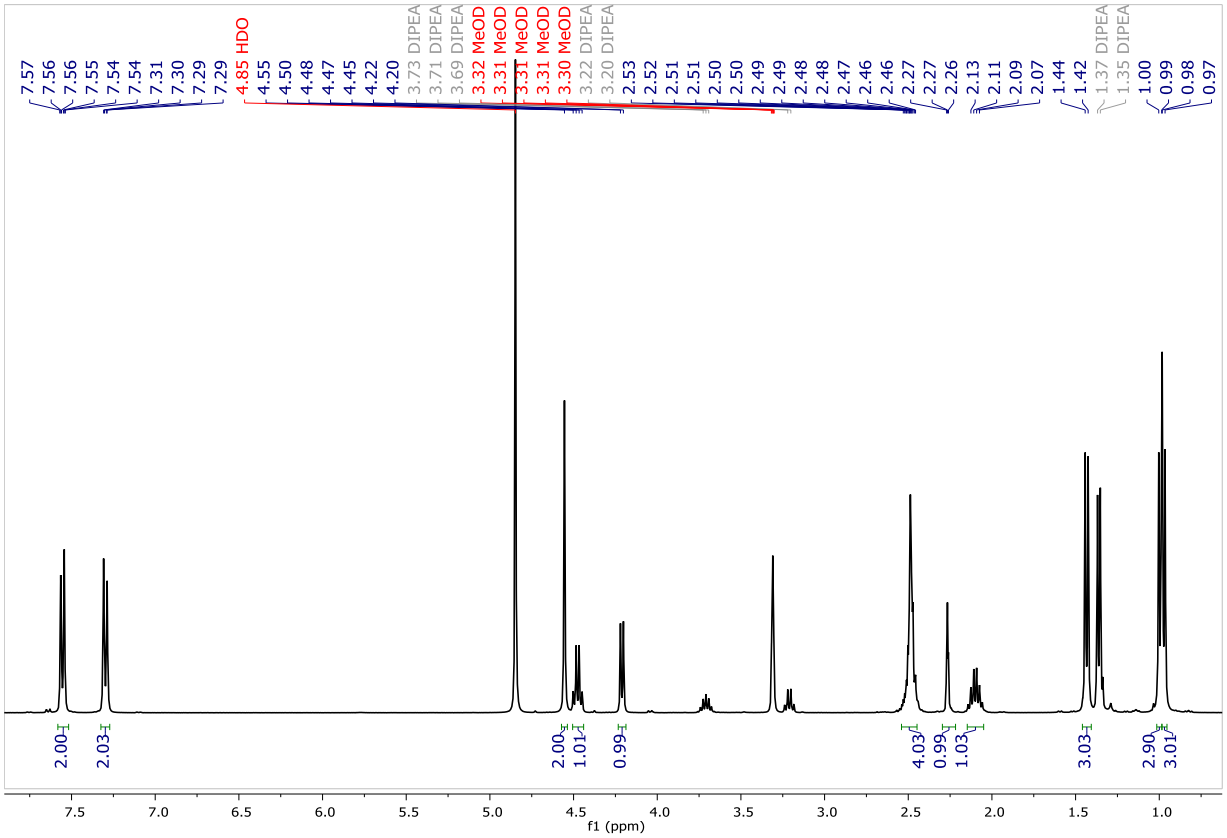

^{13}C-TOTAL NMR (101 MHz, MeOD-d_4)

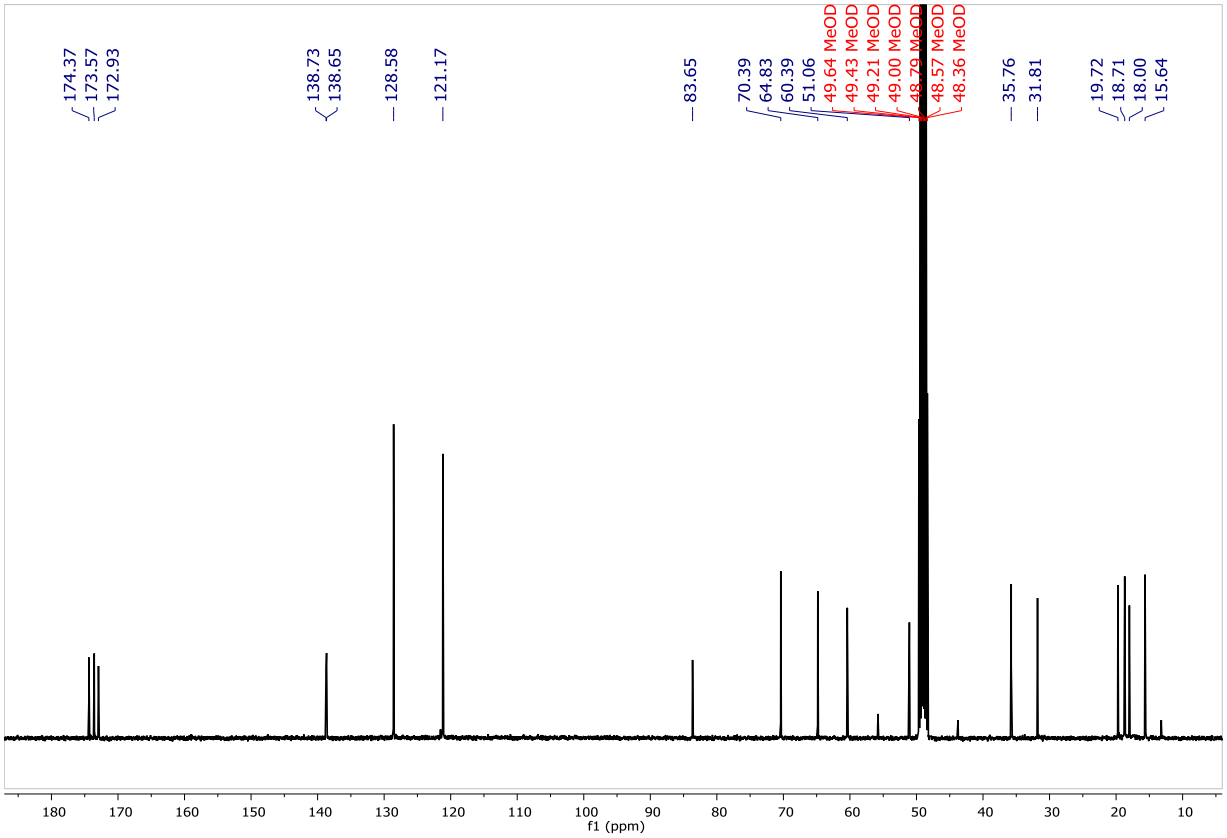

Aliphatic alkyne-Val-Ala-PABC-PNP (153)

^{1}H NMR (400 MHz, DMSO-d_6)

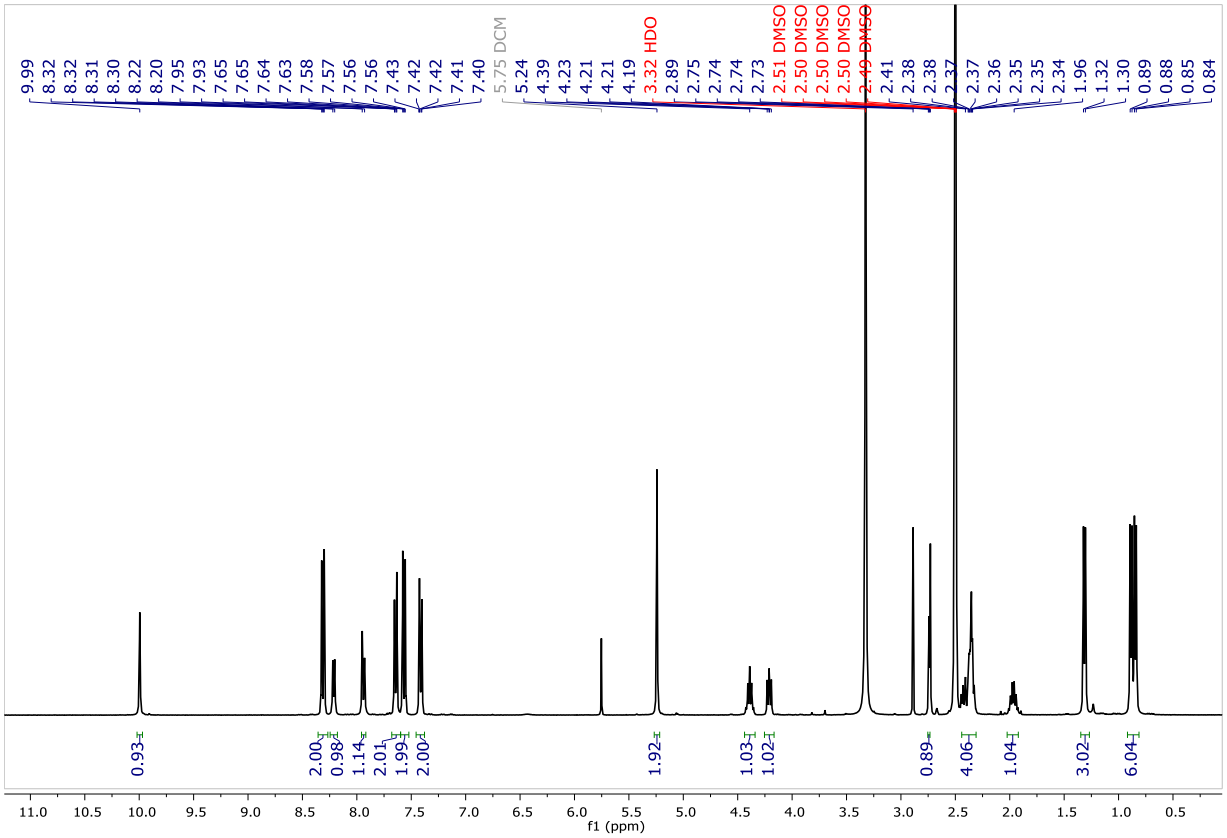

^{13}C-TOTAL NMR (101 MHz, DMSO-d_6)

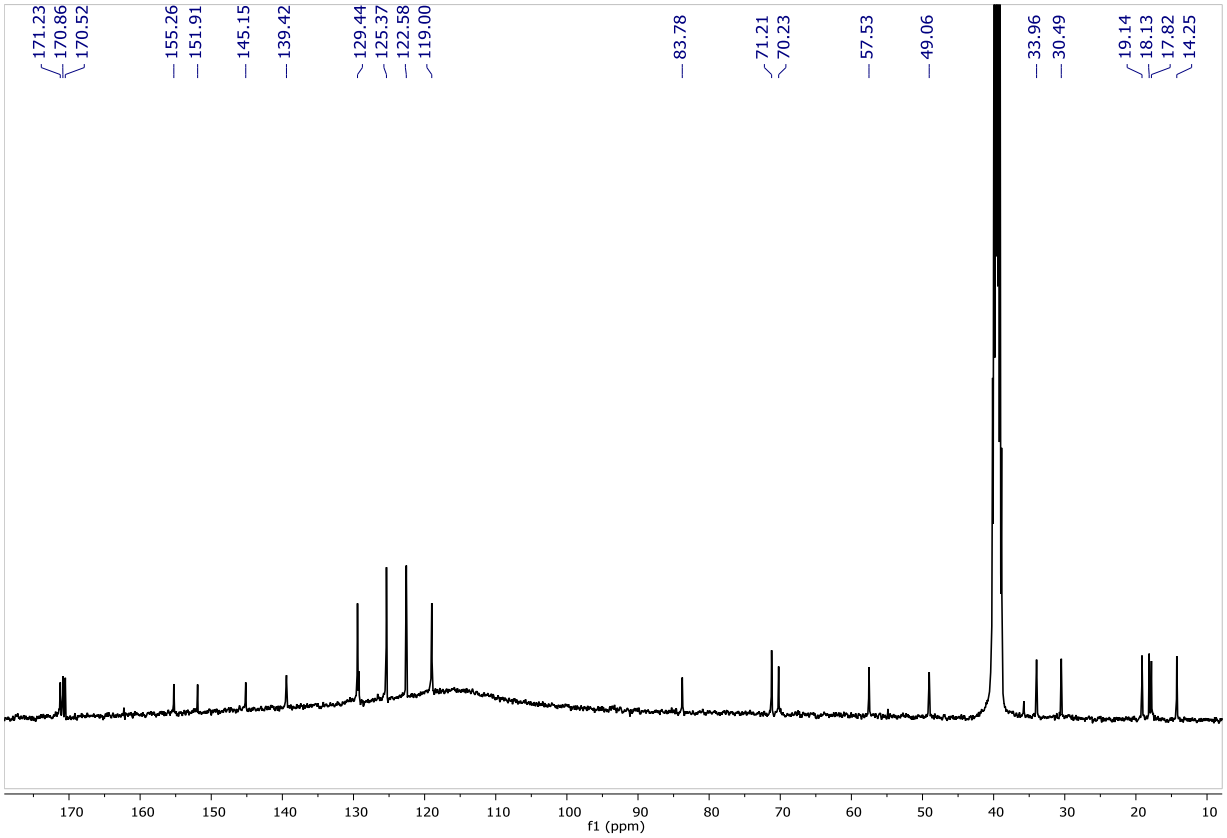

Aliphatic alkyne-Asn(Trt)-Pro-Val-PABA (160)

^{1}H NMR (400 MHz, CD_2Cl_2-d_2)

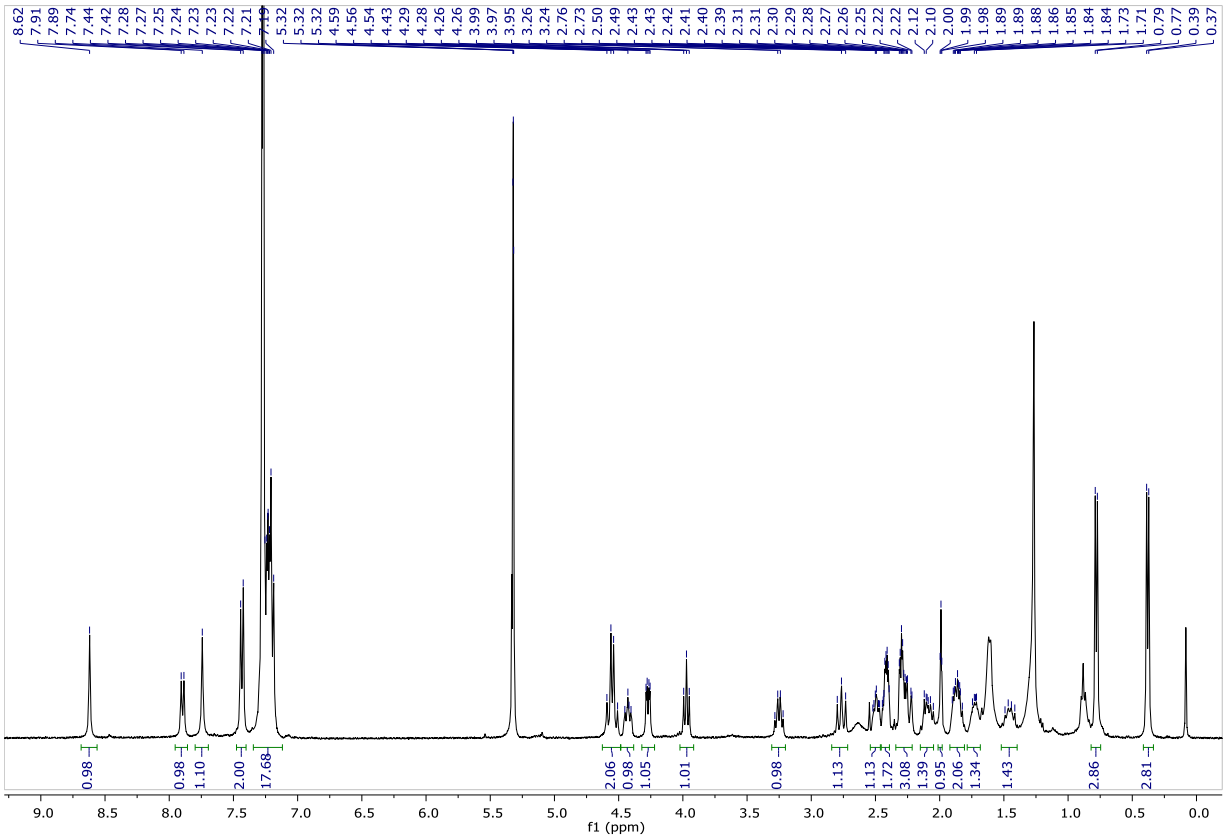

^{13}C-APT NMR (101 MHz, CD_2Cl_2-d_2)

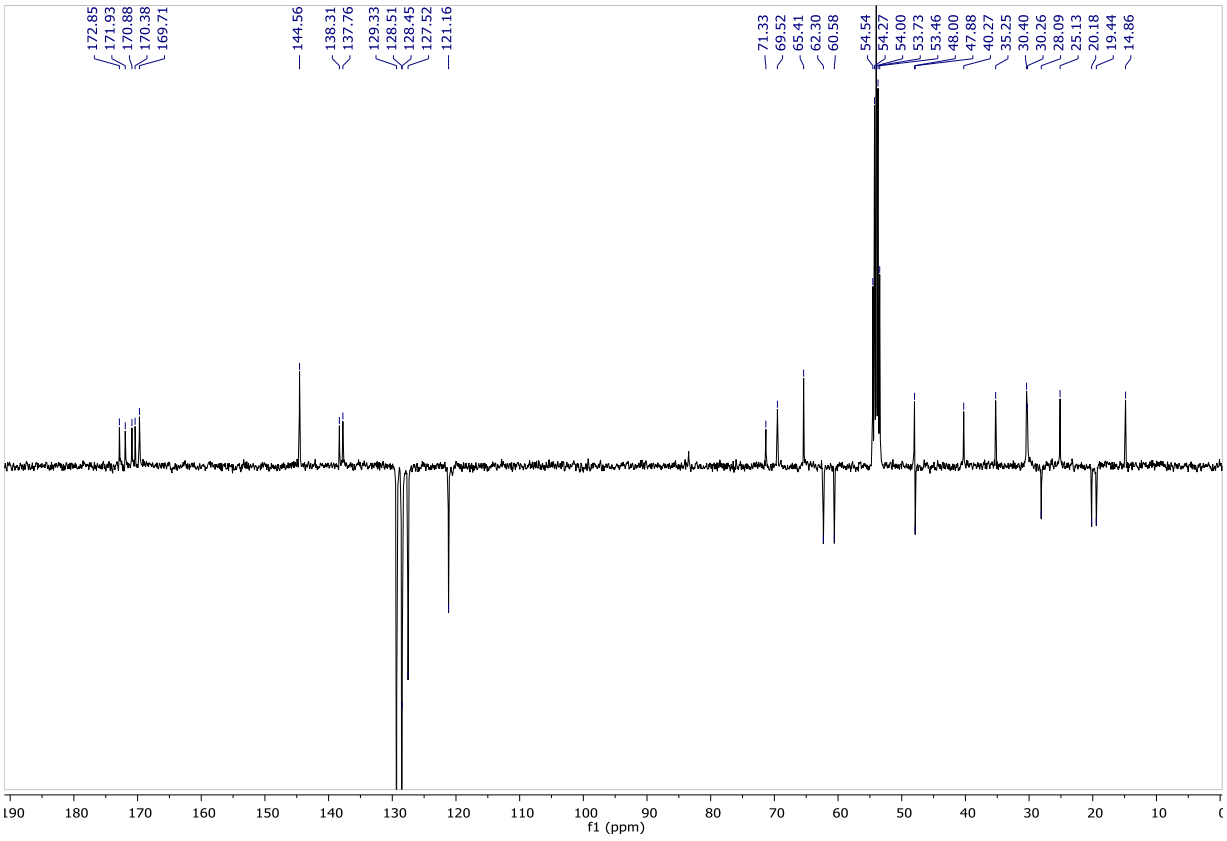

Aliphatic alkyne-Asn(Trt)-Pro-Val-PABC-PNP (161)

^{1}H NMR (400 MHz, CD_2Cl_2-d_2)

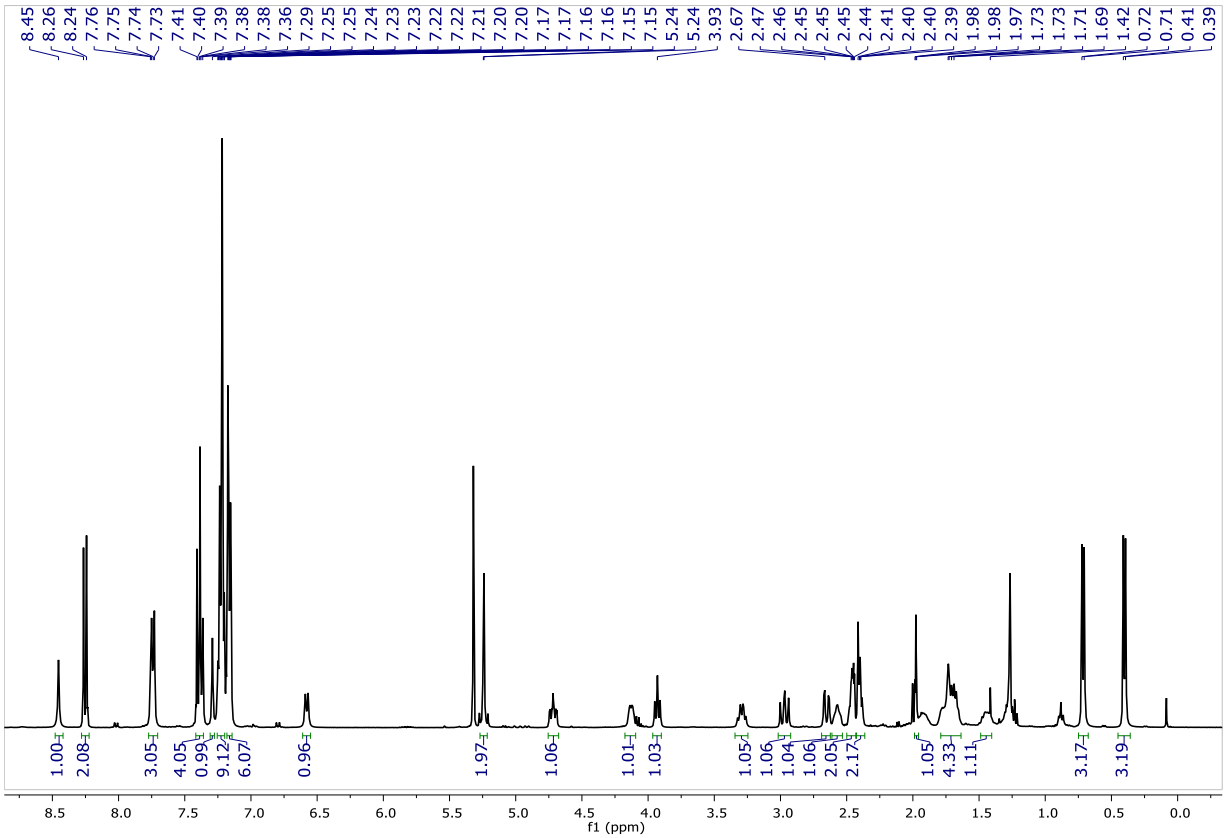

^{13}C-APT NMR (101 MHz, CD_2Cl_2-d_2)

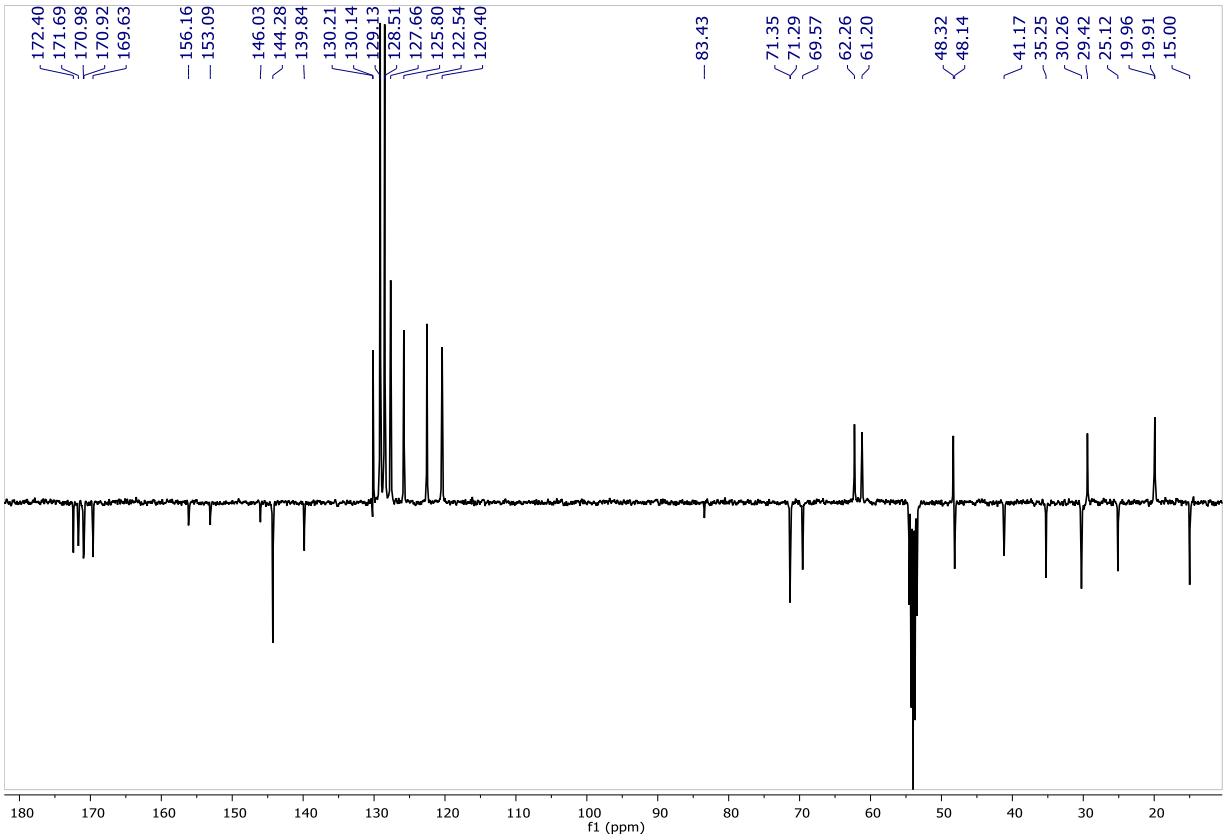

References

REFERENCES

[1] WHO Global Cancer report 2014. http://www.who.int/cancer/en/ (Accessed March 18th, 2018).

[2] WHO Global Cancer report 2014, http://www.who.int/mediacentre/factsheets/fs297/en/ (Accessed on March 18th, 2018).

[3] V. T. DeVita, E. Chu, *Cancer Res.* **2008**, *68*, 8643-8653.

[4] L. L. Brunton, *Goodman and Gilman's The Pharmacological Basis of Therapeutics* McGraw-Hill, New York, **2011**, 2084 pp.

[5] T. L. Lemke, D. A. Williams, V. F. Roche, S. W. Zito, *Foye's Principles of Medicinal Chemistry* Lippincott Williams & Wilkins Wolters Kluwer, **2012**, 1520 pp.

[6] K. Cheung-Ong, G. Giaever, C. Nislow, *Chem. Biol.* **2013**, *20*, 648-659.

[7] G. L. Patrick, *An introduction to Medicinal Chemistry* OUP Oxford, 2009, 776 pp.

[8] L. G. Dezhenkova, V. B. Tsvetkov, A. A. Shtil, *Russ. Chem Rev.* **2014**, *83*, 82-94.

[9] W. N. Haita, E. Rubina, E. Alli, S. Goodin, *Update Cancer Ther.* **2007**, *2*, 1-18.

[10] N. Carelle, E. Piotto, A. Bellanger, J. Germanaud, A. Thuillier, D. Khayat, *Cancer* **2002**, *95*, 155-163.

[11] J. Wang, R. Xu, J. Li, Y. Bai, T. Liu, S. Jiao, G. Dai, J. Xu, Y. Liu, N. Fan, Y. Shu, Y. Ba, D. Ma, S. Qin, L. Zheng, W. Chen, L. Shen, *Gastric Cancer* **2016**, *19*, 234-244.

[12] T. Lammers, F. Kiessling, W. E. Hennink, G. Storm, *J. Control. Release* **2012**, *161*, 175-187.

[13] Q. Cao, Z.-B. Li, K. Chen, Z. Wu, L. He, N. Neamati, X. Chen, *Eur. J. Nucl. Med. Mol. Imaging* **2008**, *35*, 1489-1498.

[14] K. Bosslet, R. Straub, M. Blumrich, J. Czech, M. Gerken, B. Sperker, H. K. Kroemer, J.-P. Gesson, M. Koch, C. Monneret, *Cancer Res.* **1998**, *58*, 1195-1201.

[15] A. A. van der Veldt, N. H. Hendrikse, E. F. Smit, M. P. Mooijer, A. Y. Rijnders, W. R. Gerritsen, J. J. van der Hoeven, A. D. Windhorst, A. A. Lammertsma, M. Lubberink, *Eur. J. Nucl. Med. Mol. Imaging* **2010**, *37*, 1950-1958.

[16] N. Kerru, P. Singh, N. Koorbanally, R. Raj, V. Kumar, *Eur. J. Med. Chem.* **2017**, *142*, 179-212.

[17] F. Kratz, I. A. Müller, C. Ryppa, A. Warnecke, *ChemMedChem* **2008**, *3*, 20-53.

[18] C. Weiss, B. Sammet, N. Sewald, *Nat. Prod. Rep.* **2013**, *30*, 924-940.

[19] L. Zhao, J. P. May, A. Blanc, D. J. Dietrich, A. Loonchanta, K. Matinkhoo, A. Pryyma, D. M. Perrin, *Chembiochem* **2015**, *16*, 1420-1425.

[20] N. Krall, J. Scheuermann, D. Neri, *Angew. Chem. Int. Ed.* **2013**, *52*, 1384-1402.

[21] T. Legigan, J. Clarhaut, I. Tranoy-Opalinski, A. Monvoisin, B. Renoux, M. Thomas, A. Le Pape, S. Lerondel, S. Papot, *Angew. Chem. Int. Ed.* **2012**, *51*, 11606-11610.

[22] M. L. Miller, M. Shizuka, A. Wilhelm, P. Salomon, E. E. Reid, L. Lanieri, S. Sikka, E. K. Maloney, L. Harvey, Q. Qiu, K. E. Archer, C. Bai, D. Vitharana, L. Harris, R. Singh, J. F. Ponte, N. C. Yoder, Y. Kovtun, K. C. Lai, O. Ab, J. Pinkas, T. A. Keating, R. V. J. Chari, *Mol. Cancer Ther.* **2018**, *17*, 650-660.

[23] H. Maeda, J. Wu, T. Sawa, Y. Matsumura, K. Hori, *J. Control. Release* **2000**, *65*, 271-284.

[24] T. Sun, Y. S. Zhang, B. Pang, D. C. Hyun, M. Yang, Y. Xia, *Angew. Chem. Int. Ed.* **2014**, *53*, 12320-12364.

[25] N. R. Jabir, K. Anwar, C. K. Firoz, M. Oves, M. A. Kamal, S. Tabrez, *Curr. Med. Res. Opin.* **2018**, *23*, 1-11.

[26] T. M. Allen, *Nat. Rev. Cancer* **2002**, *2*, 750.

[27] G. Casi, D. Neri, *J. Control. Release* **2012**, *161*, 422-428.

[28] E. L. Sievers, P. D. Senter, *Annu. Rev. Med.* **2013**, *64*, 15-29.

[29] a) E. Perrino, M. Steiner, N. Krall, G. J. Bernardes, F. Pretto, G. Casi, D. Neri, *Cancer Res.* **2014**, *74*, 2569-2578; b) G. Casi, D. Neri, *Mol. Pharmaceutics* **2015**, *12*, 1880-1884.

[30] R. V. Chari, M. L. Miller, W. C. Widdison, *Angew. Chem. Int. Ed.* **2014**, *53*, 3796-3827.

[31] C. A. Janeway, P. Travers, M. Walport, and M. J. Shlomchik. *The Immune System in Health and Disease,* New York: Garland Science, **2001**, Part II – Chapter 3.

[32] L. Haas, *J. Neurol. Neurosurg. Psychiatry* **2001**, *71*, 62-62.

[33] K. Strebhardt, A. Ullrich, *Nat. Rev. Cancer* **2008**, *8*, 473-480.

[34] C. Brack, M. Hirama, R. Lenhard-Schuller, S. Tonegawa, *Cell* **1978**, *15*, 1-14.

[35] a) A. Cambrosio, P. Keating, *J. Hist. Biol.* **1992**, *25*, 175-230; b) P. N. Nelson, G. M. Reynolds, E. E. Waldron, E. Ward, K. Giannopoulos, P. G. Murray. *Mol Pathol.* **2000**, *53*, 111-117.

[36] T. A. Waldmann, W. Strober in *Metabolism of immunoglobulins*, *Vol. 13* Karger Publishers, **1969**, pp. 1-110.

[37] D. C. Roopenian, S. Akilesh, *Nat. Rev. Immunology* **2007**, *7*, 715-725.

[38] F. Li, C. Zhao, L. Wang, *Int. J. Cancer* **2014**, *134*, 1257-1269.

[39] P. Chames, M. Van Regenmortel, E. Weiss, D. Baty, *Br. J. Pharmacol.* **2009**, *157*, 220-233.

[40] B. A. Teicher, R. V. Chari, *Clin. Cancer Res.* **2011**, *17*, 6389-6397.

[41] G. J. Bernardes, G. Casi, S. Trussel, I. Hartmann, K. Schwager, J. Scheuermann, D. Neri, *Angew. Chem. Int. Ed.* **2012**, *51*, 941-944.

[42] P. Trail, D. Willner, S. Lasch, A. Henderson, S. Hofstead, A. Casazza, R. Firestone, I. Hellstrom, K. Hellstrom, *Science* **1993**, *261*, 212-215.

[43] M. N. Saleh, S. Sugarman, J. Murray, J. B. Ostroff, D. Healey, D. Jones, C. R. Daniel, D. LeBherz, H. Brewer, N. Onetto, A. F. LoBuglio, *J. Clin. Oncol.* **2000**, *18*, 2282-2292.

[44] B. H. Petersen, S. V. DeHerdt, D. W. Schneck, T. F. Bumol, *Cancer Res.* **1991**, *51*, 2286-2290.

[45] N. Joubert, C. Denevault-Sabourin, F. Bryden, M.-C. Viaud-Massuard, *Eur. J. Med. Chem.* **2017**, *143*, 393-415.

[46] C. Chalouni, S. Doll, *J. Exp. Clin. Cancer Res.* **2018**, *37*, 20-32.

[47] G. Casi, D. Neri, *J. Med. Chem* **2015**, *58*, 8751-8761.

[48] S. Cazzamalli, A. D. Corso, D. Neri, *CHIMIA Int. J. for Chem.* **2017**, *71*, 712-715.

[49] M. Srinivasarao, C. V. Galliford, P. S. Low, *Nat. Rev. Drug Discov.* **2015**, *14*, 203-219.

[50] A. Dal Corso, L. Pignataro, L. Belvisi, C. Gennari, *Curr. Top. Med. Chem.* **2016**, *16*, 314-329.

[51] S. C. Alley, N. M. Okeley, P. D. Senter, *Curr. Opin. Chem. Biol.* **2010**, *14*, 529-537.

[52] M. Srinivasarao, P. S. Low, *Chem. Rev.* **2017**, *117*, 12133-12164.

[53] A. Alouane, R. Labruere, T. Le Saux, F. Schmidt, L. Jullien, *Angew. Chem. Int. Ed.* **2015**, *54*, 7492-7509.

[54] G. Russell-Jones, K. McTavish, J. McEwan, J. Rice, D. Nowotnik, *J. Inorg. Biochem.* **2004**, *98*, 1625-1633.

[55] L. B. Bailey, J. F. Gregory, *J. Nutr.* **1999**, *129*, 779-782.

[56] C. S. Kue, A. Kamkaew, K. Burgess, L. V. Kiew, L. Y. Chung, H. B. Lee, *Med. Res. Rev.* **2016**, *36*, 494-575.

[57] C. P. Leamon, Y. Wang, I. R. Vlahov, F. You, P. J. Kleindl and H. K. R. Santhapuram, WO 2009/002993 A1, **2008**.

[58] S. Park, E. Kim, W. Y. Kim, C. Kang, J. S. Kim, *Chem. Commun.* **2015**, *51*, 9343-9345.

[59] X. Warg, L. Yin, P. Rao, R. Stein, K. M. Harsch, Z. Lee, W. D. W. Heston, *J. Cell. Biochem.* **2007**, *102*, 571-579.

[60] A. Ghosh, W. D. W. Heston, *J. Cell. Biochem.* **2004**, *91*, 528-539.

[61] W. Roll, A. Bode, M. Weckesser, M. Bögemann, K. Rahbar, *Clin. Nucl. Med.* **2017**, *42*, 152-153.

[62] M. Volante, R. Rosas, E. Allìa, R. Granata, A. Baragli, G. Muccioli, M. Papotti, *Mol. Cell. Endocrinol.* **2008**, *286*, 219-229.

[63] A. Balaev, V. Osipov, D. Khachatryan, *Pharm. Chem. J.* **2015**, *49*, 345-351.

[64] M. Huo, Q. Zhu, Q. Wu, T. Yin, L. Wang, L. Yin, J. Zhou, *J. Pharm. Sci.* **2015**, *104*, 2018-2028.

[65] X. Chen, X.-Y. Zhang, Y. Shen, L.-L. Fan, M.-L. Ren, Y.-P. Wu, *Oncotarget* **2016**, *7*, 83451-83461.

[66] Y. Shen, X.-Y. Zhang, X. Chen, L.-L. Fan, M.-L. Ren, Y.-P. Wu, K. Chanda, S.-W. Jiang, *Oncol. Rep.* **2017**, *37*, 219-226.

[67] R. G. Alargova, M. T. Bilodeau, C. A. Dunbar, S. Kadiyala, R. R. Shinde, P. L. Soo, B. Sweryda-Krawiec, B. H. White, P. R. Bazinet, R. Wooster, WO 2016/004048 A2, **2016**.

[68] M. Wichert, N. Krall, *Curr. Opin. Chem. Biol.* **2015**, *26*, 48-54.

[69] N. Krall, F. Pretto, W. Decurtins, G. J. Bernardes, C. T. Supuran, D. Neri, *Angew. Chem. Int. Ed.* **2014**, *53*, 4231-4235.

[70] N. Krall, F. Pretto, D. Neri, *Chem. Sci* **2014**, *5*, 3640-3644.

[71] S. Cazzamalli, A. Dal Corso, D. Neri, *Mol. Cancer Ther.* **2016**, *15*, 2926-2935.

[72] K. Y. Choi, M. Swierczewska, S. Lee, X. Chen, *Theranostics* **2012**, *2*, 156.

[73] M. Wichert, N. Krall, W. Decurtins, R. M. Franzini, F. Pretto, P. Schneider, D. Neri, J. Scheuermann, *Nature Chem.* **2015**, *7*, 241-249.

[74] Y. Li, R. Luca, S. Cazzamalli, F. Pretto, D. Bajic, J. Scheuermann, D. Neri, *Nat. Chem.* **2018**, *10*, 441–448.

[75] S. Cazzamalli, A. Dal Corso, F. Widmayer, D. Neri, *J. Am. Chem. Soc.* **2018**, *5*, 1617-1621.

[76] R. J. D. Hatley, S. J. F. Macdonald, R. J. Slack, J. Le, S. B. Ludbrook, P. T. Lukey, *Angew. Chem. Int. Ed.* **2018**, *57*, 3298-3321.

[77] D. Cox, M. Brennan, N. Moran, *Nat. Rev. Drug Discov.* **2010**, *9*, 804-820.

[78] W. Guo, F. G. Giancotti, *Nat. Rev. Mol. Cell Biol.* **2004**, *5*, 816-826.

[79] F. Danhier, A. Le Breton, V. Préat, *Mol. Pharmaceutics* **2012**, *9*, 2961-2973.

[80] J.S. Desgrosellier, D. A. Cheresh, *Nat. Rev. Cancer* **2010**, *10*, 9-22.

[81] C. Mas-Moruno, R. Fraioli, F. Rechenmacher, S. Neubauer, T. G. Kapp, H. Kessler, *Angew. Chem. Int. Ed.* **2016**, *55*, 7048-7067.

[82] E. Ruoslahti, M. D. Pierschbacher, *Science* **1987**, *238*, 491-497.

[83] M. D. Pierschbacher, E. Ruoslahti, *Nature* **1984**, *309*, 30-33.

[84] R. S. McDowell, T. R. Gadek, *J. Am. Chem. Soc*. **1992**, *114*, 9245-9253.

[85] M. Aumailley, M. Gurrath, G. Müller, J. Calvete, R. Timpl, H. Kessler. *FEBS Lett.* **1991**, *291*, 50-54.

[86] K. E. Gottschalk, H. Kessler, *Angew. Chem. Int. Ed.* **2002**, *41*, 3767-3774.

[87] J. P. Xiong, T. Stehle, R. Zhang, A. Joachimiak, M. Frech, S. L. Goodman, M. A. Arnaout, *Science* **2002**, *296*, 151-155.

[88] C. Mas-Moruno, F. Rechenmacher, H. Kessler, *Anticancer Agents Med. Chem.* **2010**, *10*, 753-768.

[89] T. G. Kapp, F. Rechenmacher, S. Neubauer, O. V. Maltsev, E. A. Cavalcanti-Adam, R. Zarka, U. Reuning, J. Notni, H.-J. Wester, C. Mas-Moruno, J. Spatz, B. Geiger, and H. Kessler, *Sci. Rep.* **2017**, *7*, 39805.

[90] F. Zanardi, P. Burreddu, G. Rassu, L. Auzzas, L. Battistini, C. Curti, A. Sartori, G. Nicastro, G. Menchi, N. Cini, A. Bottonocetti, S. Raspanti, and G. Casiraghi, *J. Med. Chem.* **2008**, *51*, 1771-1782.

[91] G. Casiraghi, G. Rassu, L. Auzzas, P. Burreddu, E. Gaetani, L. Battistini, F. Zanardi, C. Curti, G. Nicastro, L. Belvisi, I. Motto, M. Castorina, G. Giannini, and C. Pisano, *J. Med. Chem.* **2005**, *48*, 7675-7687.

[92] L. Manzoni, L. Belvisi, D. Arosio, M. Civera, M. Pilkington-Miksa, D. Potenza, A. Caprini, E. Araldi, E. Monferini, M. Mancino, F. Podestà, and C. Scolastico, *ChemMedChem* **2009**, *4*, 615-632.

[93] R. De Marco, A. Tolomelli, E. Juaristi, L. Gentilucci, *Med. Res. Rev.* **2016**, *36*, 389-424.

[94] D. Arosio, L. Manzoni, E. M. V. Araldi, C. Scolastico, *Bioconjugate Chem.* **2011**, *22*, 664-672.

[95] L. Battistini, P. Burreddu, A. Sartori, D. Arosio, L. Manzoni, L. Paduano, G. D'Errico, R. Sala, L. Reia, S. Bonomini, G. Rassu, F. Zanardi, *Mol. Pharmaceutics* **2014**, *11*, 2280-2293.

[96] S. Lanzardo, L. Conti, C. Brioschi, M. P. Bartolomeo, D. Arosio, L. Belvisi, L. Manzoni, A. Maiocchi, F. Maisano, G. Forni, *Contrast Media Mol. Imaging* **2011**, *6*, 449-458.

[97] H. Chen, G. Niu, H. Wu, X. Chen, *Theranostics* **2016**, *6*, 78-92.

[98] Y. S. Song, H. S. Park, B. C. Lee, J. H. Jung, H. Y. Lee, S. E. Kim, *Cancer Biother. Radiopharm.* **2017**, *32*, 288-296.

[99] D. Arosio, C. Casagrande, L. Manzoni, *Curr. Med. Chem.* **2012**, *19*, 3128-3151.

[100] D. Arosio, C. Casagrande, *Adv Drug Deliv Rev* **2016**, *97*, 111-143.

[101] H. Cai, P. S. Conti, *J. Labelled Comp. Radiopharm.* **2013**, *56*, 264-279.

[102] S. Liu, *Bioconjug. Chem.* **2015**, *26*, 1413-1438.

[103] P. Caswell, J. Norman, *Trends Cell Biol.* **2008**, *18*, 257-263.

[104] P. T. Caswell, S. Vadrevu, J. C. Norman, *Nat. Rev. Mol. Cell Biol.* **2009**, *10*, 843-853.

[105] W. Arap, R. Pasqualini, E. Ruoslahti, *Science* **1998**, *279*, 377-380.

[106] F. M. de Groot, H. J. Broxterman, H. P. Adams, A. van Vliet, G. I. Tesser, Y. W. Elderkamp, A. J. Schraa, R. J. Kok, G. Molema, H. M. Pinedo, H. W. Scheeren, *Mol. Cancer Ther.* **2002**, *1*, 901-911.

[107] D. Arosio, L. Manzoni, C. Corno, P. Perego, *Recent Pat. Anticancer Drug Discov.* **2017**, *12*, 148-168.

[108] C. Ryppa, H. Mann-Steinberg, I. Fichtner, H. Weber, R. Satchi-Fainaro, M. L. Biniossek, F. Kratz, *Bioconjug. Chem.* **2008**, *19*, 1414-1422.

[109] A. Dal Pozzo, M. H. Ni, E. Esposito, S. Dallavalle, L. Musso, A. Bargiotti, C. Pisano, L. Vesci, F. Bucci, M. Castorina, R. Fodera, G. Giannini, C. Aulicino, S. Penco, *Bioorg. Med. Chem.* **2010**, *18*, 64-72.

[110] S. Katsamakas, T. Chatzisideri, S. Thysiadis, V. Sarli, *Future Med. Chem.* **2017**, *9*, 579-604.

[111] A. Dal Pozzo, E. Esposito, M. Ni, L. Muzi, C. Pisano, F. Bucci, L. Vesci, M. Castorina, S. Penco, *Bioconjug. Chem.* **2010**, *21*, 1956-1967.

[112] A. Dal Pozzo, S. Penco, G. Giannini, O. Tinti, C. Pisano, L. Vesci, M. H. Ni, WO 2005111064, **2005**.

[113] J. P. Stevenson, W. Sun, M. Gallagher, R. Johnson, D. Vaughn, L. Schuchter, K. Algazy, S. Hahn, N. Enas, D. Ellis, D. Thornton, P. J. O'Dwyer, *Clin. Cancer Res.* **2002**, *8*, 2524-2529.

[114] H. Chen, Z. Lin, K. E. Arnst, D. D. Miller, W. Li, *Molecules* **2017**, *22,* 1281-1309.

[115] C. Weiss, E. Figueras, A. N. Borbely, N. Sewald, **2017**, *23*, 514-531.

[116] M. Nahrwold, C. Weiss, T. Bogner, F. Mertink, J. Conradi, B. Sammet, R. Palmisano, S. Royo Gracia, T. Preusse, N. Sewald, *J. Med. Chem.* **2013**, *56*, 1853-1864.

[117] J. L. Crisp, E. N. Savariar, H. L. Glasgow, L. G. Ellies, M. A. Whitney, R. Y. Tsien, *Mol. Cancer Ther.* **2014**, *13*, 1514-1525.

[118] D. Boturyn, E. Defrancq, G. T. Dolphin, J. Garcia, P. Labbe, O. Renaudet, P. Dumy, *J. Pept. Sci.* **2008**, *14*, 224-240.

[119] A. Massaguer, A. Gonzalez-Canto, E. Escribano, S. Barrabes, G. Artigas, V. Moreno, V. Marchán, *Dalton Trans.* **2015**, *44*, 202-212.

[120] X. Chen, C. Plasencia, Y. Hou, N. Neamati, *J. Med. Chem.* **2005**, *48*, 1098-1106.

[121] C. Ryppa, H. Mann-Steinberg, I. Fichtner, H. Weber, R. Satchi-Fainaro, M. L. Biniossek, F. Kratz, *Bioconjug. Chem.* **2008**, *19*, 1414-1422.

[122] M. Pilkington-Miksa, D. Arosio, L. Battistini, L. Belvisi, M. De Matteo, F. Vasile, P. Burreddu, P. Carta, G. Rassu, P. Perego, N. Carenini, F. Zunino, M. De Cesare, V. Castiglioni, E. Scanziani, C. Scolastico, G. Casiraghi, F. Zanardi, L. Manzoni, *Bioconjug. Chem.* **2012**, *23*, 1610-1622.

[123] A. S. M. Ressurreição, A. Vidu, M. Civera, L. Belvisi, D. Potenza, L. Manzoni, S. Ongeri, C. Gennari, U. Piarulli, *Chem. Eur. J.* **2009**, *15*, 12184-12188.

[124] M. Marchini, M. Mingozzi, R. Colombo, I. Guzzetti, L. Belvisi, F. Vasile, D. Potenza, U. Piarulli, D. Arosio, C. Gennari, *Chem. Eur. J.* **2012**, *18*, 6195-6207.

[125] R. Fanelli, L. Schembri, U. Piarulli, M. Pinoli, E. Rasini, M. Paolillo, M. C. Galiazzo, M. Cosentino, F. Marino, *Vasc. Cell* **2014**, *6*, 11.

[126] S. Panzeri, S. Zanella, D. Arosio, L. Vahdati, A. Dal Corso, L. Pignataro, M. Paolillo, S. Schinelli, L. Belvisi, C. Gennari, U. Piarulli, *Chem. Eur. J.* **2015**, *21*, 6265-6271.

[127] R. Colombo, M. Mingozzi, L. Belvisi, D. Arosio, U. Piarulli, N. Carenini, P. Perego, N. Zaffaroni, M. De Cesare, V. Castiglioni, E. Scanziani C. Gennari, *J. Med. Chem.* **2012**, *55*, 10460-10474.

[128] M. Mingozzi, L. Manzoni, D. Arosio, A. Dal Corso, M. Manzotti, F. Innamorati, L. Pignataro, D. Lecis, D. Delia, P. Seneci, C. Gennari, *Org. Biomol. Chem.* **2014**, *12*, 3288-3302.

[129] S. Zanella, M. Mingozzi, A. Dal Corso, R. Fanelli, D. Arosio, M. Cosentino, L. Schembri, F. Marino, M. De Zotti, F. Formaggio, L. Pignataro, L. Belvisi, U. Piarulli, C. Gennari, *ChemistryOpen* **2015**, *4*, 633-641.

[130] A. Dal Corso, M. Caruso, L. Belvisi, D. Arosio, U. Piarulli, C. Albanese, F. Gasparri, A. Marsiglio, F. Sola, S. Troiani, B. Valsasina, L. Pignataro, D. Donati, C. Gennari, *Chem. Eur. J.* **2015**, *21*, 6921-6929.

[131] S. Zanella, S. Angerani, A. Pina, P. L. Rivas, C. Giannini, S. Panzeri, D. Arosio, M. Caruso, F. Gasparri, I. Fraietta, C. Albanese, A. Marsiglio, L. Pignataro, L. Belvisi, U. Piarulli,C. Gennari, *Chem. Eur. J.* **2017**, *23*, 7910-7914.

[132] A. Pina, A. Dal Corso, M. Caruso, L. Belvisi, D. Arosio, S. Zanella, F. Gasparri, C. Albanese, U. Cucchi, I. Fraietta, A. Marsiglio, L. Pignataro, D. Donati, C. Gennari, *ChemistrySelect* **2017**, *2*, 4759-4766.

[133] P. López Rivas, L. Bodero, B. Korsak, T. Hechler, A. Pahl, C. Müller, D. Arosio, L. Pignataro, C. Gennari, U. Piarulli, *Beilstein J. Org. Chem*. **2018**, *14*, 407-415.

[134] X. Wang, D. Ma, W. C. Olson, W. D. W. Heston, *Mol. Cancer Ther.* **2011**, *10*, 1728-1739.

[135] S. Kolodych, C. Michel, S. Delacroix, O. Koniev, A. Ehkirch, J. Eberova, S. Cianferani, B. Renoux, W. Krezel, P. Poinot, C. D. Muller, S. Papot, A. Wagner, *Eur. J. Med. Chem.* **2017**, *142*, 376-382.

[136] a) M. Mammen, S. K. Choi, G. M. Whitesides, *Angew. Chem. Int. Ed. Engl.* **1998**, *37*, 2754-2794; b) R. Haag, *Beilstein J. Org. Chem.* **2015**, *11*, 848-849.

[137] C. Fasting, C. A. Schalley, M. Weber, O. Seitz, S. Hecht, B. Koksch, J. Dernedde, C. Graf, E. W. Knapp, R. Haag, *Angew. Chem. Int. Ed.* **2012**, *51*, 10472-10498.

[138] A. Barnard, D. K. Smith, *Angew. Chem. Int. Ed.* **2012**, *51*, 6572-6581.

[139] S. M. Deyev, E. N. Lebedenko, *Bioessays* **2008**, *30*, 904-918.

[140] E. Mahon, M. Barboiu, *Org. Biomol. Chem.* **2015**, *13*, 10590-10599.

[141] S. Ordanini, N. Varga, V. Porkolab, M. Thepaut, L. Belvisi, A. Bertaglia, A. Palmioli, A. Berzi, D. Trabattoni, M. Clerici, F. Fieschi, A. Bernardi, *Chem. Commun.* **2015**, *51*, 3816-3819.

[142] L. Auzzas, F. Zanardi, L. Battistini, P. Burreddu, P. Carta, G. Rassu, C. Curti, G. Casiraghi, *Curr. Med. Chem.* **2010**, *17*, 1255-1299.

[143] C. Zhai, G. M. Franssen, M. Petrik, P. Laverman, D. Summer, C. Rangger, R. Haubner, H. Haas, C. Decristoforo, *Mol. Imaging Biol.* **2016**, *18*, 758-767.

[144] C. Imberti, S. Y. A. Terry, C. Cullinane, F. Clarke, G. H. Cornish, N. K. Ramakrishnan, P. Roselt, A. P. Cope, R. J. Hicks, P. J. Blower, M. T. Ma, *Bioconjugate Chem.* **2017**, *28*, 481-495.

[145] Z. H. Jin, T. Furukawa, T. Ohya, M. Degardin, A. Sugyo, A. B. Tsuji, Y. Fujibayashi, M. R. Zhang, T. Higashi, D. Boturyn, P. Dumy, T. Saga, *Nucl. Med. Commun.* **2017**, *38*, 347-355.

[146] M. Janssen, W. J. Oyen, L. F. Massuger, C. Frielink, I. Dijkgraaf, D. S. Edwards, M. Radjopadhye, F. H. Corstens, O. C. Boerman, *Cancer Biother. Radiopharm.* **2002**, *17*, 641-646.

[147] Z. Q. Zhao, Y. Yang, W. Fang, S. Liu, *Nucl. Med. Biol.* **2016**, *43*, 661-669.

[148] D. Boturyn, J. L. Coll, E. Garanger, M. C. Favrot, P. Dumy. *J. Am. Chem. Soc.* **2004**, *126*, 5730-5739.

[149] Z. H. Jin, V. Josserand, J. Razkin, E. Garanger, D. Boturyn, M. C. Favrot, P. Dumy, J. L. Coll, *Mol Imaging* **2006**, *5*, 188-197.

[150] Z. H. Jin, V. Josserand, S. Foillard, D. Boturyn, P. Dumy, M. C. Favrot, J. L. Coll, *Mol. Cancer* **2007**, *6*, 41.

[151] L. Sancey, V. Ardisson, L. M. Riou, M. Ahmadi, D. Marti-Batlle, D. Boturyn, P. Dumy, D. Fagret, C. Ghezzi, J. P. Vuillez, *Eur. J. Nucl. Med. Mol. Imaging* **2007**, *34*, 2037-2047.

[152] L. Sancey, E. Garanger, S. Foillard, G. Schoehn, A. Hurbin, C. Albiges-Rizo, D. Boturyn, C. Souchier, A. Grichine, P. Dumy, J. L. Coll, *Mol. Ther.* **2009**, *17*, 837-843.

[153] A. Grassin, M. Jourdan, P. Dumy, D. Boturyn, *Chembiochem* **2016**, *17*, 515-520.

[154] S. Foillard, P. Dumy, D. Boturyn, *Org. Biomol. Chem.* **2009**, *7*, 4159-4162.

[155] A. Bianchi, D. Arosio, P. Perego, M. De Cesare, N. Carenini, N. Zaffaroni, M. De Matteo,L. Manzoni, *Org. Biomol. Chem.* **2015**, *13*, 7530-7541.

[156] V. M. Krishnamurthy, L. A. Estroff, G. M. Whitesides, *Fragment-based Approaches in Drug Discovery: Multivalency in Ligand Design*, WILEY-VCH Verlag GmbH & Co. KGaA, Weinheim, **2006**.

[157] a) *1,3-Dipolar Cycloadditions Chemistry*, R. Huisgen, Ed., Wiley (New York), **1984**, Vol. 1, pp. 1-176; b) R. Huisgen, *Pure Appl. Chem.* **1989**, *61*, 613-628;

[158] V. M. Krishnamurthy, V. Semetey, P. J. Bracher, N. Shen, G. M. Whitesides, *J. Am. Chem. Soc.* **2007**, *129*, 1312-1320.

[159] a) Z.-X. Jiang, Y. Feng, Y. B. Yu, *Chem. Commun.* **2011**, *47*, 7233-7235; b) M. Assali, J. J. Cid, M. Pernía-Leal, M. Muñoz-Bravo, I. Fernández, R. E. Wellinger, N. Khiar, *ACS Nano* **2013**, *7*, 2145-2153.

[160] a) H. C. Kolb, M. G. Finn, K. B. Sharpless, *Angew. Chem. Int. Ed.* **2001**, *40*, 2004-2021; b) H. C. Kolb, K. B. Sharpless, *Drug Discov. Today* **2003**, *8*, 1128-1137.

[161] P. L. Rivas, I. Ranđelović, A. Raposo Moreira Dias, A. Pina, D. Arosio, J. Tóvári, G. Mező, A Dal Corso, L. Pignataro, C. Gennari, *Eur. J. Org. Chem.* **2018**, 2902-2909.

[162] A. Raposo Moreira Dias, A. Pina, A. Dal Corso, D. Arosio, L. Belvisi, L. Pignataro, M. Caruso, C. Gennari, *Chem. Eur. J.* **2017**, *23*, 14410-14415.

[163] a) M. Janssen, W. J. G. Oyen, L. F. A. G. Massuger, C. Frielink, I. Dijkgraaf, D. S. Edwards, M. Radjopadhye, F. H. M. Corstens, O. C. Boerman, *Cancer Biother. Radiopharm.* **2002**, *17*, 641-646; b) D. S. Choi, H.-E. Jin, S. Y. Yoo, S.-W. Lee, *Bioconjugate Chem.* **2014**, *25*, 216-223; c) V. López-Rodríguez, C. Galindo-Sarco, F. O. García-Pérez, G. Ferro-Flores, O. Arrieta, M. A. Ávila-Rodríguez, *J. Nucl. Med.* **2016**, *57*, 404-409; d) C. Imberti, S. Y. A. Terry, C. Cullinane, F. Clarke, G. H. Cornish, N. K. Ramakrishnan, P. Roselt, A. P. Cope, R. J. Hicks, P. J. Blower, M. T. Ma, *Bioconjugate Chem.* **2017**, *28*, 481-495.

[164] M. Dorywalska, R. Dushin, L. Moine, S. E. Farias, D. Zhou, T. Navaratnam, V. Lui, A. Hasa-Moreno, M. G. Casas, T.-T. Tran, *Mol. Cancer Ther.* **2016**, *15*, 958-970.

[165] a) T. Kline, M. Y. Torgov, B. A. Mendelsohn, C. G. Cerveny, P. D. Senter, *Mol. Pharm.* **2004**, *1*, 9-22; b) C. F. Albright, N. Graciani, W. Han, E. Yue, R. Stein, Z. Lai, M. Diamond, R. Dowling, L. Grimminger, S.-Y. Zhang, *Mol. Cancer Ther.* **2005**, *4*, 751-760; c) J. L. Crisp, E. N. Savariar, H. L. Glasgow, L. G. Ellies, M. A. Whitney, R. Y. Tsien, *Mol. Cancer Ther.* **2014**, *13*, 1514-1525.

[166] a) P. Yingyuad, M. Mével, C. Prata, S. Furegati, C. Kontogiorgis, M. Thanou, A. D. Miller, *Bioconjugate Chem.* **2013**, *24*, 343-362; b) F. Fouladi, K. J. Steffen, S. Mallik, *Bioconjugate Chem.* **2017**, *28*, 857-868; c) B. Hurt, R. Schulick, B. Edil, K. C. El Kasmi, C. Barnett, *Am. J. Surg.* **2017**, *214*, 938-944.

[167] S. Cazzamalli, A. Dal Corso,D . Neri, *J. Control. Release* **2017**, *246*, 39-45.

[168] K. Achilles, P. J. Bednarski, *Biol. Chem.* **2003**, *384*, 817-824.

[169] a) K. Yamaguchi, S. Shimada, S. Tashima, M. Ogawa, *Oncol. Rep.* **2000**, *7*, 1017-1038; b) T. Sato, S. Takahashi, T. Mizumoto, M. Harao, M. Akizuki, M. Takasugi, T. Fukutomi, J. Yamashita, *Surg. Oncol.* **2006**, *15*, 217-222.

[170] R. Firestone, L. Telan (Boehringer Ingelheim Pharmaceuticals Inc), US 6855689 B2, **2005**.

[171] H. G. D. Lerchen, J. D. Baumgarten, A. D. Schoop, M. D. Albers (Bayer HealthCare AG), EP 1372732 A1, **2002**.

[172] F. M. H. de Groot, L. W. A. van Berkom, H. W. Scheeren, *J. Med. Chem.* **2000**, *43*, 3093-3102.

[173] F. M. H. de Groot, W. J. Loos, R. Koekkoek, L. W. A. van Berkom, G. F. Busscher, A. E. Seelen, C. Albrecht, P. de Bruijn, H. W. Scheeren, *J. Org. Chem.* **2001**, *66*, 8815-8830.

[174] a) P. M. Starkey, A. J. Barrett, *Biochem. J* **1976**, *155*, 265-271; b) C. Gardi, E. Cavarra, P. Calzoni, P. Marcolongo, M. de Santi, P. A. Martorana, G. Lungarella, *Biochem. J* **1994**, *299*, 237-245.

[175] T. Legigan, J. Clarhaut, B. Renoux, I. Tranoy-Opalinski, A. Monvoisin, C. Jayle, J. Alsarraf, M. Thomas, S. Papot, *Eur. J. Med. Chem.* **2013**, *67*, 75-80.

[176] C. F. Albright, N. Graciani, W. Han, E. Yue, R. Stein, Z. Lai, M. Diamond, R. Dowling, L. Grimminger, S. Y. Zhang, D. Behrens, A. Musselman, R. Bruckner, M. Zhang, X. Jiang, D. Hu, A. Higley, S. Dimeo, M. Rafalski, S. Mandlekar, B. Car, S. Yeleswaram, A. Stern, R. A. Copeland, A. Combs, S. P. Seitz, G. L. Trainor, R. Taub, P. Huang, A. Oliff, *Mol. Cancer Ther.* **2005**, *4*, 751-760.

[177] a) J. Tian, V. J. Stella, *J. Pharm. Sci.* **2008**, *97*, 3100-3108; b) S. K. Dordunoo, H. M. Burt, *Int. J. Pharm.* **1996**, *133*, 191-201.

[178] A. Dal Corso, S. Cazzamalli, R. Gebleux, M. Mattarella,D. Neri, *Bioconjug. Chem.* **2017**, *28*, 1826-1833.

[179] T. Kline, M. Y. Torgov, B. A. Mendelsohn, C. G. Cerveny, P. D. Senter, *Mol. Pharm.* **2004**, *1*, 9-22.

[180] M. P. Johansson, H. Maaheimo, F. S. Ekholm, *Sci. Rep.* **2017**, *7*, 15920.

[181] K. G. Steube, D. Grunicke, T. Pietsch, S. M. Gignac, G. R. Pettit, H. G. Drexler, *Leukemia* **1992**, *6*, 1048-1053.

[182] H. C. Pitot, E. A. McElroy, Jr., J. M. Reid, A. J. Windebank, J. A. Sloan, C. Erlichman, P. G. Bagniewski, D. L. Walker, J. Rubin, R. M. Goldberg, A. A. Adjei, M. M. Ames, *Clin. Cancer Res.* **1999**, *5*, 525-531.

[183] S. Banerjee, Z. Wang, M. Mohammad, F. H. Sarkar, R. M. Mohammad, *J. Nat. Prod.* **2008**, *71*, 492-496.

[184] A. Maderna, C. A. Leverett, *Mol. Pharm.* **2015**, *12*, 1798-1812.

[185] S. O. Doronina, B. A. Mendelsohn, T. D. Bovee, C. G. Cerveny, S. C. Alley, D. L. Meyer, E. Oflazoglu, B. E. Toki, R. J. Sanderson, R. F. Zabinski, A. F. Wahl, P. D. Senter, *Bioconjug. Chem.* **2006**, *17*, 114-124.

[186] S. O. Doronina, T. D. Bovee, D. W. Meyer, J. B. Miyamoto, M. E. Anderson, C. A. Morris-Tilden, P. D. Senter, *Bioconjug. Chem.* **2008**, *19*, 1960-1963.

[187] A. Dal Corso, R. Gebleux, P. Murer, A. Soltermann, D. Neri, *J. Control. Release* **2017**, *264*, 211-218.

[188] a) Z.-X. Jiang, Y. Feng, Y. B. Yu, *Chem. Commun.* **2011**, *47*, 7233-7235; b) M. Assali, J. J. Cid, M. Pernía-Leal, M. Muñoz-Bravo, I. Fernández, R. E. Wellinger, N. Khiar, *ACS Nano* **2013**, *7*, 2145-2153.

[189] J. I. Gavrilyuk, U. Wuellner, S. Salahuddin, R. K. Goswami, S. C. Sinha, C. F. Barbas, *Bioorg. Med. Chem. Lett.* **2009**, *19*, 3716-3720.

[190] A. Diez-Torrubia, J. Balzarini, G. Andrei, R. Snoeck, I. De Meester, M. J. Camarasa, S. Velazquez, *J. Med. Chem.* **2011**, *54*, 1927-1942.

[191] S. C. Jeffrey, M. T. Nguyen, J. B. Andreyka, D. L. Meyer, S. O. Doronina, P. D. Senter, *Bioorg. Med. Chem. Lett.* **2006**, *16*, 358-362.

[192] W. C. Still, M. Kahn, A. Mitra, *J. Org. Chem.* **1978**, *43*, 2923-2925.

[193] G. R. Fulmer, A. J. M. Miller, N. H. Sherden, H. E. Gottlieb, A. Nudelman, B. M. Stoltz, J. E. Bercaw, K. I. Goldberg, *Organometallics* **2010**, *29*, 2176-2179.